LA COORDENADA TONAL H EN CIENCIAS ANALÍTICAS
APLICACIÓN A SENSORES QUÍMICOS

Miguel María Erenas Rodríguez

GRUPO DE INVESTIGACIÓN
ESPECTROMETRÍA EN FASE SÓLIDA

UNIVERSIDAD DE GRANADA

DEPARTAMENTO DE QUÍMICA ANALÍTICA

LA COORDENADA TONAL H EN CIENCIAS ANALÍTICAS. APLICACIÓN A SENSORES QUÍMICOS

TESIS DOCTORAL

MIGUEL MARÍA ERENAS RODRÍGUEZ

GRANADA, 2011

Diseño de cubierta:
Jorge Rodríguez Gómez
E-mail: estoypoison@hotmail.com

.

Editor: Editorial de la Universidad de Granada
Autor: Miguel María Erenas Rodríguez
D.L.: Gr 1550-2011
ISBN: 978-84-694-0953-4

LA COORDENADA TONAL H EN CIENCIAS ANALÍTICAS. APLICACIÓN A SENSORES QUÍMICOS

por

Miguel María Erenas Rodríguez

Departamento de Química Analítica

Universidad de Granada

VISADO en Granada, a 8 de Noviembre de 2010

Fdo: Prof. Dr. D. **Luis Fermín Capitán Vallvey**, Catedrático del Departamento de Química Analítica de la Universidad de Granada.

Fdo: Prof. Dr. D. **Ignacio de Orbe Payá**, Profesor Titular del Departamento de Química Analítica de la Universidad de Granada

MEMORIA presentada para aspirar al Grado de Doctor en Ciencias Químicas. Granada, a 8 de Noviembre de 2010

Fdo: **Miguel María Erenas Rodríguez**, Licenciado en Químicas.

A mis padres y mis hermanos.
A Cristina.

Agradecimientos

Esta Tesis Doctoral no se podría haber llevado a cabo sin la ayuda y colaboración de muchas personas. Desde aquí quiero expresar mi más sincero agradecimiento a todas ellas.

En primer lugar, a los directores de esta Tesis, Dr. D. Luis Fermín Capitán Vallvey y Dr. D. Ignacio de Orbe Payá, tanto por el esfuerzo y dedicación que les ha supuesto la dirección y supervisión de este trabajo, como por sus sabios consejos y sugerencias sin los cuales no habría sido posible la elaboración de esta Tesis Doctoral.

A Kevin Cantrell y Deanna Cantrell, quienes me hicieron sentir como en casa a pesar de encontrarme en la otra punta del mundo.

Al Departamento de Química Analítica de la Universidad de Granada, por su soporte técnico, disponibilidad y hospitalidad. A cada uno de sus miembros, que de una u otra forma han puesto su granito de arena contribuyendo a la realización de este trabajo.

A todos los compañeros que han estado conmigo durante este tiempo, Clara, Eduardo, Javier, Emilio, Alejandro, Olga, Ismael, Sonia, Cristina y Estefanía. Con ellos he pasado mis buenos y malos momentos en el laboratorio y siempre han estado ahí.

A electrónicos, Migue, Antonio y Nuria, porque a pesar de coincidir poco con ellos (aunque cada vez más), es como si hubieran estado siempre en el laboratorio (sobre todo con el Facebook).

De modo especial me acuerdo de Juanfra, Julio y Younes con los que viví mañanas en el laboratorio de instrumentación que no olvidaré jamás. Tenía ganas de ir a trabajar todos los días para poner el himno del Granada, el video de Madonna o tan solo recordar el día en que los mejores albañiles del mundo taparon el agujero de la pared del laboratorio. Fueron, sin duda, de los mejores momentos que he vivido en estos años y que nunca olvidaré. También quiero acordarme de Isa, la "secretaria" que nunca tuve y que casi mandaba más que su jefe. Al principio no le hablé mucho, pero menos mal que ella se acercó a mí, porque nunca me habría perdonado no haberla conocido. A María, la que da alegría al laboratorio, que tanto deja todo por ayudarte en los momentos más difíciles como puedes pasar los momentos más divertidos y entrañables. A Paulina y Carmen, quienes a pesar de no haber compartido el laboratorio, siempre han sido fieles compañeras, incluso de desayuno.

No quiero, por supuesto, olvidarme de mis amigos que, aunque no se lo crean, me han aguantado cuando no estaba bien y me han ayudado sin ellos saberlo. En especial a Jorge, que gentilmente me ha diseñado la portada de esta Memoria y al que estoy muy agradecido por ello.

No quiero terminar sin mi más sentida dedicatoria a mis padres, mis hermanos y a Cristina, sin los cuales no podría haber comenzado ni terminado este Doctorado y que siempre, independientemente de la hora o de lo que tuvieran que hacer, han estado a mi lado dándome ánimos y ayudándome en todo momento.

Por último, mi recuerdo a D. Juan Manuel, profesor del Colegio H.H. Maristas, que me enseñó a estudiar y gracias al cual soy lo que hoy soy.

Índice

Capítulo 4

Aproximación a lenguas ópticas de un solo uso para iones alcalinos 131

Objetivos

Esta Tesis Doctoral se enmarca en el campo de los métodos rápidos de análisis químico empleando sensores ópticos de un solo uso. El objetivo general que se persigue es la simplificación de la metodología analítica a través del empleo de dispositivos de captura digital de imágenes con los sensores y uso de espacios de color que proporcionen parámetros analíticos robustos. De esta manera se abre camino hacia el empleo de dispositivos ubicuos que pueden conjugar la recogida de imágenes con capacidad de procesamiento y comunicación inalámbrica como son los teléfonos móviles provistos de cámara digital.

En resumen, se pretende que estos ensayos rápidos lleguen a ser lo más independientes posible del laboratorio de análisis y puedan ser llevados a cabo por usuarios sin preparación específica.

Para lograr este objetivo general se han planteado una serie de objetivos particulares que van a ir desarrollando diferentes aspectos del mismo:

1. Estudiar la posibilidad de llevar a cabo medidas de transflexión para calibrar sensores ópticos de un solo uso.
2. Establecer una carta de color teórica para sensores de un solo uso a partir de espectros de transflexión y su evaluación experimental.
3. Evaluar la coordenada tonal H del espacio de color HSV obtenida a partir de dispositivos de captura de imagen para su uso como parámetro analítico de sensores de un solo uso.
4. Usar diferentes dispositivos de captura de imagen digital como son escáneres, cámaras fotográficas o teléfonos móviles tanto en modo transmisión como reflexión, para obtener imágenes de sensores ópticos de un solo uso a partir de las cuales establecer procedimientos analíticos

5. Desarrollar lenguas ópticas de un solo uso para la determinación simultánea de distintos analitos.
6. Aprovechar las características de teléfonos móviles provistos de cámara digital, referidas la adquisición de imágenes y la capacidad de procesamiento para su empleo como dispositivo analítico completo utilizando sensores de un solo uso.

Capítulo 1

Introducción

La aparición de los dispositivos electrónicos de captura digital de imágenes en el campo de las ciencias analíticas ocurrió tímidamente en la década de los 80 y ya en la década de los 90 tuvo un enorme impacto, incrementando su importancia tal y como se observa en la Figura 1. Representaron una revolución principalmente en el campo de la espectroscopia óptica llegando a ser excelentes detectores de imagen para análisis químico en los que se originaban, frecuentemente, bajos flujos de fotones. Para un gran número de aplicaciones analíticas que requerían información espacial, se convirtieron en el detector ideal por su gran resolución espacial, amplio rango dinámico lineal, alta sensibilidad, desde rayos X hasta infrarrojo próximo, y su capacidad para integrar señales durante largos periodos de tiempo [1].

De forma similar, a partir de los años 90 se observa un desarrollo explosivo de la electrónica de consumo en las sociedades del primer mundo con características de: 1) reducción continua de precios por la mayor eficiencia de la fabricación, reducción de costos de mano de obra por el desplazamiento de la fabricación a países del tercer mundo y la mejora en la tecnología de semiconductores; 2) convergencia de tecnologías por incorporación de funcionalidades en productos (fotocopiadora con funcionalidad de escáner y fax); 3) inclusión de conectividad a internet en muchos productos, desde televisores a neveras, a través de tecnologías Wi-Fi, Bluetooth ó Ethernet.

Como consecuencia de este desarrollo de la electrónica de consumo se ha puesto en manos del usuario final, una variedad de dispositivos ópticos – escáneres, cámaras de video, webcams, cámaras fotográficas – con unas carac-

terísticas de sensibilidad, ubicuidad, asequibilidad y portabilidad que las hacen atractivas como potenciales herramientas analíticas. A este hecho se une que el ciudadano cada vez demanda una mayor cantidad de información química acerca de cuestiones diversas relacionadas con salud, medioambiente, bienestar u otras.

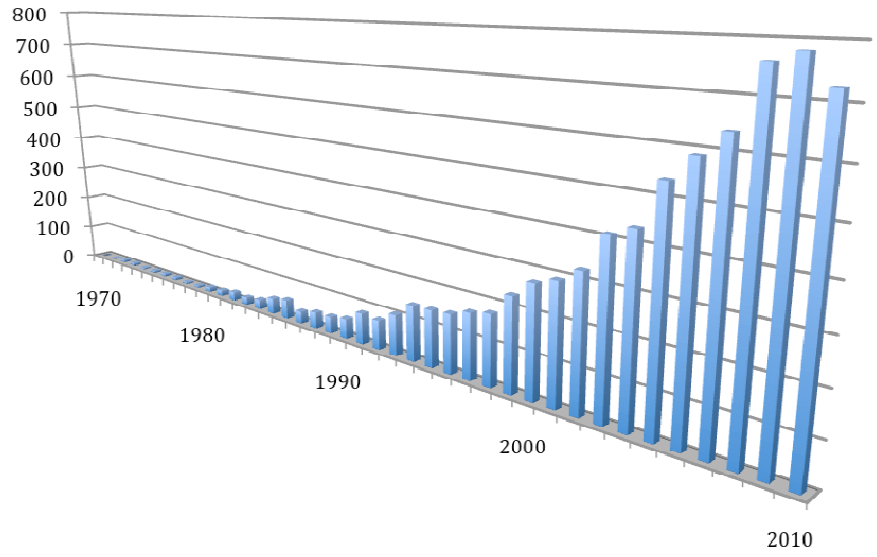

Figura 1. Evolución del número de publicaciones por año referidas al uso de dispositivos de captura digital

En esta Memoria de Doctorado se aborda el reto de utilizar dispositivos de imagen de propósito general, actualmente de amplia utilización por el ciudadano, altas prestaciones y bajo precio, como instrumentos para la obtención de información analítica. Para ello nos centraremos en el estudio de la adquisición del parámetro analítico a partir de la información contenida en las imágenes de los sensores ópticos utilizados, llegando a proponer un nuevo parámetro analítico con buenas características de robustez y fiabilidad, demostrando su utilidad con diversos tipos de dispositivos de detección óptica.

1. Dispositivos de captura digital

En esta sección, se pretende dar una visión sucinta de los dispositivos de imagen de uso común incorporados en la electrónica de consumo y que serán usados en esta Memoria, pasando a continuación a revisar el estado del arte del empleo de estos dispositivos de imagen en las ciencias analíticas.

Un dispositivo de carga acoplada o Charge-Coupled Device (CCD) es un circuito integrado que contiene una matriz de condensadores de tecnología MOS (*Metal-Oxide-Semiconductor*). Bajo el control de circuitería interna, cada condensador puede transferir su carga eléctrica a uno o a varios de los condensadores adyacentes en el circuito impreso. La alternativa actual a los CCD son los dispositivos CMOS (*Complementary Metal Oxide Semiconductor*) utilizados en algunas cámaras digitales y en numerosas webcam. En la actualidad los CCD son mucho más habituales en aplicaciones profesionales y en cámaras digitales de altas prestaciones.

El dispositivo CCD fue inventado por Willard Boyle y George Smith en 1969 en los Laboratorios Bell, siendo premiados por ello con diversas distinciones como el Stuart Ballantine Medal del Instituto Franklin en 1973, el IEEE Morris N. Liebmann Memorial Award en 1973, el Charles Stark Draper Prize en 2006 y el Premio Nobel de Física de 2009. Curiosamente, el objetivo inicial de su desarrollo fue como dispositivo de almacenamiento de información (memoria), aunque muy pronto se comprobó su potencial como detector bidimensional de imágenes.

Los sensores CCD (Figura 2) están compuestos por un sustrato de silicio sobre el cual se dispone una matriz de fotodiodos MOS dispuestos uno al lado del otro [2-4]. En cada uno de estos fotodiodos, también llamado píxel, se va a generar una carga como consecuencia de la incidencia de fotones que se va a ir almacenando durante el llamado tiempo de integración, tiempo durante el cual los fotones llegan a los fotodiodos. La carga generada en cada uno de ellos va a

depender de la intensidad del flujo de luz que llega a los fotodiodos, del tiempo de integración y de la eficiencia cuántica de los mismos.

Una vez generada, la carga ha de ser llevada a un amplificador de señal, el cual se encuentra conectado a los fotodiodos más externos de la matriz que componen los mismos. Por tanto, es necesario transferir dicha carga de un píxel al adyacente hasta llegar al amplificador. La transferencia de carga es controlada por el procesador que se incluye en el sensor CCD y que consiste en modular el voltaje de los fotodiodos de manera que se vaya transfiriendo la carga hasta la posición deseada [2].

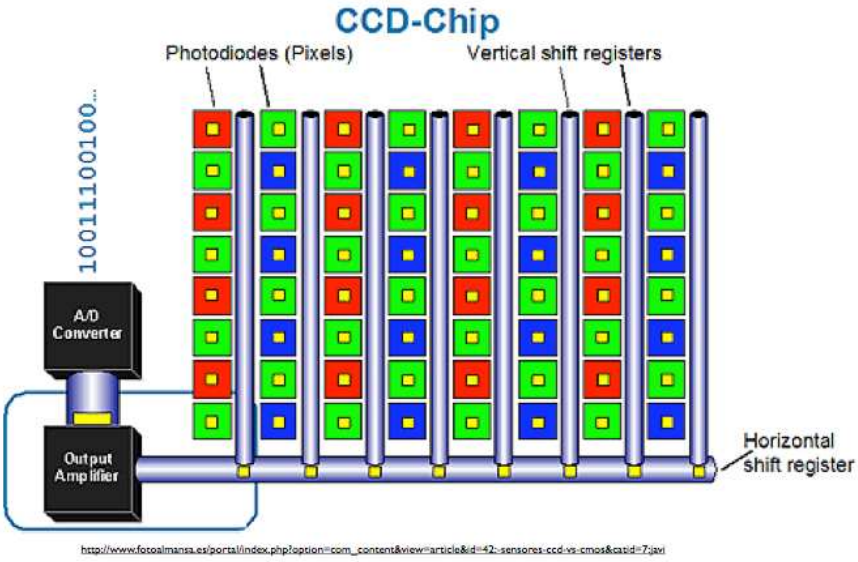

Figura 2. Esquema de un sensor CCD

El proceso de conversión carga-voltaje se va realizar, como se ha dicho anteriormente, en un amplificador de señal al que va a llegar de manera secuencial la carga de cada uno de los píxeles. El amplificador de señal está compuesto por un transistor MOS dispuesto en emisor común con un transistor de puesta a cero. La carga alcanza la etapa en emisor común, generándose el voltaje a partir

de la mencionada carga. Una vez generado el voltaje, el amplificador se reinicia de manera que esté preparado para recibir la siguiente carga procedente de otro píxel.

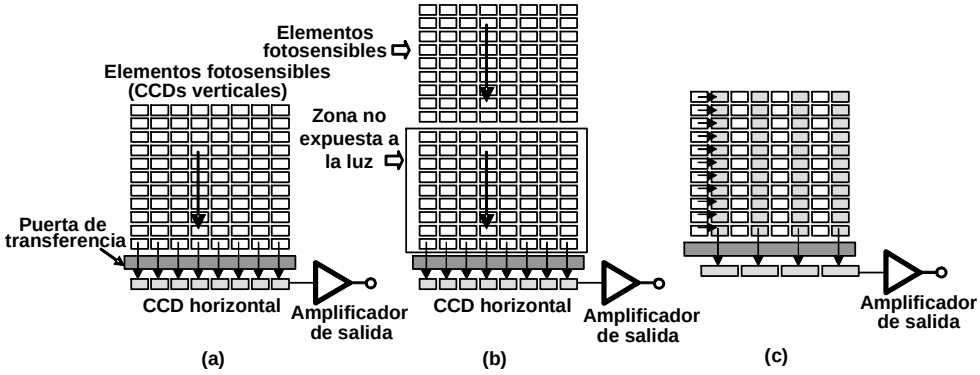

Figura 3. Configuraciones de transferencia de la imagen

El principal problema de este tipo de detectores es que en el momento en que uno de los píxeles que componen la matriz de los mismos se deteriora, no puede llegar la carga al amplificador de dicho píxel, y, en consecuencia, a todos los que dependen de él. Tal y como se muestra en la Figura 3, estos píxeles se encuentran conectados entre sí normalmente formando columnas que llegan hasta el amplificador, son las matrices lineales (a); aun así existen otros tipos de configuraciones como la transferencia de imagen completa (b) o la transferencia interlínea (c) [2].

Finalmente, el voltaje llega a un convertidor analógico-digital donde se obtiene una señal interpretable por el procesador, almacenando la imagen digitalizada en la memoria del dispositivo.

En el caso de tratarse de dispositivos a color, se emplea junto con el detector CCD un mosaico de Bayer [5] (Figura 4). Dicho mosaico es una cuadrícu-

la de filtros rojos, verdes y azules que se van a situar delante de los elementos que componen el detector y va a hacer llegar la radiación transmitida por cada filtro proporcionando información sobre la intensidad de radiación en cada una de las zonas rojas, verdes y azules del espectro que por síntesis aditiva permitirá establecer el color de cada píxel. La proporción de filtros de cada color en el mosaico no es igual, sino que existen un 50% de filtros verdes, 25% de rojos y 25% de azules, al objeto de imitar la respuesta óptica del ojo humano, cuyos bastones son más sensibles al verde que a otros colores. Debido a esta distribución, el color de cada píxel que compone la imagen va a venir dado por la interpolación de la tonalidad de cuatro fotodiodos, dos verdes, uno azul y otro rojo.

Aunque el filtro de Bayer es de amplio uso, existen filtros alternativos para realizar una función similar, como es el filtro CYMG (*cyan, yellow, green, magenta*) o el filtro RGBE (*red, green, blue, emerald*). Otras disposiciones se encuentran en el sensor Foveon X3 que sitúa verticalmente los filtros rojos, verdes y azules en vez de la disposición en mosaico. En otras ocasiones se han utilizado disposiciones de tres distintas CCD, una para cada color con sus filtros correspondientes.

Para reconstruir la imagen a color, con las intensidades de los tres colores primarios representadas para cada píxel, a partir de la imagen en bruto capturada por el dispositivo CCD provisto del filtro, se emplea un algoritmo de interpolación, operación a la que se denomina *demosaicing*. La reproducción final del color depende de la transmitancia espectral de los elementos del filtro utilizado y del algoritmo de reconstrucción de color utilizado. Como las respuestas de los filtros generalmente no corresponden con las funciones de ajuste de color CIE, es frecuente convertir los valores triestímulo a un espacio de color absoluto como el CIEXYZ o el sRGB.

Aunque ampliamente conocidas con anterioridad, por motivos tecnológicos, no fue hasta la década de los 90 cuando aparecieron las estructuras semi-

conductor-óxido-metal complementarias (Complementary Metal-Oxide-Semiconductor CMOS) como una alternativa, también basada en el efecto foto-eléctrico, a los sensores CCD [5-7]. Una de sus principales características es la utilización conjunta de transistores de tipo pMOS y nMOS configurados de manera que en estado de reposo, el consumo de energía se debe exclusivamente a las corrientes parásitas. Estos sensores de luz basados en tecnología CMOS se conocen como Active Pixel Sensor (APS) o simplemente sensores CMOS.

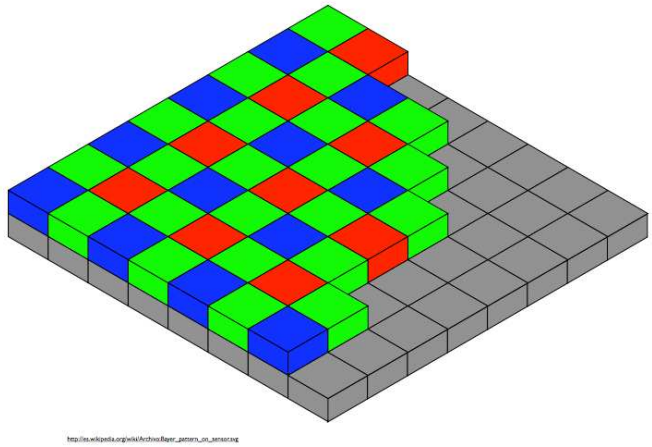

Figura 4. Mosaico de Bayer

El sensor CMOS está formado por un conjunto de fotositos, uno para cada píxel, que trabajan de manera independiente unos de otros y originan una carga eléctrica. En el CMOS, a diferencia del CCD, se incorpora un amplificador de la señal eléctrica integrado en cada fotosito siendo común incluir el conversor analógico-digital en el propio chip. La carga generada va a parar directamente al amplificador de señal integrado en el mismo píxel, sin necesidad de trasladarlo a través del resto de fotodiodos, obteniendo un voltaje que en la interfase analógica-digital se convierte en información interpretable por el dispositivo de imagen (Figura 5).

Como en el caso de los sensores CCD, cuando se quiere trabajar con imágenes en color se utiliza el mosaico de Bayer situado sobre el sensor CMOS, y de nuevo el color de cada píxel se integra a partir del color obtenido de cuatro píxeles diferentes, dos de ellos con un filtro verde, uno con filtro rojo y otro con azul.

La principal diferencia existente entre los sensores CCD y CMOS es el modo en que trabajan una vez que se genera la carga al impactar los fotones sobre el fotodiodo. Como consecuencia de ello, cada tipo de sensor va a tener sus ventajas y sus inconvenientes.

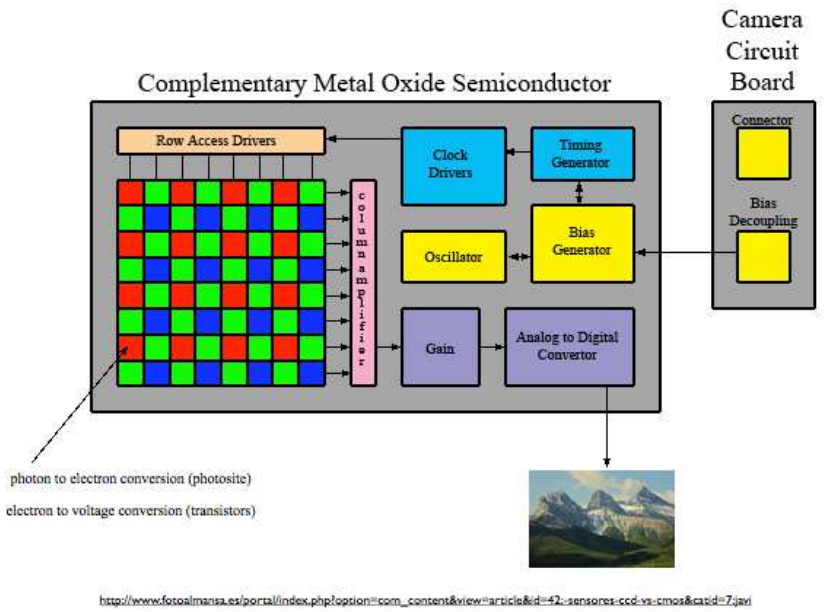

Figura 5. Esquema de un sensor CMOS

Así, los sensores CMOS van a necesitar un menor voltaje para el reseteo de cada uno de los píxeles, así como para el proceso de conversión de la carga en voltaje. Además, en los sensores CCD no pueden trabajar todas las columnas al mismo tiempo de manera que al amplificador de señal van llegando las cargas

de los píxeles de una sola columna de fotodiodos, y una vez finalizado el proceso para esa columna comienza el de la siguiente. Todo esto se va a traducir en un mayor consumo de energía por parte de los sensores CCD frente a los CMOS.

El ruido generado también es diferente en los sensores CCD y CMOS. En los primeros, al tener tanto la interfase analógica-digital como el amplificador de señal fuera del sensor, puede utilizar mejores sistemas que permiten reducir el ruido de la señal. Además, el CMOS al tener elementos no fotosensibles integrados en la placa, no puede captar tanta luz a igualdad de superficie del chip. La solución utilizada fue aumentar la densidad de integración, reduciendo de tamaño la electrónica y utilizando microlentes para concentrar la luz de cada celda en su fotosito.

La respuesta de todos los fotodiodos frente a la misma radiación debería producir teóricamente la misma señal, cosa que no ocurre en la práctica, sobre todo en el caso de los sensores CMOS frente a los CCD donde la señal es más uniforme debido al paso de la carga de un fotodiodo a otro. No obstante mediante la inclusión en los sensores CMOS de circuitos con realimentación, subsana en gran medida el problema.

Una ventaja de los sensores CMOS es que la electrónica puede leer directamente la señal de cada píxel con lo que se soluciona el problema conocido como blooming. Éste se refiere al efecto de la sobreexposición de un píxel, esto es, la recepción de una gran intensidad lumínica en un punto influye en los píxeles adyacentes.

Por último, una ventaja de los sensores CCD frente a los CMOS es su mayor rango dinámico, cociente entre el nivel de saturación de los píxeles y el umbral por debajo del cual no captan señal, que suele ser el doble para los primeros frente a los últimos.

Debido a estas diferencias, los sensores CCD tienden a ser usados en

cámaras de muy alta sensibilidad que pretenden lograr imágenes de alta calidad con buena sensibilidad luminosa y gran número de píxeles. Aunque tradicionalmente los sensores CMOS presentan menor calidad, resolución y sensibilidad, sus características han mejorado de forma que en la actualidad sus prestaciones son similares con la ventaja de su menor precio y consumo energético [2].

2. Escáneres en análisis químico

Un escáner óptico o de computadora es un dispositivo que explora ópticamente imágenes, textos u objetos convirtiéndolos en imágenes digitales. Existen de diverso tipo: de rodillo, de barras, de mano, plano, cenital, de tambor u otros de propósito más específico como los escáneres 3D o los de alta resolución (hasta 1 $\mu m \cdot pixel^{-1}$) usados en investigación biomédica para la lectura de microarrays de DNA.

Mientras que los escáneres más antiguos empleaban tubos fotomultiplicadores como sensores de imagen, los escáneres actuales utilizan dispositivos de carga acoplada (CCD) o bien sensores de imagen por contacto (Contact Image Sensor, CIS), que están reemplazando a los CCD en aplicaciones portátiles y de bajo consumo. Al contrario que los escáneres CCD convencionales en los que se usa un sensor estacionario al que llega la luz reflejada mediante un espejo al moverse la fuente de radiación sobre el objeto a escanear, el CIS sitúa la imagen el sensor de imagen en contacto casi directo con el objeto. Un escáner CIS consta de un array lineal de detectores, con las lentes de enfoque sobre ellos y un conjunto de LEDs para iluminación.

El escáner de sobremesa o plano, que será el que se utilice en esta Tesis Doctoral, dispone de una superficie plana de vidrio sobre la que se sitúa el elemento a escanear y bajo la cual de desplaza un elemento móvil donde se ubica

la fuente de luz y el sensor en los escáneres de reflexión o sólo el sensor o bien espejos en los escáneres de transmisión, estando localizada la fuente de luz encima del documento a escanear. En cualquier caso, el sensor óptico convierte la luz en carga eléctrica que con la ayuda de un software de conversión analógico/digital transforma la señal eléctrica generada en una señal electrónica en forma de una imagen de mapa de bits.

La calidad de un escáner y, en consecuencia, de las imágenes digitales que genera viene determinada por tres aspectos: 1) profundidad del color, medida en bits por píxel (ppi), que se refiere a la cantidad de bits de información necesarios para representar el color de un píxel (acrónimo de Picture Element); 2) resolución, que es la cantidad de píxeles que contiene una imagen y se mide en píxeles por pulgada (ppp); y 3) rango de densidad entendida como la capacidad de un escáner para recoger el rango completo de densidades de la imagen de partida o para distinguir variaciones, así como la linealidad de la diferenciación.

Como resultado del escaneo se obtiene una imagen RGB no comprimida que puede comprimirse, y preprocesarse previamente a transferirse al ordenador con algún firmware embebido en el periférico. Los formatos más habituales de las imágenes escaneadas son JPEG, TIFF, mapa de bits o PNG dependiendo del uso que se vaya a dar a dicha imagen. Los formatos más comunes, algunos de los cuales serán usados en esta Memoria, son los siguientes:

GIF (Graphics Interchange Format): formato de archivo utilizado normalmente para representar gráfico e imágenes de color indexado en páginas web. En este tipo de archivo se comprime del orden de 1.5:1 a 2:1.

PNG (Portable Network Graphic): formato de imagen similar al anterior con la diferencia de que en lugar de utilizar un formato de compresión licenciado, utiliza uno que no está patentado con la consiguiente ventaja.

TIFF (Tagged Image File Format): formato de imagen etiquetado de alta resolución. Por tanto, además de los datos de la imagen propiamente dicha,

llevan la información sobre las características de la imagen, que sirve para su tratamiento posterior. Pueden operar con diferentes niveles de compresión: sin compresión, compresión entre 1.5:1 a 2:1 y compresión entre 10:1 a 20:1.

JPEG (Join Photograph Expert Group): formato de archivo gráfico que se utiliza para mostrar imágenes en color de alta resolución. Las imágenes JPEG aplican un esquema de compresión especificado por el usuario que puede reducir considerablemente los tamaños de archivos grandes de imágenes de alta calidad. La compresión que se aplica a este tipo de archivos está comprendida desde 10:1 hasta 100:1.

Los escáneres de ordenador como dispositivo o periférico de entrada para digitalizar documentos o imágenes procedentes de papel, libros, negativos o diapositivas se utilizan principalmente en ofimática, entendida como el conjunto de técnicas, aplicaciones y herramientas informáticas que se utilizan en funciones de oficina (para archivado, fax, microfilmado, gestión de archivos y documentos, etc.) y por una amplia gama de usuarios, para optimizar, automatizar y mejorar los procedimientos o tareas relacionados con propósitos diversos.

Además de su amplia utilización ofimática, los escáneres de tipo óptico se han empleado con diferentes propósitos como alternativa a otros tipos de instrumentación más compleja, debido a su fácil uso y a la posibilidad de analizar la imagen capturada para determinar o cuantificar los datos de luminosidad correspondientes al objeto en estudio. Así, han sido utilizados en diferentes campos como mineralogía [8], ciencias de la tierra [9], odontología [10], radiología [11], procesamiento de alimentos [12-15], biología [16] ó arqueología [17], entre otros.

En el campo de las ciencias analíticas, los escáneres han sido utilizados con diferentes propósitos. Uno de ellos pretende conseguir información de procesos de separación bidimensionales, como por ejemplo en cromatografía en capa fina, permitiendo la obtención de densitometrías a partir de imágenes en

blanco y negro, análisis de imágenes coloreadas o imágenes fluorescentes con fines de archivo o análisis [18-20]. También se han usado en conexión con la electroforesis sobre gel de poliacrilamida, técnica de amplio uso para la separación de biomoléculas. Así por ejemplo, en la técnica Western blot o inmunoblot que se emplea para la detección de proteínas inmovilizadas en membrana mediante anticuerpos mono o policlonales, se realiza una separación de las proteínas mediante electroforesis sobre gel de poliacrilamida con lo que se obtiene información acerca de peso molecular, estructura, hidrofobicidad o existencia de isoformas en las proteínas bajo estudio. La detección se puede hacer con ayuda de diferentes tipos de escáner (convencional, escáner laser) dependiendo del tipo de marcado utilizado en la reacción antígeno-anticuerpo, así reacciones coloreadas o marcadores coloreados, fluorescencia o quimioluminiscencia [21-23].

Los escáneres se utilizan habitualmente para la recogida de información en dispositivos tipo lab-on-a-chip. Estos dispositivos integran una o más operaciones analíticas en un simple chip de dimensiones que varían entre los pocos milímetros a varios centímetros, permitiendo el manejo de volúmenes muy pequeños de muestra, en torno a los picolitros, con bajo consumo de reactivos, tiempos de análisis cortos, buen control de procesos, alta paralelización y precio relativamente bajo. No obstante presenta problemas debido a que los procesos son más complejos a esa escala que en un laboratorio convencional. Por ello, la detección suele conducir a bajas relaciones señal/ruido y a falta de precisión debida a microfabricación. Se utilizan para PCR en tiempo real, ensayos bioquímicos, inmunoensayos para moléculas, bacterias o virus, screening de canales iónicos, ensayos de nuevos medicamentos, etc.

Una de las formas de detección es con la ayuda de escáneres de propósito específico que pueden incluir tubos fotomultiplicadores o CCD como sensores de imagen, con discriminación de longitud de onda, alta velocidad de escaneo, medida de fluorescencia o cambio de parámetros durante el registro [24].

A modo de ejemplo, se puede citar un array radial de 96 canales basado en electroforesis capilar para obtención del genotipo con alta eficiencia en el que la detección se hace con un escáner confocal rotatorio que emplea un láser como fuente y usa cuatro canales de color [25]. Una propuesta de gran originalidad es la de Abe *et al.* [26] en la que prepara el dispositivo microfluídico con celulosa mediante técnicas de impresión por chorro con zonas hidrófilas e hidrófobas, lo que permite el movimiento por capilaridad del problema y su llegada a las zonas sensoras. Se ha propuesto para la determinación de pH, proteínas totales y glucosa en orina usando la información de color procedente de un escáner utilizando el espacio de color L*a*b*.

Un tercer tipo de empleo de los escáneres concierne a análisis en disolución. Diferentes tipos de procedimientos analíticos llevados a cabo en disolución se ha desarrollado utilizando placas micropocillo que tras reaccionar son medidas con escáneres; así para determinación de proteínas [27] o para test de toxicidad basados en microorganismos [28]. Dentro de este grupo se puede incluir el análisis de gases, pudiéndose citar como ejemplo la combinación de tubos detectores de gases con escáneres ópticos para la monitorización de malos olores en ambientes habitados [29].

Sin embargo, una de las formas de mayor uso de los escáneres en análisis es la que obtiene información cuantitativa o cualitativa de un análisis llevado a cabo en fase sólida. Dentro de esos ensayos de fase sólida, los denominados sistemas verticales son más sencillos de llevar a cabo y en ellos el fluido conteniendo el analito atraviesa perpendicularmente la capa o capas que constituyen la zona reactiva sufriendo un conjunto de reacciones y procesos que permitirán desarrollar una propiedad analítica [30,31].

Uno de las situaciones más simples es aquella en que se determina exclusivamente un analito. Este es el caso, por ejemplo, de la determinación de proteínas sobre membrana de nitrocelulosa utilizando ponceau S como coloran-

te y utilizando los valores de intensidad que ofrece la escala de grises de la imagen obtenida utilizando la opción de autoexposición [32]. Un caso similar es la determinación semicuantitativa de mercurio en pescado basándose en la recogida de vapores de mercurio sobre papel de carboximetil celulosa recubierto con yoduro cuproso y medida del color del tetrayodomercuriato cuproso insoluble formado [33]. En otro ejemplo, se ha propuesto determinar Fe(III) basándose en ensayos en membranas con tiocianato inmovilizado [34] o el antiséptico polividona yodada [34], en ambos casos utilizando un escáner de mano, aunque mejorando la calibración a partir de las coordenadas RGB de la imagen mediante análisis de componentes principales.

Un esquema de transducción utilizado para cationes y aniones y en menor medida para compuestos orgánicos, es el basado en la química ionóforo-cromoionóforo, también llamado de segundo componente [35]. El cambio de color de una membrana, conteniendo un ionóforo selectivo a la especie de interés y un cromoionóforo, debido a la complejación del analito en la membrana permite la determinación de esa especie. Así, se ha propuesto la determinación escanométrica de potasio en agua entre $6{,}58\cdot10^{-6}$ y 10^{-2} M con una precisión expresada como RSD entre 0,45 y 1,80% basada en el cambio de color de violeta a azul [36].

La medida con escáneres se ha utilizado para la determinación multianalito usando sensores de un solo uso. A modo de ejemplo podemos indicar la determinación de potasio, magnesio y dureza en agua a partir de medidas escanométricas [37]. En este caso la linealización de las funciones respuesta obtenidas a partir de las coordenadas RGB de la imagen escaneada permite la determinación de potasio entre $5{,}4\cdot10^{-6}$ y $2{,}7\cdot10^{-7}$ M, de magnesio entre $1{,}4\cdot10^{-4}$ y $2{,}0\cdot10^{-6}$ M y de dureza entre 1,7 y $2{,}0\cdot10^{-2}$ $mg\cdot L^{-1}$ expresado como $CaCO_3$ con precisiones que oscilan entre el 2 y el 8%.

Un caso diferente dentro de este grupo se refiere a las denominados ensayos de un solo uso de tipo horizontal [38]. En este tipo de ensayo, se obliga a que la muestra se mueva a través del dispositivo mediante flujo fluido de manera que haga posible que se tome la muestra directamente evitando contaminación cruzada y que se dispongan secuencialmente una serie de operaciones analíticas llevando a cabo separaciones cromatográficas de reactivos o interferentes. Se han usado especialmente en sensores inmunológicos de tipo heterogéneo – las llamadas tiras inmunocromatográficas- en los que se aplica una etapa inmunocromatográfica tras la inmovilización de anticuerpos y/o oligonucleótidos en posiciones predefinidas de la membrana, las llamadas zonas de captura. La mezcla de la muestra con marcadores (nanopartículas de oro, carbón, látex, partículas de poliestireno con colorantes, enzimas, liposomas con colorantes o etiquetas fluorescentes) se introduce en la membrana por capilaridad hasta llegar a las zonas de captura donde los analitos y/o los marcadores se unen a los ligandos inmovilizados. Se han usado diversos formatos habituales en inmunoensayo, principalmente sándwich y competitivo.

La recogida de la imagen con ayuda de un escáner convencional de sobremesa permite la cuantificación del analito de interés. Como ejemplo podemos citar la determinación de inmunoglobulina E, en el rango de atomoles, utilizando partículas de carbono como marcador de los anticuerpos [39], la de gonadotropina coriónica humana HGC en ensayos de embarazo [40] o la del pesticida tiabendazol en zumos de frutas con un límite de detección de 0,08 $ng \cdot mL^{-1}$ [41]. Otros tipos de marcadores, como lo son las partículas de oro, han sido usadas para la determinación de HGC en inmunoensayos tipo sándwich [42] o de sulforadamina B marcada con biotina encapsulada en liposomas usada en inmunoensayos rápidos de una sola etapa para biotina [43]. La combinación de redes neuronales con sistemas de análisis de imagen han sido empleadas para cuantificar α-fetoproteina en suero humano haciendo uso de tiras inmunocromatográficas [44].

Dentro de este grupo se puede ubicar también el empleo de escáneres para la tecnología de microrray o chips de ADN que es una tecnología multiplex consistente en una secuencia ordenada de cientos o miles de oligonucleótidos de ADN (sondas) dispuestos sobre una superficie sólida - vidrio, plástico e incluso chips de silicio – capaces de hibridar con cADN o cARN dianas presentes en la muestra. La detección de los eventos de hibridación se hacen usando dianas marcadas con nanopartículas, fluoróforos o quimioluminóforos, determinándose así la abundancia relativa de secuencias de ácidos nucléicos en la muestra, lo que permite la realización de ensayos genéticos al monitorizarse miles de ellos de forma simultánea.

Esta detección se puede realizar de diversas maneras pero la más habitual es la basada en escáneres de alta sensibilidad como los ya citados. Este es el caso del esquema de detección basado en nanopartículas, que utiliza como sonda nanopartículas de oro unidas covalentemente a oligonucleótidos que son complementarios a la diana de interés [45]. Otro caso descrito, usa moléculas diana no etiquetadas y está basado en la interacción electrostática entre nanopartículas de oro y moléculas diana hibridadas [46] o la detección colorimétrica que utiliza un etiquetado enzimático a través de la química de la biotina [47]. También se han utilizado microarrays de proteínas para parametrización proteómica basadas igualmente en medidas con un escáner [48]. Otro tipo de arrays, macroarrays en este caso, se han propuesto para diversas finalidades; este es el caso de un array colorimétrico para determinación de compuestos orgánicos volátiles (VOC) capaces de determinar unos 100 VOC mediante diferentes técnicas multicomponentes [49-51].

3. Cámaras CCD en análisis químico

Una cámara CCD que como hemos visto es una matriz bidimensional de elementos fotosensibles que permiten la resolución espacial de áreas ilumi-

nadas y su uso combinado con la preparación de membranas sensoras espacialmente separadas permite la resolución multianalito.

El uso de cámaras CCD como sistemas detectores ha aumentado notablemente en los últimos tiempos, siendo las imágenes obtenidas utilizadas para diferentes propósitos. Así, se han usado CCD para técnicas de screening [52-54], en el campo de la proteómica [55,56], en el diagnóstico de enfermedades [57] o la detección simultánea de antibióticos en leche [58]. De forma general, la determinación simultánea se realiza situando las zonas de reconocimiento en distintas posiciones dentro del array [59], o utilizando la tecnología de los microchips [60], todo ello en conjunción con dispositivos de alto rendimiento. Se han empleado también en detección de proteínas sobre geles empleando técnicas no radiativas [61] y usando polímeros impresos (MIP) en técnicas enzimáticas tipo ELISA en lugar de anticuerpos [62-64].

La adquisición de imagen juega un importante papel en el campo de la alimentación [13,65], habiendo sido usada para determinar bacterias en cerveza [66]. Otras aplicaciones de las cámaras CCD se encuentra en la detección de bajos niveles de explosivos, especialmente explosivos gaseosos [67], discriminación entre diferentes fragancias [68] o para la fabricación de sensores ópticos de alta densidad [69,70].

Las cámaras CCD se han empleado para la detección simultánea de analitos en métodos separativos como electroforesis [71-74] o cromatografía [75]. Haciendo uso de una cámara CCD, es posible determinar Al(II) y Fe(II) en aleaciones, aplicando redes neuronales (ANN) [76] o incluso especiar Fe(II) y Fe(III) inmovilizando un ionóforo sobre distintos soportes como puede ser una lámina de papel o una placa de cromatografía en capa fina [77]. En una publicación se ha propuesto la determinación de la alcalinidad total del agua utilizando una cámara CCD como instrumento de medida [78] o el uso de sensores de

afinidad paralela (PASA, *parallel affinity sensor array*) en el campo medioambiental para la detección de contaminantes en el agua [79].

También se ha empleado una cámara CCD para determinar Ca^{2+}, Na^{+}, Mg^{2+}, SO_4^{2-}, Cl_2 y Hg^{2+} en agua mediante medidas de fluorescencia sobre microplacas [80].

Las continuas mejoras en cámaras digitales de fotografía ha hecho posible el desarrollo de instrumentos potentes que pueden ser utilizados para diversas aplicaciones, aparte de la propia fotografía, en aplicaciones científicas y de ingeniería. Así se ha utilizado la cámara de fotografía digital KODAC DCS640c en sistemas fotográficos aéreos para la medida de vegetación. También, debido a la manejabilidad que ofrecen las cámaras digitales, se han utilizado en cirugía, como por ejemplo la cámara digital Nikon Coopix 995 [81]. Otras aplicaciones de las cámaras de fotografia digitales se han realizado en el campo de la tecnología alimentaria [13,65]. En el campo de la Química Analítica se ha descrito la determinación de Al(II) y Fe(II) utilizando una cámara de fotografía digital Canon EOS-d30 [76].

Se ha propuesto el empleo de una cámara digital para análisis convencionales en disolución junto con un LED apropiado a la sustancia a determinar, mejor a la reacción a emplear, de manera que las señales de intensidad luminosa se procesan en escala de grises como una señal de absorbancia [82].

Por último cabe citar a Filippini y colaboradores, quienes han realizado propuestas interesantes de análisis usando cámaras web para medidas en el rango visible [83-85] e incluso medidas de fluorescencia [86].

No nos extendemos más en las aplicaciones analíticas tanto de cámaras CCD como de cámara fotográficas digitales ya que serán tratadas extensamente en la introducción de cada uno de los capítulos de que consta esta Memoria de Doctorado.

4. Bibliografía

1. M.B. Denton, H.A. Lewis, G.R. Sims, Charge-injection and charge-coupled devices in practical chemical analysis. Operation characteristics and considerations, ACS Symp.Ser. 236 (1983) 133.

2. G. C. Holst, T. S. Lomheim. CMOS/CCD Sensors and Camera Systems, PM172 ed., JCD Publishing, Winter Park, Florida USA, 2007

3. Kodak,. Technical Overview: CCD Technology, http://www.kodak.com/global/en/service/professional/tib/tib4131.jhtml, 2010.

4. Spring, Kenneth R., Fellers, Thomas J., Davidson, Michael W. Introduction to Charge-Coupled Devices (CCDs), Molecular Expressions; Florida State University; Nikon,Inc., http://www.microscopyu.com/articles/digitalimaging/ccdintro.html, FL, USA, 2010.

5. Bayer, Brice E., Color imaging array, US 3971065, 1976.

6. Dickinson, Alexander G., Eid, El-Sayed I., Inglis, David A., Active pixel sensor and imaging system having differential mode, US 5631704, 1997.

7. Gerald C.Holst, Terrence S.Lomheim, Active Pixel Sensors: Are CCD's Dinosaurs?, Proceedings of SPIE 1900 (1993) 2.

8. P. Armienti, S. Tarquini, Power law olivine crystal size distributions in lithospheric mantle xenoliths, Lithos 65 (2002) 273.

9. S. Aydemir, S. Keskin, L.R. Drees, Quantification of soil features using digital image processing (DIP) techniques, Geoderma 119 (2004) 1.

10. A.G. Attaelmanan, E. Borg, H.G. Grondahl, Signal-to-noise ratios of 6 intraoral digital sensors, Oral Surg.Oral Med.Oral Pathol.Oral Radiol.Endod. 91 (2001) 611.

11. K.W. Schulze Ralf, T.R. Rosing Stephan, B. D'Hoedt, Contrast perception in digitized panoramic radiographs compared with their film-based origin, Oral Surg.Oral Med.Oral Pathol.Oral Radiol.Endod. 94 (2002) 388.

12. D.W. Hatcher, S.J. Symons, U. Manivannan, Developments in the use of image analysis for the assessment of oriental noodle appearance and colour, J.Food Eng. 61 (2004) 109.

13. K.L. Yam, S.E. Papadakis, A simple digital imaging method for measuring and analyzing color of food surfaces, J.Food Eng. 61 (2004) 137.

14. G.van Dalen, Determination of the size distribution and percentage of broken kernels of rice using flatbed scanning and image analysis, Food Res.Intern. 37 (2004) 51.

15. U. Gonzalez-Barron, Francis Butler, A comparison of seven thresholding techniques with the k-means clustering algorithm for measurement of bread-crumb features by digital image analysis, J.Food Eng. 74 (2006) 268.

16. A.K. Davis, B.D. Farrey, S. Altizer, Variation in thermally induced melanism in monarch butterflies (Lepidoptera: Nymphalidae) from three North American populations, J.Therm.Biol. 30 (2005) 410.

17. D. Miriello, G.M. Crisci, Image analysis and flatbed scanners.A visual procedure in order to study the macro-porosity of the archaeological and historical mortars, J.Cult.Her. 7 (2006) 186.

18. M. Blazsek, O. Istvanfy, S. Roman, Use of high-performance thin-layer chromatography and flatbed scanner for the quantitative determination of metabolic byproducts of the antibiotic salinomycin, Chemicke Listy 98 (2004) 989.

19. A. Zeb, M. Murkovic, Thin-layer chromatographic analysis of carotenoids in plant and animal samples, J.Planar Chromatogr.--Mod.TLC 23 (2010) 94.

20. G.E. Morlock, Sample application and chromatogram development, Chromatogr.Sci.Ser. 95 (2006) 99.

21. S.G. Velleman, Quantifying immunoblots with a digital scanner, BioTechniques 18 (1995) 1056.

22. B. Lewis, S. Rathman, R.J. McMahon, Detection and quantification of biotinylated proteins using the Storm 840 Optical Scanner, J.Nut.Biochem. 14 (2003) 196.

23. C. Harada, H. Tajima, S. Hirohashi, T. Kondo, Toward high performance western blotting using vacuum-driven system and laser scanner; comparison between two signal detection methods based on chemiluminescent and immunofluorescent imaging, J.Electrophor. 53 (2009) 63.

24. K. E. Herold, A. Rasooly. Lab-on-a-Chip Technology (Vol. 2): Biomolecular Separation and Analysis , Caister Academic Press, Norwich, UK, 2009.

25. Y. Shi, P.C. Simpson, J.R. Scherer, D. Wexler, C. Skibola, M.T. Smith, R.A. Mathies, Radial Capillary Array Electrophoresis Microplate and Scanner for High-Performance Nucleic Acid Analysis, Anal.Chem. 71 (1999) 5354.

26. K. Abe, K. Suzuki, D. Citterio, Inkjet-printed microfluidic multianalyte chemical sensing paper, Anal.Chem. 80 (2008) 6928.

27. N.C. Birch, D.F. Stickle, Example of use of a desktop scanner for data acquisition in a colorimetric assay, Clin.Chim.Acta 333 (2003) 95.

28. J. Gabrielson, I. Kuhn, P. Colque-Navarro, M. Hart, A. Iversen, D. McKenzie, R. Mollby, Microplate-based microbial assay for risk assessment and (eco)toxic fingerprinting of chemicals, Anal.Chim.Acta 485 (2003) 121.

29. Y. Tanaka, T. Nakamoto, T. Moriizumi, Study of highly sensitive smell sensing system using gas detector tube combined with optical sensor, Sens.Actuators B B119 (2006) 84.

30. Lange, H., Rittersdorf, W., Rey, H. G., Diagnostic device, US 3,897,214, 2001.

31. G.-Q. Shi, G. Jiang, A dip and read test strip for the determination of Hg(II) in aqueous samples based on urease activity inhibition, Anal.Sci. 18 (2002) 1215.

32. S.V. Bannur, S.V. Kulgod, S.S. Metkar, S.K. Mahajan, J.K. Sainis, Protein Determination by Ponceau S Using Digital Color Image Analysis of Protein Spots on Nitrocellulose Membranes, Anal.Biochem. 267 (1999) 382.

33. A.V. Yallouz, R. Calixto de Campos, S. Paciornik, A low-cost non instrumental method for semiquantitative determination of mercury in fish, Fresenius J.Anal.Chem. 366 (2000) 461.

34. M. Kompany-Zareh, S. Mirzaei, Genetic algorithm-based method for selecting conditions in multivariate determination of povidone-iodine using hand scanner, Anal.Chim.Acta 521 (2004) 231.

35. E. Bakker, P. Bühlmann, E. Pretsch, Carrier-Based Ion-Selective Electrodes and Bulk Optodes. 1. General Characteristics, Chem Rev. 97 (1997) 3083.

36. A. Lapresta-Fernandez, L.F. Capitan-Vallvey, Scanometric potassium determination with ionophore-based disposable sensors, Sens.Actuators B 134 (2008) 694.

37. Lapresta-Fernandez, A., Ph.D. Thesis. University of Granada, 2007.

38. L. F. Capitan-Vallvey , in: Grimes, C. A.; Dickey, E. C.Pishko, M. V., Eds. (Ed.), Encyclopedia of Sensors, The Pennsylvania State University, Pennsylvania, USA, 2005, pp. 55-93 .

39. M. Lonnberg, J. Carlsson, Quantitative detection in the attomole range for immunochromatographic tests by means of a flatbed scanner, Anal.Biochem. 293 (2001) 224.

40. A. van Amerongen, D. van Loon, L.B.J.M. Berendsen, J.H. Wichers, Quantitative computer image analysis of a human chorionic gonadotropin colloidal carbon dipstick assay, Clin.Chim.Acta 229 (1994) 67.

41. M. Blazkova, P. Rauch, L. Fukal, Strip-based immunoassay for rapid detection of thiabendazole, Biosens.Bioelectron. 25 (2010) 2122.

42. T. Yuhi, N. Nagatani, T. Endo, K. Kerman, M. Takata, H. Konaka, M. Namiki, Y. Takamura, E. Tamiya, Resin-based micropipette tip for immunochromatographic assays in urine samples, J.Immunol.Methods 312 (2006) 54.

43. D. Martorell, S.T. Siebert, R.A. Durst, Liposome Dehydration on Nitrocellulose and Its Application in a Biotin Immunoassay, Anal.Biochem. 271 (1999) 177.

44. L. Chuang, J.Y. Hwang, H.C. Chang, F.M. Chang, S.B. Jong, Rapid and simple quantitative measurement of a-fetoprotein by combining immunochromatographic strip test and artificial neural network image analysis system, Clin.Chim.Acta 348 (2004) 87.

45. T.A. Taton, C.A. Mirkin, R.L. Letsinger, Scanometric DNA array detection with nanoparticle probes, Science 289 (2000) 1757.

46. Y. Sun, W.H. Fan, M.P. McCann, V. Golovlev, Microarray gene expression analysis free of reverse transcription and dye labeling, Anal.Biochem. 345 (2005) 312.

47. J. Petersen, M. Stangegaard, H. Birgens, M. Dufva, Detection of mutations in the b-globin gene by colorimetric staining of DNA microarrays visualized by a flatbed scanner, Anal.Biochem. 360 (2007) 169.

48. S. Nishizuka, N.R. Washburn, P.J. Munson, Evaluation method of ordinary flatbed scanners for quantitative density analysis, BioTechniques 40 (2006) 442,444,446,448.

49. M.C. Janzen, J.B. Ponder, D.P. Bailey, C.K. Ingison, K.S. Suslick, Colorimetric Sensor Arrays for Volatile Organic Compounds, Anal.Chem. 78 (2006) 3591.

50. C. Zhang, K.S. Suslick, A colorimetric sensor array for organics in water, J.Am.Chem.Soc. 127 (2005) 11548.

51. K.S. Suslick, N.A. Rakow, A. Sen, Colorimetric sensor arrays for molecular recognition, Tetrahedron 60 (2004) 11133.

52. R.A. Potyrailo, R.C. Conrad, A.D. Ellington, G.M. Hieftje, Adapting selected nucleic acid ligands (aptamers) to biosensors., Anal.Chem. 70 (1998) 3419.

53. D. Boecker, A. Zybin, V. Horvatic, C. Grunwald, K. Niemax, Differential Surface Plasmon Resonance Imaging for High-Throughput Bioanalyses, Anal.Chem. 79 (2007) 702.

54. Y. Matsubara, K. Kerman, M. Kobayashi, S. Yamamura, Y. Morita, E. Tamiya, Microchamber array based DNA quantification and specific sequence detection from a single copy via PCR in nanoliter volumes, Biosensors Bioelectron. 20 (2005) 1482.

55. R.Q. Liang, C.Y. Tan, K.C. Ruan, Colorimetric detection of protein microarrays based on nanogold probe coupled with silver enhancement, J.Immunol.Methods 285 (2004) 157.

56. W. Budach, D. Neuschaefer, C. Wanke, S.D. Chibout, Generation of transducers for fluorescence-based microarrays with enhanced sensitivity and their application for gene expression profiling, Anal.Chem. 75 (2003) 2571.

57. M. Schuettpelz, C. Mueller, H. Neuweiler, M. Sauer, UV Fluorescence Lifetime Imaging Microscopy: A Label-Free Method for Detection and Quantification of Protein Interactions, Anal.Chem. 78 (2006) 663.

58. B.G. Knecht, A. Strasser, R. Dietrich, E. Maertlbauer, R. Niessner, M.G. Weller, Automated Microarray System for the Simultaneous Detection of Antibiotics in Milk, Anal.Chem. 76 (2004) 646.

59. C.A. Rowe, L.M. Tender, M.J. Feldstein, J.P. Golden, S.B. Scruggs, B.D. MacCraith, J.J. Cras, F.S. Ligler, Array Biosensor for Simultaneous Identification of Bacterial, Viral, and Protein Analytes, Anal.Chem. 71 (1999) 3846.

60. P. Angenendt, J. Gloekler, Z. Konthur, H. Lehrach, D.J. Cahill, 3D protein microarrays: Performing multiplex immunoassays on a single chip, Anal.Chem. 75 (2003) 4368.

61. E. Scrivener, B.A. Boghigian, E. Golenko, A. Bogdanova, P. Jackson, A. Mikulskis, E. Denoyer, P. Courtney, M.F. Lopez, W.F. Patton, Performance validation of an improved Xenon-arc lamp-based CCD camera system for multispectral imaging in proteomics, Proteomics 5 (2005) 4354.

62. I. Surugiu, B. Danielsson, L. Ye, K. Mosbach, K. Haupt, Chemiluminescence imaging ELISA using an imprinted polymer as the recognition element instead of an antibody, Anal.Chem. 73 (2001) 487.

63. I. Surugiu, J. Svitel, L. Ye, K. Haupt, B. Danielsson, Development of a flow injection capillary chemiluminescent ELISA using an imprinted polymer instead of the antibody, Anal.Chem. 73 (2001) 4388.

64. I. Alexandre, S. Hamels, S. Dufour, J. Collet, N. Zammatteo, F. De Longueville, J.L. Gala, J. Remacle, Colorimetric silver detection of DNA microarrays, Anal.Biochem. 295 (2001) 1.

65. A. Antonelli, M. Cocchi, P. Fava, G. Foca, G.C. Franchini, D. Manzini, A. Ulrici, Automated evaluation of food colour by means of multivariate image analysis coupled to a wavelet-based classification algorithm, Anal.Chim.Acta 515 (2004) 3.

66. C. March, J.J. Manclus, A. Abad, A. Navarro, A. Montoya, Rapid detection and counting of viable beer-spoilage lactic acid bacteria using a monoclonal chemiluminescence enzyme immunoassay and a CCD camera, J.Immunol.Methods 303 (2005) 92.

67. K.J. Albert, D.R. Walt, High-Speed Fluorescence Detection of Explosives-like Vapors, Anal.Chem. 72 (2000) 1947.

68. K.J. Albert, D.R. Walt, D.S. Gill, T.C. Pearce, Optical multibead arrays for simple and complex odor discrimination, Anal.Chem. 73 (2001) 2501.

69. K.L. Michael, L.C. Taylor, S.L. Schultz, D.R. Walt, Randomly Ordered Addressable High-Density Optical Sensor Arrays, Anal.Chem. 70 (1998) 1242.

70. L.C. Taylor, D.R. Walt, Application of high-density optical microwell arrays in a live-cell biosensing system, Anal.Biochem. 278 (2000) 132.

71. E.T. Bergstroem, D.M. Goodall, B. Pokric, N.M. Allinson, A charge coupled device array detector for single-wavelength and multiwavelength ultraviolet absorbance in capillary electrophoresis, Anal.Chem. 71 (1999) 4376.

72. J.V. Sweedler, J.B. Shear, H.A. Fishman, R.N. Zare, R.H. Scheller, Fluorescence detection in capillary zone electrophoresis using a charge-coupled device with time-delayed integration, Anal.Chem. 63 (1991) 496.

73. A.T. Timperman, K.E. Oldenburg, J.V. Sweedler, Native fluorescence detection and spectral differentiation of peptides containing tryptophan and tyrosine in capillary electrophoresis, Anal.Chem. 67 (1995) 3421.

74. Q. Gao, E.S. Yeung, High-Throughput Detection of Unknown Mutations by Using Multiplexed Capillary Electrophoresis with Poly(vinylpyrrolidone) Solution, Anal.Chem. 72 (2000) 2499.

75. M. Lancaster, D.M. Goodall, E.T. Bergstroem, S. McCrossen, P. Myers, Real-Time Image Acquisition for Absorbance Detection and

Quantification in Thin-Layer Chromatography, Anal.Chem. 78 (2006) 905.

76. N. Maleki, A. Safavi, F. Sedaghatpour, Single-step calibration, prediction and real samples data acquisition for artificial neural network using a CCD camera, Talanta 64 (2004) 830.

77. A. Abbaspour, M.A. Mehrgardi, A. Noori, M.A. Kamyabi, A. Khalafi-Nezhad, M.N. Soltani Rad, Speciation of iron(II), iron(III) and full-range pH monitoring using paptode: A simple colorimetric method as an appropriate alternative for optodes, Sens.Actuators B 113 (2006) 857.

78. E.d.N. Gaiao, V.L. Martins, W.d.S. Lyra, L. Farias de Almeida, E. Cirino da Silva, M.C.U. Araujo, Digital image-based titrations, Anal.Chim.Acta 570 (2006) 283.

79. M.G. Weller, A.J. Schuetz, M. Winklmair, R. Niessner, Highly parallel affinity sensor for the detection of environmental contaminants in water, Anal.Chim.Acta 393 (1999) 29.

80. T. Mayr, G. Liebsch, I. Klimant, O.S. Wolfbeis, Multi-ion imaging using fluorescent sensors in a microtiterplate array format, Analyst 127 (2002) 201.

81. W.B. Schroder, Practical digital photography for surgeons, Curr Surg 59 (2002) 581.

82. R.A. Minamisawa, L.E.R. Santos, M.A. Parada, K.R.P. Daghastanli, P. Ciancaglini, A. De Almeida, Digital Image Analysis to Standardize a Photometric Method in Colorimetric Quantification, Instrumentation Science & Technology 36 (2008) 97.

83. D. Filippini, G. Comina, I. Lundstroem, Computer screen photo-assisted reflectance fingerprinting, Sens.Actuators B 107 (2005) 580.

84. D. Filippini, K. Tejle, I. Lundstroem, ELISA test for anti-neutrophil cytoplasm antibodies detection evaluated by a computer screen photo-assisted technique, Biosensors Bioelectron. 21 (2005) 266.

85. D. Filippini, P. Asberg, P. Nilsson, O. Inganas, I. Lundstroem, Computer screen photo-assisted detection of complementary DNA strands using a luminescent zwitterionic polythiophene derivative, Sens.Actuators B 113 (2006) 410.

86. J.W.P. Bakker, D. Filippini, I. Lundstroem, Enhancing classification capabilities of computer screen photo-assisted fluorescence fingerprinting, Sens.Actuators B 110 (2005) 190.

Capítulo 2

Sensor de un solo uso para potasio basado en medidas de transflectancia

1. Planteamiento

Los sensores ópticos de un solo uso son dispositivos analíticos autocontenidos en el sentido de que son formulaciones analíticas que incluyen todos los reactivos necesarios en estado sólido y que puestos en contacto con el problema, inician una serie de reacciones y/o procesos que conducen a la determinación del analito presente a través de su reconocimiento y modificación de una propiedad, óptica en este caso, que permitirá su cuantificación [1,2].

Los ensayos en fase sólida se pueden clasificar como antes se ha dicho, en dos grupos: sistemas verticales y sistemas horizontales, atendiendo a como se relaciona el problema conteniendo el analito con el sensor de un solo uso [1]. En los sistemas verticales el fluido atraviesa perpendicularmente la capa o capas que constituyen la zona reactiva, teniendo lugar un conjunto de reacciones y procesos que permitirán desarrollar una propiedad analítica [3,4]. En los sistemas horizontales la muestra se deposita sobre una zona de recepción y se mueve por flujo fluido a través del sensor produciéndose, como consecuencia de esa migración, separaciones cromatográficas, reacciones y/o retenciones de analito o interferentes, que originaran la propiedad analítica [5-7]. En esta Memoria de Doctorado sólo trataremos de ensayos de tipo vertical, por lo que a ellos nos atendremos en lo que sucesivo.

Para lograr el reconocimiento del analito mediante sensores de un solo uso de tipo óptico o visual, se han utilizado diferentes esquemas dependiendo del tipo de analito y de la muestra en la que se encuentre. De una manera general, un ligando –portador de iones, ionóforo, indicador o agente complejante- o

un reactivo o reactivos se enlazan químicamente o bien se entrapan físicamente cerca de la interfase o bien en el seno de la capa sensora o bien se inmovilizan directamente en la superficie de la zona sensora. La señal óptica se genera mediante la interacción del reactivo, que cambia sus propiedades ópticas por reacción con el analito, bien solo o con la ayuda de compuestos adicionales-cromoionóforos, fluoroionóforos, colorantes indicadores, reactivos auxiliares-.

En concreto nos vamos a centrar en sensores para la determinación de cationes, basados en una química ionóforo-cromoionóforo. Estos sensores se basan en los cambios de concentración en el seno de una fase completa –bulk membranes- que contiene todos los componentes necesarios, disueltos en una membrana polimérica plastificada para la extracción y reconocimiento del analito y para la transducción de la energía libre del proceso en una señal de tipo óptico.

Los sensores basados en películas hidrófobas no pueden responder a un solo ión, debido a que se debe cumplir el principio de electroneutralidad en el seno de la membrana y, en consecuencia, no puede haber una transferencia neta de carga hacia la misma. Por ello, se utiliza un equilibrio de transferencia de fase que involucre dos iones diferentes, -uno de ellos el analito y el otro un ión de referencia- de manera que permita la transferencia de iones en ambos sentidos y se mantenga en todo momento la electroneutralidad en la membrana. Generalmente, la reacción de complejación de uno de los dos iones –el analito- con el ionóforo es el que conduce o desencadena la respuesta de tipo óptico debida al segundo ión o ión de referencia [8-10]. Esto significa que la respuesta del sensor se ha descompuesto en dos procesos diferentes: el de reconocimiento del analito por parte del ionóforo y el de transducción de la energía libre del proceso anterior mediante el reconocimiento del ión de referencia, a través de un ionóforo específico denominado cromoionóforo.

Concretamente, en este estudio emplearemos un sensor para potasio desarrollado previamente por nuestro grupo de investigación [11] y basado en una membrana de PVC plastificada con o-nitrofeniloctiléter conteniendo el éter dibenzo18-corona-6 como ionóforo, (1,2-benzo-7-(dietilamino)-3-(octadecanoilimino) fenoxazina (azul Nilo lipofilizado) como cromoionóforo y tetrakis (4-clorofenil)borato potásico como sal lipofílica.

Cuanto más analito -potasio- entre en la membrana, más cromoionóforo se desprotonará y mayor será el cambio de color de la membrana desde el color de la forma ácida del cromoionóforo, azul para el azul Nilo lipofilizado, al color magenta de la forma básica.

El cociente de actividades de los iones de referencia y analito a_{H^+}/a_{K^+} en medio acuoso se relaciona a través de una constante de equilibrio con el parámetro experimental que es una señal óptica relativa y que se puede calcular a partir de medidas de absorbancia [9], fluorescencia [12], reflectancia [13], índice de refracción [14], o coordenadas cromáticas RGB [15], originando una función respuesta de tipo sigmoidal.

La mayor parte de las medidas ópticas usadas en sensores de tipo ionóforo-cromoionóforo se basan en la transmisión de radiación en membranas transparentes [16,17] aunque también se han usado medidas basadas en reflexión, como es el caso de las tiras reactivas usadas en análisis clínicos para iones alcalinos y alcalinotérreos en suero sanguíneo que suelen ser opacas y de tipo multicapa para permitir su determinación directamente en sangre, implementando toda una serie de procesos de separación [13,18].

En este capítulo se trata de utilizar la transflexión de radiación para construir el parámetro analítico y poder cuantificar la concentración de potasio a partir de un sensor de un solo uso.

Aparte de la reflexión especular que ofrece poca información sobre la muestra, los dos métodos reflectométricos más usados para muestras sólidas o líquidas con partículas en suspensión son la reflexión difusa y la transflexión.

La reflexión difusa ocurre cuando la radiación penetra en el seno de la muestra ocurriendo múltiples reflexiones, refracciones y difracciones antes de que una fracción de la radiación regrese a la superficie y alcance el detector. La gran cantidad de interacciones radiación-muestra que tienen lugar hace que la radiación difusa reflejada contenga información sobre la muestra a una profundidad que depende de la longitud de onda de la radiación y de la absortividad de la muestra.

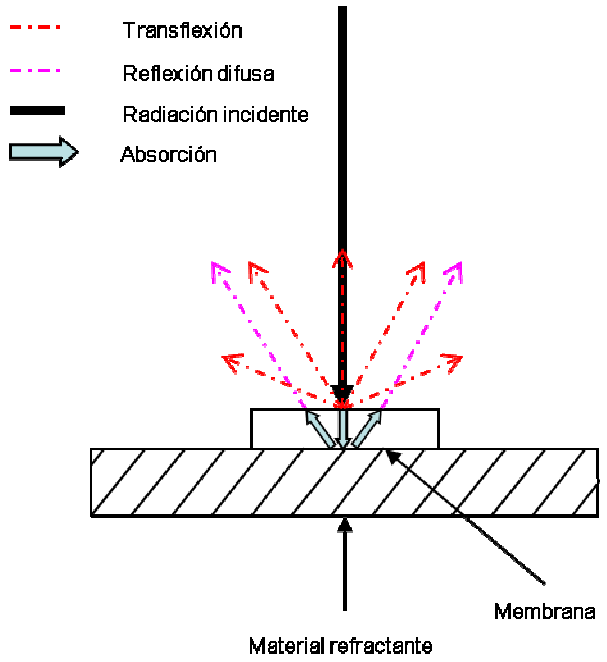

Figura 1. Medida de transflectancia.

La transflexión participa de la transmisión y de la reflexión especular. Cuando una radiación incide sobre una superficie reflectante sobre la que está

dispuesta la muestra trasparente, bien sólida o líquida (Figura 1), ocurren dos procesos: reflexión en la superficie de la muestra y transmisión de radiación seguida de reflexión en la superficie especular, seguida de una segunda transmisión. Como para la mayoría de los materiales la reflexión en la superficie es menor que la reflexión en el espejo, la radiación total recogida corresponde a la medida de transmisión con el camino óptico duplicado [19]. Este principio permite la construcción de sondas compactas y muy versátiles.

La transflexión es un fenómeno híbrido entre la absorción y la reflectancia difusa (Figura 1). Consiste en que una radiación incide sobre el sensor que se encuentra dispuesto sobre un material reflectante. Parte de dicha radiación se refleja de forma difusa y llega al detector, pero otra parte pasa a través de la membrana, llegando así al material reflectante y emergiendo de nuevo a través de la membrana hacia el detector. Al pasar la radiación a través de la membrana, se va a dar un proceso de absorción de radiación por parte de la membrana, de manera que la radiación emergente no va a ser igual que la radiación reflejada de forma difusa ya que se está produciendo un proceso de absorción por parte de la membrana.

Un segundo objetivo de este estudio es la obtención de una carta de color para poder utilizar el sensor de potasio antes comentado como sensor visual y así obtener información de tipo semicuantitativa. Un sensor de un solo uso de tipo visual se basa en la comparación del color del sensor con una carta de colores normalizada que contiene un número discreto de bloques de color correspondientes a diferentes concentraciones de analito. El ajuste del color del sensor, una vez reaccionado con la muestra, con un bloque de color dado o la interpolación entre dos bloques consecutivos, permite estimar la concentración. Estos sensores visuales basados en el emparejamiento de colores deben utilizar reglas simples y bien definidas para obtener resultados confiables que pueden ser cualitativos, concentración por encima del valor de corte, o bien semicuantitativos si

se encuentra dentro de algunos de los grupos previamente establecidos en la carta de color [1].

Aquí se tratará de establecer a partir de los espectros de transflectancia del sensor, los posibles grupos de color que el ojo es capaz de discriminar y en consecuencia se tratará de construir una posible carta de color que luego se comparará con los resultados obtenidos a partir de un panel de observadores.

Para ello hay que calcular las coordenadas de color en el espacio de color CIELAB, espacio de color independiente del dispositivo y desarrollado por la Commission Internationale d'Eclairage (Comisión Internacional de Iluminación), razón por la cual se abrevia como CIE. Los tres parámetros en el modelo representan la luminosidad de color (L*, L*=0 indica negro y L*=100 indica blanco), su posición entre magenta y verde (a*, valores negativos indican verde mientras valores positivos indican magenta) y su posición entre amarillo y azul (b*, valores negativos indican azul y valores positivos indican amarillo).

Aquí se va a usar una fórmula basada en CIELAB y denominada CIEDE20002 [20,21] que incorpora correcciones a las simples diferencias en claridad (ΔL^*), croma (ΔC^*) y tono (ΔH^*), calculadas de acuerdo con CIELAB [22], debido a la no uniformidad de este espacio CIELAB. A partir de esas coordenadas se calcula el coeficiente ΔE_{00}, el cual, cuando al comparar dos colores presenta un valor mayor de 0.75, indica que el ojo humano es capaz de diferenciar dichos colores.

Available online at www.sciencedirect.com
ScienceDirect
Sensors and Actuators B 127 (2007) 586–592
SENSORS AND ACTUATORS B CHEMICAL
www.elsevier.com/locate/snb

Potassium disposable optical sensor based on transflectance and cromaticity measurements

I. de Orbe-Payá, M.M. Erenas, L.F. Capitán-Vallvey*

Solid Phase Spectrometry Research Group, Department of Analytical Chemistry, Faculty of Sciences, Campus Fuentenueva, University of Granada, E-18071 Granada, Spain

Received 20 February 2007; received in revised form 3 May 2007; accepted 13 May 2007
Available online 21 May 2007

Abstract

This paper presents the study of a disposable optical sensor to determine potassium by an ion-exchange mechanism based on the conventional ionophore dibenzo-18-crown-6. The normalised signal used as analytical parameter is obtained from measurements in transflectance mode and the results are compared with those obtained by transmission mode. The sensor responds linearly in activities up to 100 mM with a detection limit of 19 mM and a precision around 7%. It is possible to linearise the sigmoidal calibration curve by means of a decimal logistic transformation applied to transflectance data, in this way increasing the linear dynamic range with a detection limit of 8.4 mM. The potential utility of the disposable sensor was checked in the determination of potassium in different types of waters, validating the results against a reference procedure. The viability of the semi-quantitative determination of potassium using this disposable sensor was studied using a colour-difference CIELAB-base formula, designed to give quantitative values of the perceived colour difference between a pair of coloured samples under specific experimental conditions, obtaining seven intervals of discriminable concentrations in the colour chart between 10^{-7} and 10^{-1} M.

Keywords: Potassium determination; Optical disposable sensor; Transflectance mode; Ionophore–chromoionophore chemistry; Water analysis

1. Introduction

Disposable sensors, also known as one-shot sensors, are analytical devices that use an insoluble solid phase containing reagents immobilised by chemical or physical procedures on a support. The contact of the problem solution, by immersion, passing it through or deposit, with the analytical element and subsequent measurement or observation of a property conducted over this same solid support makes it possible to determine the concentration.

Different properties have been used in optical disposable sensors for measurement, including radiation absorption by transmission [1,2] as well as other techniques which rely on luminescence, both fluorescence [3] and phosphorescence [4] and chemiluminescence [5,6]. The measurement of fluorescence excited within the evanescent field has been proposed in connection with a one-shot sensor chip [7]. One suggested alternative is using the chromaticity characteristics of the one-shot sensor for the analytical parameters; these would be colour lightness, chromaticity or other coordinates as well as the combination of such parameters [8] and the digital colour analysis technique [9,10].

However, the most widely used property with quantitative disposable sensors is reflectance spectrometry [11]. Given the structure of different types of optical disposable sensors, these are usually opaque, which is why the usual measurement method is by diffuse reflectance spectroscopy, with measurements at one or two wavelengths [12]. This technique involves measuring the intensity that may result from the interaction of radiation with the reaction volume of the carrier when irradiation with electromagnetic radiation due to absorption, transmission and scattering by materials occurs.

Different approaches have been used depending on the type of disposable sensor [13]. In the case of monolayer systems, both homogeneous and heterogeneous, the homogenous are the simplest and they achieve a homogenous distribution of chemicals through the impregnation of an adsorbent (fibre-impregnated systems), deposit of a solution of reagents on a non-absorbent

* Corresponding author.
E-mail address: lcapitan@ugr.es (L.F. Capitán-Vallvey).

0925-4005/$ – see front matter © 2007 Elsevier B.V. All rights reserved.
doi:10.1016/j.snb.2007.05.016

Potassium disposable optical sensor based on transflectance measurements

I. de Orbe-Payá, M.M. Erenas and L.F. Capitán-Vallvey*

Solid Phase Spectrometry Research Group,
Department of Analytical Chemistry,
Faculty of Science, Campus Fuentenueva, University of Granada.
E-18071 Granada. Spain.

Abstract

This paper presents the study of a disposable optical sensor to determine potassium by an ion-exchange mechanism based on the conventional ionophore dibenzo-18-crown-6. The normalised signal used as analytical parameter is obtained from measurements in transflectance mode and the results are compared with those obtained by transmission mode. The sensor responds linearly in activities up to 100 mM with a detection limit of 19 mM and a precision around 7%. It is possible to linearise the sigmoidal calibration curve by means of a decimal logistic transformation applied to transflectance data, in this way increasing the linear dynamic range with a detection limit of 8.4 mM. The potential utility of the disposable sensor was checked in the determination of potassium in different types of waters, validating the results against a reference procedure. The viability of the semi-quantitative determination of potassium using this disposable sensor was studied using a colour-difference CIELAB-base for-

mula, designed to give quantitative values of the perceived colour difference between a pair of coloured samples under specific experimental conditions, obtaining 7 intervals of discriminable concentrations in the colour chart between 10^{-7} and 10^{-1} M.

Keywords. Potassium determination; optical disposable sensor; transflectance mode; ionophore-chromoionophore chemistry; water analysis.

* Corresponding author. E-mail: lcapitan@ugr.es

2. Introduction

Disposable sensors, also known as one-shot sensors, are analytical devices that use an insoluble solid phase containing reagents immobilised by chemical or physical procedures on a support. The contact of the problem solution, by immersion, passing it through or deposit, with the analytical element and subsequent measurement or observation of a property conducted over this same solid support makes it possible to determine the concentration.

Different properties have been used in optical disposable sensors for measurement, including radiation absorption by transmission [1,23] as well as other techniques which rely on luminescence, both fluorescence [24] and phosphorescence [25] and chemiluminescence [26,27]. The measurement of fluorescence excited within the evanescent field has been proposed in connection with a one-shot sensor chip [28]. One suggested alternative is using the chromaticity characteristics of the one-shot sensor for the analytical parameters; these would be colour lightness, chromaticity or other coordinates as well as the combination of such parameters [29] and the digital colour analysis technique [16,30].

However, the most widely used property with quantitative disposable sensors is reflectance spectrometry [31]. Given the structure of different types of optical disposable sensors, these are usually opaque, which is why the usual measurement method is by diffuse reflectance spectroscopy, with measurements at one or two wavelengths [32]. This technique involves measuring the intensity that may result from the interaction of radiation with the reaction volume of the carrier when irradiation with electromagnetic radiation due to absorption, transmission and scattering by materials occurs.

Different approaches have been used depending on the type of disposable sensor [33]. In the case of monolayer systems, both homogeneous and heterogeneous, the homogenous are the simplest and they achieve a homogenous distribution of chemicals through the impregnation of an adsorbent (fibre-

impregnated systems), deposit of a solution of reagents on a non-absorbent support or by fabrication of a film using a film-forming material along with the reagents on a plastic support. In the last case, the phenomenological theory of Kubelka-Munk [34] is applied and simplified to an equation analogous to Beer's law and they are similarly used in analytical applications.

Another type of disposable sensor uses multilayer systems that attempt to segregate the individual functions of the analytical element into discrete layers of different natures through which the sample runs vertically, producing a sequential series of analytical operations, along with chemical reactions [35]. Different types of layers can be structured in different ways for each possible case, with the most common being: reflecting layer, spreading layer or metering layer and reagent layer. In this case the mathematical treatment of the radiation measured is more complicated and it is necessary to consider diffuse reflectance, transmittance, and specular reflectance of hemispherically distributed incident radiation. The mathematical model of Williams and Clapper [36] is used for multilayer systems [33].

We have studied the use of transparent membranes containing the necessary reagent in disposable sensors for the optical determination of different analytes measuring the optical property (absorption, luminescence) in transmission mode [37-40]. In this paper we investigate the use of these disposable sensors in reflectance mode. Here the membrane containing the sensing area is measured on a white nontransparent reflective material. When the radiation reaches the transparent membrane, it is transmitted through it and then it is reflected from the reflective material and transmitted back through the sample before finally arriving at the detector. A sum of effects due to multiple absorption and reflection occurs and the term transflectance, as a hybrid of transmittance and reflectance, rather than reflectance, is used to describe the measurement mode.

Transflectance measurements are used in near-infrared (NIR) spectroscopy especially in food and pharmaceutical analysis for use with non-transparent liquids [41] and has also been used in flow-through sensors for organic compounds, such as amines [42] or alcohols [43].

In this paper, we study a disposable sensor to determine potassium in beverages and waters that works based on ionophore-chromoionophore chemistry and measures by transflectance. The results compared favourably with those obtained by transmission mode.

3. Experimental

3.1 Reagents and materials

The chemicals used were of analytical-reagent grade and all aqueous solutions were prepared using reverse-osmosis type quality water produced by a Milli-RO 12 plus Milli-Q purification system (Millipore, Bedford, MA).

Potassium chloride stock solution (1,000 $mg \cdot L^{-1}$) was prepared in water by exactly weighing analytical reagent grade dry potassium chloride (Aldrich, Steinheim, Germany). Solutions of lower concentration were prepared by dilution with water. Stock solutions of 1,000 $mg \cdot L^{-1}$ of the following ions were also used: Mg (II), Ca (II), Na (I) and Li (I) as chloride all supplied by Merck (Darmstadt, Germany). pH 9.0 Tris(hydroxymethyl) aminomethane 1.0 M buffer solution supplied by Sigma (Sigma-Aldrich Química S.A., Madrid, Spain).

For preparing the optode films poly(vinylchloride) (PVC; high molecular weight), dibenzo18-crown-6-ether, o-nitrophenyloctylether (NPOE), and tetrahydrofuran (THF) were purchased from Sigma and potassium tetrakis (4-chlorophenyl)borate (TCPB) was purchased from Fluka (Fluka, Madrid, Spain). The chromoionophore (1,2-benzo-7-(diethylamino)-3-(octadecanoylimino) phenoxazine was synthesised, purified and identified by us according to Morf *et*

al.[44]. Sheets of Mylar-type polyester (Goodfellow, Cambridge, UK) were used as support.

3.2 Apparatus and Software

To perform the absorbance measurements of the membranes, a Hewlett Packard diode array spectrophotometer (model 8453; Nortwalk, CT, US) equipped with a 44 mm high, 12 mm wide homemade membrane cell holder made of a matte black painted iron block and containing a 1 mm thick space for the introduction of the disposable sensor was used. The diameter of the central hole of the cell holder was 5 mm and it was situated 11.5 mm from the base [45]. The transflectance measurements of the disposable membranes were obtained using an Ocean Optics USB2000 UV-Vis spectrophotometer connected by optical fibre to an ISP-R integrating sphere with fibre ports at 90º to the spectrometer and 8º to the light source (LS-1 tungsten halogen light source). To perform the transflectance measurement we used a holder (Figure 2 and Figure 3) composed of two plates of black methacrylate with a white reflecting material between them and a hole in the top black plate the diameter of the integrating sphere to fit it. Additionally, the white reflecting material has a superficial notch with the same dimensions as the disposable sensors to laterally insert the sensor and present its sensing area to the sample port of the integrating sphere placed directly over it. As diffuse reflectance standard we used WS-1 (PTFE) from Ocean Optics.

The acquisition and manipulation of the spectral data were carried out using the Chemstation software package supplied by HP for absorbance measurements and OOIIRRAD-C software for transflectance and colour measurements. Later statistical calculations were performed with the Statgraphics software package (Manugistics Inc. and Statistical Graphics Corporation, USA, 1992), ver. 6.0 STSC Inc. Statistical Graphics Corporations, USA, 1993,

Graphmatica for Win 32 ver. 1:60d, 1998 edited by K. Hertzer and adapted by J. Garrido and Mathematica ver. 5.0, 1988-2003 (Wolfram Research).

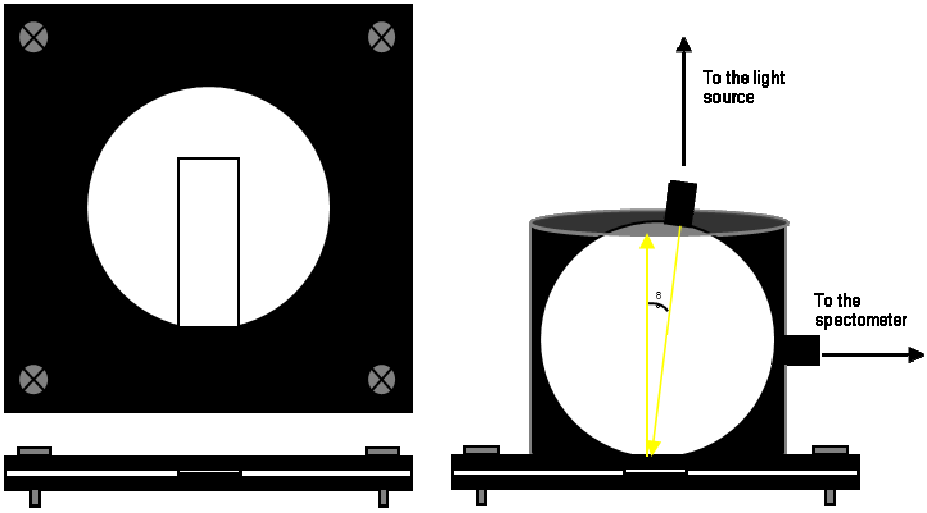

Figure 2. Integrating sphere and homemade holder

3.3 Preparation of disposable membranes

The membranes were produced on a polyester substrate using a spin-coating technique[46]. Mixtures for the potassium-sensitive membranes were made from a batch of 26.0 mg (28.0 wt %) of PVC, 63.0 mg (68.5 wt %) of NPOE, 0.8 mg (0.87 wt %) of DB18C6, 1.3 mg (1.4 wt %) of (1,2-benzo-7-(diethylamino)-3-(octadecanoylimino) phenoxazine and 1.1 mg (1.2 wt %) of TCPB. All components were dissolved in 1 mL of freshly distilled THF. The disposable sensors were cast by placing 20 µL of the cocktail on a 14 mm x 4 cm x 0.5 mm thick polyester sheet by means of a laboratory-made spin-on device and stored in a vacuum dryer at room temperature to enable slow solvent

evaporation. The prepared red sensing area was 6 mm in diameter and around 5 μm in thickness.

Figure 3. Modular transflectance instrument.

3.4 Measurements

The response of the potassium sensitive disposable sensors was evaluated by adding an aliquot of test solution containing between $1 \cdot 10^{-7}$ and $1 \cdot 10^{-1}$ M ($8.7 \cdot 10^{-8}$ and $7.6 \cdot 10^{-2}$ M in activities) of potassium in a 25 mL flask along with 0.5 mL pH 9.0 Tris 1.0 M buffer solution and levelling off with water. 10 mL of the above solution was placed in a 10x1.5 cm polyethylene plastic tube and a disposable sensor was introduced for 5 min into the tube without shaking. Once equilibrium was reached, the membrane was pulled out of the solution and the water droplets were gently removed from its surface. Each membrane was pre-

viously conditioned with 10^{-2} M HCl, and $2x10^{-2}$ M Tris buffer, and after equilibration with potassium containing the problem or standard, with 10^{-2} M NaOH solution. After the different conditioning processes, each membrane was scanned in transflectance mode and absorbance mode consecutively, recording their spectra between 400 and 800 nm in both cases. In the case of transflectance, the working wavelength used was 482 nm and 660 nm in the case of absorbance.

With application to real samples, i.e. water samples and beverages, 10 mL of each sample was introduced in a polyethylene tube together with 1 mL of pH 9.0, 0.2 M Tris buffer solution operating as described above.

Additionally, the colour coordinates X, Y, and Z of each membrane after reaction with the potassium standards, the units used in the Tristimulus colour space, were obtained with the same set-up used for transflectance measurements and the software mentioned above. In this case, the selected illuminant was D65 and the observer CIE 1931

3.5 Calculations

The extension of the recognition process is measured by the degree of protonation 1-α of the chromoionophore. As the chromoionophore cannot be fully protonated (1-α ≅ 0.9) at the working pH (9.0), we use an effective α value, α_{eff} [11]. This α_{eff} value is evaluated by the optical property measured, which in the case of absorbance is:

$$1-\alpha_{eff}=\frac{A_x-A_C}{A_{HC^+}-A_C} \quad (1)$$

in which A_{HC^+} is the absorbance of the membrane in 2x10^{-2} M Tris buffer, the absorbance in 10^{-2} M NaOH and A_x the absorbance in potassium containing problem or standard.

In the case of transflectance measurements, the experimental parameter R (eq. 2) is defined as the ratio of the intensity of light read by the detector from a sample to intensity of light from a reflection standard, although in terms of reflection density we use D_R, which is analogous to the absorbance in transmission mode [33,35] (eq. 3).

$$R = \frac{I_x}{I_{std}} \tag{2}$$

$$D_R = \log \frac{I_{std}}{I_X} = \log \frac{1}{R} \tag{3}$$

Consequently, the normalised parameter 1-α_{eff} (eq. 4) is obtained using the reflection density corresponding to the membrane in 2x10^{-2} M Tris buffer ($D_{R_{HC^+}}$), in 10^{-2} M NaOH (D_{R_C}) and in potassium containing problem or standard (D_{R_x}).

$$1 - \alpha_{eff} = \frac{D_{R_x} - D_{R_C}}{D_{R_{HC^+}} - D_{R_C}} \tag{4}$$

The K_{exch} value to obtain an optimal fit of the experimental data was calculated according to [47]. In all cases the activities were calculated according to the two-parameter Debye-Hückel formalism [48]. All measurements were carried out at room temperature.

4. Results and Discussion

The sensing zone of the disposable sensor in contact with an aqueous solution containing potassium ions holds an ion-exchange equilibrium [11], in which barred species are in membrane phase (eq. 5), assuming the formation of a 1:1 potassium complex:

$$\overline{L} + \overline{HC^+} + \overline{R^-} + K^+ \leftrightarrow \overline{C^-} + \overline{KL^+} + \overline{R^-} + H^+ \tag{5}$$

The ion activities ratio a_{H^+}/a_{K^+} in aqueous phase is related to the equilibrium constant K_{exch} and the experimental parameter α_{eff} through the response function [9,11] (eq. 6):

$$a_{I^{\nu+}} = \frac{1}{K_{exch}}\left(\frac{a_{H^+}\alpha_{eff}}{1-\alpha_{eff}}\right)^{\nu} \frac{C_R - (1-\alpha_{eff})C_C}{\nu\left(C_L - \frac{p}{\nu}\left(C_R - (1-\alpha_{eff})C_C\right)\right)^{p}} \tag{6}$$

where C_L, C_C and C_R are the analytical concentrations of ionophore, chromoionophore and lipophilic anion, respectively, and p is the stoichiometric factor for the complex formed and ν is the analyte charge. The extension of the ion-exchange process can be measured by the degree of protonation 1-α_{eff} of chromoionophore ($[HC^+]/C_C$), the only measurable species in membrane phase.

The absorption spectra of the disposable sensor show two sets of bands in equilibrium corresponding to the protonated neutral form (610 and 660 nm) and the deprotonated (540 nm) with an isosbestic point (565 nm). The increase in potassium concentration decreases the 660 nm band and increases at 540 nm. Contrarily, the transflectance spectrum that is deprotonated in form show a minimum (660 nm) and a maximum (640 mm) and a maximum for the protonated (482 nm), with an isosbestic point at the same wavelength as in absorption (565 nm). As a working wavelength we used 660 nm in absorbance mode and 482 nm in transflectance mode because they generate the highest signal varia-

tion, namely a decrease in signal with potassium concentration both in absorption and transflectance modes.

The composition of the membrane used here was the same as with the previously described sensor for potassium [11]. The values of the selectivity coefficients (SSM method), as $\log K_{K,j}^{opt}$ obtained using membranes with the composition indicated above are -4.27 Li(I); -1.99 Na(I), -3.13 Ca(II), and -2.99 Mg(II) and are of the same magnitude order as the values previously described for the same sensor working in absorbance mode [11]. This membrane exhibits sufficient potassium selectivity against the usual concomitant ions in natural waters to make determination possible.

The response of the disposable sensor to potassium activities between 8.7×10^{-8} and 7.6×10^{-2} M (10^{-7} and 10^{-1} M in concentrations) at pH 9.0 is shown in Figure 4 along with the theoretical response function using eq. 6 for the stoichiometric ratio of ionophore/potassium, p = 1. Figure 4 also shows that the results obtained in absorption mode are very similar to those obtained in transflectance mode. Thus the summation of residual squares between the experimental points and theoretical curve (p = 1) are 0.999 (as r^2) for α values obtained in absorbance mode and 0.997 for values obtained from transflectance mode. Additionally, the fit by least-squares of the experimental points in the linear maximum slope zone (11 different concentration levels and 3 replicates of each one) of the response function to potassium to the mathematical model indicated by eq. 6 gives us for log K_{exch} the value 2.46×10^{-6} using data from absorption and 2.29×10^{-6} using transflectance data. The data obtained suggest that the model and the analytical parameter α used here and obtained from transflectance measurements are viable for the description of this transflectance disposable sensor.

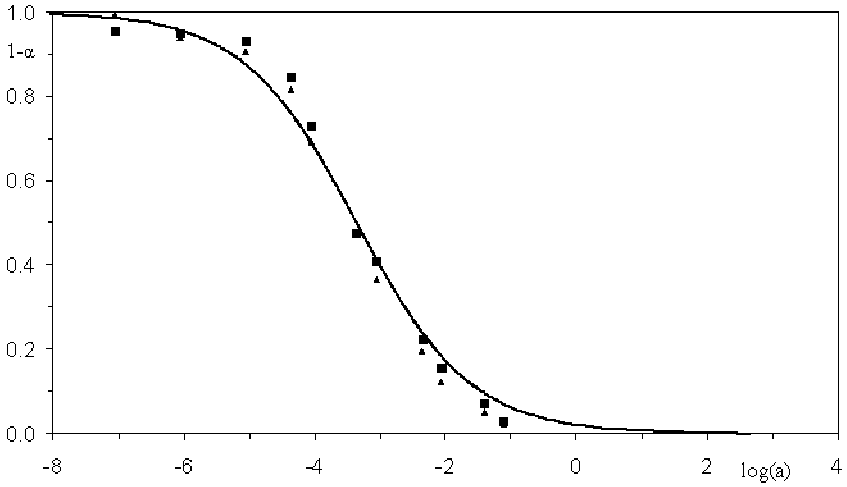

Figure 4. Calibration functions. ■ From transmission data; ▲ From transflectance data

4.1. Analytical Characterisation of Transflectance Sensor

The measuring range of the sensors based on bulk optode membranes, which exhibits a sigmoidal shape response function, can be obtained in two main ways: i] assimilating the central part of the sigmoidal response curve to a straight line; this option is the most commonly employed one and has been defined in various forms [47]; and ii] linearising the whole sigmoidal curve by means of a mathematical transformation [49]. Here we test the two options. In the case of the linear relationship in the middle of the sigmoidal response function, the measuring range is defined by means of a lack-of-fit test and the detection limit is obtained from the intersection of the linear calibration function and a linear function adjusted in the minimal slope zone at low analyte concentration.

The linearisation of the sigmoidal response function is obtained through a decimal logistic-type transformation of the sigmoidal response curve [49]. In brief, as the analytical concentrations of ionophore, chromoionophore and lipo-

philic salt are the same in this sensing membrane, $C_L = C_C = C_R = C$, and, additionally, $\nu = 1$ and $p = 1$ [11], we can reduce eq. 6 to:

$$a_{K^+} = \frac{a_{H^+}}{K_{exch}^{K^+}} \left(\frac{\alpha_{eff}}{1-\alpha_{eff}} \right)^2 \tag{7}$$

Taking decimal logarithms results in the linearised equation:

$$\log\left(\frac{\alpha_{eff}}{1-\alpha_{eff}} \right) = \frac{1}{2} \log \frac{K_{exch}^{K^+}}{a_{H^+}} + \frac{1}{2} \log a_{K^+} \tag{8}$$

In this case the detection limit is defined as the cation concentration which yields a value significantly different from zero. It is possible to establish a minimum value for a such that it fulfils the condition $a \geq 3 \cdot s_0$, where s_0 is the standard deviation of experimental α values when the analyte concentration is near zero and DL is the corresponding analyte concentration calculated from the calibration curve.

To determine the range and detection limit of the method based on the described disposable sensor, we prepared 11 potassium standards with activities ranging between 8.7×10^{-8} and 7.6×10^{-2} (1×10^{-7} and 10^{-1} M in concentrations). Three different sensing membranes were tested consecutively against the standard solutions measuring each equilibrated membrane in transflectance mode and absorbance mode consecutively.

To obtain the calibration function using the straight line of the central part of the sigmoidal response curve, we apply a lack-of-fit test and the linear functions obtained were: $1 - \alpha_{eff} = -0.489 - 0.300 \log a_{K^+}$ ($r^2 = 0.990$) in transflectance and $1 - \alpha_{eff} = -0.519 - 0.300 \log a_{K^+}$ ($r^2 = 0.997$) in absorbance, respectively.

The interception of these functions with those linear functions adjusted in the zone at low analyte concentrations $(1-\alpha_{eff}) = 0.871 - 0.012 \log a_{K^+}$ in transflectance and $(1-\alpha_{eff}) = 0.680 - 0.044 \log a_{K^+}$ in absorbance give us the detection limits: 1.90×10^{-5} M and 2.00×10^{-5} M in transflectance and absorbance, respectively, expressed as activities (2.18×10^{-5} M and 2.28×10^{-5} M in concentrations). As upper limit of linear range we use the maximum concentration tested, which in all cases was 0.1 M (0.08 M in activity).

Using the same disposable sensor, the precision, expressed as relative standard deviation (RSD), was obtained at three activity levels of K^+, namely $4.3 \cdot 10^{-5}$, $4.3 \cdot 10^{-4}$ and $4.3 \cdot 10^{-3}$ M ($5 \cdot 10^{-5}$, $5 \cdot 10^{-4}$ and $5 \cdot 10^{-3}$ M in concentrations) and ten replicates of each, with values of 3.2, 7.5 and 18.6% for $\log a_{K^+}$ from transflectance measurements and 4.9, 8.0 and 15.1 from absorbance measurements. The RSD values found using the same disposable sensor were higher than usual, which suggests that the behaviour is not completely reversible, an assumption corroborated by the decreasing trend observed in $1-\alpha_{eff}$ vs the number of replicate plots, especially from 5-6 times reuse which may be related to plasticiser leaching. However, the disposable format used for this sensor minimises the problem. The repeatability of the procedure when using different disposable sensors with ten replicates of each had values of 2.4, 4.4, and 7.9% for $\log a_{K^+}$ from transflectance measurements and 3.3, 2.1 and 7.5% from absorbance measurements. As usual, the precision decreases when the analyte activity decreases due to the inverse relationship between the measured signal (transflectance or absorbance) and the activity. Table 1 shows these and other analytical parameters.

Table 1. Analytical Parameters

Parameter	Transflectance	Linearised transflectance	Absorbance	Linearised absorbance
Intercept	-0.498	1.693	-0.519	1.994
Slope	-0.300	0.511	-0.300	0.560
Lineal range (activity)	1.9×10^{-5} - 0.08 M	8.4×10^{-6} - 0.08 M	2.0×10^{-5} - 0.08 M	9.3×10^{-7} - 0.08 M
Detection limit (activity)	1.9×10^{-5} M	8.4×10^{-6} M	2.0×10^{-5} M	9.3×10^{-7} M
Intramembrane precision (RSD%)				
5×10^{-5} M	3.2	12.2	4.9	20.8
5×10^{-4} M	7.5	----	8.0	---
5×10^{-3} M	18.6	16.1	15.1	12.0
Intermembrane precision (RSD%)				
5×10^{-5} M	2.4	10.9	3.3	13.6
5×10^{-4} M	4.4	---	2.1	---
5×10^{-3} M	7.9	7.9	7.5	6.3

When the linearised model described above is applied, the dynamic linear range for K^+ is from 8.4×10^{-6} M to 0.08 M using transflectance data. This means an increase (in 1 order of magnitude) in the linear dynamic range with respect to the previous methodology (from 1.90×10^{-5} M to 0.08 M in activities; $\log\left(\frac{\alpha_{eff}}{1-\alpha_{eff}}\right) = 0.52 \log a_{K^+} + 1.78$; R^2=0.95). Using absorbance data, we obtained similar results from the linearised model, the dynamic linear range for K^+ is from 9.3×10^{-7} M to 0.08 M using absorbance data

($\log\left(\frac{\alpha_{eff}}{1-\alpha_{eff}}\right) = 0.56 \log a_{K^+} + 1.99$; R^2= 0.98), instead of the previous results obtained from the sigmoidal model in which we obtained a smaller linear range (from 2.00×10^{-5} M to 0.08 M in activities).

The precision of the activity logarithm measurements was studied at the different concentrations mentioned above. From the results we can observe that in both cases, intramembrane and intermembrane, the precision is better for transflectance than for absorbance measurements. Also we can see that the precision is better in lower concentrations of potassium than in higher concentrations. The reason for this behavior is the fact that this kind of membrane is especially designed to work at low concentrations. Also, although these sensors are disposable, they can be used more than once, obtaining very good results up to 6 or 7 times (Table 1).

4.2. Analytical applications

To assess the usefulness of the proposed transflectance disposable sensor for K^+ we selected samples of beverages and waters (mineral, tap, well, and rain) with different K^+ contents. Table 2 shows the results obtained using the disposable sensor in transflectance compared to an atomic absorption spectrometry method used as a reference method. Table 2 also includes the mean values from three determinations of each sample and the standard deviation of these measurements and the probability value (P_{val}) of the test used for the comparison of the measurements obtained for both methods. As can be seen, the results obtained with this disposable sensor in transflectance mode are statistically similar to those of a standard procedure (AAS).

Table 2. Determination of potassium in different types of matrices using AAS as a reference method

	AAS (mM)	s	Transflectance (mM)	s	p-value	Linearised transflectance (mM)	s	p-value
Cider (El Gaitero)	24.33	0.312	21.150	8.216	0.5385	14.657	7.433	0.873
Mineral water (Bezoya)	0.008	0.0002	0.037	0.032	0.195	0.015	0.022	0.616
Mineral water (Mondariz)	0.130	0.0009	0.184	0.103	0.419	0.115	0.075	0.740
Well water (Valderubio, Granada,)	0.045	0.009	0.139	0.045	0.047	0.088	0041	0.156
Well water (Otura, Granada)	0.040	0.016	0.087	0.040	0.020	0.050	0.011	0.438
Running water (Almuñecar, Granada)	0.076	0.013	0.095	0.076	0.205	0.056	0.013	0.136

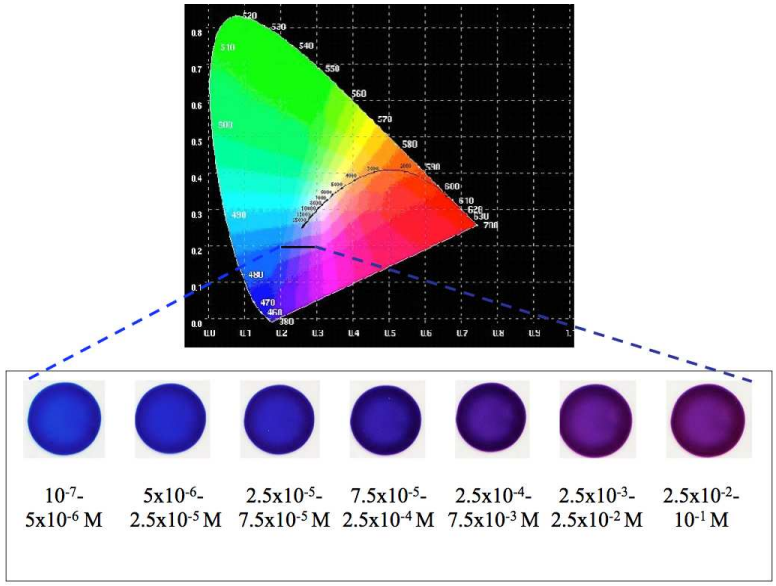

Figure 5. Color chart

4.3. Visual potassium determination based on colour analysis

To study the viability of the semi-quantitative determination of K^+ using the described disposable sensor we used a colour-difference formula designed to give a quantitative value of the perceived colour difference between a pair of coloured samples in specific experimental conditions. We use a CIELAB-based formula, namely CIEDE20002 [20,21] which incorporates corrections to simple differences in lightness (ΔL*), croma (ΔC*) and hue (ΔH*), calculated according to CIELAB[22], for nonuniformity of CIELAB space; namely, lightness, croma and hue weighting functions, S_L , S_C , S_H, parametric factors accounting for the influence of illuminating and viewing conditions in colour-difference evaluation, K_L, K_C, K_H, rotation term R_T and correction for neutral colours (eq. 9).

$$\Delta E_{00} = \sqrt{\left(\frac{\Delta L^*}{K_L S_L}\right)^2 + \left(\frac{\Delta C^*}{K_C S_C}\right)^2 + \left(\frac{\Delta H^*}{K_H S_H}\right)^2 + R_T\left(\frac{\Delta C^*}{K_C S_C}\right)\left(\frac{\Delta H^*}{K_H S_H}\right)} \qquad (9)$$

Two colours are considered to be distinguishable by the naked eye if the ΔE_{00} value is higher than 0.75 [21]. To prepare the semi-quantitative colour chart, an experiment was made using 11 potassium standard solutions equally spaced between $1 \cdot 10^{-7}$ and $1 \cdot 10^{-1}$ M. After equilibrating a disposable sensor with the solution, from the most diluted to the most concentrated, the chromatic coordinates were obtained and the ΔE_{00} parameter was obtained comparing each value with each of the other values. This experiment was repeated with three different disposable sensors to corroborate the results. The analysis of the results indicates 9 different discriminable colours, each one defining a concentration interval; however the experimental inspection of these classes using a panel of 5 people indicates that it is only possible to differentiate 7 intervals in reality (Figure 5). Table 3 shows the possible concentration intervals for potassium estimation using the described disposable sensor. The colours that the membrane takes on when it is introduced in the different potassium standard solutions are in-

cluded in the interval defined by the colours shown by the membranes when introduced in HCl 0.01M solution (deep blue colour; colour coordinates X=9.48, Y=9.69, Z=28.0) and in NaOH 0.01M solution, (pink colour; X=8.39, Y=6.26, Z=16.0).

Table 3. Values of ΔE_{00} parameter

[K], M	ΔE_{00}	Interval, M
$1x10^{-7}$		10^{-7}-$5x10^{-6}$
$1x10^{-6}$	0.32	
$1x10^{-5}$	1.04	$5x10^{-6}$- $2.5x10^{-5}$
$5x10^{-5}$	2.95	$2.5x10^{-5}$-$7.5x10^{-5}$
$1x10^{-4}$	2.31	$7.5x10^{-5}$- $2.5x10^{-4}$
$5x10^{-4}$	3.74	$2.5x10^{-4}$ -$2.5x10^{-3}$
$1x10^{-3}$	0.85	
$5x10^{-3}$	1.51	$2.5x10^{-3}$-$2.5x10^{-2}$
$1x10^{-2}$	0.83	
$5x10^{-2}$	1.86	$2.5x10^{-2}$-10^{-1}
$1x10^{-1}$	0.36	

5. Conclusion

An optical disposable sensor coupled to absorption spectroscopy in transflectance mode for quantifying potassium was evaluated for the determination of potassium in natural waters. The results obtained are very similar to those found when measuring in transmission mode. The described disposable sensor

makes it possible to monitor potassium *in situ* for most practical situations. It is environmentally friendly and has an estimated lifetime of at least two months when protected from light in normal conditions. Additionally, we have considerably enlarged the linear dynamic range of this ionophore-chromoionophore based sensor by using a simple mathematical linear model.

This new approach described here has considerable potential as a useful and inexpensive tool for obtaining chemical information *in situ* for a wide range of analyte samples that can be implemented easily in portable equipment. Moreover, we have studied the feasibility of this disposable sensor for the semi-quantitative determination of potassium proving, by using a colour-difference CIELAB-base formula, that the use of a colour chart with 7 intervals of discriminable concentrations between 10^{-7} and 10^{-1} M is possible.

Acknowledgements

We acknowledge financial support from the *Ministerio de Educación y Cultura, Dirección General de Enseñanza Superior* (Spain) (Projects CTQ2005-09060-CO2-01 and CTQ2005-09060-CO2-02).

6. Conclusión

En este capítulo se ha detallado el estudio llevado a cabo sobre un sensor basado en química ionóforo-cromoionóforo que trabaja por intercambio iónico para la determinación de potasio en muestras de bebidas y aguas de distinto tipo. Para ello, se ha medido una propiedad distinta de la absorción de radiación como es la transflexión y se ha comprobado la validez de la propuesta comparando los resultados con las medidas de absorbancia habituales. El objetivo de este estudio es obtener el parámetro analítico, una señal óptica relativa, a partir de medidas de transflectancia de membranas sensoras de potasio y establecer las funciones de calibrado, tanto lineales como sigmoidales, así como las características del procedimiento. El empleo de medidas de transflectancia abre las puertas al diseño de instrumentación portátil más compacta que la basada en absorción de radiación así como a sensores de un solo uso de tipo multicapa con mayor capacidad de separación.

De los resultados obtenidos se deduce que la determinación de potasio con este tipo de sensores por medio de medidas de transflectancia, proporciona unos resultados similares a los obtenidos con medidas de absorción. Así, los límites de detección son prácticamente idénticos con transflectancia y absorbancia ($1.9x10^{-5}$ M para transflexión y $2.0x10^{-5}$ M para absorción) así como los rangos de medida. Si observamos los resultados de precisión obtenidos, en el caso de la precisión intramembrana son, en ambos casos, muy similares, obteniendo un valor de desviación estándar relativa media de 9.7% con medidas de transflectancia y 9.3% para medidas de absorbancia. En el caso de la precisión intermembrana se han encontrado unos valores de 4.9% y 4.3%, respectivamente, en términos de desviación estándar relativa igualmente.

Cuando se utiliza la función linealizada a través de una linealización logística, se mejora muy considerablemente el rango de medida del sensor, bajando el límite de detección de $1.9x10^{-5}$ M a $8.4x10^{-6}$ M. Todas las medidas de

transflectancia fueron tomadas usando una instrumentación portable modular; por tanto, los resultados obtenidos poseen un valor añadido ya que no se realizaron con una instrumentación de sobremesa como en el caso del espectrofotómetro usado para las medidas de absorción.

Un segundo objetivo marcado en este trabajo fue el desarrollo teórico de una carta de color a partir de las medidas de transflectancia anteriores y su posterior validación frente a un panel de observadores. Todo ello con la intención de usar el sensor de un solo uso para potasio como un sensor de tipo visual que ofrezca información semicuantitativa sin necesidad de utilizar ningún tipo de instrumentación. Para ello, a partir de los espectros de transflexión se calcularon las coordenadas cromáticas del color que adquieren las membranas con los diferentes patrones de potasio de concentración variable utilizados.

El número de intervalos de concentración que se van a poder definir va a depender del número de colores distintos que va a tomar el sensor y que el ojo humano pueda diferenciar. El número de colores discriminables teóricamente fueron nueve, sin embargo, los resultados del panel de observadores muestra que son sólo siete los intervalos de concentración discernibles por su color. Por tanto esta herramienta permite predecir la utilidad de un sensor de un solo uso como un sensor de tipo visual así como establecer cuales tienen que ser las variaciones de color para poder definir un conjunto de concentraciones dado.

7. Bibliografía

1. L. F. Capitan-Vallvey, in: Grimes, C. A.; Dickey, E. C.Pishko, M. V., Eds. (Ed.), Encyclopedia of Sensors, The Pennsylvania State University, Pennsylvania, USA, 2005, pp. 55-93 .

2. Yu. Zolotov, V.M. Ivanov, V.G. Amelin, Test methods for extra-laboratory analysis, TrAC 21 (2002) 302.

3. Lange, H., Rittersdorf, W., Rey, H. G., Diagnostic device, US 3,897,214, 2001.

4. G.-Q. Shi, G. Jiang, A dip and read test strip for the determination of Hg(II) in aqueous samples based on urease activity inhibition, Anal.Sci. 18 (2002) 1215.

5. M. Blazkova, P. Rauch, L. Fukal, Strip-based immunoassay for rapid detection of thiabendazole, Biosens.Bioelectron. 25 (2010) 2122.

6. C. Shi, S. Zhao, K. Zhang, G. Hong, Z. Zhu, Preparation of colloidal gold immunochromatography strip for detection of methamidophos residue, J.Environ.Sci.(Beijing, China) 20 (2008) 1392.

7. B.A. Cadle, K.C. Rasmus, L.S. Leverich, C.E. O'Neill, R.K. Bachtell, D.C. Cooper, Cellular phone-based image acquisition and quantitative ratiometric method for detecting cocaine and benzoylecgonine for biological and forensic applications, Subst.Abuse: Res.Treat. 4 (2010) 21.

8. U. E. Spichiger-Keller, in: Chemical Sensors and Biosensors for Medical and Biological Applications, Wiley-VCH, Weinheim, 1998, pp. 259-319.

9. E. Bakker, P. Bühlmann, E. Pretsch, Carrier-Based Ion-Selective Electrodes and Bulk Optodes. 1. General Characteristics, Chem Rev. 97 (1997) 3083.

10. P. Bühlmann, E. Pretsch, E. Bakker, Carrier-Based ion-Selective Electrodes and bulk Optodes. 2.Ionophores for Potentiometric and optical Sensors, Chem.Rev. 98 (1998) 1953.

11. L.F. Capitan-Vallvey, M.D. Fernandez Ramos, M. Al Natsheh, A disposable single-use optical sensor for potassium determination based on neutral ionophore, Sens.Actuators B 88 (2003) 217.

12. A. Ceresa, Y. Quin, S. Peper, E. Bakker, Mechanistic insights into the development of optical chloride sensor based on the mercuracarborand-3 ionophore, Anal.Chem. 75 (2003) 133.

13. R.H. Ng, K.M. Sparks, B.E. Statland, Colorimetric determination of potassium in plasma and serum by reflectance photometry with a dry-chemistry reagent, Clin.Chem. 38 (1992) 1371.

14. D. Freiner, R.E. Kunz, D. Citterio, U.E. Spichiger, M.T. Gale, Integrated optical sensors based on refractometry of ion-selective membranes, Sens.Actuators B 29 (1995) 277.

15. A. Lapresta-Fernandez, L.F. Capitan-Vallvey, Scanometric potassium determination with ionophore-based disposable sensors, Sens.Actuators B 134 (2008) 694.

16. E. Hirayama, T. Sugiyama, H. Hisamoto, K. Suzuki, Visual and Colorimetric Lithium Ion Sensing Based on Digital Color Analysis, Anal.Chem. 72 (2000) 465.

17. M. Shamsipur, S. Rouhani, A. Mohajeri, M.R. Ganjali, PVC-membrane ion-selective bulk optode for Ag^+ ion based on hexathia-18-crown-6 and 1,2-benzo-3-octadecanoylimino-7-diethylaminophenoxazine, Anal. Bioanal. Chem. 375 (2003) 692.

18. S.C. Charlton, R.L. Fleming, A. Zipp, Solid-phase colorimetric determination of potassium, Clin.Chem. 28 (1982) 1857.

19. F. Baldini, A. N. Chester, J. Homola. Optical Chemical Sensors, Springer, 2006

20. M. Melgosa, R. Huertas, R.S. Berns, Relative significance of the terms in the CIEDE2000 and CIE94 color-difference formulas, J.Opt.Soc.Am.A 21 (2004) 2269.

21. M. Melgosa, M.M. Perez, A. Yebra, R. Huertas, E. Hita, Algunas reflexiones y recientes recomendaciones internacionales sobre evaluación de diferencias de color, Óptica Pura y Aplicada 34 (2001) 1.

22. CIE, Colorimetry, CIE Publication 15-2, Viena,1986.

23. Hildebrand, K., Von Döhren, H. H., Perrey, H, Wehling, K., Transparent test strip system, US 4,824,640, 1989.

24. Eisinger, R. W., Khalil, M. H., Katz, D. H., Sargeant, R. B., Lateral flow, non-bibulous membrane assay protocols, US 4,943,522, 1990.

25. L.F. Capitan-Vallvey, O.M.A. Al-Barbarawi, M.D. Fernandez-Ramos, R. Avidad-Castañeda, Determination of oxolinic acid in cow´s milk and human urine by means of a single-use optical sensor, Talanta 60 (2003) 247.

26. Akhavan-Tafti, H., Sugioka, K., Sugioka, Y., Reddy, L. V., Chemiluminescent detection methods using dual enzyme-labeled binding partners, US 5,843,666, 1998.

27. J. Ballesta Claver, M.C. Valencia-Miron, L.F. Capitan-Vallvey, Determination of hypochlorite in water using a chemiluminescent test strip, Anal.Chim.Acta 522 (2004) 267.

28. K. Schult, A. Katerkamp, D. Trau, F. Grawe, K. Cammann, M. Meusel, Disposable Optical Sensor Chip for Medical Diagnostics: New Ways in Bioanalysis, Anal.Chem. 71 (1999) 5430.

29. N.I. Ershova, V.M. Ivanov, Application of chromaticity characteristics for direct determination of trace aluminum with Eriochrome cyanine R by diffuse reflection spectroscopy, Anal.Chim.Acta 408 (2000) 141.

30. K. Suzuki, E. Hirayama, T. Sugiyama, K. Yasuda, H. Okabe, D. Citterio, Ionophore-Based Lithium Ion Film Optode Realizing Multiple Color Variations Utilizing Digital Color Analysis, Anal.Chem. 74 (2002) 5766.

31. L.K. Chau, M.D. Porter, Optical Sensor for Calcium: Performance, Structure and Reactivity of Calciochrome Immobilized at an Anionic Polymer, Anal.Chem. 62 (1990) 1964.

32. Phillips, R., McGarraugh, G., Jurik, F. A., Underwood, R. D., Whole blood glucose test strip, US 5,563,042, 1996.

33. J. Greyson, Problems and possibilities of chemistry on dry reagent carriers, J.Autom.Chem. 3 (1981) 66.

34. P. Kubelka, F.Z. Munk, Tech.Physik. 12 (1931) 593.

35. H.G. Curme, R.L. Columbus, G.M. Dappen, T.W. Eder, W.D. Fellows, J. Figueras, C.P. Glover, C.A. Goffe, D.E. Hill, W.H. Lawton, E.J. Muka, J.E. Pinney, R.N. Rand, K.J. Sanford, T.W. Wu, Multilayer film

elements for clinical analysis: general concepts, Clin.Chem. 24 (1978) 1335.

36. F.C. Williams, F.R. Clapper, Multiple internal reflections in photographic color prints, J.Opt.Soc.Am. 43 (1953) 595.

37. L.F. Capitan-Vallvey, P. Alvarez de Cienfuegos, M.D. Fernandez-Ramos, R. Avidad-Castañeda, Determination of Calcium by a Single-Use Optical Sensor, Sens.Actuators B 71 (2000) 140.

38. L.F. Capitan-Vallvey, C. Cano-Raya, C. Esparza del Valle, M.D. Fernandez-Ramos, I. De Orbé Payá, R. Avidad-Castañeda, A Multilayer Optical Test Strip For Copper Determination In Human Plasma, Anal.Lett. 35 (2002) 615.

39. L.F. Capitan-Vallvey, E. Arroyo-Guerrero, M.D. Fernandez-Ramos, F. Santoyo-Gonzalez, Disposable receptor-based optical sensor for nitrate, Anal.Chem. 77 (2005) 4459.

40. C. Cano-Raya, M.D. Fernandez-Ramos, L.F. Capitan-Vallvey, Fluorescence resonance energy transfer disposable sensor for copper(II), Anal.Chim.Acta 555 (2006) 299.

41. B. G. Osborne , in: Meyers, R. A., Ed. (Ed.), Encyclopedia of Analytical Chemistry, John Wiley & Sons Ltd, Chichester, 2005.

42. A. Moradian, G.J. Mohr, M. Linnhoff, M. Fehlmann, U.E. Spichiger-Keller, Continuous optical monitoring of aqueous amines in transflectance mode, Sens.Actuators B 62 (2000) 154.

43. P. Blum, G.J. Mohr, K. Matern, J. Reichert, U.E. Spichiger-Keller, Optical alcohol sensor using lipophilic Reichardt's dyes in polymer membranes, Anal.Chim.Acta 432 (2001) 269.

44. W.E. Morf, K. Seiler, B. Rusterholz, W. Simon, Design of calcium-selective optode membrane based on neutral ionophores, Anal.Chem. 62 (1990) 738.

45. L.F. Capitan-Vallvey, M.D. Fernandez-Ramos, P. Alvarez de Cienfuegos, F. Santoyo-Gonzalez, Characterization of a transparent optical test strip for quantification of water hardness, Anal.Chim.Acta 481 (2003) 139.

46. K. Seiler, W. Simon, Theoretical aspects of bulk optode membranes, Anal.Chim.Acta 266 (1992) 73.

47. L.F. Capitan-Vallvey, M.D. Fernandez-Ramos, P. Alvarez de Cienfuegos, Optical test strip for calcium determination based on neutral ionophore, Anal.Chim.Acta 451 (2002) 231.

48. P.C. Meier, Two-Parameter Debye-Hückel Aproximation for the Evaluation of Mean Activity Coefficient of 109 Electrolytes, Anal.Chim.Acta 136 (1982) 363.

49. L.F. Capitan-Vallvey, A. Lapresta-Fernandez, M.D. Fernandez-Ramos, L. Cuadros-Rodriguez, Establishment of wide-range linear response curves in bulk optode sensors for cations based on ion exchange, Sens.Actuators B 117 (2006) 27.

Capítulo 3

Coordenada tonal H del espacio HSV
como parámetro analítico
para sensores ópticos

1. Planteamiento

En este capítulo se profundiza en el empleo de color como parámetro para obtener información analítica. Al ser el color una propiedad organoléptica de la materia, esto es, apreciable por los sentidos, se ha utilizado tradicionalmente en Química Analítica como una señal analítica cualitativa observada en reacciones de separación o de identificación para el análisis cualitativo o para una estimación de la concentración -semicuantitativa- de especies. Recordemos a este respecto el uso del color de precipitados, disoluciones, extractos en disolventes, gases generados o llamas coloreadas, de amplia tradición y utilización en marchas cualitativas y ensayos directos.

El color es una percepción visual que se genera en el cerebro al interpretar las señales nerviosas enviadas por la retina ocular procedente de la radiación electromagnética visible que le llega. En consecuencia, el color se refiere a cualidades que se presentan o representan en experiencias visuales y por su naturaleza, es subjetivo. Por otra parte, hay que recordar que el color no pertenece intrínsecamente a los objetos a los que asociamos un color, sino que es una propiedad de la luz que vemos después de reflejarse en ellos o de ser transmitida por los mismos [1].

Aunque se pueda describir de forma precisa un color midiendo la distribución de energía espectral de la luz que origina ese color -energía por unidad de área y longitud de onda de una iluminación dada-, esto lleva a un alto grado de redundancia debido a que la retina del ojo es sensible a color en tres zonas amplias de longitudes de onda correspondientes aproximadamente a luz roja, verde y azul. Las señales eléctricas de estas células de la retina (conos) junto con las de las células

sensibles a intensidad (bastones) se combinan en el cerebro dando lugar a las diferentes sensaciones de color: claridad, tono, saturación, forma, tamaño, textura, localización u otras, de las que las tres primeras son intrínsecamente visuales y se denominan atributos psicológicos del color.

Aunque, como sabemos, el color es subjetivo y depende de cómo se perciba por el observador, se puede especificar numéricamente a partir de las leyes experimentales de emparejamiento cromático obtenidas a partir de la generalización empírica conocida como generalización tricromática [2].

A partir de medidas físicas de potencia radiante, para lo que se utilizan diversos tipos de detectores, es posible llegar a definir un color. Los dispositivos más habituales son térmicos y fotónicos, estando en este último caso basados en efecto fotoeléctrico externo (fotoemisión) o en efecto fotoeléctrico interno (fotoconductivo y fotovoltaico), siendo muy frecuentes los dispositivos de carga acoplada CCD y los dispositivos CMOS (Complementary Metal Oxide Semiconductor).

La forma de especificar, crear y visualizar colores es mediante los denominados espacios de color. Un espacio de color es la combinación de un modelo de color y de una apropiada función de representación gráfica de este modelo. Un modelo de color es un modelo matemático abstracto que describe los colores como secuencias de números, habitualmente tres o cuatro valores dependiendo del modelo, así RGB o CMYK [2]. Se puede clasificar estos espacios de color en cuatro grupos que se relacionan mediante diferentes tipos de transformaciones: a) triestímulo lineales (CIE XYZ, RGB), b) cromáticos xy (CIE xyY), c) perceptualmente uniformes (CIE L*u*v*; CIE L*a*b*, R'G'B' no lineal) y d) orientados al tono (HLS, HSV) [3] .

En Química Analítica se ha utilizado la información procedente de diferentes dispositivos de imagen con propósitos cuantitativos. Así escáneres manuales [4] o de sobremesa trabajando tanto por reflexión [5] como por transmisión [6], dispo-

sitivos CCD [7], video cámaras [8], cámaras fotográficas digitales [9] y analizadores digitales de color [10-12].

De todos los espacios de color antes citados, los más utilizados bajo el punto de vista del análisis químico son los espacios triestímulo (RGB) y los de cromaticidad xy. El problema de estos espacios es que los colores se definen como mezcla de colores básicos y es frecuente el utilizar un solo canal de los tres, con la consiguiente pérdida de información que ello supone, o bien varios de ellos a la vez, principalmente como cocientes de coordenadas. Pero dicha elección supone un problema de fondo que es la pérdida de información de los canales no utilizados. Por tanto hay que enfrentarse a la decisión de o bien emplear un procedimiento en el que sean necesarias las tres coordenadas de color para así definir correctamente el color que adquiere el sistema analítico, lo que hace que el procedimiento sea más complejo, o bien utilizar un solo canal con la pérdida de información que ello conlleva aunque dando lugar a un procedimiento más sencillo. Esta pérdida de información se traduce a su vez en una disminución de la robustez de la señal.

Para resolver estas cuestiones, se propone en este capítulo el uso analítico del espacio de color HSV (Hue, Saturation, Value) y en concreto su coordenada H correspondiente al tono. Este espacio HSV va a definir los colores como una combinación de estos tres parámetros que se corresponde con el tono (H), saturación (S) y luminosidad (V). Por tanto, en este espacio el tono de un color va a venir perfectamente definido por el parámetro H, mientras que las otras dos coordenadas van a añadir matices al tono, como son la saturación (intensidad del color) y la luminosidad (claridad u oscuridad del color). De esta manera podemos tener definido el tono que adquiere el sensor mediante una sola coordenada y no mediante tres como ocurre en las coordenadas RGB y sin estar influenciado por la saturación o la luminosidad, resultando así un parámetro analítico mucho más robusto.

El objetivo que nos planteamos no es sólo ver si es posible el uso de este parámetro para calibrar y cuantificar con estos sensores, sino llevar a cabo previa-

mente un estudio teórico acerca del comportamiento del parámetro H al variar factores del propio sensor como es el grosor de la membrana y la cantidad de indicador o en general de reactivos coloreados o generadores de color presentes en la misma, así como factores externos al sensor como son los dispositivos de imagen utilizados para digitalizarlo y la iluminación. De esta manera comprobamos de manera fehaciente la robustez de este parámetro.

Todas las imágenes tomadas tanto con el escáner como con las cámaras fotográficas que a continuación se indican se obtuvieron trabajando en modo transmisión, es decir, iluminando la membrana sensora por el lado contrario al que se encuentra el dispositivo de medida.

Anal. Chem. 2010, 82, 531–542

Use of the Hue Parameter of the Hue, Saturation, Value Color Space As a Quantitative Analytical Parameter for Bitonal Optical Sensors

K. Cantrell,[†] M. M. Erenas,[‡] I. de Orbe-Payá,[‡] and L. F. Capitán-Vallvey*,[‡]

Department of Chemistry, The University of Portland, Portland, Oregon 97203, and Solid Phase Spectrometry Research Group, Department of Analytical Chemistry, Campus Fuentenueva, University of Granada, E-18071 Granada, Spain

The hue or *H* component of the hue, saturation, value (HSV) color space has been studied as a quantitative analytical parameter for bitonal optical sensors. The robust nature of this parameter provides superior precision for the measurement of sensors which change colors with the speciation of some indicator molecule. This parameter has been compared to red, green, blue (RGB) intensity and RGB absorbance along with differences and ratios of both intensity and absorbance and has been demonstrated to be 2 to 3 times superior. The *H* value maintains this superior precision with variations in indicator concentration, membrane thickness, detector spectral responsivity, and illumination. Because this parameter is stable, simple to calculate, easily obtained from commercial devices such as scanners and digital cameras, continuous over the entire color gamut, and bound between values of 0 and 1, it shows great promise for use in a variety of sensing applications including imaging, automated analysis, pharmaceutical sensing, lab-on-a-chip devices, and quality control applications.

The latent information contained in a material sample is encoded into an analytical signal from chemical reaction or energetic interaction with an analyte. Usually this interaction with the sample is inelastic and involves an energetic exchange between the measurement system and measured sample. Signals resulting from this energetic exchange contain information regarding both the types and the amounts of constituents in the sample. In the signal domain these are coded into a signal position which typically gives qualitative information about the chemical entities whereas the intensity at that position is connected to quantitative information about the chemical entities.[1,2] For example, in traditional molecular absorbance spectrometry, wavelength is the qualitative signal position and absorbance is the quantitative signal intensity.

Quantitative analysis is based on absolute, relative, or reference measurements of intensity related to concentration by means of a continuous function, linear in most cases, estimated mainly by experimentation. However, it is possible to determine the amounts of analytes using a qualitative variable under certain circumstances. For instance, consider a chemical A characterized by a signal position z_A that by direct or indirect reaction or interaction with the analyte X produces the chemical B with a signal position z_B. If the qualitative relationship for the transformation of z_A to z_B is represented by a continuous function, it is possible to extract quantitative information from the continuous qualitative variable. The difference in the signal between the two ends, z_A and z_B, is related to the displacement of reaction by the analyte and thus with the concentration of analyte X through an experimental calibration function. Examples of this type of analysis include the determination of composition of a defined solvent mixture by using the wavelength displacement of a solvatochromic dye used as a probe[3] and the monitoring of slag composition by measurement of density.[4]

A one-shot sensor for potassium previously studied using spectrophotometric[5] and transflectance (a measurement of reflected light for semitransparent samples) measurements[6] meets the criteria previously described. This sensor relies on an ion-exchange equilibrium[7,8] between the aqueous solution containing the analyte and the sensing membrane as shown in the reaction below, where the bar indicates a membrane bound species.

$$\bar{L} + \overline{HC^+} + K^+ \rightleftharpoons \overline{KL^+} + \bar{C} + H^+$$

A plasticized PVC sensing membrane contains the selective ionophore L, which drives the reaction, the chromoionophore C, which is selective for H^+, and the highly lipophilic anion R$^-$. When potassium enters the membrane to bind with the ionophore, the chromoionophore must become deprotonated to maintain electroneutrality within the membrane phase. Thus the color of the membrane turns from the chromoionophore's acidic form, HC^+ (blue for the lipophilic Nile Blue chromoiono-

* Corresponding author. E-mail: lcapitan@ugr.es.
[†] The University of Portland.
[‡] University of Granada.

(1) Danzer, K. *Anal. Bioanal. Chem.* **2004**, *380*, 376–382.
(2) Danzer, K. *Analytical Chemistry: Theoretical and Metrological Fundamentals*; Springer-Verlag: Berlin, Germany, 2007.
(3) Citterio, D.; Kaneda, T.; Yagi, J.; Ishigaki, T.; Hisamoto, H.; Suzuki, S. I.; Suzuki, K. *Anal. Chim. Acta* **2003**, *482*, 19–28.
(4) Oliveira, R.; Bruno, M. P.; Lang, H. *Metall. Trans. B* **1991**, *22B*, 205–207.
(5) Capitán-Vallvey, L. F.; Fernández Ramos, M. D.; Al Nashash, M. *Sens. Actuators, B* **2003**, *90*, 217–222.
(6) Orbe-Payá, I. d.; Erenas, M.; Capitán-Vallvey, L. F. *Sens. Actuators, B* **2007**, *125*, 586–592.
(7) Bakker, E.; Bühlmann, P.; Pretsch, E. *Chem. Rev.* **1997**, *97*, 3083–3132.
(8) Spichiger-Keller, U. E. *Chemical Sensors and Biosensors for Medical and Biological Applications*; Wiley-VCH: Weinheim, Germany, 1998.

10.1021/ac901753c © 2010 American Chemical Society
Published on Web 12/15/2009

The use of the Hue parameter of the HSV color space as a quantitative analytical parameter for bitonal optical sensors

K. Cantrell[1], M.M. Erenas[2], I. de Orbe-Payá[2], L.F. Capitán-Vallvey[2*]

[1]Department of Chemistry, The University of Portland, Portland, OR 97203, USA
[2]Solid Phase Spectrometry Research Group, Department of Analytical Chemistry, Campus Fuentenueva, University of Granada, E-18071,Granada, Spain

Abstract

The hue or H component of the HSV (Hue, Saturation, Value) color space has been studied as a quantitative analytical parameter for bitonal optical sensors. The robust nature of this parameter provides it superior precision for the measurement of sensors which change colors with the speciation of some indicator molecule. This parameter has been compared to RGB (Red, Green, Blue) intensity and RGB absorbance along with differences and ratios of both intensity and absorbance, and has been demonstrated to be 2 to 3 times superior. The H value maintains this superior precision with variations in indicator concentration, membrane thickness, detector spectral responsivity, and illumination. Because this parameter is stable, simple to calculate, easily obtained from commercial devices such as scanners and digital cameras, continuous over the entire color gamut, and bound between values of 0 and 1, it shows great promise for use in a variety of sensing applications in-

cluding imaging, automated analysis, pharmaceutical sensing, lab-on-a-chip devices, and quality control applications.

Keywords: H coordinate; HSV color space; bitonal optical sensors; potassium sensor; imaging

* Corresponding author; *e-mail:* lcapitan@ugr.es

2. Introduction

The latent information contained in a material sample is encoded into an analytical signal from chemical reaction or energetic interaction with an analyte. Usually this interaction with the sample is inelastic and involves an energetic exchange between the measurement system and measured sample. Signals resulting from this energetic exchange contain information regarding both the types and the amounts of constituents in the sample. In the signal domain those are coded into a signal position which typically gives qualitative information about the chemical entities whereas the intensity at that position is connected to quantitative information about the chemical entities [13,14]. For example in traditional molecular absorbance spectrometry, wavelength is the qualitative signal position and absorbance is the quantitative signal intensity.

Quantitative analysis is based on absolute, relative, or reference measurements of intensity related to concentration by means of a continuous function, linear in most cases, estimated mainly by experimentation. However, it is possible to determine the amounts of analytes using a qualitative variable under certain circumstances. For instance, consider a chemical A characterized by a signal position z_A that by direct or indirect reaction or interaction with the analyte X produces the chemical B with a signal position z_B. If the qualitative relationship for the transformation of z_A to z_B is represented by a continuous function, it is possible to extract quantitative information from the continuous qualitative variable. The difference in the signal between the two ends, z_A and z_B, is related to the displacement of reaction by the analyte and thus with the concentration of analyte X through an experimental calibration function. Examples of this type of analysis include the determination of composition of a defined solvent mixture by using the wavelength displacement of a solvatochromic dye used as a probe [15] and the monitoring of slag composition by measurement of density [16].

A one-shot sensor for potassium previously studied using spectrophotometric [17] and transflectance (a measurement of reflected light for semi-transparent samples**)** measurements [18] meets the criteria previously described. This sensor relies on an ion-exchange equilibrium [19,20] between the aqueous solution containing the analyte and the sensing membrane as shown in the reaction below.

$$\overline{L} + \overline{HC^+} + K^+ \leftrightarrow \overline{KL^+} + \overline{C} + H^+$$

A plasticized PVC sensing membrane contains the selective ionophore L, which drives the reaction, the chromoionophore C, which is selective for H^+, and the highly lipophilic anion R^-. When potassium enters the membrane to bind with the ionophore, the chromophore must become deprotonated to maintain electroneutrality within the membrane phase. Thus the color of the membrane turns from the chromoionophore's acidic form, HC^+ (blue for the lipophilic Nile Blue chromoionophore used in the potassium membranes studied here), to the basic form, C (magenta for the lipophillic Nile Blue chromoionophore).

The degree of protonation of the chomoionphore, 1-α, is related to the activity of the analyte potassium, a_{K^+}, through the sigmoidal response function [18] given in eq. 1.

$$a_{K^+} = \frac{1}{K_{exch}}\left(\frac{a_{H^+}\alpha}{1-\alpha}\right)\frac{C_R - (1-\alpha)C_C}{\left(C_L - 0.5\left(C_R - (1-\alpha)C_C\right)\right)^{0.5}} \quad (1)$$

Here 1-α is the fraction of protonated chromionophore, K_{exch} is the equilibrium constant for the ion-exchange reaction, and C_L, C_C and C_R are the analytical concentrations of ionophore, chromoionophore and lipophilic anion, respectively. Eq. 1 assumes that the stoichiometric factor for the analyte to ionophore complex is 0.5, and the charge of analyte is 1. The extent of the ion-exchange process can be measured by the degree of protonation, and there is a sigmoidal relationship between 1-α and the concentration of the analyte, potassium. Thus the color of the

chromoionophore, which depends on the fraction of it that is deprotonated, can be used to track the extent of interaction between the analyte and the sensing membrane.

Colors are qualities that are present or represented in visual experiences [21] and can be quantified using a number of methods or color spaces that specify color from the three primary colors, similar to human color perception. Color systems can be classified into four groups related by different types of transformations: linear-light tri-stimulus (CIE XYZ, RGB), xy chromaticity (CIE xyY), perceptually uniform (CIE L*u*v*; CIE L*a*b*, non-linear R'G'B') and hue oriented (HLS, HSV) [3] .

The RGB color space is an additive representation of color used by devices such as CRT monitors, scanners, and digital cameras. In this representation, all the colors in the gamut can be represented as a combination of red, green, and blue primaries. In input devices such as scanners and cameras, spectral band filters for these three regions of the spectra are used to calculate a numerical representation of the intensity of each of these color channels. Thus the value for a channel represents the total photons in that region of the spectra as given by eq. 2a, 2b and 2c, where P is incident intensity and S is spectral responsivity for a particular channel.

$$R = \int_{\lambda} P(\lambda) S_R(\lambda) d\lambda \tag{2a}$$

$$G = \int_{\lambda} P(\lambda) S_G(\lambda) d\lambda \tag{2b}$$

$$B = \int_{\lambda} P(\lambda) S_B(\lambda) d\lambda \tag{2c}$$

The spectral responsivity of each channel varies from device to device, but they are roughly Gaussian functions with typical ranges of 400-500 nm, 500-580 nm, and 580-700 nm for the blue, green, and red channels, respectively. Typically, scanners are designed primarily to deal with printed material where the printed color comes from mixing of ink. Thus their spectral responsivity tends to be more narrowly distributed than those in general purpose digital cameras. Most devices such as cameras and scanners use the sRGB color space which is a device-independent color space based on the CIE XYZ master color space [22]. These devices use internal calibration data to transform the measured RGB values into the sRGB color space [23].

HSV is an alternate representation of color derived from the red, green, and blue intensity values of the RGB color space. A pixel in this color space is defined by its Hue (H), Saturation (S), and Value (V) coordinates. In broad terms, H is a numerical representation of the color, S gives the degree to which a single channel dominates, and V represents the brightness. The equations for calculating H, S, and V are given in eq. 3a, 3b, and 3c, respectively [24].

$$H = \begin{cases} \left(\dfrac{G-B}{\max_{channel}-\min_{channel}}+0\right)\Big/6; & if\ \max = R^{*} \\ \left(\dfrac{B-R}{\max_{channel}-\min_{channel}}+2\right)\Big/6; & if\ \max = G \\ \left(\dfrac{R-G}{\max_{channel}-\min_{channel}}+4\right)\Big/6; & if\ \max = B \end{cases} \tag{3a}$$

* *if H is less than* 0 *then add* 1 *to H*

$$S = \frac{\max_{channel} - \min_{channel}}{\max_{channel}} \tag{3b}$$

$$V = \max_{channel} \tag{3c}$$

Because of the circular nature of H (the values are bounded between 0 and 1, with both 0 and 1 representing the same hue), it is often reported as an angle that varies between 0 and 360° and represented as a color wheel where 0° is located at the top of the wheel. Figure 1 shows a color wheel in which H values change with angle while S and V are held constant as 1. To gain a qualitative understanding of the relationship between H and the more familiar absorbance spectrum of a molecule, one must divide the visible wavelengths into three regions corresponding to red, green and blue. The region in which the least absorbance occurs will determine the starting position on the color wheel at 0° (red), 120° (green), or 240° (blue). The value of hue will then shift, where the direction of the shift is determined by which of the two remaining regions has a smaller total absorbance, and the magnitude of the shift is determined by the difference in the absorbances within the three regions. For example, the H values for the fully protonated and deprotonated forms of lipophilized Nile Blue, the chromophore used for potassium membranes studied here, are indicated in Figure 1. The blue acid form of the indicator has a hue of 0.560 or 201°, and the magenta base form has a hue of 0.812 or 292°.

Color has been used traditionally in analytical chemistry as a qualitative analytical signal resulting from separation or identification reactions (e.g. color of precipitates, solutions, extracts, gases, or flames). Although color is subjective, depending on how it is perceived by an observer, the introduction of different color spaces and imaging devices have allowed the use of objective color measurements in analytical chemistry for different purposes. One of the first such applications was complementary tri-stimulus colorimetry in which the trichromatic coordinates and the coordinates of the absorbed color are calculated from the transmittance or

absorbance values. This technique was used for the evaluation of color changes at the end-point in visually indicated titrations and for multicomponent analysis of mixtures among other applications [25,26].

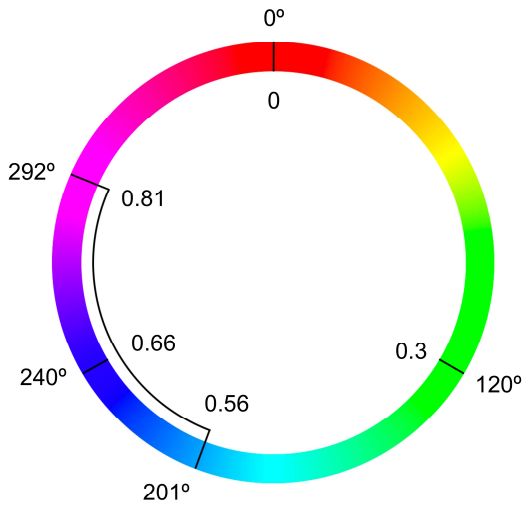

Figure 1. Color wheel showing the range of possible values for H. The values of S and V are held constant at 1. The values of the H coordinate for the K(I) one-shot sensor studied are shown in the range between 0.56 (acid form) and 0.81 (base form).

Signals coming from different imaging devices have been used for quantitative purposes including hand-held [4] and desktop scanners working both in reflection [5] or transmission mode [6], CCD arrays [7], video cameras [8], digital photographic cameras [9] and digital color analyzers [10-12]. The analytical use of color-based methods is very diverse. Examples of single analyte determinations include total protein [27], Fe(III) [4] , Hg(II) [28] , dopamine [29] and chlorophyll [30]. Some multianalyte determinations are iron speciation and pH [31], Fe(III) and Al(III) [32] , the identification of VOC's [33] or organics in water [34], and the simultaneous determination of pH, proteins and glucose [28,35].

The most commonly used color space is tri-stimulus RGB intensity and, if the measurement is selective enough, the calibration function is obtained from the most sensitive color coordinate through a curvilinear [36] or linearized function [37] although a ratio or some other transformation of coordinates is also possible [29]. In other cases multivariate calibration (PLS, NNA) is a better option for linearization [4], or multianalyte determination [32]. For classification purposes hierarchical cluster analysis is often used [38]. In all these examples the R, G or B intensity is used as the quantitative analytical signal. In some cases other color spaces have been tested with good results, as is the case of CIE L*a*b* used by Suzuki *et al* [10-12] for semiquantitative determination of different analytes. The Hue coordinate has been used to characterize and detect flames from digital images and video. The subtractive CMYK and the hue oriented HLS were both used by Campos *et al.* [28,39] for mercury determination. This is the only occasion, to the best of our knowledge, in which the H coordinate of the HSV color space is used in a conventional chemical quantitative analysis.

The main feature of the HSV color space is the representation of the cognitive color information in a single parameter, the hue component or H. In this way, the color coordinate H from this space can be considered as a qualitative signal, independent of variations in color intensity coming from concentration and optical path. But if the conditions stated above hold, that is chemical equilibrium is displaced by an analyte with at least two distinct colors, it is possible to use the qualitative H coordinate as a quantitative analytical signal. This approach is of particular interest for membrane optical sensors, especially those in the disposable format. These sensors typically lack homogeneity within the same membrane, and even greater variation exists between different sensors thus lowering the precision of the measurement. Here the properties of the H coordinate are studied as an analytical parameter using a disposable K(I) sensor developed in our laboratory [17] and compare the results with other possible analytical parameters that can be derived from images of these sensor membranes.

3. Experimental

3.1. Reagents

Potassium chloride stock solution (1.000 M) was prepared in DI water by exactly weighing analytical reagent grade dry KCl (Aldrich, Steinheim, Germany). Tris and HCl supplied by Sigma (Sigma-Aldrich Química S.A., Madrid, Spain) was used to prepare a pH 9.0 tris(hydroxymethyl)aminomethane 1 M buffer.

The chemicals used for preparing potassium sensitive films were high molecular weight polyvinyl chloride (PVC), the ionophore dibenzo18-crown-6-ether (DB18C6), the plasticizer o-nitrophenyloctylether (NPOE) and tetrahydrofuran (THF) purchased from Sigma, along with the lipophilic salt potassium tetrakis (4-chlorophenyl)borate (TCPB) and the chromoionophore (1,2-benzo-7-(diethylamino)-3-(octadecanoylimino) phenoxazine (liphophilized Nile Blue) purchased from Fluka (Fluka, Madrid, Spain). Sheets of Mylar-type polyester (Goodfellow, Cambridge, UK) were used as support. All chemicals used were of analytical-reagent grade. Reverse-osmosis quality water type III (Milli-RO 12 plus Milli-Q station from Millipore) was used throughout.

3.2. Instruments and Software

Two different instruments were used to acquire images of the K(I) membranes: a) Microtek ScanMaker i700 scanner (Microtek, CA, USA) (Figure 2); b) Olympus E-500 single-lens reflex digital photographic camera equipped with a Zuiko Digital 17.5-45 mm f 3.5-5.6 objective with a 4/3 type full frame transfer primary color CCD detector. A fluorescent photographic light box was used to illuminate the membranes (daylight, 4.66 Klx). The light source and cameras were mounted on a Vibraplane optical breadboard (Kinetic Systems, Inc., Boston, MA), and a digital luxometer (DigiPro F; PCE Group Ibérica, Tobarra, Murcia, Spain) was used for illuminance measurements. To perform the absorbance measurements

of the membranes for comparative purposes, a Hewlett Packard diode array spectrophotometer (model 8453; Nortwalk, CT, US) equipped with a membrane cell holder was used [40].

Figure 2. Scanner used to imaging the sensing membranes in transmission mode

The program used to manage the scanner was Silver Fast Ai provided by Microteck. The images were processed with a set of scripts and functions developed in Matlab r2007b. The acquisition and manipulation of the spectral data were carried out using the Chemstation software package supplied by HP for absorbance measurements. Statistical calculations were performed with Statgraphics software package (Manugistics Inc. and Statistical Graphics Corporation, USA, 1992), and Microsoft Excel (Microsoft Corp., Redmond, WA, USA) was used for general calculations.

The acquisition of the images with the scanner was performed in transmission mode with the membranes placed on the glass surface of the scanner and illu-

minated by a cold cathode fluorescent lamp (2.72 Klux) as shown in Figure 3. The resolution and color depth were set to 300 dpi and either 48 or 28 bits of color respectively. The obtained images were stored in TIFF (True Image File Format) format to avoid loss of information due to compression. The scanner was calibrated each time using an IT8 calibration target which is designed to measure the performance of input devices and generate ICC (International Colour Consortium) profiles that characterize the color space behavior of a device. With a color management system such as Silverfast software, it is possible to make the values obtained from the scanner match the established reference values for the standard colors printed on the card.

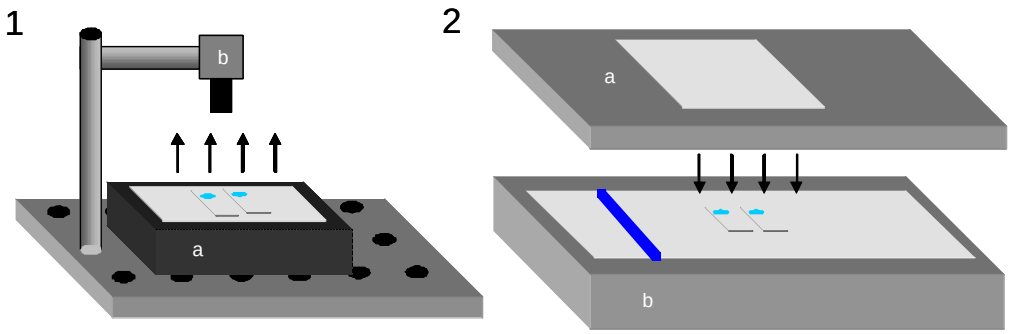

Figure 3. Arrangement used for measurements with 1) a digital photographic camera and 2) a scanner. The light sources are labeled with the letter "a" and detectors are labeled with a "b".

The pictures of sensing membranes using the photographic camera were obtained in a dark room to avoid external light interference and reflections. The digital camera was mounted on an optical table using a rotational and translation stage to position it at the desired angle to the measuring area. Membranes were placed on a light box (4.66 Klux) in order to acquire the images by transmission as

shown in Figure 3. The camera images were in TIFF format with a resolution of 3264x2448 pixels. The white balance setting of the camera was changed depending on the circumstances.

3.3 Disposable Membrane Preparation

Potassium sensing films were produced on a polyester support (14 mm x 40 mm x 0.5 mm) by spin-coating a cocktail of 26.0 mg of PVC, 63.0 mg of NPOE, 0.8 mg of DB18C6, 1.3 mg of chromoionophore and 1.1 mg of TCPB in 1.0 mL of freshly distilled THF [17]. Membranes of different thickness were prepared by using different cocktail volumes (10, 15, 20, 25 and 40 μL) while maintaining a constant membrane diameter of 12 mm. The calculated membrane thicknesses were 1.4, 2.0, 2.7, 3.4 and 5.5 μm, respectively. Membranes without spin coating were produced by simply pipetting 20 μL of the same cocktail previously described onto the polyester support. The shape of the sensing area was nearly circular at 12 mm in diameter.

3.4 Response evaluation

The responses of membrane sensors were evaluated at room temperature using 11 K(I) standard solutions with concentrations ranging from $1.0x10^{-7}$ to $1.0x10^{-1}$ M, buffered with pH 9.0 Tris buffer ($2x10^{-2}$ M). Sensors were activated by introducing them for 3 min into $1.0x10^{-2}$ M HCl and afterwards were equilibrated without shaking for 3 min in the standard or unknown solution. After reaction, the sensor was removed from solution and imaged using the scanner or photographic camera. For comparative purposes the absorbance was measured using a spectrophotometer. In addition to the potassium solutions, the absorbance of the membranes at 660 nm were measured after reacting in $1.0x10^{-2}$ M HCl and $1.0x10^{-2}$ M

NaOH. The values of the fully protonated and deprotonated forms of the chromoionophore were then used to calculate the fraction of protonated indicator, 1-α.

3.5. Matlab Processing

All images were processed using routines in the Matlab programming environment. After the image files were opened and read into memory as separate RGB channels, the first step, referred to here as masking, was to determine which pixels are parts of the colored membrane and which are not. In the first step of this process each channel was normalized independently of each other. Thus the resulting values for R, G, and B range from 0 to 1. After normalization the difference between the channels that produce the maximum and minimum values was then determined for each pixel in the image. These differences were then compared to the maximum observed difference in the entire image multiplied by some threshold fraction, where pixels with greater differences were interpreted as colored and pixels with smaller differences were interpreted as grey background. The value used for all images discussed here was 0.3. Larger values result in a more selective mask that interprets more pixels as being grey rather than colored. Adjustment of this value is only necessary when the sensor membranes are very thin or diluted (decreasing the threshold includes the pixels that are almost white) or when the white balance has not been properly corrected (increasing the threshold excludes the pixels not part of the sensor material that appear colored). It should be noted that although the threshold value influences which pixels are included in subsequent steps, a minimum size restriction (see below) makes large miscategorization of the pixels obvious and correctable, while small changes in the number of included pixels have no effect on the most frequently occurring value.

After each pixel was sorted into a colored or non-colored category, the image was then divided into smaller sub-images, one for each membrane in the image. This process searched the image for entire rows and columns that did not con-

tain colored pixels. In this way the image was cut into smaller rectangles that contain colored pixels. Images that contained a sufficient number of colored pixels (typically 16,000 or more) were retained, and the process was repeated twice more so that there was a single membrane per rectangle. Because the membranes are circular and the cuts were vertical and horizontal, the cut images have corners that contained non-colored pixels. These pixels could be used in a subsequent step to rebalance the color channels relative to each other to control the appearance of white in the image.

After masking and slicing, the RGB channels for each sub-image were then scaled. Two different methods were used to scale each channel to values between 0 and 1. In the first method, each channel was divided by the same number, which is the maximum possible value for a channel, 255 for 8-bit color depth or 65,535 for 16-bit color depth image. The second method used different values for each of the channels, and affects the white balance of the image. This method was important when processing images taken with the digital camera as discussed later, but for images from the scanner, both methods gave equivalent results. Here, each channel was divided by the maximum value observed for that channel in the white spaces in the corners of each of the squares. After these steps, the scaled RGB values were the basis for all of the analytical parameters considered here.

4. Results and Discussion

4.1. Modeling Results

Unlike RGB intensity, hue is largely independent of the concentration or path length of the absorbing species. It is primarily this insensitivity that gives H its superior precision when quantifying data from bitonal optical sensors, where the quantification of the analyte is based on the change in the color of the sensor material. For molecules that have different absorptivities in all three color channels,

this path/indicator concentration dependence is more pronounced than in molecules that have two color channels that are similar to each other. In an effort to further reduce or eliminate the path/concentration dependence of hue, an alternate method of calculating H based on absorbance was devised which is here designated as H'. The calculation of H' is shown in eq. 4 where A_R, A_G, and A_B are the negative logarithms of the red, green, and blue channels respectively after the intensity is scaled to values between 0 and 1; A_{max} and A_{min} are the channels with highest and lowest absorbance.

$$H' = \begin{cases} \left(\dfrac{A_B - A_G}{A_{\max} - A_{\min}} + 0\right) \Big/ 6 & if\ \min = A_R \\ \left(\dfrac{A_R - A_B}{A_{\max} - A_{\min}} + 2\right) \Big/ 6 & if\ \min = A_G \\ \left(\dfrac{A_G - A_R}{A_{\max} - A_{\min}} + 4\right) \Big/ 6 & if\ \min = A_B \end{cases} \quad (4)$$

* *if* H' *is less than* 0 *then add* 1 *to* H'

The values of H, based on RGB intensity, and H', based on RGB absorbance, converge as the indicator concentration approaches zero.

In order to predict the values of H and H' in the presence of polychromatic light, an existing polychromatic modeling approach [41] was adapted to include calculations in the HSV color space. In this approach the molar absorptivity (ε), incident intensity (P_0), and spectral responsivity of a channel (S_I) are all functions of wavelength, and each discrete wavelength can be treated as a monochromatic case. The intensities of the RGB channels are calculated according to eq. 5 where b is pathlength and c is indicator concentration.

$$R = \frac{\sum_{\lambda} P_O(\lambda) 10^{-\varepsilon(\lambda) bc} S_R(\lambda)}{\sum_{\lambda} P_O(\lambda) S_R(\lambda)} \tag{5a}$$

$$G = \frac{\sum_{\lambda} P_O(\lambda) 10^{-\varepsilon(\lambda) bc} S_G(\lambda)}{\sum_{\lambda} P_O(\lambda) S_G(\lambda)} \tag{5b}$$

$$B = \frac{\sum_{\lambda} P_O(\lambda) 10^{-\varepsilon(\lambda) bc} S_B(\lambda)}{\sum_{\lambda} P_O(\lambda) S_B(\lambda)} \tag{5c}$$

For this model the incident light source was assumed to be homogeneous with an intensity of 1 at all wavelengths. The spectral responsivities for each of the three color channels were taken from the data sheet for a Hamamatsu S9706 CMOS RGB detector. By summing up the product of the monochromatic incident intensity and spectral responsivity at each wavelength, a numerical estimate of the total possible light intensity in a particular color channel is obtained. This value is then divided into the sum of the product of the monochromatic incident intensity and spectral responsivity now attenuated by the transmission of the indicator molecule to obtain the polychromatic transmission of a color channel. Once the theoretical values for RGB intensities (scaled between 0 and 1) are obtained, the values for H and H' are then calculated using eqs 4a and 5.

Results of this polychromatic model for both the acid and base forms of liphophilized Nile Blue are given in Figure 4.

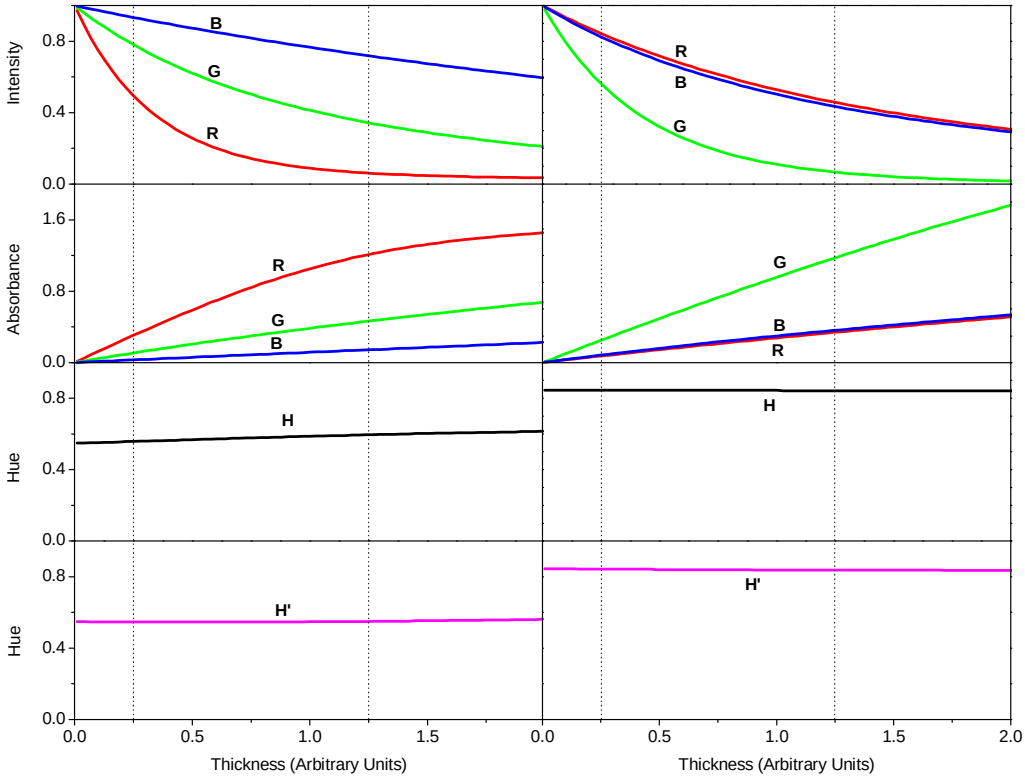

Figure 4. Modelling results for the RGB intensities and Hue parameters. This model assumes homogenous illumination intensity over the entire visible region of the spectrum and spectral responsivities for each of the three color channels approximately equivalent to a Hamamatsu S9706 CMOS RGB detector. The left column shows results for the (blue) acid form of the chromophore Nile Blue, and the right hand column has results for the (magenta) base form of the chromophore. The results shown in the first row are RGB intensities. The results in the second row are the RGB absorbances calculated by taking the negative log of the RGB intensities. The third and fourth rows show the results for H and H' respectively

The left-hand column shows calculated values for the blue acid form of the indicator and the right-hand column has values for the magenta base form. In the first row of the figure, the RGB intensity data calculated using eq. 2 are shown as the pathlength is increased from 0 to 3 (arbitrary units). Here the exponential relationship between indicator concentration/pathlength and the RGB intensity is evident. The second row in the figure shows the theoretical values for the absorbance of the red, green, and blue channels calculated by taking the negative logarithm of the intensity data. The familiar non-linear behavior is observed due to the effects of polychromatic radiation [41]. The third and fourth rows of the figure show the theoretical values for H and H' calculated from RGB intensity. Both H and H' exhibit some dependence on indicator amount/pathlength due to saturation of a color channel in the case of H or non-linear effects of polychromatic radiation in the case of H'. Both effects are predicted to be more pronounced for the base form of the indicator than the acid form which can be seen by comparing the slopes of the lines in the left-hand column with those in the right-hand column. In the acid form, the intensities of the red and blue color channels are similar. This condition makes the H and H' values less susceptible to changes in amount/path. Clearly, the modeling data for these parameters predict that the H and H' parameters will be less sensitive to changes in membrane thickness and indicator amount than the intensity or absorbance parameters.

4.2 Experimental Results

A sensing membrane for K(I) based in ionophore-chromoionophore chemistry that changes color from blue (H = 0.560) in the absence of potassium to magenta (H = 0.812) in the presence of potassium (Figure 1) was selected to study the characteristics and possibilities of various analytical parameters. For these types of sensors the position of acid-base equilibrium coupled to analyte complexation with ionophore is calculated from an optical parameter coming from one of the chemical

forms in equilibrium. The usual analytical parameter is the degree of protonation, 1-α, defined as the ratio of protonated chromoionophore to its analytical concentration C_C, obtained from absorbance [19], fluorescence [42], reflectance [43], transflectance [18], refractive index [44], and even one RGB channel [6]. For any optical measurement, 1-α is calculated as shown in eq. 6, where X is the value of the analytical parameter for a given measurement, and X_{HC^+} and X_C are the values coming from fully protonated and deprotonated chromoionophore species.

$$1-\alpha = \frac{[HC^+]}{[C]_o} = \frac{X - X_C}{X_{HC^+} - X_C} \tag{6}$$

Alternatively, other analytical parameters have been used for calibration purposes instead of the normalized value 1-α, such as the direct absorbance value [45], reflectance [46] and fluorescence intensity [47]. Normalized or relative signals are more convenient for sensor measurements and calibration because they avoid sensor-to-sensor variations and indicator photobleaching, although they involve measuring optical signals related to fully protonated and deprotonated species in addition to the signals from the sample or standards. For disposable sensors the use of normalized signals is cumbersome and requires the acquisition of different measurements with the same sensor.

In this study the analytical parameters were obtained from imaging devices such as scanners or digital cameras instead of conventional optical instrumentation. The RGB intensity values from the image were used as the basis to calculate potential analytical parameters including H, H', RGB absorbances and different RGB absorbance ratios. A typical image scanned at 300 dpi resolution contained approximately 16,000 pixels. In order to obtain a single value for a parameter from an image of a sensing membrane, the most frequently occurring value was selected.

Histograms of the RGB color channels, H, and H' are shown in Figure 5 with data from an image of the acid form of the indicator shown as a solid line and

data from the base form shown as a dashed line. The first row of the figure shows the Red, Green, and Blue intensity channels. The broad distribution in intensity values (resulting in short and wide peaks in the first row of histograms) is attributed primarily to variations in membrane thickness. During the spin coating process the outer edge of the circular membrane becomes thicker than the center, resulting in the bi-modal distribution of values seen in the first row of Figure 5. The second row of Figure 5 shows the values for H and H' for the same images. As predicted by the modeling calculations (section 3.1), the values for the hue based parameters are more narrowly distributed than the RGB intensity values, resulting in much taller and narrower peaks in the histogram. Also in confirmation of the model, the values for H and H' of the acid form of the indicator are slightly more widely variable than those for the base form of the indicator as can be seen by comparing the widths of the solid lines to those of the dashed lines. Because the pixels in the image of a single membrane have similar values for the hue based parameters, it allows us to extract a singular value (the mode) that is clearly representative of the entire membrane. Thus H and H' have superior precision and are better suited for quantification.

4.3. Influencing factors on H coordinate

The precision of the H value was compared with the precision of other analytical parameters that can be derived from an image along with the influence of different factors (such as membrane thickness) on the resilience of these parameters. First the precision of the intra- and inter-membrane measurements was considered, and then the influences of membrane thickness, indicator concentration, membrane making procedure, and the use of different imaging devices were studied. These deliberate changes were made in the experimental conditions in order to evaluate how robust the possible analytical parameters are by measuring their insensitivity to alterations in the operating conditions [48].

In order to compare the robustness of different color coordinates for the quantitative determination of an analyte, a quantitative measure of it, here designated Rb, was devised according to eq. 7.

$$Rb = \frac{Max_{avg} - Min_{avg}}{s_{pooled}} \tag{7}$$

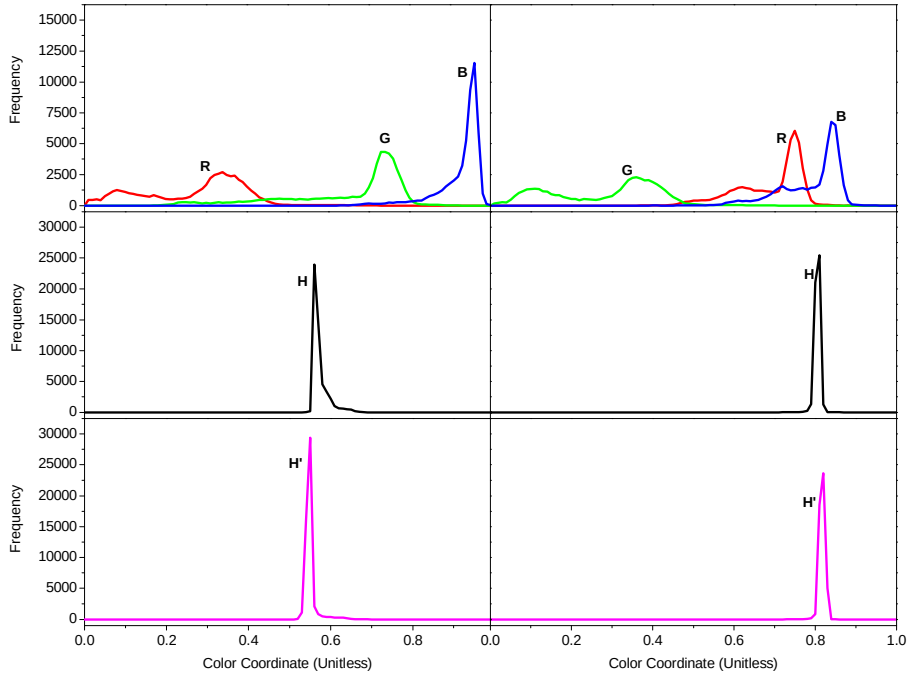

Figure 5. Experimental histograms for the RGB intensities and Hue parameters. The aggregated histograms for 4 distinct membranes are show here. The left column shows results for images taken after equilibration with 1.0×10^{-2} M HCl, and the right hand column has results for 1.0×10^{-2} M NaOH. The results shown in the first row are RGB intensities. The second and third rows show the results for H and H' respectively. Note that the scale for the first row (RGB intensity data) is exactly ½ that of the second and third rows so that details can be more easily observed.

In eq. 7, Max_{avg} is the average signal for all membranes that were exposed to the solution that gave the largest value and Min_{avg} is the average signal for all membranes in the solution that gave the smallest value. For example the minimum H value of 0.56 is obtained when the indicator is in the acid form and the maximum value of 0.82 is obtained when the indicator is in the base form. The pooled standard deviation for all of the membranes studied is s_{pooled}. Thus Rb is a measure of the sensitivity of the analytical parameter to changes in indicator speciation divided by an estimate of the precision of a particular measurement, or how many standard deviations are present in the range of possible values. To calculate the figure of merit Rb, a set of experiments was performed using different membranes and conditions, acquiring the images of multiple membranes after exposure to at least three K(I) concentrations ($5.0x10^{-5}$, $5.0x10^{-4}$ and $5.0x10^{-3}$ M). An increase in Rb indicates either greater change in the analytical parameter as the membrane is exposed to different solutions or smaller differences between individual sensor membranes in the same solution; thus larger values indicate a parameter that is better suited for quantification.

4.4. Membrane-related factors

The precision of H measurements coming from replicate membrane images was studied. From H values of 10 different membranes measuring three different K(I) concentrations each, the coefficient of variation CV ranges between 0.2 and 0.4% as shown in Table 1. These values are similar to values obtained when the same membrane is sequentially exposed to a solution and imaged ten times (n: 10, CV: 0.3%). The results using H are much better than those obtained when using 1-α calculated from absorbance measurements which ranges usually from 4 to 10% [18].

Thickness dependence. One of the reasons for the lack of precision in intensity-based analytical parameters is the influence of membrane thickness. So the

influence of thickness was studied by preparing a set of sensing membranes using different volumes of the same cocktail (10, 15, 20, 25 and 40 μl) but maintaining a constant spot diameter of 12 mm. Thus, the calculated thickness varies between 1.4 and 5.5 μm. The results from 10 different membranes of each thickness, equilibrated with three different K(I) concentrations each are presented in Table 1. The H value for each K(I) concentration is almost independent of the membrane thickness, and the results do not show bias when the membrane thickness increases. Considering the precision in H using all membranes of different thickness (50 membranes) for the three K(I) solutions, the CV values are 0.86, 0.55, and 1.01%, respectively, for the H values obtained for each solution. Consequently, the small variations in membrane thickness can be avoided by the use of H parameter, thus improving the sensor-to-sensor precision.

Shown in Table 2 are the Rb values for some of the possible analytical parameters that can be derived from an image of the sensor membrane. The values are calculated from a set of 17 membranes with 5 different thicknesses. This set of membranes was exposed to 5 different solutions sequentially (acid, base, and three K(I) solutions) for a total of 85 distinct images. Comparing the results obtained from the H parameter with other possible analytical parameters using the Rb value, it is clear that Rb for the hue related parameters (H, H') are the highest. As the thickness is varied, the single channel RGB intensity and RGB absorbance values are almost useless – all giving fewer than 3 standard deviations within the possible range of values. Only the ratios of the RGB absorbances are able to provide some quantitative information, but these are still approximately 2 times inferior to H.

Indicator concentration dependence. The amount of chromoionophore in the sensor membrane is another influential factor on the efficacy of analytical parameters. To study the influence of chromoionophore concentration on H, 20 membranes were prepared using two different cocktails, 10 with the concentrations described in the Experimental section and another 10 with half of the concentration

in all constituents previously used. Note that this variation in chromoionophore concentration has the same effect as variations in membrane thickness discussed above, and only two cases were studied to verify the predicted results. As shown in Table 1, the CVs calculated from all 20 membranes equilibrated in the same solution were 0.21, 0.24 and 1.06% for each K(I) solution. Similar to previous results, there is no bias with the increase in indicator concentration. The results considering the Rb parameter are shown in Table 2, and again the hue based parameters are superior to the others studied.

Membrane preparation. In order to check the independence of the H parameter from the procedure used for membrane preparation, a set of 10 sensors was prepared manually without using the standard spin coating procedure. Using a micropipette, 20 μL of cocktail was cast onto the Mylar support trying to obtain a circular spot. The results, shown in Table 1, were reasonably similar to those previously obtained, although the H values obtained are greater than those from spin-coated membranes. The inter-membrane precision of these membranes was also calculated, and the CV values were 0.75, 0.14 and 0.25%. The manual preparation of membranes only results in a difference between 1.6 and 3.4 % with respect to spin-coated membranes. This result is favorable considering the poor reproducibility of the preparation system used. A comparison of Rb values for a data set that included the two preparation techniques is included in Table 2. Here the Rb value for H is smaller than the thickness or concentration studies, but it still shows approximately twice as many standard deviations over the range of possible values than its nearest competition.

The H coordinate is insensitive to variation in thickness, indicator concentration and even membrane preparation technique. For this reason the traditionally qualitative parameter can overcome the differences between lots, and is superior to the usual intensity-based parameters for quantitative measurement of one-shot sensors.

Table 1. Influence of different factors on the precision of the H measurement

	$[K^+] = 5.0x10^{-5}$ M	$[K^+] = 5.0x10^{-4}$ M	$[K^+] = 5.0x10^{-3}$ M
Thickness	**Hue Coordinate**		
1.4	0.585±0.001	0.649±0.005	0.749±0.001
2.0	0.582±0.001	0.644±0.001	0.740±0.001
2.7	0.588±0.006	0.647±0.002	0.738±0.003
3.4	0.585±0.001	0.640±0.001	0.733±0.001
5.5	0.596±0.002	0.646±0.003	0.730±0.001
CV	0.86%	0.55%	1.01%
Indicator Concentration	**Hue Coordinate**		
Diluted	0.591±0.003	0.645±0.005	0.753±0.005
Normal	0.589±0.002	0.649±0.005	0.742±0.003
CV	0.21%	0.24%	1.06%
Membrane Making Procedure	**Hue Coordinate**		
Spin coating	0.588±0.006	0.647±0.002	0.738±0.003
Hand made	0.605±0.004	0.669±0.001	0.750±0.002
White Balance	**Hue Coordinate**		
Auto	0.592±0.001	0.614±0.006	0.762±0.002
Sun light (5300K)	0.558±0.001	0.626±0.005	0.778±0.013
Cloudy(6000K)	0.576±0.002	0.606±0.009	0.781±0.001
Lamp(3000K)	0.566±0.003	0.674±0.003	0.763±0.003
Fluorescent(4000K)	0.572±0.003	0.625±0.001	0.757±0.001
CV	2.3%	3.7%	1.7%
Average CV*	1.10%	1.49%	1.25%

* The average CV is calculated from data sets that include variations in thickness, concentration, and white balance setting.

Table 2. Robustness (Rb) of various analytical parameters as experimental conditions (e.g. membrane thickness) is varied.

Analytical Parameter	Rb values			
	Membrane Thickness	**Indicator Concentration**	**Membrane Making Procedure**	**White Balance**
R	2	2	9	14
G	2	2	3	11
B	2	2	6	9
Ar	2	2	5	10
Ag	2	1	3	9
Ab	2	2	6	9
Ar/Ag	5	27	3	13
Ab/Ar	24	15	18	14
Ag/Ab	1	2	1	1
H	45	**44**	**34**	**24**
H'	**56**	37	8	22

4.5. Influence of imaging device

All the measurements performed in the previous section were acquired with a calibrated scanner working in transmission mode and characterized to use an internal light source in such a way that the sensing membrane was illuminated in a reproducible manner. In order to study the influence of the imaging device on the analytical parameters, a digital photographic camera and fluorescent light box (used to view color slides) were used so that the measurement was still made in transmission mode. Additionally, the use of this device under less controlled conditions is a good test for the ruggedness of the H parameter relative to the other analytical parameters under consideration.

Membrane images for a single experiment were acquired under the same conditions. The camera was set to macro mode and focused manually, and the membranes were lit from below with a fluorescent photographic light box as shown in Figure 3. The results, given in Table 1 and obtained using the same experimental procedure as previous studies (10 membranes, 3 concentrations of K(I) standards), are very similar, showing differences between 0.5 and 0.8 % with respect to previous scanner values. Interestingly, the CV calculated is of the same order of magnitude of that obtained with scanners.

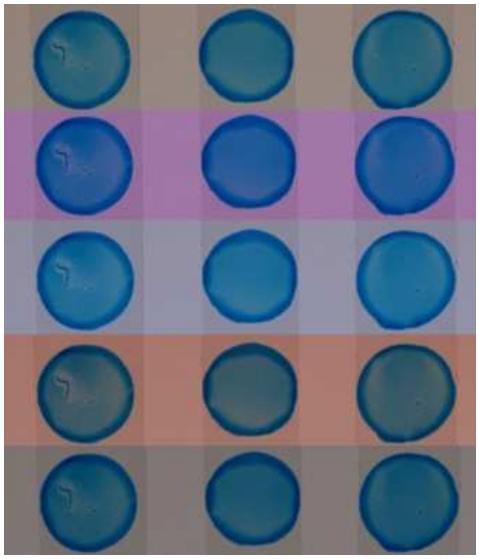

Figure 6. Images obtained using different white balance settings. The white balance settings of the Olympus E-500 camera used were Auto, Sun light (5300K), Cloudy (6000K), Lamp (3000K), and Fluorescent (4000K).

The influence of different lighting conditions on the H values obtained from photographic cameras was also studied. Because the work presented here is focused on images from transmitted light, the illumination (such as sunlight, camera flash, fluorescent, or tungsten lighting) was not varied. Instead, to simulate

different lighting conditions, different white balance settings for the camera were used. By maintaining a constant light source and changing the white balance setting, the responsivity of the camera's sensors to different color channels changes, resulting in photos that appear as if they were illuminated differently. The images resulting from white balance settings of sun light (5300K), cloudy (6000K), lamp (3000K), and fluorescent (4000K) are given in Figure 6. These images show dramatic differences, but the resulting H values (Table 1) show differences ranging only between 3 and 10%. Additionally, the coefficient of variation for each concentration including all membranes and all white balance settings ranges from 1.5 to 3.6%. The Rb value for the H parameter, as shown in Table 2, is more than two times superior to any of the other analytical parameters considered.

Thus it is possible to acquire images for analytical purposes using different imaging devices and under different lighting conditions and still get stable values for the H parameter.

4.6. Analytical parameter

The degree of deprotonation, 1-α, can be calculated using H as shown in eq. 7. Advantages of 1-α include its insensitivity to sensor-to-sensor variations and indicator photobleaching along with its fit with an established theoretical model [19]. The disadvantage is the necessity to measure the signals from the fully protonated and deprotonated species in addition to the signal coming from the sample or standard. The results using 1-α based on the absorbance measured with a spectrometer and the H coordinate measured with the scanner are shown in Figure 7 along with a comparison to theoretical values. The results are similar to those obtained for the same one-shot sensor when absorbance [17], transflectance [18] or RGB color coordinates [6] are used to calculate the degree of deprotonation.

With an interest in simplifying the experimental procedure to avoid the use of calibrants for the protonated and deprotonated forms of the chromoionophore, the reproducibility of the H parameter was examined for both the fully protonated and deprotonated forms of chromoionophore. A total of 215 membranes prepared over the course of one year using different cocktails for sensor preparation and different HCl and NaOH calibrants were studied. The coefficients of variations were 0.4% for the acid form and 0.7% for the basic form (H_{HC^+} = 0.560±0.002; H_C = 0.812±0.006). Thus, it is possible to calculate 1-α from only one experimental H value considering the other two values (H_{HC^+}, H_C) as constant.

Because the H parameter is bound between values of 0 and 1 (eq. 2) and there is small sensor-to-sensor variation, it is possible to use it directly in a calibration for potassium concentration. Once again, the H coordinate gives better precision (0.2-0.4%) than other calibration parameters including 1-α calculated from absorbance (4.2-10.7%), A/A_{HC^+} (1.6-3.1%) [49] and A/A_C (1.6-5.2%) [50]. The two last values were used in a portable photometer that uses pretreated sensors in their acidic form [49] or basic form [50]. The use of H directly simplifies the procedure, only requires one measurement, and avoids the absorbance measurement before and after equilibration with calibrants.

To obtain the calibration function 10 different membranes were used measuring 11 standards each ranging from 1.0×10^{-7} to 1.0×10^{-1} M. The resulting sigmoidal function has the same shape as the conventional 1-α graphs and is shown in Figure 7. The analytical range can be estimated by fitting a straight line to the region of maximum slope to obtain a linear function, H = 0.94(±0.02) + 0.082(±0.007) [K(I)]. This relationship has an R^2 = 0.9911 and a limit of detection of 3.64×10^{-5} M, obtained from the intersection of the linear calibration function and the linearized background at low concentration. This detection limit is similar to that calculated from absorbance measurements (1.25×10^{-5} M) [17].

Additionally, the dynamic range of the procedure can be increased by fitting results to the sigmoidal relationship given by eq. 8 where a_0 to a_3 are adjusting coefficients.

$$H = a_2 + \frac{a_2 - a_1}{1 + \exp\left(\frac{\left([K(I)] - a_o\right)}{a_3}\right)} \tag{8}$$

The dataset fit well (a_0 = -2.95; a_1 = 0.564; a_2 = 0.803; a_3 = 0.637) showing an excellent correlation (R^2 = 0.9994). The experimental values and calculated fit are labeled with a as Hue in Figure 7. The high precision with which H can be measured allows for the improvement of the analytical range and the detection limit of the procedure. Using the IUPAC criteria (3s) for the lower and upper limits, a wider measurement range ($4.5 \cdot 10^{-6}$ M to $1.0 \cdot 10^{-1}$ M) is achieved.

The precision of the procedure using different one-shot sensors was obtained at three potassium concentrations, namely 5.0×10^{-5}, 5×10^{-4} and 5×10^{-3} M using 10 replicates each. The CV values were 0.2, 0.4, and 0.4%, respectively, using H as the calibrating parameter and 4.9, 8.0, and 15.1% when using 1-α based on absorbance measurements. These results show that the precision is much higher using H than with traditional absorbance measurements due to the independence of H to the thickness and concentration of chromoionophore in the membrane.

The precision of the procedure using different one-shot sensors was obtained at three potassium concentrations, namely 5.0×10^{-5}, 5×10^{-4} and 5×10^{-3} M using 10 replicates each. The CV values were 0.2, 0.4, and 0.4%, respectively, using H as the calibrating parameter and 4.9, 8.0, and 15.1% when using 1-α based on absorbance measurements. These results show that the precision is much higher using H than with traditional absorbance measurements due to the independence of H to the thickness and concentration of chromoionophore in the membrane.

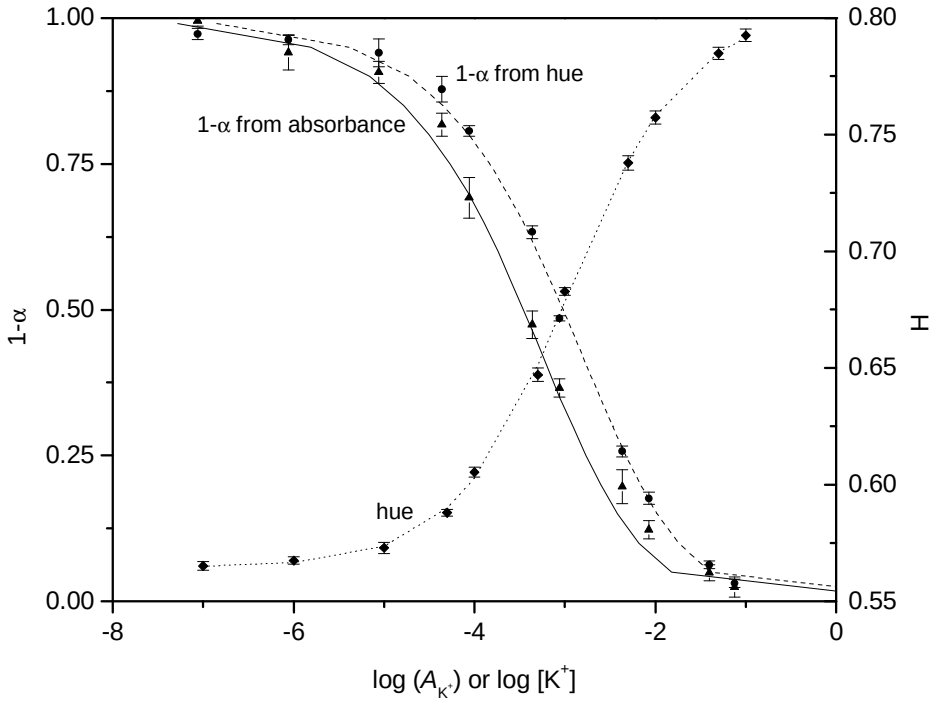

Figure 7. Calibration functions using different analytical parameters. The triangular data points are 1-a values calculated from absorbance (K_{exc}=2.57·10^{-7}); The circular data points are 1-a values calculated from H (K_{exc}=9.35·10^{-8}); The diamond data points are H parameter directly. The solid and dashed lines represent the results of a theoretical calculation based on eq. 1. The dotted line is the best fit for the experimental data using eq. 8.

The precision of the H coordinate (CV of 0.2 to 0.4%) is evident when ompared with other techniques using the same sensor material but a different type of optical measurement. With a diode array spectrophotometer the CV values range between 3.3 and 7.7% [17]; using transflectance measurements they are from 2.4 to 7.9 % [18], and with CIELAB cylindrical coordinates coming from spectroradiometric measurements they are between 2.8 to 3.5 % [51]. With a portable elec-

tronic photometer, the CV values range between 1.6 and 2.1 % [49], from 0.4 to 1.8 % using scanometric measurements and RGB coordinates [6], and from 2.3 to 3.7 % working with a black and white CCD camera and RGB [52]. The calibration using the H value is obtained directly without the need for any type of normalization. It is not necessary to obtain the H values for the acidic and basic forms of the chromoionophore, thus simplifying the procedure and requiring less time and solutions to calibrate.

To test the usefulness of the H-based procedure, it was applied to waters of diverse provenance (spring, mineral, tap) from Andalucia, Spain, for potassium content. H values for the sensors were determined, and the concentration of potassium was calculated using H directly as the analytical parameter. The method was validated by comparison with results from atomic absorption spectroscopy. The results obtained using H were comparable to the established techniques as shown in Table 3.

Table 3. Determination of K(I) in different types of waters using AAS as a reference method.

Water Sample	Sensor	Reference	p-value
Tap (Algeciras)	7.3×10^{-5}	1.1×10^{-4}	0.4330
Tap (Torremolinos)	6.1×10^{-5}	3.8×10^{-5}	0.7368
Tap (Otura)	6.3×10^{-5}	6.2×10^{-5}	0.4066
Well (Otura)	6.8×10^{-5}	6.8×10^{-5}	1.0000
Mineral water 1	5.7×10^{-5}	6.0×10^{-5}	0.3558
Mineral water 2	5.0×10^{-5}	5.2×10^{-5}	0.0522
Mineral water 3	5.3×10^{-5}	4.6×10^{-5}	0.1301

5. Conclusions

The use of hue coming from images of sensing membranes and quantified as the H coordinate from HSV color space is proposed as an analytical parameter with the aim to improve the robustness of one-shot sensors as opposed to the usual intensity-based measurements. A traditionally qualitative color property is used as an analytical parameter for quantitative determination of chemicals based in the use of bitonal optical sensors that change their color by reaction. The primary advantage of this approach is its high precision, between 4 and 10 times superior CV, as compared to other optical signals such as absorbance. Additional advantages include insensitivity to changes in membrane thickness, indicator concentration, and membrane preparation procedures that overcome the differences between lots. The one-shot sensor for potassium highlights the small influence of the imaging device used for image acquisition which opens many interesting analytical possibilities. Additionally, the calibration using the H value can be obtained directly, without the need of any type of normalization as is usual in this type of optical one-shot sensors. It is not necessary to obtain the H values for the acidic and basic forms of the chromoionophore, which greatly simplifies the establishment of the analytical function.

The use of commercial imaging devices such as digital cameras or desktop scanners to obtain analytical information from one-shot (multi)sensors has many advantages over traditional spectrometers. These devices are relatively inexpensive, easy to use, and ubiquitous. An optical sensor can be quickly photographed just after exposure to a sample, and multiple membranes can be included in a single picture rather than being analyzed separately. If the sensing chemistry and calibration are sufficiently developed, it would be possible to send a set of membranes on a transparent card that could be exposed to a sample and then imaged by the end user. Because the technique is robust and all of the sophistication is contained with-

in the image processing program, an untrained person with no specialized equipment can easily obtain useful measurements.

Acknowledgements

We acknowledge financial support from *Ministerio de Educación y Ciencia, Dirección General de Enseñanza Superior* (Spain) (Projects CTQ2005-09060-CO2-01, CTQ2005-09060-CO2-02, CTQ2009-14428-C02-01) and *Junta de Andalucia* (Proyecto de Excelencia P06-FQM-01467).

6. Conclusión

En este capítulo se demuestra la posibilidad de utilizar dispositivos de captura de imágenes, operando en modo transmisión, para la obtención de información analítica. Dichos dispositivos pueden ser una cámara fotográfica convencional o un escáner de sobremesa. Con ellos es posible la digitalización de membranas sensoras, provenientes en este caso de sensores de un solo uso para la determinación de potasio.

Una vez comprobado que dicho uso es posible, se ha propuesto el empleo de una coordenada de color diferente de los canales del espacio RGB, que es el más utilizado. Se ha llevado a cabo un estudio teórico del comportamiento de dicho parámetro H del espacio de color HSV antes de su utilización práctica.

El estudio teórico realizado nos muestra que este parámetro analítico, al contrario de lo que ocurre con los canales RGB, presenta una gran insensibilidad frente a variaciones tanto del dispositivo de medida como de condiciones de iluminación o grosor, concentración de indicador o modo de fabricación de la membrana. Por tanto, como demuestra el coeficiente de robustez calculado para cada una de las condiciones, el parámetro H es el más estable frente a todo este tipo de variaciones de condiciones de un conjunto de posibles parámetros analizados, obteniendo unos valores de coeficiente de variación medio de todas estas pruebas del 1.2%

No sólo presenta ventajas frente a otras coordenadas de color sino que además, debido a la alta precisión que se obtiene con este parámetro, pues sólo medimos información tonal y por tanto variaciones en intensidad de color entre membranas no afecta al parámetro H, es posible su uso de forma directa sin necesidad de normalización de la señal mediante el empleo del parámetro 1-α, como es habitual en este tipo de sensores. El uso directo de este parámetro además nos va a permitir una simplificación del procedimiento de trabajo con estos sensores, ya que para el cálculo del parámetro 1-α son necesarias tres medidas, a saber: del sensor

completamente virado a forma ácida la primera, una segunda del sensor en forma básica y, por último, del sensor tras reacción con el problema conteniendo el analito. Sin embargo, al ser pequeñas las diferencias de sensor a sensor, se simplifica el procedimiento, pasando de ser necesarias tres medidas a sólo una. Además también debido a la alta precisión de las medidas, es posible emplear una ecuación sigmoidal tipo ecuación de Boltzman para calibrar el sensor y así alcanzar un límite de detección más bajo, $4.5 \cdot 10^{-6}$ M, frente al obtenido con medidas de absorción, 2.0×10^{-5} M o transflexión, 1.9×10^{-5} M.

Hablando en términos de precisión, de nuevo tenemos mejores resultados que los obtenidos con otros parámetros analíticos. En el caso de la coordenada H, la precisión de las medidas en términos de coeficiente de variación varía entre 0.2 y 0.4%, frente a los resultados obtenidos usando un espectrofotómetro, 3.3-7.7%, medidas de transflectancia, 2.4-7.9 %, fotómetro portátil, 1.6-2.1% o medidas escanométricas usando coordenadas RGB, 0.4-1.8 %.

7. Bibliografía

1. E. Hita Villaverde. El mundo del color, 1 ed., Editorial Universidad de Granada, Granada, 2001

2. G. Wyszecki, W.S.Stiles. Color Science: Concepts and Methods, Quantitative Data and Formulae, 2nd Edition ed., John Wiley & Sons, New York, 1982

3. G. Wyszecki, W. S. Stiles. Color Science: Concepts and Methods, Quantitative Data and Formulae, Wiley Classics Library, Denver USA, 2000

4. M. Kompany-Zareh, M. Mansourian, F. Ravaee, Simple method for colorimetric spot-test quantitative analysis of Fe(III) using a computer controlled hand-scanner, Anal.Chim.Acta 471 (2002) 97.

5. J. Gabrielson, M. Hart, A. Jarelov, I. Kuhn, D. McKenzie, R. Mollby, Evaluation of redox indicators and the use of digital scanners and spectrophotometer for quantification of microbial growth in microplates, J.Microbiol.Methods 50 (2002) 63.

6. A. Lapresta-Fernandez, L.F. Capitan-Vallvey, Scanometric potassium determination with ionophore-based disposable sensors, Sens.Actuators B 134 (2008) 694.

7. J.J. Lavigne, S. Savoy, M.B. Clevenger, J.E. Ritchie, B. McDoniel, S.J. Yoo, E.V. Anslyn, J.T. McDevitt, J.B. Shear, D. Neikirk, Solution-Based Analysis of Multiple Analytes by a Sensor Array: Toward the Development of an "Electronic Tongue", J.Am.Chem.Soc. 120 (1998) 6429.

8. K. Tohda, M. Gratzl, Micro-miniature autonomous optical sensor array for monitoring ions and metabolites 1: design, fabrication, and data analysis, Anal.Sci. 22 (2006) 383.

9. V.V. Apyari, S.G. Dmitrienko, Using a digital camera and computer data processing for the determination of organic substances with diazotized polyurethane foams, J.Anal.Chem. 63 (2008) 530.

10. E. Hirayama, T. Sugiyama, H. Hisamoto, K. Suzuki, Visual and Colorimetric Lithium Ion Sensing Based on Digital Color Analysis, Anal.Chem. 72 (2000) 465.

11. K. Suzuki, E. Hirayama, T. Sugiyama, K. Yasuda, H. Okabe, D. Citterio, Ionophore-Based Lithium Ion Film Optode Realizing Multiple Color Variations Utilizing Digital Color Analysis, Anal.Chem. 74 (2002) 5766.

12. Y. Suzuki, K. Suzuki, Optical sensors for ions and protein based on digital color analysis, Springer Series on Chemical Sensors and Biosensors 3 (2005) 343.

13. K. Danzer, A closer look at analytical signals, Anal.Bioanal.Chem. 380 (2004) 376.

14. K. Danzer. Analytical Chemistry. Theoretical and Metrological Fundamentals, 1 ed., Springer-Verlag, Berlin, 2007

15. D. Citterio, T. Kawada, J. Yagi, T. Ishigaki, H. Hisamoto, S.I. Sasaki, K. Suzuki, Molecular design, characterization, and application of multiinformation dyes for optical chemical sensing IV. Multiinformation dyes with extended spectral sensitivity in the near-infrared spectral range, Anal.Chim.Acta 482 (2003) 19.

16. R. Olivares, M.P. Brungs, H. Liang, Monitoring of slag composition changes by density measurements, Metall.Trans.B 22B (1991) 305.

17. L.F. Capitan-Vallvey, M.D. Fernandez Ramos, M. Al Natsheh, A disposable single-use optical sensor for potassium determination based on neutral ionophore, Sens.Actuators B 88 (2003) 217.

18. I.d. Orbe-Paya, M. Erenas, L.F. Capitan-Vallvey, Potassium disposable optical sensor based on transflectance measurements, Sens.Actuators B 127 (2007) 586.

19. E. Bakker, P. Bühlmann, E. Pretsch, Carrier-Based Ion-Selective Electrodes and Bulk Optodes. 1. General Characteristics, Chem Rev. 97 (1997) 3083.

20. U. E. Spichiger-Keller. Chemical Sensors and Biosensors for Medical and Biological Applications, 1 ed., Wiley-VCH, Weinheim, 1998 p. 1.

21. Maund, Barry. Color. 2006. Metaphysics Research Lab, CSLI, Stanford University. Stanford Encyclopedie of Philosophy.

22. P. Green, W. MacDonald. Colour Engineering: Achieving Device Independent Colour, 2002

23. J. Y. Hardeberg. Acquisition and Reproduction of Color Images: Colorimetric and Multispectral Approaches, Universal-Publishers.com., 2001

24. A.R. Smith, Color gamut transform pairs, Proceedings of the 5th Annual Conference on Computer Graphics and Interactive Techniques (1978) 12.

25. C.N. Reilley, H.A. Flaschka, S. Laurent, B. Laurent, Characterization of the color quality of indicator transition. Complementary tristimulus colorimetry, Anal.Chem. 32 (1960) 1218.

26. C.N. Reilley, E.M. Smith, Chemical applications of complementary tristimulus colorimetry, Anal.Chem. 32 (1960) 1233.

27. S.V. Bannur, S.V. Kulgod, S.S. Metkar, S.K. Mahajan, J.K. Sainis, Protein Determination by Ponceau S Using Digital Color Image Analysis of Protein Spots on Nitrocellulose Membranes, Anal.Biochem. 267 (1999) 382.

28. A.V. Yallouz, R. Calixto de Campos, S. Paciornik, A low-cost non instrumental method for semiquantitative determination of mercury in fish, Fresenius J.Anal.Chem. 366 (2000) 461.

29. A. Abbaspour, A. Khajehzadeh, A. Ghaffarinejad, A simple and cost-effective method, as an appropriate alternative for visible spectrophotometry: development of a dopamine biosensor, Analyst 134 (2009) 1692.

30. D.N. Dani, S.V. Bannur, S.V. Kulgod, J.K. Sainis, Estimation of chlorophyll in leaves using portable digital camera, Physiol.Mol.Biol.Plants 11 (2005) 321.

31. A. Abbaspour, M.A. Mehrgardi, A. Noori, M.A. Kamyabi, A. Khalafi-Nezhad, M.N. Soltani Rad, Speciation of iron(II), iron(III) and full-range pH monitoring using paptode: A simple colorimetric method as an appropriate alternative for optodes, Sens.Actuators B 113 (2006) 857.

32. N. Maleki, A. Safavi, F. Sedaghatpour, Single-step calibration, prediction and real samples data acquisition for artificial neural network using a CCD camera, Talanta 64 (2004) 830.

33. M.C. Janzen, J.B. Ponder, D.P. Bailey, C.K. Ingison, K.S. Suslick, Colorimetric Sensor Arrays for Volatile Organic Compounds, Anal.Chem. 78 (2006) 3591.

34. C. Zhang, K.S. Suslick, A colorimetric sensor array for organics in water, J.Am.Chem.Soc. 127 (2005) 11548.

35. K. Abe, K. Suzuki, D. Citterio, Inkjet-printed microfluidic multianalyte chemical sensing paper, Anal.Chem. 80 (2008) 6928.

36. Y. Shishkin, S.G. Dmitrienko, O.M. Medvedeva, S.A. Badakova, L.N. Pyatkova, Use of a scanner and digital image-processing software for the quantification of adsorbed substances, J.Anal.Chem. 59 (2004) 102.

37. N.C. Birch, D.F. Stickle, Example of use of a desktop scanner for data acquisition in a colorimetric assay, Clin.Chim.Acta 333 (2003) 95.

38. K.S. Suslick, N.A. Rakow, A. Sen, Colorimetric sensor arrays for molecular recognition, Tetrahedron 60 (2004) 11133.

39. S. Paciornik, A.V. Yallouz, R.C. Campos, D. Gannerman, Scanner image analysis in the quantification of mercury using spot-tests, J.Braz.Chem.Soc. 17 (2006) 156.

40. L.F. Capitan-Vallvey, M.D. Fernandez-Ramos, P. Alvarez de Cienfuegos, F. Santoyo-Gonzalez, Characterization of a transparent optical test strip for quantification of water hardness, Anal.Chim.Acta 481 (2003) 139.

41. R. Smith, K. Cantrell, Modeling the effect of polychromatic light in quantitative absorbance spectroscopy, J.Chem.Ed. 84 (2007) 1021.

42. A. Ceresa, Y. Quin, S. Peper, E. Bakker, Mechanistic insights into the development of optical chloride sensor based on the mercuracarborand-3 ionophore, Anal.Chem. 75 (2003) 133.

43. R.H. Ng, K.M. Sparks, B.E. Statland, Colorimetric determination of potassium in plasma and serum by reflectance photometry with a dry-chemistry reagent, Clin.Chem. 38 (1992) 1371.

44. D. Freiner, R.E. Kunz, D. Citterio, U.E. Spichiger, M.T. Gale, Integrated optical sensors based on refractometry of ion-selective membranes, Sens.Actuators B 29 (1995) 277.

45. H. Hisamoto, N. Miyashita, K. Watanabe, E. Nakagawa, N. Yamamoto, K. Suzuki, Ion sensing film optodes: disposable ion sensing probes for the determination of Na^+, K^+, Ca^{2+}, and Cl^- concentrations in serum, Sens.Actuators B 29 (1995) 378.

46. Vogel, P., Thym, D., Fritz M., Mosoiu, D., Test Carried for the Determination of Ions, US 5,211,914, 1993.

47. D. Citterio, M. Omagari, T. Kawada, S. Sasaki, Y. Suzuki, K. Suzuki, Chromogenic Betaine Lariates for highly selective calcium ion sensing in aqueous enviroment, Anal.Chim.Acta 504 (2004) 227.

48. D. C. Harris. Quantitative Chemical Analysis, W.H. Freeman and Company, 2007

49. A.J. Palma, A. Lapresta-Fernandez, J.M. Ortigosa-Moreno, M.D. Fernandez-Ramos, M.A. Carvajal, L.F. Capitan-Vallvey, A simplified measurement procedure and portable electronic photometer for disposable sensors based on ionophore-chromoionophore chemistry for potassium determination, Anal.Bioanal.Chem. 386 (2006) 1215.

50. M.D. Fernandez-Ramos, M. Greluk, A.J. Palma, E. Arroyo-Guerrero, J. Gomez-Sanchez, L.F. Capitan-Vallvey, The use of one-shot sensors with a dedicated portable electronic radiometer for nitrate measurements in aqueous solutions, Meas.Sci.Technol. 19 (2008) 095204/1.

51. A. Lapresta-Fernandez, R. Huertas, M. Melgosa, L.F. Capitan-Vallvey, Colourimetric characterisation of disposable optical sensors from spectroradiometric measurements, Anal.Bioanal.Chem. 393 (2009) 1361.

52. A. Lapresta-Fernandez, R. Huertas, M. Melgosa, L.F. Capitan-Vallvey, Multianalyte imaging in one-shot format sensors for natural waters, Anal.Chim.Acta 636 (2009) 210.

Capítulo 4

Aproximación a lenguas ópticas de un solo uso para iones alcalinos

1. Planteamiento

Una de las cuestiones que suscitan mayor interés en el campo de los sensores químicos son los sistemas multianalito. La aproximación convencional se basa en disponer de un sensor distinto para cada analito de interés, lo que exige preparar un conjunto de receptores específicos para el conjunto de analitos en el problema a través del diseño y síntesis de receptores específicos usando conceptos tipo llave-cerradura [1]. Los inconvenientes de este enfoque se refieren a la dificultad de lograr buena selectividad para analitos similares y al número de sensores necesarios, que crece linealmente con el número de analitos. Por ello, ha surgido un paradigma alternativo de sensado basado en una imitación de la estructura y propiedades de sistemas sensoriales biológicos, en concreto de los sistemas del gusto y olfato de los mamíferos. De esta manera, han aparecido los conceptos de nariz y lengua electrónicas que se han mostrado muy eficaces para tareas de reconocimiento, esto es, para clasificación, identificación y discriminación, abriendo las puertas a una correlación objetiva con los sentidos humanos gusto y olfato [2].

En el caso del olfato, la discriminación (> 10.000 sustancias) se atribuye a un gran número de receptores poco selectivos, de alta reactividad cruzada, en combinación con un procesado de señales en los sistemas nerviosos central y periférico. Para el sentido del gusto el número de receptores -al menos en humanos- es menor y con los cinco tipos existentes se pueden describir y evaluar cuantitativamente el sabor de los alimentos [3], tanto referido a la sensación de sabores básicos como a la impresión global producida por un alimento junto con el olfato y las somatosensaciones [4]. En resumen, el resultado es la fabricación de una “imagen” interna del objeto sensado.

La idea inicial de nariz electrónica surge en 1982 con el trabajo de Persaud y Dodd en Nature [5] y pocos años después se extiende como una consecuencia natural apareciendo el concepto de lengua electrónica para las medidas en líquidos. En general, ambos conceptos suponen el uso de un conjunto (matriz) de sensores no específicos o de baja selectividad que producen señales analíticamente útiles para el análisis de matrices multicomponentes que son tratadas posteriormente mediante procedimientos matemáticos avanzados de procesamiento de señal por reconocimiento de patrones y/o análisis multivariado (redes neuronales, análisis por componentes principales u otros) [6]. Con el uso de estos procedimientos es posible la identificación empleando sensores no selectivos y además se pueden identificar gran número de especies con un pequeño conjunto de sensores. Aunque el nombre de estos dispositivos puede ser diferente, y sujeto a controversia en ocasiones, se ha preferido mantener la denominación de lengua y nariz electrónica a lo largo de esta Memoria de Doctorado.

Una de las características de mayor interés de estos dispositivos es que han permitido abordar problemas analíticos irresolubles con las aproximaciones tradicionales, como son las descripciones cualitativas de productos naturales (café, vino o té) lo que no es rastreable con la simple inspección de constituyentes.

La eficiencia de estos sistemas se puede lograr aumentando la cantidad de información químicamente ortogonal generada por el conjunto. Se puede conseguir este objetivo de varias formas: 1) aumentando el número de sensores en la matriz con materiales de diferente sensibilidad y que usan el mismo principio de transducción; 2) midiendo varias propiedades físicas de cada sensor individual usando diferentes transductores; o bien 3) modulando las condiciones de operación de cada sensor individual [7].

De cualquiera de estas maneras, la matriz de sensores que constituyen tanto narices como lenguas electrónicas, produce señales que no son necesariamente específicas de ninguna especie en concreto, sino que el patrón de señales originado

se correlaciona con ciertas características o cualidades de la muestra. Esto es, suministran información cualitativa sobre la muestra analizada, siendo éste el enfoque más utilizado. La aplicación industrial de la clasificación mediante lenguas y narices electrónicas aumenta continuamente como una parte de la monitorización de procesos industriales, especialmente en industrias agroalimentarias [2].

Un segundo uso de estos dispositivos es para determinaciones cuantitativas, pues algunos analitos que originan señales solapadas o interferencias se pueden cuantificar directamente usando un conjunto de sensores que caractericen la respuesta cruzada junto con la adecuada calibración multivariada [4]. Esta posibilidad es especialmente importante para la detección de sustancias nocivas o peligrosas y en análisis en el ámbito biosanitario. En resumen, los objetivos de estos dispositivos en análisis cualitativo son la discriminación, la clasificación y la identificación y en análisis cuantitativo la determinación multicomponente.

Se han utilizado diferentes principios para la preparación de matrices de sensores tanto para narices como para lenguas electrónicas. Para narices electrónicas los más usados son: sensores catalíticos de óxido de estaño, de polímeros conductores, de onda acústica, de microbalanza de cristal de cuarzo, basados en tecnología MOSFET, sistemas basados en espectrometría de movilidad iónica así como en técnicas de espectrometría de masas como API o PTR y, por último, técnicas ópticas principalmente basadas en fibra óptica y medida de fluorescencia [2,8].

En el caso de lenguas electrónicas, los sensores electroquímicos son los más comunes, así potenciométricos, amperométricos y voltamétricos, aunque también se han descrito sistemas basados en sensores ópticos y en biosensores [9,10]. Sin embargo, la mayoría de estos sistemas se basan en sensores potenciométricos, especialmente electrodos selectivos de iones (ISE). La principal desventaja de las medidas potenciométricas es la influencia de la temperatura, aunque puede ser minimizada mediante el control de la misma o la atemperación.

Las aplicaciones de estos dispositivos son muy amplias existiendo muy pocos instrumentos comerciales [9,10]. En concreto, existen diez compañías en todo el mundo que comercializan lenguas electrónicas: Atsugi (Japón), Alpha MOS (Francia), McScience (Corea del Sur), Food Valley Netherlands (Holanda), CMP (Holanda), Erie Foods International (EE.UU.), Nerac Inc. (EE.UU.), Millipore Corp. (EE.UU.), TNO Food & Nutrition Research (Holanda) y Lianyungang Mupro Fi Plant Lianyungang (China).

En resumen, la principal ventaja de los sistemas de lengua electrónica es la posibilidad de ajustar el modo de operación a la aplicación deseada. Esto significa que, después de una calibración apropiada, tales dispositivos pueden realizar: 1) análisis cuantitativo multianalito (análisis detallado de un vino); 2) discriminación; 3) clasificación (tipo de vino); 4) reconocimiento (madurez de frutos); 5) simulación de paneles de cata humanos.

La mayoría de las lenguas electrónicas se basan en medidas de tipo electroquímico y en mucha menor extensión en medidas de tipo óptico, como más adelante se verá al resumir el estado de la técnica. Salvo muy contadas excepciones, los diferentes dispositivos ópticos simplemente se han estudiado para demostrar las posibilidades de uso sin que se hayan aplicado en la práctica [3].

La mayoría de las diferentes aproximaciones ópticas usadas tanto para lenguas como narices se basan en la medida de color usando diferentes espacios de color obtenidos a partir de la imagen generada por dispositivos fotosensibles, cámaras CCD y escáneres principalmente. Con mucho, el espacio más utilizado es el RGB, prácticamente el único, siendo estas coordenadas las que son procesadas por el sistema de reconocimiento de pautas y/o análisis multivariado.

Los requerimientos básicos para los sistemas tipo lengua óptica referidos a la matriz de sensores, clave del sistema, es que los sensores presenten baja selectividad o lo que es lo mismo alta sensibilidad cruzada y que tengan una características analíticas reproducibles [3]. Por otra parte, se busca que los sensores sean cada vez más sensi-

bles y más robustos, lo cual es contradictorio a partir de cierto punto, pues una mayor sensibilidad del sensor se traduce en menor robustez [11]. Una solución es el empleo de sensores desechables y por tanto no integrados en el dispositivo. Requerimientos adicionales se refieren a costo y portabilidad.

Uno de los problemas que presentan muchos de los sistemas descritos es la falta de precisión de las medidas lo que incrementa el error de las predicciones. Falta de precisión que se debe a la variabilidad en la preparación de los sensores y a la variabilidad lote a lote. Algunas de las alternativas propuestas, como las microesferas situadas en un chip de Si micromecanizado [12] conducen a sistemas de buenas prestaciones aunque complejos experimentalmente y de alto precio. La segunda alternativa más usada es la comercializada por la empresa ChemSensing, Inc. [13] aunque más útil para narices que para lenguas ópticas. La forma de preparación de estas matrices por deposición de microvolúmenes de una disolución de los reactivos sobre una cromatoplaca, presenta cierta variabilidad que se traduce en dificultades para la cuantificación de analitos.

La reciente y escasa instrumentación comercial en lenguas electrónicas mencionada anteriormente tiene como denominador común la necesidad de realizar la medida en condiciones controladas de laboratorio por personal experto, en muchos casos, con complejos sistemas de inserción y extracción de muestras. Esta característica es común a la mayoría de las técnicas instrumentales durante la fase inicial de desarrollo, y ya ha sido recorrida por otras técnicas analíticas más asentadas, permitiendo el diseño y fabricación de equipos portátiles concebidos para trabajar “sobre el terreno” y por personal no experto en la materia. El diseño y fabricación de tales sistemas requiere de la colaboración del conocimiento de varias ramas de la ciencia y la tecnología: tecnologías de sensores, tecnologías de instrumentación electrónica, métodos de reconocimientos de patrones, inteligencia artificial y herramientas quimiométricas.

La alternativa que se ha utilizado es este capítulo es el empleo de espacios de color diferentes del RGB, en concreto del espacio orientado hacia el tono HSV, ya descrito en el capítulo anterior y cuya principal característica es que representa la información cognitiva del color en un único parámetro, la coordenada H (tono), no siendo necesarias las tres coordenadas para definir el tono como ocurre en RGB. Se propone el uso de este espacio de color HSV a pesar de no ser el habitualmente empleado para el intercambio de datos exactos de color, como es el CIE L*a*b* y similares, porque no se busca aquí la reproducción exacta de un color, sino un parámetro robusto que de forma simple nos indique el tono. Esta coordenada H, como hemos visto con anterioridad, se puede considerar como una señal cualitativa que es independiente de concentración y camino óptico, esto es, no le afectan diferencias en espesor, falta de homogeneidad de las membranas o de concentración de reactivos entre lotes de sensores, que reducen la precisión de las medidas.

La propuesta que presentamos consiste en la combinación de lenguas ópticas desechables obtenidas por impresión sobre soportes transparentes con la medida de color de los diferentes sensores mediante escáneres convencionales.

Como ejemplo se ha elegido los iones alcalinos sodio y potasio y la química de reconocimiento será de tipo ionóforo-cromoionóforo aunque de baja selectividad. Para ello se procederá inicialmente a diseñar los sensores que van a componer la lengua y para ello se estudiaran diversos ionóforos tipo éter corona que reaccionen de manera no selectiva frente a los analitos a determinar, Na(I) y K(I).

Una vez desarrollada, se plantearon dos estrategias diferentes para procesar los datos de color extraídos de la lengua electrónica. El primer planteamiento consiste en construir una superficie 3-D en el rango de concentraciones de los analitos y del valor de tono de cada sensor. Posteriormente, partiendo de los dos valores de tono de una lengua, se utiliza el algoritmo de los k vecinos más cercanos (k-Nearest Neighbours, k-NN) para obtener la concentración de los analitos a deter-

minar. El segundo enfoque se fundamenta en el uso de una red neuronal para predecir los analitos partiendo de los valores de tono de la lengua.

El algoritmo k-NN es uno de los algoritmos de clasificación más simples en el ámbito del aprendizaje automático. Su funcionamiento consiste en determinar el grupo al que pertenece un objeto a clasificar de acuerdo a una función de distancia -como por ejemplo la distancia Euclídea- a los k objetos más cercanos. El valor de k debe ser un número natural (entero positivo), habitualmente pequeño. Si k = 1, entonces el objeto se asigna simplemente a la clase de su vecino más cercano (dígase aquel cuya distancia al objeto es mínima). También puede variarse la ponderación de los vecinos de manera que los más cercanos contribuyan más al cálculo de la clase que los que se encuentren más distantes.

Por otra parte, la segunda estrategia consiste en el uso de redes neuronales artificiales (Artificial Neural Networks, ANNs). Las ANNs son modelos matemáticos inspirados en la estructura y funcionamiento de las neuronas biológicas y su interconexión. Al igual que en el modelo biológico, una red neuronal artificial recibe un estímulo externo (datos de entrada) que es procesado y transmitido a través de la red de neuronas para obtener el resultado deseado para el que se entrenó la red (datos de salida). Del mismo modo también pueden distinguirse diferentes tipos de conexiones neuronales dentro de una red neuronal: las neuronas de entrada reciben los datos externos y los transmiten a las demás neuronas de la red (neuronas intermedias u ocultas). Éstas procesan a su vez la información recibida y vuelven a transmitir el resultado a las neuronas encargadas de proporcionar el dato de salida esperado (neuronas de salida). Existen diferentes tipos de redes neuronales atendiendo a la estructura de interconexión de la que dispongan sus neuronas y al tipo de procesamiento interno de la información. Ejemplos conocidos de ANNs son el Perceptrón Multicapa (también conocido como red feedforward) o redes RBF.

El entrenamiento o aprendizaje de una red neuronal consiste en la optimización de la ponderación de cada estímulo de entrada a cada neurona de la red, con

el fin de proporcionar el mínimo error en las neuronas de salida. Este proceso de optimización es usualmente no lineal, dado que el procesamiento típico de los datos de entrada de una neurona se corresponde con una función sigmoidal. Finalmente, al igual que en todo método de optimización en ingeniería, el resultado de este proceso de optimización se debe comprobar sobre otros datos no utilizados en el entrenamiento con el fin de verificar que la red ha aprendido el comportamiento deseado.

Capítulo 4A

A Surface Fit Approach with a Disposable Optical Tongue for Alkaline Ion Analysis

M.M. Erenas[a], O. Piñeiro[b], M.C. Pegalajar[b], M.P. Cuellar[b], I. de Orbe-Payá[a], and L.F. Capitán-Vallvey[a]

ECsens. [a]Department of Analytical Chemistry. Faculty of Sciences. [b]Department of Computer Science and Artificial Intelligence. High Technical School of Computer Sciences and Telecommunications. University of Granada, E-18071 Granada, Spain.

Abstract

A disposable optical tongue for the alkaline ions Na(I) and K(I) is described. The two-sensor array prepared on a transparent support consists of non-specific polymeric membranes working by ionophore-chromoionophore chemistry. The non-specific behaviour of the membranes was controlled by means of the crown ether-type ionophore present. The imaging of the tongue, after reaction for 3 min with the unknown solution, by means of a conventional flatbed scanner working by transmission mode, makes it possible to calculate the H (hue) value of the hue, saturation, value (HSV) colour space used as a robust and precise analytical parameter. The modelling of the response of the two-sensor tongue as a sigmoidal surface is used to characterize the behaviour of the tongue and as a basis to infer the concentration values. To compute the concentration of two analytes from the

two hue values obtained using the optical tongue, a surface fit approach was used. The tongue works over a wide dynamic range ($1.0 \cdot 10^{-4}$ to 0.1 M both in Na(I) and K(I)). The sensing membranes show good intramembrane (1.4% RSD) and inter-membrane precision (0.71% RSD) and lifetime (around 45 days in darkness). The procedure was used to analyze Na(I) and K(I) in different types of natural waters (tap and mineral), validating the results against a reference procedure.

Keywords: Disposable optical tongue; HSV color space; Sodium and potassium determination; Water analysis; Answer surface modelling

*Corresponding author; e-mail: lcapitan@ugr.es

2. Introduction

One of the questions that raise interest in the chemical sensor field concerns multi-analyte systems. The disadvantages of the conventional approach based on specific receptors –difficulties in obtaining good selectivity against similar analytes and the number of sensors needed, which increases proportionally with the number of analytes – have led to an alternative paradigm based on differential receptors [1].

This alternative concept proposes the use of an array of non-specific or low selective sensors (electronic tongues) that produce analytical signals useful for the analysis of multi-component samples that are later treated through advanced mathematical procedures for signal processing by pattern recognition and/or multivariate analysis both for quantitative and qualitative analysis [6].

A number of approaches based on chemical sensor arrays have been reported, although most are based on electrochemical sensors (voltammetric, potentiometric), and to a much lesser extent, optical type measurements [2,9,14].

In the discussion of optical type electronic tongues, different approaches have been described:

1) Use of optical fiber with a group of fluorescent reagents, like reagents for pH, O_2 and CO_2, attached by a covalent bond or entrapped in the distal end of the same fiber in such a way that the signal transmitted by the fiber generates a characteristic fingerprint [15]; these can also be reagents deposited in different optical fibers [16] or incorporated into microspheres situated in microcavities etched into the end of the fiber [17] and whose signals are later deconvoluted using multivariate algorithms.

2) Use of polymeric microsphere arrays with a chemically modified surface that will enable the covalent binding of receptors (conventional reagents, enzymes, antibodies). These microspheres are arranged in micromachined cavities

fabricated in Si structures using diverse procedures to place the sample in contact with the device [12,18]. This experimental design has been used with various types of recognition systems along with different pattern recognition algorithms or principal component analysis to address different problems: a) reagents covalently bound to PEG-PS microspheres [18]; b) differential receptors fixed over microspheres [19]; c) multilayered microspheres with a reagent that changes colours on the inside and colourless binding groups on the outside (called microspheres with chromatographic layers and integrated detection) [20]; d) using polymeric membrane arrays containing quantum dots suspended in Si wafer cavities and with binding reagents that change their colour by interacting with the analytes, and measured by spectrophotometry or conventional fluorimetry [21].

3) Molecular printing polymers (MIPs) have been used to discriminate between aromatic amines using the absorbance variation of the same analytes retained in the MIP after the interaction and linear discriminant analysis [22]. The restriction that assumes that the same analytes generate the signal was resolved in a later study using the displacement of a dye [23].

4) The arrangement of reagents in microplate wells was used to obtain an image by means of a CCD camera. An array has been described for protein detection using tetraphenylporphyrin derivatives on the periphery with amino acids and peptides producing receptors that differ in charge, size, hydrophobicity and symmetry, and that will allow the fluorescent transduction through intensity variation or quenching [24]. In another example, the use of an array of different oligonucleotides with recognition zones based on three-way junctions functionalized with a fluorophore capable of interacting with different molecules are used to discriminate cocaine and diverse steroids [25]. Contrary to the previous examples, the recognition reagents can be fixed on the microplate itself. This way, diverse fluorescent markers have been immobilized in PEG for the detection of commons ions using Dual Lifetime Referencing technique with a CCD camera [26,27]}.

5) Systems based on different colorimetric membrane arrays placed bi-dimensionally over a flat hydrophobic silica base. The color change after the reaction is retrieved using a scanner. The RGB coordinates of each membrane are used for the classification by HCA, having been proposed for the recognition of organic compounds in water [13]. Other types of systems have been suggested, like speciation Fe(II)/Fe(III) with reagents placed on filter paper [28].

6) A very different strategy is used by Edelman and col. [29] for the estimation of wine astringency based on the interaction of polyphenols with proline-rich proteins immobilized in the cell of a flow system monitored by IR spectroscopy.

One of the problems that many of the described systems have is a lack of measurement precision, which increases prediction errors. The lack of precision is due to the variability in preparing the sensors and the batch-to-batch variability.

Some of the different optical approaches used for optical tongues are based on the measurement of color using different color spaces obtained from the image generated mainly by imaging devices, such as CCD cameras or scanners. By far, the most commonly used space is RGB [18,19,28], with these coordinates being the ones that are processed by the pattern recognition system and/or multivariate analysis.

In this paper we use the HSV hue-oriented color space, whose main characteristic is that it represents the cognitive information of the color in one single parameter, the coordinate H (hue), meaning that it is not necessary to have the three coordinates to define the hue, as occurs with RGB. The use of this HSV color space is proposed even though it is not normally used to exchange exact color data, as in the case of CIElab and the like, because we are not looking for the exact reproduction of a color but rather a robust parameter that will show us the hue in a simple way. The H coordinate can be considered as a qualitative signal independent from reagent concentration and the optical path, meaning that it will not be

affected by differences in thickness or the lack of membrane homogeneity, or the reagent concentration between batches of sensors, which reduces the precision of measurements. Previous studies have shown that the use of the H coordinate in bitonal sensors that produce a color change by reaction yields a substantial improvement in precision and is better suited for quantification [30].

In this paper we study a disposable optical tongue for the quantification of Na(I) and K(I) in natural waters based on non-selective optical sensors working by ionophore-chromoionophore chemistry, which to the best of our knowledge has not been used previously for this approach.

3. Experimental

3.1. Reagents

Potassium chloride, sodium chloride, calcium chloride and magnesium chloride stock solutions (1.000 M) were prepared in water by exactly weighing analytical reagent grade dry KCl, NaCl, $CaCO_3$ and $MgCO_3$ (Aldrich, Steinheim, Germany) and standardized by atomic absorption spectrometry. pH 9.0 tris(hydroxymethyl)aminomethane (Tris) 1 M buffer solution was prepared from Tris and HCl supplied by Sigma (Sigma-Aldrich Química S.A., Madrid, Spain).

Chemicals for preparing alkaline ions sensitive films, high molecular weight poly (vinyl chloride) (PVC), 12-crown-4-ether (12C4), bis[(12-crown-4)methyl] dodecylmethylmalonate (BC12C4), dibenzo-15-crown-5-ether (DB15C5), dibenzo-18-crown-6-ether (DB18C6), dibenzo-24-crown-8-ether (DB24C8), dibenzo-30-crown-10-ether (DB30C10), o-nitrophenyloctylether (NPOE) and tetrahydrofuran (THF) were purchased from Sigma and potassium tetrakis (4-chlorophenyl)borate (TCPB) and the chromoionophore (1,2-benzo-7-(diethylamino)-3-(octadecanoylimino) phenoxazine (lipophilized Nile Blue) were purchased from Fluka (Fluka, Madrid, Spain). Sheets of Mylar-type polyester (Goodfellow, Cam-

bridge, UK) were used as support. All chemicals used were of analytical-reagent grade. Reverse-osmosis type quality water (Milli-RO 12 plus Milli-Q station from Millipore) was used throughout.

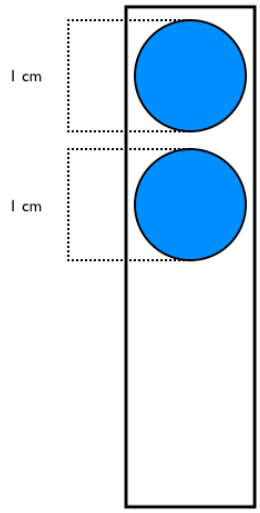

Figure 1. Diagram of the optical tongue.

3.2. Disposable optical tongue preparation

The disposable optical tongue consists of two sensing membranes placed on a polyester substrate (Figure 1) using a spin-coating technique. Each one was cast by placing 20 µL of its cocktail on a 14 mm x 40 mm x 0.5 mm thick polyester sheet using a homemade spin-coater. The two spots were placed on the same sheet of Mylar, first the A cocktail and then the B cocktail. The A cocktail was prepared from a solution of 26.0 mg (28.0 wt %) PVC, 63.0 mg (68.5 wt %) NPOE, 0.8 mg (0.87 wt %) DB18C6, 1.3 mg (1.4 wt %) chromoionophore and 1.1 mg (1.2 wt %) TCPB dissolved in 1.0 mL of freshly distilled THF. The B cocktail was prepared from 26.0 mg (28.0 wt %) PVC, 63.0 mg (68.5 wt %) NPOE, 1.4 mg (0.87 wt %)

BC12C4, 1.3 mg (1.4 wt %) chromoionophore and 1.1 mg (1.2 wt %) TCPB dissolved in 1.0 mL of freshly distilled THF. Both sensing membranes were calculated to have a thickness of about 5 μm. Other cocktails prepared with different ionophores use the same proportion of all components.

3.3. Response evaluation

In order to select the adequate ionophores, all the sensors were tested using seven standard solutions ranging from $1.0 \cdot 10^{-7}$ to $1.0 \cdot 10^{-1}$ M of Na(I), K(I), Ca(II) and Mg(II), respectively. In this way, the behavior of the sensors against the different cations was tested and compared to determine the sensor's selectivity. The procedure introduced the membrane in a solution of HCl $1.0 \cdot 10^{-2}$ M for 3 min in order to activate the membranes which were then equilibrated for 3 min in the standard solution. Each solution was measured 3 times with 3 different membranes. After that, the membranes were also equilibrated in NaOH $1.0 \cdot 10^{-2}$ M solution. All the measurements were performed spectrophotometrically. This procedure was only used for the selection and characterization study of sensing membranes.

The response of the disposable optical tongue was evaluated using a set of standard solutions containing Na(I) and K(I), whose concentrations ranged from $1.0 \cdot 10^{-7}$ to $1.0 \cdot 10^{-1}$ M with 3 replicates each and buffered with pH 9 Tris buffer $2.0 \cdot 10^{-2}$ M. The procedure used was to activate the optical tongue in an HCl solution $1.0 \cdot 10^{-2}$ M for 3 minutes and then they were equilibrated for 3 minutes in the standard or problem solution. After equilibration, the sensor was pulled out of the solution and imaged using a scanner. In this case the measurement of protonated and deprotonated forms of the indicator in each membrane was not necessary because the H parameter was used directly as analytical parameter.

Finally, the real water samples used to check the method were prepared adding 1 mL of pH 9 Tris buffer $2.0 \cdot 10^{-2}$ M to 49 mL of the sample. Then the opti-

cal tongue was introduced after an activation step as before for 3 min in the standard or problem solution. After equilibration, the membrane was pulled out of the solution and imaged as before.

3.4 Apparatus and Software

The images were acquired with a Microtek scanner model ScanMaker i700 (Microtek, CA, USA). The program used to manage the scanner was Silver Fast Ai provided by Microteck. The scanner was calibrated using an IT8 calibration target which is designed to measure the performance of input devices and generate ICC (International Colour Consortium) profiles. The treatment of the images obtained from the scanner was performed with a set of programs that were developed by us using Matlab r2007b (The MathWorks, Inc, Natick, MA, USA). Another instrument used was a Crison digital pH-meter with combined glass-saturated calomel electrode (Crison Instruments Barcelona, Spain). Characterization of membranes in terms of selectivity was performed spectrophotometrically using a Hewlett Packard diode array spectrophotometer (DAD) (model 8453; Nortwalk, CT, US) equipped with a 44 mm high, 12 mm wide homemade membrane cell holder [31].

Statistical calculations were performed with Statgraphics software package (Manugistics Inc. and Statistical Graphics Corporation, USA, 1992), ver. 5.0 and Matlab. Excel software (Microsoft Corp., Redmond, WA, USA) was used for general calculations.

3.5 Image acquisition and treatment

The acquisition of the images with the scanner was performed in transmission mode lighting the membranes placed on the glass surface of the scanner with cold cathode fluorescent (2.72 Klx). The resolution and color bits were configured at 300 dpi and 48-to-24 bits of color. The obtained images were stored in TIFF

(True Image File Format) file format because this format does not compress the image, thus preventing any loss of information. The image as usually obtained contains more than one sensing area captured, so the information (H value) of the different sensing areas that form the image must be obtained as previously we described [30]. For this purpose, a program was developed to estimate the position of the membranes in the image. Then the RGB coordinates of each pixel that makes up the membranes were calculated and from these values, the H parameter was also calculated for each pixel. The image is usually composed of 16,000 pixels, and the H value that we take as representative of the membrane is the most repeated value of H (mode). Thus, H has better precision and is better suited for quantification.

4. Rationale

4.1. Sensing design for optical tongue

The disposable sensors used in this tongue were optical sensors based on an ionophore-chromoionophore design [32,33]. When a sensor of this type is introduced into an aqueous solution containing the analyte I^{z+}, the next equilibrium (eq.1) is fulfilled (barred species means membrane phase):

$$I^{z+} + p\overline{L} + z\overline{HC^{+}} \leftrightarrow \overline{IL_p^{z+}} + z\overline{C} + zH^{+} \quad (1)$$

The plasticized sensing membrane contains the ionophore L, which drives the reaction, the chromoionophore C which is selective for H^+, and the highly lipophilic anion R^- to give needed ion-exchange properties to membrane. As the analyte is transferred into the bulk membrane, the chromoionophore is deprotonated and, hence, the color of the membrane turns from the chromoionophore's acidic form, HC^+, to the basic form C.

Figure 2. Acquisition of analytical signals from optical tongue by scanner working in transmission mode.

The ratio of ion activities, $a_{H^+}^{z} / a_{I^{z+}}$, in aqueous phase is related to the equilibrium constant $K_e^{IL_p}$ and the analytical parameter 1-α through a sigmoidal response function (eq. 2):

$$a_{I^{z+}} = \frac{1}{K_e^{IL_p}} \left(\frac{a_{H^+} \alpha}{1-\alpha} \right)^z \frac{C_R - (1-\alpha) C_C}{z \left(C_L - \frac{p}{z} \left(C_R - (1-\alpha) C_C \right) \right)^p} \qquad (2)$$

where C_L, C_C and C_R are the analytical concentrations of ionophore, chromoionophore and lipophilic anion, respectively, p is the stoichiometric factor for the analyte:ionophore complex and z is the charge of the analyte I. The extent of the ion-exchange process, i.e., the recognition process, can be measured by the degree of protonation 1-α of the chromoionophore ($[HC^+]/C_C$).

The usual way to acquire this analytical parameter is by measuring an intensity-based parameter (eq. 3):

$$1-\alpha=\frac{X-X_B}{X_A-X_B} \tag{3}$$

where X can be the absorbance, fluorescence, luminosity of a component of RGB color space or another signal. This relative parameter, which varies from 0 to 1, is obtained from the signals at a given equilibrium X, totally displaced to A (X_A) and totally displaced to B (X_B).

The selectivity of these sensing membranes against the analyte is measured using the selectivity coefficients K_{ij}^{opt} [34].

The optical tongue presented here involves broadly selective sensors defined by their cross-sensitivity, defined as the tendency of a sensor to change its response if different species are present [9]. The cross-selectivity needed for these optical sensors can be achieved by modifying the composition of the sensing membrane, mainly the ionophore [34] and plasticizer [35]. In this way, the amount of information that can be gained using these broadly selective optical sensors is greater than with the usual selective sensors.

In the case of an optical tongue, each membrane reacts with all of the analytes, meaning that as many reactions are carried out in the membrane as analytes are present in the sample. Furthermore, as many sensing membranes are needed as the analytes that we want to determine. The composition of the sensing areas that make up the tongue must be different and the behaviour of each membrane against the analytes must also be different, so the information obtained from the membranes is different and not redundant, making the calculation of the analyte concentration possible.

4.2. Modelling the sensor response

Usually with this type of sensor, the degree of protonation 1-α is used as the analytical parameter and the relationship between this parameter and the logarithm of concentration, actually activity, of the analyte shows a sigmoidal dependence [32]. The main disadvantage of the 1-α parameter is the need to measure signals from the fully protonated and deprotonated chromoionophore species in addition to the signal coming from the sample or standard. Thus, based on previous studies [30] we decided to use the H value from the HSV color space as the analytical parameter. H represents the hue that the membranes take on when they are equilibrated in solutions of different analyte concentrations. H is a qualitative parameter that can be used as a quantitative one, because indicate the displacement of the chemical equilibrium and plays the same role as 1-α in eq. 2. It also presents other advantages against 1-α, such as its insensitivity to sensor-to-sensor variations and indicator photobleaching along with its fit to an established theoretical model, which means a very high precision when compared to 1-α and the other optical parameters used.

If a measurement is made of the changes in color, quantified by a color coordinate independent of intensity, as is the HSV color space, a relative signal defined similarly to eq. 3 can be used to indicate the displacement on the chemical equilibrium and plays the same role as 1-α in eq. 2.

The relationship between the H parameter and the logarithm of the concentration of the analyte I^{z+}, similarly to 1-α, is sigmoidal and can be defined mathematically by a Boltzmann type equation

$$H = a_2 + \frac{(a_1 - a_2)}{1 + e^{\frac{[I^{z+}] - x0}{x1}}} \tag{4}$$

where a_1, and a_2 correspond to values of H of the lower and top asymptotes of the sigmoidal function, respectively, and these match the values of H for totally proto-

nated and deprotonated chromoionophore. x0 and x1 are the constants that must be calculated to fit the experimental data with eq. 4.

In the case that the sensors are not selective and respond to various analytes that satisfy the property given by the eq. 4, the values of a_1 and a_2 that correspond to both asymptotes do not change, but the H value depends on the analyte concentration in the standard or sample. For n analytes, I_i^{z+}, i=1,..., n, the behavior of the sensor against the concentration of the n analytes is defined by an (n+1)-dimensional representation that has the shape of a sigmoidal surface and is characterized by eq. 5. Thus, an optical tongue of this type needs as many equations as membranes that it contains. For each of the sensors j, j=1,…, m, and each of the n analytes I_i^{z+},i=1,…, n :

$$H_j = a_2 + \frac{a_1 - a_2}{1 + \sum_{i=1}^{n} z_1^i \cdot e^{\frac{z_2^i \cdot \left(\left[I_i^{z+}\right] + z_3^i x_0^i\right)}{x_1^i}}} \tag{5}$$

where a_1, a_2, x_0^i and x_1^i have the same meaning as the constants calculated for the individual model (eq. 4) and z_1^i, z_2^i and z_3^i constants are calculated by an iterative method to fit the surfaces that are defined by these equations to the experimental data.

The computation of the constants z_1^i, z_2^i and z_3^i is performed in our approach with an iterative non-linear optimization method whose objective is the minimization of the squared error between the real H_j data and the approximated H_j obtained from eq. 5. This procedure needs an input matrix with the values of the concentrations of the analytes homogeneously distributed over the entire space and the experimental H value obtained with each of the tongue sensors.

4.3. Building the surfaces to predict analyte concentration

In general terms, our goal is to predict the values of the concentration of *n* analytes from the hues H_j obtained from *m* sensors ($1 \leq j \leq m$) using eq. 5. In our approach, we build *m* surfaces with (*n+1*) dimensions, one for each analyte and the last one with the H coordinate associated with the respective sensor and computed with eq. 5.

The construction of each surface starts with the approximation of the sensors response according to eq. 5, where the parameters to be optimized are the values z_1^i, z_2^i and z_3^i, and the optimization criteria is the minimization of the error in the hue H response of the formula. After that, a surface is built for each sensor with a predefined precision between consecutive points in the analyte concentrations bound. Each point in the last dimension n+1 of the surfaces is then assigned with the value resulting of the evaluation of the point with eq. 5 and the z_j^i parameters that corresponds to the sensor.

We remark that it is required that the calibration data contain data vectors of n+1 dimensions ($(\lfloor I_1^{z+} \rfloor, \lfloor I_2^{z+} \rfloor, \lfloor I_3^{z+} \rfloor, ..., \lfloor I_n^{z+} \rfloor)$, H_j) must be uniformly distributed along the analyte concentrations bound, in order to achieve a suitable sensor's surface approximation in all the areas of the n-dimensional concentrations space.

4.4. Inferring the concentration values from the response surfaces

In the previous section, *m* surfaces were built in order to model the hue of each sensor for a set of *n* analytes concentration. Now we assume that the sensors in the optical tongue provides us a vector of hue values ($h_1, h_2, ... h_m$) to predict the concentration values of the *n* analytes. To achieve this purpose, we have used the k-nearest neighbors classification method [36,37], with k=1. The basis of this procedure is to find the concentration of the analytes that matches the hues of the sen-

sors in all the surfaces. This problem is formulated as the minimization of a distance criterion $D(\vec{x},\vec{y})$ over the sensors' response and the hues (H_1,H_2,...H_m) in the surfaces, as stated in eq. 6:

$$(I_1^{Z+},I_2^{Z+},I_3^{Z+}...,I_n^{Z+}) = \min_{(I_1^{Z+},I_2^{Z+},I_3^{Z+}...,I_n^{Z+})}\{D([h_1,h_2,...,h_m],[H_1,H_2...,H_m])\} \quad \text{(eq.6)}$$

Since the domain of the hue values of a sensor is the real line, then the domain of the hue vectors is $\Re^m$ and the classic Euclidean distance may be used here as distance criterion (eq. 7).

$$D([h_1,...,h_m],[H_1,...,H_m]) = \sqrt{\sum_{j=1}^{m}(H_j - h_j)^2} \quad (7)$$

5. Results and discussion

As a proof of concept in this paper we present an optical tongue for the determination of two alkaline ions, Na(I) and K(I) in natural waters based on the measurement of a color coordinate, a modeling of each sensor response against both analytes and a surface fit approach to infer their concentrations.

5.1. Selection and characterization of optical membranes

As an initial hypothesis, we used only two non-selective membranes for the resolution of Na(I) and K(I) mixtures in the simplest way. The criteria for the optical tongue membrane selection was based on: 1) different selectivity patterns for Na(I) and K(I); 2) fit of the working range for Na(I) and K(I) to the usual alkaline ion concentration in natural waters; 3) sufficient selectivity against concomitant alkaline earth ions.

The sensing membranes present in the optical tongue studied are based on an ion-exchange mechanism using an ionophore-chromoionophore design [32]. For the sake of simplicity, the sensing chemistry used here is based on the same chro-

moionophore, thus the same color, which changes from an acid form to a basic one allowing the acquisition of the analytical parameter. Consequently, the non-specific and different behavior between membranes will be controlled only by the ionophore included. As ionophore, we tested different commercial crown ethers of different crown size used for both potentiometric and optical sensors; namely 12C4, BC12C4, DB15C5, DB18C6, DB24C8, and DB30C10. Different membranes were prepared using the same membrane polymer (PVC), plasticizer (NPOE) and lipophilic salt (TCPB) and the above-mentioned chromoionophore (lipophilized Nile Blue) working at the same C_L, C_C and C_R concentrations (See Experimental section).

The selectivity coefficients $K_{I^{z+}}^{j}$ for K(I), Na(I), Mg(II), and Ca(II) using all the membranes prepared with the above-indicated ionophores plus another one containing no ionophore were determined by means of the separate solutions method [32]. Table 1 shows that the membranes containing 12C4, BC12C4 and the membranes without ionophore are potential candidates for Na(I). However, taking into account the great difference in selectivity between Na(I) and K(I), the substantial interference of Mg(II) in the case of 12C4, and, on the other hand, the selectivity of the membrane without ionophore towards alkaline earth, we selected the BC12C4 membrane, as a non-specific but more selective membrane for Na(I).

Table 1. Selectivity coefficients $K_{I^{z+}}^{j}$ for alkaline and alkaline-earth ions in the sensing membranes studied and using the response to Na(I) as a reference.

	Without	**12C4**	**BC12C4**	**DB15C5**	**DB18C6**	**DB24C8**	**DB30C10**
Na(I)	0	0	0	0	0	0	0
K(I)	-1.96	-4.04	-1.17	2.40	1.3	0.41	n.r.
Ca(II)	0.38	-0.04	-2.12	0.17	-0.18	-1.03	-0.72
Mg(II)	3.24	1.02	-2.77	1.30	-0.63	-1.14	-1.65

n.r.: no reaction

In the same way, but for K(I), the DB15C5, DB18C6 and DB24C8 membranes appeared to be possible candidates. In this case, it is apparent that DB15C5 is quite selective for K(I) and in addition more selective for Ca(II) and Mg(II) than Na(I), and was rejected for that reason. In the case of the membrane containing DB24C8, the difference in selectivity for K(I) against Na(I) is not enough to discriminate between ions and, thus, determine the concentrations of both of them. Consequently, the ionophore DB18C6 was selected as a non-selective ionophore for K(I). Additionally, the working range for the two membranes selected for Na(I) and K(I) was adequate for a real sample application.

Once the ionophores for the sensing membranes were selected (DB18C6 and BC12C4), the response of membranes containing them against concentrations of both alkaline ions was studied individually. By using both spectrophotometric and scanometric measurements through absorbance and H coordinate, respectively, we checked that they fit the model defined by eq. 2. The $K_e^{IL_p^{z+}}$ values obtained are displayed in Table 2, concluding that the H coordinate is a good parameter for sensor calibration considering the similar results in $K_e^{IL_p^{z+}}$ obtained from a different experimental setup.

Table 2. Equilibrium constant $K_e^{IL_p^{z+}}$ for alkaline and alkaline-earth ions for the different sensing membranes studied.

Ion	$K_e^{IL_p^{z+}}$						
	Without	**12C4**	**BC12C4**	**DB15C5**	**DB18C6**	**DB24C8**	**DB30C10**
Na(I)	$5.62\cdot10^{-9}$	n.r.	$3.30\cdot10^{-7}$	$2.41\cdot10^{-9}$	$4.79\cdot10^{-8}$	$3.24\cdot10^{-7}$	$5.99\cdot10^{-7}$
K(I)	n.r.	n.r.	$1.76\cdot10^{-8}$	$4.71\cdot10^{-7}$	$1.97\cdot10^{-6}$	$1.41\cdot10^{-6}$	$4.85\cdot10^{-6}$
Ca(II)	$2.81\cdot10^{-19}$	$2.07\cdot10^{-19}$	n.r.	$1.05\cdot10^{-19}$	$5.65\cdot10^{-19}$	$2.99\cdot10^{-18}$	$2.17\cdot10^{-17}$
Mg(II)	$5.53\cdot10^{-17}$	$1.86\cdot10^{-17}$	n.r.	$1.00\cdot10^{-17}$	$2.62\cdot10^{-19}$	$2.83\cdot10^{-18}$	$1.35\cdot10^{-17}$

n.r. no reaction

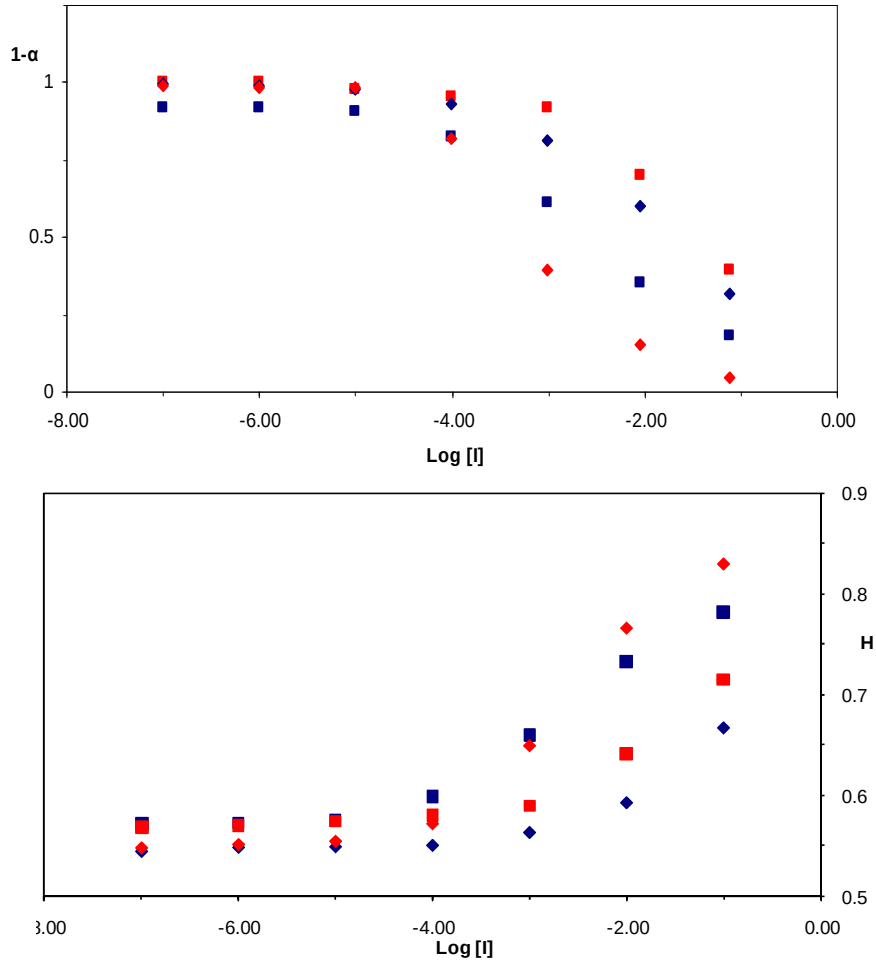

Figure 3. The behaviour of optical tongue membranes showing their sigmoidal dependence, fitted using 1-α get from H values (A) and using H values (B). The blue points represent values at different Na(I) concentrations and the red ones from K(I). The ■ are the results from the BC12C4 sensor and ♦ the results from DB18C6 sensor.

The hue coordinate H varies for the sensing membranes studied here between 0.54 and 0.82, the first value being that obtained when the lipophilized Nile blue is totally protonated and the second when it is totally deprotonated. All the H

values for the different solutions must be within the above range. The behavior of both membranes fitted using only the H value by means of the sigmoid Boltzmann type eq. 4 is shown in Figure 3.

5.2. Building the alkaline ion surface response

A preliminary study was performed using the full range concentration of both sensors, with the result being that the response at low concentrations of both analytes shows very small changes in H in such a way that the procedure was unable to solve the system. Thus, it was decided to select an effective range of concentrations where the H changes were sufficient to perform the determination of both analytes. As the effective range of concentration, from $1.0 \cdot 10^{-4}$ to 0.1 M was used both in Na(I) and K(I) because in those ranges the maximum slope of the response function is found.

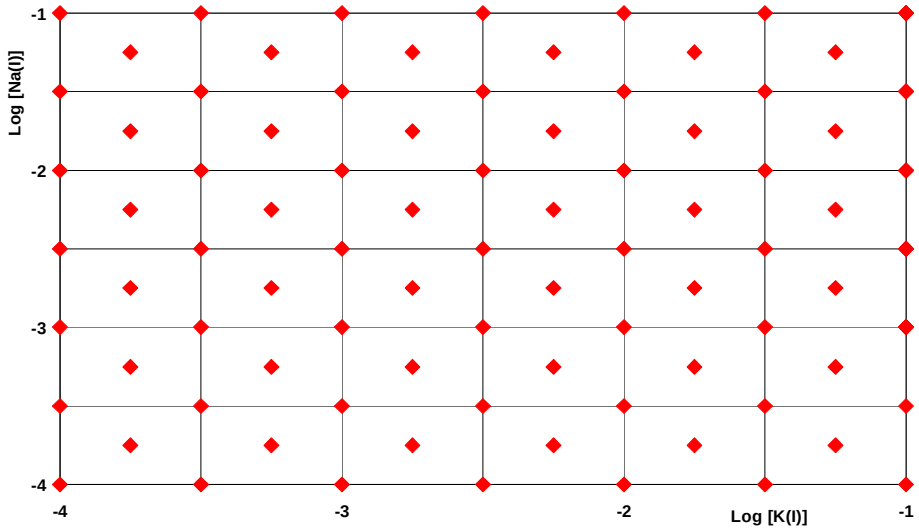

Figure 4. 2-D grid concentration matrix used to model the tongue.

Before obtaining the response surface for each membrane, a study of the precision in the acquisition of the H parameter was made. For this preliminary study of intramembrane and intermembrane precision, 8 solutions of different concentrations of Na(I) and K(I) covering the above concentration range were selected. For the intramembrane study, we repeated the cycle of acid-standard-base solutions 3 times for all standards, obtaining the H value in each case. The average values for the relative standard deviations were 1.3% for the DB18C6 membrane and 1.7% for BC12C4 membrane. The intermembrane study was performed using 10 different tongues measuring the H value according to the usual procedure. The average values for RSD % of the 8 solutions were 0.73% for the DB18C6 membrane and 0.70% for the BC12C4 membrane. In all cases the precision values are good, but the worst figure obtained using the same membrane comes from the fact that the behavior observed for both membranes composing the tongue is not totally reversible; namely there is a tendency for the H value to rise with the repeated use of the membranes. The results reveal a good precision for this optical tongue measurement and suggest a disposable use.

The response for each sensor when the Na(I) and K(I) concentration vary simultaneously in the range indicated above was obtained with 80 standard solutions covering the whole concentration range according to the experimental procedure previously discussed (Figure 4). Adjusting eq. 6 to the optical tongue studied results in a set of calculated constants for each membrane (eq. 8 and 9). Figures 5A and 5B shows the surface response evaluated for DB18C6 and BC12C4 membranes, respectively. According to the calculated selectivities for alkaline ions, the shape and orientation of the surfaces is different for each membrane, thus allowing the resolution.

5.3. Resolving the system

The calibration data used to optimize the parameters z_1^i, z_2^i and z_3^i of eq. 8 on both surfaces has 80 pairs of concentration values of K(I) and Na(I), with the corresponding hue values from the sensors BC12C4 and DB18C6. In addition, we used another 48 data pairs for the model validation.

For two analytes, K(I) and Na(I), the behavior of the tongue against the concentration of the two analytes is defined by a 3D representation that has the shape of a sigmoidal surface and is characterized by the equations:

$$H_{BC12C4} = 0.84 + \left(\frac{(0.56 - 0.82)}{1 + 1.6993 \cdot e^{\left(2.2890 \frac{([K(I)]+1.1566)}{0.68}\right)} + 1 \cdot 2.9071 \cdot e^{\left(0.7512 \frac{([Na(I)]+1.9804)}{0.72}\right)}} \right) \quad (8)$$

$$H_{DB18C6} = 0.84 + \left(\frac{0.56 - 0.82}{1 + 1.5518 \cdot e^{\left(0.2439 \frac{([K(I)]+2.61)}{0.34}\right)} + (-1.2951) \cdot 0.2439 \cdot e^{\left(-0.1787 \frac{[Na(I)]+1.50}{0.68}\right)}} \right) \quad (9)$$

In order to compute the concentration of the two analytes from the two hue values obtained using the optical tongue, two 3D surfaces were first built – one for each sensor – where the X and Y axes contains the concentration of each analyte in the calibration data set, and the Z axis contains the hue value of the sensor. Figures 5a and 5b illustrate the shape of the surfaces built for each sensor.

Given two values of H, h_{DB18C6} and h_{BC12C4}, the associated concentrations are calculated using the k-nearest neighbor algorithm. The base point ([K(I)], [Na(I)]) of the surfaces was sought that minimizes the Euclidean distance between (H_1, H_2) on the surfaces and the hues (h_1, h_2) obtained from the sensors. After that, the pair of concentrations ([K(I)], [Na(I)]) were returned as the predicted concentrations (Figure 6).

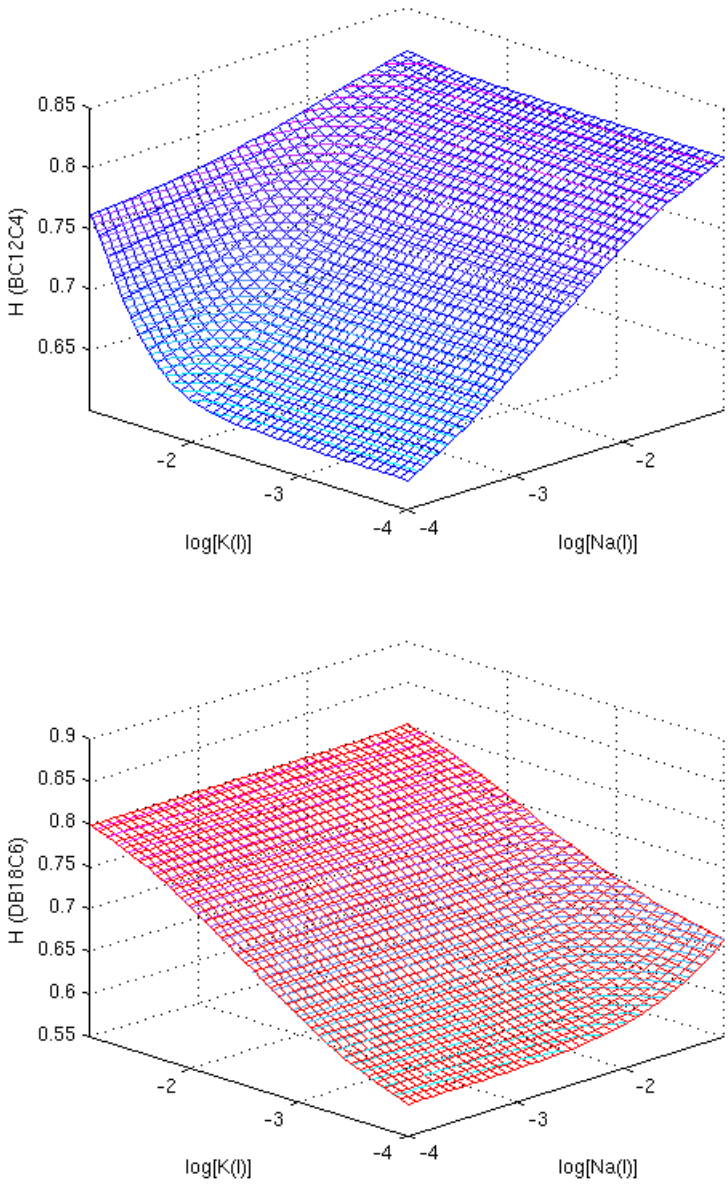

Figure 5. Approximated surfaces of the sensors' hue response in respect to the reference analyte concentrations. A: BC12C4 sensor; B: DB18C6 sensor.

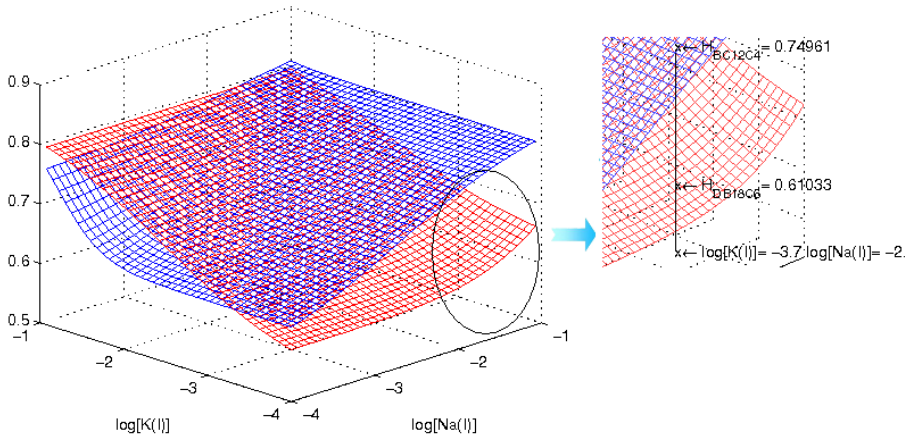

Figure 6. Surface fit approach for analyte concentration prediction.

5.4. Validation of the optical tongue

The disposable optical tongue presented here was applied to the determination of alkaline ions studied in real samples in order to assess its usefulness. To perform the validation we selected samples of waters from diverse sources (tap and mineral). Table 4 shows the average results (three replicates each) obtained using the optical tongue described here and expressed in $mg \cdot l^{-1}$ compared to atomic absorption spectrometry (AAS) used as a reference method.

The mean squared error obtained in the prediction of the concentrations is 0.10438, which suggests that the approach provides a suitable generalization of the calibration data. In order to ensure that the prediction suits the real concentrations, we also applied a Pearson correlation test between the concentration values predicted and the real ones measured. The results of the test provide a probability value of 0.004 for the comparison of the real and predicted log([K(I)]) concentration data, and 0.003 for the log([Na(I)]). These values suggest that there is a significant correlation between the reference and predicted analyte concentration. Furthermore, the coefficient R describes a high degree of correlation between both

the real and predicted values, whose value is 0.9773 for the correlation between the reference and predicted concentrations of log([K(I)]), and 0.9774 for the correlation between the reference and predicted concentrations of log([Na(I)]).

Table 3. Determination of K(I) and Na(I) in different types of natural water using the proposed optical tongue and AAS as reference method.

	K(I) mg·l^{-1}		**Na(I) mg·l^{-1}**	
Water sample	AAS*	Tongue	AAS*	Tongue
Tap (Granada)	1.59	1.57	4.07	4.62
Mineral water 1	2.35	2.35	2.16	1.99
Mineral water 2	1.79	1.80	4.81	4.92
Mineral water 3	2.27	2.17	3.80	3.76
Mineral water 4	1.94	2.03	4.17	4.22

* AAS: Atomic Absorption Spectrometry reference method

6. Conclusions

An optical tongue for the simultaneous determination of Na(I) and K(I) has been developed and characterized. The tongue consists of an array of two polymeric membranes that work by ionophore-chromoionophore chemistry. Both membranes use the same chromoionophore, meaning that the same color change and their non-selective behavior are achieved by modifying the crown ether used as ionophore on the basis of their selectivity coefficients $K^{j}_{I^{z+}}$ for alkaline and alkaline-earth ions. The color that the two-sensor optical tongue attains in the presence of the sample solution is used as the analytical signal. The color is measured from the image of the tongue in a scanner working in transmission mode, considering the H parameter (hue) of the HSV color space, which affords robust and precise measurements. The prediction of the analyte concentration, based on the hues obtained

from the multimembrane, was carried out using Machine Learning techniques: a surface model was developed in order to model the possible hues provided from the multimembrane with their respective analyte concentration. Then, the k-nearest neighbors classification method was used over the surface model to provide the prediction of the analyte concentration. This model has provided suitable results using a multimembrane with two sensors for the prediction of concentrations of Na(I) and K(I). Statistical tests were applied to validate the model over real data, showing a high correlation between the reference and predicted analyte concentration.

Acknowledgements

We acknowledge financial support from the *Ministerio de Ciencia e Innovación, Dirección General de Investigación y Gestión del Plan Nacional de I+D+i* (Spain) (Projects CTQ2009-14428-C02-01 and CTQ2009-14428-C02-02); and the *Junta de Andalucía* (*Proyecto de Excelencia* P08-FQM-3535). These projects were partially supported by European Regional Development Funds (ERDF).

Capítulo 4B

Disposable Optical Tongue for Alkaline Ion Analysis

M.M. Erenas[a], M.C. Pegalajar[b], M.P. Cuellar[b], I. de Orbe-Payá[a], and L.F. Capitán-Vallvey[a]

ECsens. [a]Department of Analytical Chemistry. Faculty of Sciences. [b]Department of Computer Science and Artificial Intelligence. High Technical School of Computer Sciences and Telecommunications. University of Granada, E-18071 Granada, Spain.

Abstract

A disposable optical tongue has been developed with a two-sensor array prepared on a transparent support. The array consists of polymeric membranes working by ionophore-chromoionophore chemistry with non-specific behaviour controlled by the crown ether-type ionophore present. The system was used for the simultaneous determination of Na(I) and K(I) ions in natural waters. The imaging of the element – after reaction for 3 min with the solution – by a conventional scanner makes it possible to calculate the hue coordinate H of the HSV colour space used as the analytical parameter. The signals were processed using an optimized multilayer artificial neural network (ANN). The individual sensing membranes show good precision (0.3% RSD) and lifetime (around 45 days in darkness). The tongue works over a wide dynamic range ($1.0 \cdot 10^{-4}$ to 0.1 M both in Na(I) and K(I)) and when the procedure was applied, the mean square error obtained by the ANN approach was 0.0569 for the prediction of K(I) and 0.0401 for Na(I). The

procedure was used to analyze Na(I) and K(I) in different types of natural waters (tap and mineral), validating the results against a reference procedure.

Keywords: Disposable optical tongue; HSV color space; Sodium and potassium determination; Artificial neural network modelling; Water analysis

*Corresponding author; e-mail: lcapitan@ugr.es

7. Introduction

A recent trend to obviate the difficulties of obtaining single analyte sensors based on specific receptors – problems of selectivity – is to combine non-specific sensors in an array that produce a set of analytical signals (electronic tongue for gaseous species/electronic nose for species in solution). This information with higher dimensionality, encoded in the overlapping measurements, can be processed to extract qualitative and quantitative information through advanced mathematical procedures of pattern recognition and/or multivariate analysis [6,9], improving in this way the performance of the sensors [38]. The characteristics of cross sensitivity and reproducibility make it possible to extract the analytical information without any separation of interferent species or matrix effect elimination. Different sensing principles have been employed in electronic tongues, the most prevalent being electrochemical, both potentiometric and amperometric, piezoelectric and optical [9].

The analysis of the data acquired by sensor arrays is performed by various numeric procedures from the measurement of standard solutions to build the chemometric tool [4,9].

One of the mathematical procedures used is the Artificial Neural Network (ANN), very popular for tasks such as classification, automatic control, pattern recognition, learning and non-linear regression [39-41]. Inspired by brain models, a neural network contains simpler computing elements (neurons) which are organized in a parallel/distributed structure. An artificial neuron receives one or more weighted stimuli (neuron inputs) that are added and processed inside the neuron to provide an output response (neuron activation). Different neural network approaches exist depending on the way that neuron inputs are added, the processing model for neuron activation, and the links structure between the neurons [39,42,43].

The most popular ANN approach is Multilayer Perceptron networks, whose neurons are structured in layers and have a sigmoid processing kernel. The input stimuli to a neuron at layer l are the sum of the weighted outputs of the neurons at layer l-1, and provide a response or activation according to a sigmoid function. This concept is described by eq. 10 and 11, where $f_i^l(\cdot)$ is the response of the i-th neuron at layer l, net_i^l is the weighted sum of all the responses of the neurons at layer l-1 connected to the i-th neuron at layer l, n_{l-1} is the number of neurons at layer l-1, w_{ki}^{l-1} stands for the weight matched with the connection between the k-th neuron at layer l-1 and the i-th neuron at layer l, and x_k^{l-1} is the response of the k-th neuron at layer l-1.

$$f_i^l(net_i^l) = \frac{1}{1+e^{-net_i^l}} \tag{10}$$

$$net_i^l = \sum_{k=1}^{n_{l-1}} w_{ki}^{l-1} x_k^{l-1} \tag{11}$$

For the neurons at the first layer, x_k^{l-1} stands for the k-th input value to the network, i.e. the independent variables of the problem to be solved. Finally, the response of the neurons at the last layer is assumed to be the network outputs, i.e. the dependent variables to be approximated in the problem.

The training of a neural network is the optimization procedure to find the optimal weights which make the network provide the best performance. During training, a set of patterns containing input/desired output values are provided to the network and its weights are modified in order to provide the best approximation of the desired output values for each pattern, considering a global error measure to be minimized. The most common error measure is the Mean Square Error (MSE) (eq. 12), in which T stands for the number of data patterns presented to the network, O is the number of network outputs, $desired_v^p$ is the desired value for the v-th output

neuron in the network for the pattern p, and $output_v^p$ is the response value provided by such neuron.

$$MSE = \left(\frac{1}{T}\sum_{p=1}^{T}\sum_{v=1}^{o}(output_v^p - desired_v^p)^2\right) \quad (12)$$

Traditional training algorithms are based on error backpropagation [39,42]; however other approaches based on evolutionary computation or Quasi-Newton algorithms have provided a good performance [44,45] and will be used in this study.

Different approaches have been described for optical electronic tongues, with the most interesting being: a) arrays of individual micrometer-scale prepared at the distal end of an optical fiber with fluorescent reagents covalently attached or entrapped generating a characteristic fingerprint in the presence of analytes [15], although the reagents can be deposited in different optical fibers [16] or incorporated into microspheres situated in microcavities etched into the end of the fiber and whose signals are later deconvoluted using multivariate algorithms [17]; b) Using polymeric microsphere arrays with a chemically modified surface binding receptors, arranged in micromachined cavities fabricated in Si structures to contact the sample [12,18]. This experimental design has been implemented in different ways: b1) reagents covalently bound to PEG-PS microspheres [18]; b2) differential receptors bound on microspheres [19]; b3) multilayered microspheres with a chromogenic reagent inside and colourless binding groups outside [20]; b4) polymeric membrane arrays containing quantum dots suspended in Si wafer cavities with binding reagents that change their colour by interacting with the analytes [21]; c) A set of molecular imprinted polymers (MIP) have been used to discriminate between aromatic amines using both the absorbance variation of the same analytes retained in the MIP [22] and dye displacement technique [23] followed by linear discriminant analysis; d) Microplate wells containing reagents and imaged after reaction with a CCD camera are described for protein detection using tetraphenylporphyrin

derivatives through fluorescent transduction [24]. Similarly, an array of different oligonucleotides with recognition zones based on three-way junctions functionalized with a fluorophore is used to discriminate cocaine and diverse steroids in microtiter plate format [25]. Alternatively, the recognition elements can be fixed on the microplate itself. This way, diverse fluorescent markers have been immobilized in PEG for the detection of common ions using the Dual Lifetime Referencing technique with a CCD camera [26,27]; e) Colorimetric membrane arrays placed bidimensionally over a flat hydrophobic silica base have been proposed for the recognition of organic compounds in water, based on the retrieval of the colour change after reaction with a scanner and classification by HCA from RGB coordinates of each membrane [13]. Other examples have been suggested using filter paper with reagents immobilized for Fe(II)/Fe(III) speciation [28].

Some of the different optical approaches described for optical tongues are based on the measurement of colour using different colour spaces, mainly RGB, from the imaging of optical tongue by imaging devices, such as CCD cameras or scanners processed by pattern recognition and/or multivariate analysis [18,19,28].

In this study, we use the HSV hue-oriented colour space which represents the colour information in one single parameter, the coordinate H (hue), unlike what occurs with RGB, which needs the three coordinates to define the hue. Previous studies have shown that the use of the H coordinate in bitonal sensors that produce a colour change by reaction yields a substantial improvement in precision and is better suited for quantification [30].

In this paper we study a disposable optical tongue based on non-selective optical sensors working by ionophore-chromoionophore chemistry for the quantification of Na(I) and K(I) in natural waters using the colour coordinate H as analytical parameter and a neural network as the signal processing technique.

8. Experimental

8.1. Reagents

Potassium and sodium stock solutions (1.000 M) were prepared in water by exactly weighing analytical reagent grade dry KCl and NaCl (Aldrich, Steinheim, Germany) standardized by atomic absorption spectrometry. pH 9.0 tris(hydroxymethyl)aminomethane (Tris) 1 M buffer solution was prepared from Tris and HCl supplied by Sigma (Sigma-Aldrich Química S.A., Madrid, Spain).

Chemicals for preparing alkaline ion sensitive films, high molecular weight poly (vinyl chloride) (PVC), bis[(12-crown-4)methyl] dodecylmethylmalonate (BC12C4), dibenzo-18-crown-6-ether (DB18C6), o-nitrophenyloctylether (NPOE) and tetrahydrofuran (THF) were purchased from Sigma and potassium tetrakis (4-chlorophenyl)borate (TCPB) and the chromoionophore (1,2-benzo-7- (diethylamino)-3-(octadecanoylimino) phenoxazine (lipophilized Nile Blue) were purchased from Fluka (Fluka, Madrid, Spain). Sheets of Mylar-type polyester (Goodfellow, Cambridge, UK) were used as support. All chemicals used were of analytical-reagent grade and reverse-osmosis type quality water (Milli-RO 12 plus Milli-Q station from Millipore) was used throughout.

8.2. Disposable optical tongue fabrication

The disposable optical tongue consists of two sensing membranes, next to each other and placed on the same transparent plastic substrate using a spin-coating technique. Each was cast by placing 20 μL of the corresponding A or B cocktail on a 14 mm x 40 mm x 0.5 mm thick polyester sheet using a homemade spin-coater. Cocktail A was prepared from a solution of 26.0 mg (28.0 wt %) PVC, 63.0 mg (68.5 wt %) NPOE, 0.8 mg (0.87 wt %) DB18C6, 1.3 mg (1.4 wt %) chromoionophore and 1.1 mg (1.2 wt %) TCPB all dissolved in 1.0 mL of freshly distilled THF. Cocktail B was prepared from 26.0 mg (28.0 wt %) PVC, 63.0 mg (68.5 wt

%) NPOE, 1.4 mg (0.87 wt %) BC12C4, 1.3 mg (1.4 wt %) chromoionophore and 1.1 mg (1.2 wt %) TCPB dissolved as the above cocktail in 1.0 mL of THF. Both sensing membranes were calculated to have a thickness of about 5 μm.

8.3. Apparatus and Software

The tongues were digitalized by scanning using a Microtek scanner model ScanMaker i700 (Microtek, CA, USA) managed by the proprietary software Silver Fast Ai. The scanner was calibrated using an IT8 calibration target. The treatment of the images obtained from the scanner was performed with a set of programs that were developed by us using Matlab r2007b (MathWorks, MA, USA). Other apparatus used included a Crison digital pH-meter with combined glass-saturated calomel electrode (Crison Instruments Barcelona, Spain). Statistical calculations were performed with the Statgraphics software package (Manugistics Inc. and Statistical Graphics Corporation, USA, 1992), ver. 5.0. and Excel software (Microsoft Corp., Redmond, WA, USA) was used for general calculations. Finally, the application of Artificial Neural Networks was carried out using the Neural Networks Toolbox in Matlab.

8.4. Optical tongue performance

The optical tongue was activated before use by introducing it for 3 minutes in a solution of HCl $1.0 \cdot 10^{-2}$ M. Then, it was equilibrated for another 3 minutes in the standard solution or problem. The response of the tongue was evaluated using a set of standard solution mixtures containing K(I) and Na(I) at concentrations ranging from $1.0 \cdot 10^{-4}$ to $1.0 \cdot 10^{-1}$ M each and buffered with pH 9 Tris buffer $2.0 \cdot 10^{-2}$ M. After equilibration, the sensor was pulled out of the solution and imaged using a scanner.

8.5. Image acquisition and treatment

The acquisition of the images with the scanner was performed working in transmission mode lighting the membranes placed on the glass surface of the scanner with cold cathode fluorescent (2.72 Klx). The resolution and bits of color were settled on 300 dpi and 48-to-24 bits of color. The obtained images were stored in TIFF (True Image File Format) file format to prevent any loss of information since this does not compress the image. As the image obtained contains more than one sensing area captured, we needed to obtain the analytical parameter (H value) from each area that formed part of the image. For this purpose, images were processed using routines developed in Matlab r2007b.

First, to recognize the sensing membranes digitalized in the image, the software detects pixels in each normalized R, G and B channels, coming from the non-colored area of the image (background) by comparing each pixel with the maximum observed difference in the entire image multiplied by a predefined threshold value [30].

$$H = \begin{cases} \left(\dfrac{G-B}{\max_{channel} - \min_{channel}} + 0 \right) \Big/ 6; & if \ \max = R^{*} \\ \left(\dfrac{B-R}{\max_{channel} - \min_{channel}} + 2 \right) \Big/ 6; & if \ \max = G \\ \left(\dfrac{R-G}{\max_{channel} - \min_{channel}} + 4 \right) \Big/ 6; & if \ \max = B \end{cases} \tag{13}$$

* *if H is less than* 0 *then add* 1 *to H*

After slicing the image of each membrane from the whole image, which typically contains 16,000 pixels, the R, G and B channels of each membrane were

scaled and the H coordinate calculated from the R, G and B coordinates of each pixel using eq. 13. The most repeated value, the mode, of the set values of H for each membrane was used as the analytical parameter for optical tongue calculation by ANN.

8.6. Artificial Neural Network settings

The tongues designed in this work depend non-linearly on two hue values from the sensing elements, and therefore a suitable processing technique for the data is needed to relate both signals with the concentrations of the analytes. For this, it was decided to use ANN [39] to predict the concentrations of K(I) and Na(I) in solution from the hue resulting from the sensing elements in the tongue (Figure 7). The network structure used in this work is a Multilayer Perceptron whose number of network inputs is the number of sensing elements in the tongue, and each receives the hue response from each sensor. The number of network outputs is the number of analytes for which their concentration in the solution must be predicted. Thus, since the model must predict the concentration of both alkaline ions, the network is designed with 2 output neurons, each providing the concentration of each analyte. The neurons for the input and the hidden layers have a sigmoid kernel, while the neurons in the output layer perform a linear processing to achieve prediction values in the range of the concentrations of the data set (10^{-4} to 10^{-1} M) from -4 to -1, resulting from the transformations $\log[\mathrm{Na(I)}]$ and $\log[\mathrm{K(I)}]$. Finally, the number of hidden layers and neurons per layer were obtained experimentally using a *trial-and-error* procedure, testing the network structures from 1 to 3 hidden layers containing a number of hidden neurons from 3 to 12 per layer. The best results were obtained with 2 hidden layers and 4 neurons per layer. Networks with a lower number of layers and neurons were able to learn the training data suitably, but they presented limitations in the generalization of the data learnt and provided poor results in the test. On the other hand, the networks with higher num-

ber of neurons and layers were not capable of learning the data correctly due to the complexity of the networks' structure.

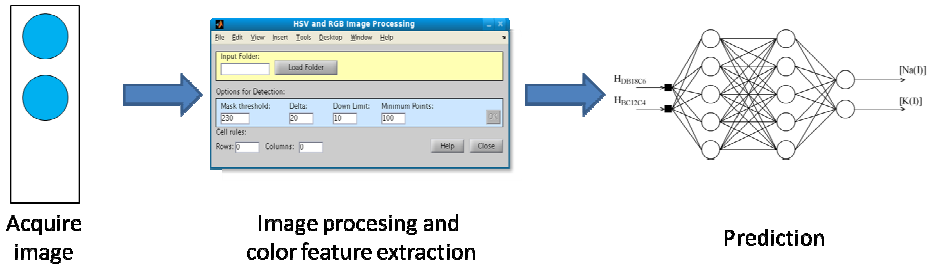

Figure 7. Procedure for color feature extraction and analyte concentration prediction.

The training method used to calibrate the network weights is the non-linear optimization Levenberg-Marquardt algorithm [44,46], and the error measure to be minimized is the Mean Squeare Error (MSE) [39]. The stopping criterion for the optimization is reaching 1000 algorithm iterations, and the alternative criterion is to obtain an MSE below 0.01. The methodology for the training followed a cross-validation procedure: the calibration data were subdivided into two random sets with 70% of the data for the training and the remaining 30% for testing the generalization capabilities of the network. This random division was carried out a total of 20 times, and for each subdivision 5 networks with different initial random weights were trained.

8.7. Applications

Once the ANN method applicability was demonstrated against some synthetic samples, the method was applied to real water samples and the results compared with those by atomic absorption spectrometry used as reference method. A set of real water samples was used. The water selected was different brands of

mineral water and tap water from different towns from the South of Spain. To validate the optical tongue with the water samples, the preparation procedure used was to take 1 mL of pH 9 Tris buffer $2.0 \cdot 10^{-2}$ M and 49 mL of the water sample. Then, the optical tongue was activated, equilibrated in the sample and imaged as before. We measured three replications from each sample to ensure robustness in the experimental validation of the Neural Network.

9. Results and Discussion

In general, an electronic tongue is a multisensor device composed of an array of sensors with a cross-sensitivity pattern that produces analytical signals useful for the analysis of multi-component samples in solution that are later treated using the mathematical procedures of signal processing to perform quantitative multi-analyte analysis, classification, recognition or the simulation of human tasting panels [6,9]. The optical tongue for Na(I) and K(I) presented in this paper is based on an array of membranes working by an ionophore-chromoionophore system of non-selective behaviour against analytes and modelling using ANN.

9.1. Optical tongue composition

The sensors that compose the tongue are disposable optical sensors based on an ionophore-chromoionophore system. The ionic analyte present in the sample goes into the membrane thanks to an ion exchange equilibrium (eq. 14) between the ionophore L and the H^+-selective chromoionophore C.

$$\overline{L} + \overline{HC^+} + \overline{R^-} + I^{z+} \leftrightarrow \overline{C} + \overline{IL^{z+}} + zH^+ + \overline{R^-} \qquad (14)$$

The plasticized sensing membrane, containing the lipophilic anion R^- to impart ion-exchange properties, extracts the analyte I^{z+} from the solution at the same time that the chromoionophore is deprotonated to maintain the electroneutral-

ity, turning the colour of the membrane from the chromoionophore's acidic form, HC^+, to the basic form C. From the phase transfer and complexation equilibrium, it is possible to derive an implicit sigmoidal response function, through an equilibrium constant K_e^{IL-p}, between a normalized analytical parameter (from absorbance, fluorescence, etc.) related to the degree of protonation of the chromoionophore and the ratio of free sample ion activities ($a_{I^{z+}} / a_{H^z}$) in solution [32].

The selectivity of a sensing membrane, expressed by the selectivity coefficients K_{ij}^{opt} [34], depends on the charge of analytes and interferents, the stoichiometry of complexes, composition of membrane, type of ionophore and chromoionophore and plasticizer present [34,35].

In this case, broadly selective sensing membranes must be used in such a way that their response changes if different species are present [9]. The strategy used here to build the optical tongue consists of maintaining the same chromoionophore in order to use the same colour change in all the membranes, simplifying the operational scheme and changing the ionophore present to achieve low selectivity against the analyte, but with a different selectivity pattern in each membrane, obtaining in this way different and non-redundant information from the membranes that enable the analytical calculation.

For the problem considered here, the resolution of Na(I) and K(I) mixtures, we used two non-selective membranes with different selectivity patterns for both ions and sufficient selectivity against concomitant alkaline earth ions. The membranes were prepared using the same membrane polymer (PVC), plasticizer (NPOE), lipophilic salt (TCPB), chromoionophore (lipophilized Nile Blue) and working with the same ionophore, chromoionophore and liphophilic salt concentrations. The different behaviour between membranes was only controlled by the ionophore included. Of the different commercial crown ethers of the different crown sizes tested, the best results were obtained using bis[(12-crown-4)methyl]

dodecylmethylmalonate (BC12C4) in one membrane and dibenzo-18-crown-6-ether (DB18C6) in the other. A repeatability study with a single sensor showed a figure of 0.3% RSD.

The membrane containing BC12C4 as ionophore imparted a greater selectivity to the sensor to Na(I) than to K(I) (K^{opt}_{NaK} = -1.17; $K_e^{NaL^+}$ = 3.30·10^{-7}; $K_e^{KL^+}$ = 1.76·10^{-8}); whereas the DB18C6 containing membrane presented greater selectivity to K(I) than to Na(I) (K^{opt}_{NaK} = 1.30; $K_e^{NaL^+}$ = 4.79·10^{-8}; $K_e^{KL^+}$ = 1.97·10^{-6}) but not enough for individual determinations in any case. At the same time, both membranes offered adequate selectivity against alkaline earth ions at their usual levels in natural waters.

9.2. Analytical parameter

The extension of the ion-exchange process in the sensing membrane, that is the recognition process, is usually measured by the degree of protonation of the chromoionophore ([HC$^+$]/C$_C$) coming from an intensity-based property (absorbance [47], reflectance [48,49], transflectance [50], fluorescence [51], refraction index [52]; RGB color coordinate [53]) as a normalized signal, which varies from 0 to 1. However in this optical tongue the tonal coordinate H of the color space HSV is used as the analytical signal.

The reasons for the choice of colour as the signal are: easy acquisition by imaging and calculation from RGB coordinates and the advantages of a qualitative parameter to determine the amounts of the analytes. Here an optical sensor contains the reporter molecule Nile Blue, characterized by a colour z_A that by indirect reaction with the analyte, alkaline ions, produces the transformation of the reporter molecule structure with a new colour z_B. If the qualitative relationship for the transformation of the reporter (colour z_A to z_B) is represented by a continuous function, it

is possible to extract quantitative information from the continuous qualitative variable. The position between the two ending colours, z_A and z_B, is related to the displacement of the reaction by the analyte and thus with its concentration through an experimental calibration function. In this case, the colour of the membrane turned from the chromoionophore's acidic form, i.e., blue for the lipophilic Nile Blue, to the basic form, magenta.

For colour measurement, the most common linear-light tristimulus RGB was not used here, but rather the hue oriented colour space HSV, the main feature of which is the representation of the cognitive colour information in a single parameter, the hue component H. The main advantage of the use of H is its high precision, between 4 and 10 times superior to CV, as compared to other optical signals commonly used such as absorbance. Additional advantages include insensitivity to changes in membrane thickness, chromoionophore concentration, membrane preparation procedure, thus insensitivity to sensor-to-sensor variations, indicator photobleaching, and the low influence of the imaging device used for image acquisition.

Usually in disposable sensors, the signal obtained must be normalized because the raw data obtained from different sensors cannot be compared directly, but using the H value the calibration can be obtained directly, without the need for any type of normalization which simplifies the analytical procedure [30]. For the chromoionophore used in this optical tongue, the hue changed from the blue acid form with a hue of 0.560 or 201°, expressed as an angle that varied between 0 and 360°, and the magenta basic form had a hue of 0.812 or 292°.

9.3. Neural networks for prediction of analyte concentration

A preliminary study was performed using the full range concentration of both sensors, with the result being that the response at low concentrations of both analytes shows very small changes in H in such a way that the procedure was un-

able to solve the system. Thus, it was decided to select an effective range of concentrations where the H changes were sufficient to perform the determination of both analytes. The effective range of concentration from $1.0 \cdot 10^{-4}$ to 0.1 M was used both in Na(I) and K(I), because the maximum slope of the response function is found in those ranges.

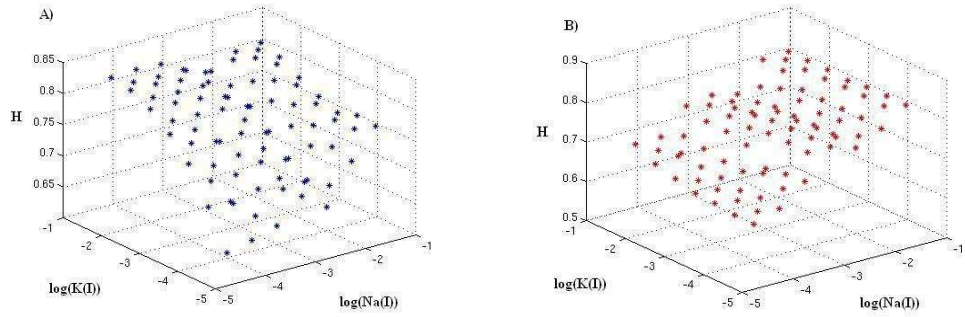

Figure 8. Calibration data set used to train the neural network. A) H value from DB12C4 membrane with respect to log[Na(I)] and log[K(I)]. B) H value from BC18C6 membrane with respect to log[Na(I)] and log[K(I)].

The response for each sensor when the Na(I) and K(I) concentrations vary simultaneously in the range indicated above was obtained with 85 standard solutions covering the whole concentration range according to the experimental procedure previously discussed. We obtained three pairs of H values from each standard solution using three different tongues. The range of the concentrations of Na(I) and K(I) studied varied from 0.1 M to $1x10^{-4}$ M, analyzing 7 concentrations levels of each equally distributed ion, resulting in 49 standards; additionally 36 intermediate standards were included in the experimental set. From this calibration experiment, 255 tuples of H, Na(I) and K(I) concentrations per membrane were obtained and used to train and test the neural network. Figure 8 shows the experimental data obtained in the calibration experiment.

For calibration purposes, an ANN was used to relate the analytical signal with the analyte concentration working with the settings described in Section 2.6. The average value of the concentration and H values measured in the three replications of the 85 solutions in the calibration data were used to build the training and test data sets for the neural network. 70% of these data, selected randomly in a cross-validation training procedure, were used for training and the remaining 30% to test the generalization capabilities of the network.

Table 4 describes the Mean Square Error obtained for the prediction of analyte concentrations by the best network obtained in the network training and test sets. These results suggest that the network is able to provide a fine prediction of the concentration. However, to ensure this assumption we made the following statistical analyses of the test data set. Firstly, a Kolmogorov-Smirnov test with an 80% confidence level was applied to the reference with the predicted analyte concentrations to check the normality assumption and secondly, the data distributions of the reference and predicted concentration values were compared using a T-test with a 95% confidence level, to check if there were any statistical differences between both data sets. Finally, we used a Pearson correlation test to corroborate that the predicted concentration values fit the reference data correctly.

Table 4. Mean Square Error obtained for the prediction of K(I) and Na(I) concentrations.

	Error for K(I)	**Error for Na(I)**
Training data set	0.0695	0.0748
Test data set	0.0569	0.0401

The Kolmogorov-Smirnov test concluded that all the data distributions fulfilled the normality assumption, providing the probability values 0.6437 and 0.6045 for the reference concentrations of K(I) and Na(I), respectively, and 0.2156 and 0.8444 for the predicted concentration values. The Student's T-test supported that there were no significant differences between the reference and predicted data and it returned the probability values 0.9084 and 0.8201 for the comparison of the

reference and predicted concentration values of K(I) and Na(I), respectively. In addition, the results of the Pearson test provided a correlation coefficient R equals 0.9645 and 0.9763 for the comparison of the predicted and reference concentration values of K(I) and Na(I). These values support the fact that the prediction made by our approach has a high positive correlation with the reference data and we may therefore assume that the neural network model performs suitably. Figure 9 supports this analysis and shows the regression line between the reference and predicted values for both analytes.

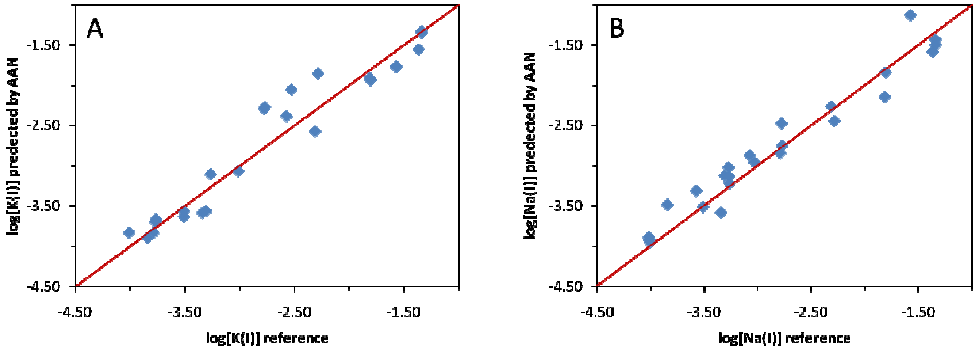

Figure 9. Regression line between the reference and predicted concentration values for both analytes in the calibration data set for ANN. A. For K(I). B. For Na(I).

9.4. Validation of the optical tongue

The disposable optical tongue presented here was applied to the determination of alkaline ions studied in real samples in order to assess its usefulness. To perform the validation, we selected 16 samples of waters from diverse sources (tap and mineral) applying the proposed procedure analyzed by atomic absorption spectrometry (AAS).

The hues of the optical tongue from equilibration in real water samples were used to predict the analyte concentrations using the trained previously ANN. The Mean Square Error obtained in the prediction of the concentrations provided by the ANN was 0.0064 for K(I) and 0.0451 for Na(I). These error values are in the same order of magnitude as the ones obtained during the training stage, and this fact suggests that the network obtained good generalization capabilities and therefore is a suitable model for the prediction in our approach. In addition, the regression line between the results obtained by AAS and the predicted concentrations in Figure 10 also suggests promising results. To support these assumptions, we carried out a statistical analysis in order to verify the network performance. Firstly, a Kolmogorov-Smirnov test was applied to the AAS data and predicted data distribution to check the normality assumption with an 80% confidence level. This provided the probability values 0.3454 and 0.0232 for the AAS concentration data of K(I) and Na(I), respectively, and the probability values 0.3336 (K(I)) and 0.0277 (Na(I)) for the concentrations predicted. According to these results, a parametric T-Student test must be used to compare the AAS and predicted concentrations for K(I), while the non-parametric Kruskal-Wallis test was applied to the data regarding the Na(I) since the normality assumption was not fulfilled in these data distributions. Both statistical tests were applied with a 95% confidence level, providing the probability values 0.8568 (T-test) and 0.775 (Kruskal-Wallis test). Considering these values, we may conclude that there are no significant differences between the predictions of the concentrations for both analytes with respect to their AAS values. Finally, we applied a Pearson correlation test to learn whether the reference and predicted data fit correctly for both analytes. This test returned a correlation coefficient R with values 0.7238 and 0.9687 for the analytes K(I) and Na(I), respectively. These results suggest a high positive correlation between the concentration values provided by the neural network and their respective AAS concentration values. Using this analysis, we may conclude that the network outputs are coherent

with the real values of the analyte concentrations, and that the neural network proposed is able to predict the concentration of the analytes correctly.

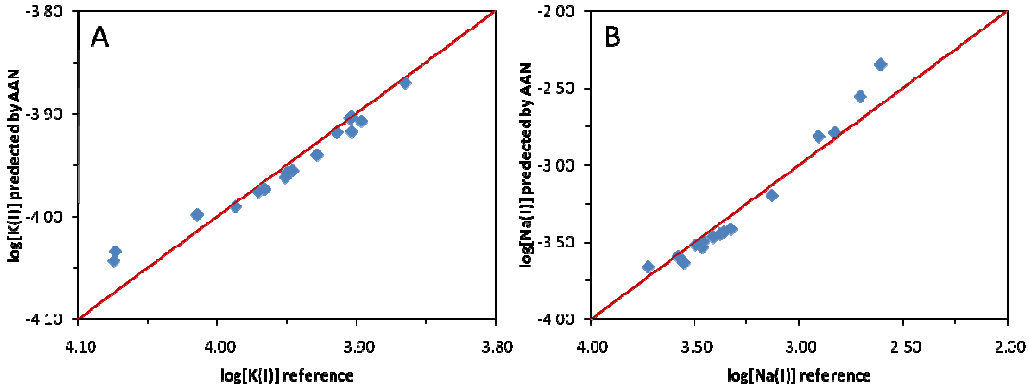

Figure 10. Regression line between the AAS and predicted concentration values for both analytes in the real water samples data set for the ANN used. A. For K(I). B. For Na(I).

9.5. Comparison with other methods

To test the capabilities of the ANN approach, in this section we compare the results of the analyte concentration predictions in the real water data with previous techniques developed, such as the 1-Nearest Neighbour (1-NN) procedure used previously [54]. The same calibration data set was used to optimize the parameters of this proposal and to build the prediction surface. The Mean Square Error obtained by the surface approach was 0.0926 for the prediction of K(I) and 0.5668 for Na(I). The comparison of these values with the error in Section 10.4 suggests that the ANN approach improves the prediction performance, especially in the case of Na(I). To support these results, a Kruskal-Wallis test was applied to the predicted concentration values of both approaches, with a 95% confidence

level. The tests provided a probability value of 0.5374 for the distributions regarding K(I), and 0.0001 for the comparison of the distributions of the prediction of Na(I). Using these results, we can conclude that there are no significative differences in the use of the surface approach and artificial neural networks for the prediction of K(I). However, there are differences regarding the prediction of Na(I), and the method that provides the best results is the one with the lowest MSE. Thus, the artificial neural network approach described in this work is able to provide the best performance for the simultaneous prediction of the analytes considered.

10. Conclusions

In this work, we have proposed a method for the prediction of alkaline ion concentrations in natural waters using a disposable optical tongue, which consists of an array of two membranes that work by ionophore-chromoionophore chemistry. By sharing the same chromoionophore, both membranes exhibit different selectivity by changing the crown ether used as the ionophore. The change in colour from the reaction of the array is measured by imaging with a scanner and the hue coordinate H of the HSV colour space is used as the analytical parameter. The prediction of the analyte concentration, based on the hues obtained from the array was carried out using Artificial Neural Network techniques.

This model provided suitable results using an optical tongue with two sensors for the prediction of concentrations of Na(I) and K(I) for its application to their analysis in natural waters.

Acknowledgements

We acknowledge financial support from the *Ministerio de Ciencia e Innovación, Dirección General de Investigación y Gestión del Plan Nacional de I+D+i* (Spain) (Projects CTQ2009-14428-C02-01 and CTQ2009-14428-C02-02); and the *Junta de Andalucía* (*Proyecto de Excelencia* P08-FQM-3535). These projects were partially supported by European Regional Development Funds (ERDF).

11. Conclusión

En este capítulo se ha descrito el desarrollo y posterior tratamiento de los resultados obtenidos con la lengua óptica para determinar la concentración de K(I) y Na(I).

El primer paso de este estudio fue el diseño de la lengua electrónica. Para ello se estudió el comportamiento de sensores que contenían diferentes ionóforos de tipo éter corona. Se calculó la selectividad frente al resto de alcalinos y alcalinotérreos mediante el método de las disoluciones separadas y de esta manera se seleccionaron los éteres corona más adecuados de manera que los dos sensores que forman parte de la lengua reaccionen uno de ellos de manera ligeramente más selectiva para potasio y el otro para sodio, aunque en ambos casos originando los dos analitos señal. Los ionóforos seleccionados fueron el éter 18-corona-6, más selectivo para potasio que para sodio, y el éter bis[(12-corona-4)methil] dodecilmetilmalonato, más selectivo en sentido contrario.

Una vez elegidos los componentes de la lengua electrónica, se plantearon dos estrategias diferentes para la resolución del sistema. El primero de ellos es el uso del algoritmo de k-Nearest Neighbour. En este caso se planteó una matriz de calibrado a partir de la cual modelar el comportamiento del sensor, viendo cómo variaba el valor del parámetro H en función de las concentraciones de sodio y potasio. A partir de estos resultados se calculó la ecuación que definía el comportamiento de los sensores que componen la lengua, y mediante dichas funciones y usando el algoritmo anteriormente citado, fue posible calcular las concentraciones de ambos analitos. Este procedimiento se aplicó y validó utilizando muestras reales de agua, demostrando de esta manera su posibilidad de uso. Como resultado se obtuvo una lengua para la determinación de ambos analitos en concentraciones comprendidas entre $1x10^{-4}$ a 0.1 M de ambos analitos, que son las concentraciones en las que se suelen encontrar dichos analitos en las muestras reales a las que se aplicó esta lengua. También, para así caracterizar el sistema, se realizó un estudio

de precisión tanto intramembrana como intermembrana, obteniendo unos valores de coeficiente de variación de 1.3 y 0.7% para el sensor DB18C6 y 1.7 y 0.7% para el caso del BC12C4. Finalmente, se determinó el error cuadrático medio cometido en la determinación tanto de Na(I) como de K(I) obteniendo unos valores de 0.5668 y 0.0926, respectivamente.

La segunda estrategia planteada, fue el uso de una red. De las distintas de redes existentes, se seleccionó una del tipo perceptrón ya que es la más simple que se puede utilizar, necesitando de esta manera menos recursos para su cálculo y aplicación. Para determinar el número de capas ocultas, así como de número de neuronas por capa, se llevó a cabo un estudio de ensayo-error con redes de distinta composición, obteniéndose como óptima la compuesta por dos capas ocultas, cada una de las cuales contiene cuatro neuronas. De esta manera vamos a tener un sistema con dos canales de entrada que son los valores de H procedentes de cada sensor, dos capas ocultas con cuatro neuronas por capa, y dos canales de salida que se corresponden a los valores de concentración de nuestros analitos, Na(I) y K(I). De igual manera que en el caso anterior, la lengua va a tener como objetivo muestras cuya concentración en Na(I) y K(I) esté comprendida entre $1x10^{-4}$ a 0.1 M calculándose el error cuadrático medio cometido en la determinación Al igual que en el caso del algoritmo k-NN, la lengua fue aplicada a muestras reales de manera satisfactoria. En este caso se calculó de nuevo el error cuadrático medio cometido en esta determinación, siendo éste 0.0064 para K(I) y 0.0451 para Na(I). Por tanto, podemos concluir que los resultados obtenidos usando la red neuronal son mejores, cometiendo menor error en la determinación de ambos analitos que usando el algoritmo k-NN.

Por último, se ha demostrado la posibilidad de uso del parámetro H del espacio de color HSV obtenido de membranas sensoras digitalizadas en modo transmisión, como parámetro analítico, no sólo para sistemas monoanalito, sino también para casos más complejos como son lenguas electrónicas, las cuales están compuestas por varias membranas sensoras.

12. Bibliografía

1. J.J. Lavigne, E.V. Anslyn, Sensing a paradigm shift in the field of molecular recognition: from selective to differential receptors, Angew.Chem.Int.Ed. 40 (2001) 3118.

2. A.K. Deisingh, D.C. Stone, M. Thompson, Applications of electronic noses and tongues in food analysis, Intern.J.Food Sci.Tech. 39 (2004) 587.

3. Y.G. Vlasov, A.V. Legin, A.M. Rudnitskaya, Multisensor systems of the electronic tongue type as novel opportunities in design and application of chemical sensors, Rus.Chem.Rev. 75 (2006) 125.

4. F. Winquist, C. Krantz-Rulcker, I. Lundstrom, Electronic tongues and combinations of artificial senses, Sensors Update 11 (2003) 279.

5. K. Persaud, G. Dodd, Analysis of discrimination mechanisms in the mammalian olfactory system using a model nose, Nature 299 (1982) 352.

6. Y. Vlasov, A. Legin, A. Rudnitskaya, C. Di Natale, A. D'Amico, Nonspecific sensor arrays (electronic tongue) for chemical analysis of liquids: (IUPAC technical report), Pure Appl.Chem. 77 (2005) 1965.

7. J. Mitrovics, H. Ulmer, U. Weimar, W. Goepel, Modular Sensor Systems for Gas Sensing and Odor Monitoring: The MOSES Concept, Acc.Chem.Res. 31 (1998) 307.

8. T. C. Pearce, S. S. Schiffman, H. T. Nagle, J. W. Gardner. Handbook of Machine Olfaction - Electronic Nose Technology, John Wiley & Sons, 2003

9. P. Ciosek, W. Wroblewski, Sensor arrays for liquid sensing - electronic tongue systems, Analyst 132 (2007) 963.

10. A. Legin, A. Rudnitskaya, Y. Vlasov, Electronic tongues: new analytical perspective for chemical sensors, Comprehensive Analytical Chemistry 39 (2003) 437.

11. M.C. Janzen, J.B. Ponder, D.P. Bailey, C.K. Ingison, K.S. Suslick, Colorimetric Sensor Arrays for Volatile Organic Compounds, Anal.Chem. 78 (2006) 3591.

12. A.P. Goodey, J.J. Lavigne, S.M. Savoy, M.D. Rodriguez, T. Curey, A. Tsao, G. Simmons, J. Wright, S.J. Yoo, Y. Sohn, E.V. Anslyn, J.B. Shear,

D.P. Neikirk, J.T. McDevitt, Development of multianalyte sensor arrays composed of chemically derivatized polymeric microspheres localized in micromachined cavities, J.Am.Chem.Soc. 123 (2001) 2559.

13. C. Zhang, K.S. Suslick, A colorimetric sensor array for organics in water, J.Am.Chem.Soc. 127 (2005) 11548.

14. Y. Vlasov, A. Legin, A. Rudnitskaya, Electronic tongues and their analytical application, Anal.Bioanal.Chem. 373 (2002) 136.

15. B.G. Healey, D.R. Walt, Fast Temporal Response Fiber-Optic Chemical Sensors Based on the Photodeposition of Micrometer-Scale Polymer Arrays, Anal.Chem. 69 (1997) 2213.

16. K.L. Michael, L.C. Taylor, S.L. Schultz, F. Szurdoki, D.R. Walt, Making sensors out of disarray: optical sensor microarrays, Proc.SPIE 3270 (1998) 34.

17. D.R. Walt, Techview: molecular biology. Bead-based fiber-optic arrays, Science 287 (2000) 451.

18. J.J. Lavigne, S. Savoy, M.B. Clevenger, J.E. Ritchie, B. McDoniel, S.J. Yoo, E.V. Anslyn, J.T. McDevitt, J.B. Shear, D. Neikirk, Solution-Based Analysis of Multiple Analytes by a Sensor Array: Toward the Development of an "Electronic Tongue", J.Am.Chem.Soc. 120 (1998) 6429.

19. A.T. Wright, M.J. Griffin, Z. Zhong, S.C. McCleskey, E.V. Anslyn, J.T. McDevitt, Differential receptors create patterns that distinguish various proteins, Angew.Chem.Int.Ed. 44 (2005) 6375.

20. A.P. Goodey, J.T. McDevitt, Multishell Microspheres with Integrated Chromatographic and Detection Layers for Use in Array Sensors, J.Am.Chem.Soc. 125 (2003) 2870.

21. H. Hogan, Suspended and Placed over Microcavities, Quantum Dots Become Brighter, Photon.Spectra 11 (2007) 98.

22. N.T. Greene, S.L. Morgan, K.D. Shimizu, Molecularly imprinted polymer sensor arrays, Chem.Comm. (2004) 1172.

23. N.T. Greene, K.D. Shimizu, Colorimetric molecularly imprinted polymer sensor array using dye displacement, J.Am.Chem.Soc. 127 (2005) 5695.

24. L. Baldini, A.J. Wilson, J. Hong, A.D. Hamilton, Pattern-based detection of different proteins using an array of fluorescent protein surface receptors, J.Am.Chem.Soc. 126 (2004) 5656.

25. M.N. Stojanovic, E.G. Green, S. Semova, D.B. Nikic, D.W. Landry, Cross-reactive arrays based on three-way junctions, J.Am.Chem.Soc. 125 (2003) 6085.

26. T. Mayr, G. Liebsch, I. Klimant, O.S. Wolfbeis, Multi-ion imaging using fluorescent sensors in a microtiterplate array format, Analyst 127 (2002) 201.

27. T. Mayr, C. Igel, G. Liebsch, I. Klimant, O.S. Wolfbeis, Cross-Reactive Metal Ion Sensor Array in a Micro Titer Plate Format, Anal.Chem. 75 (2003) 4389.

28. A. Abbaspour, M.A. Mehrgardi, A. Noori, M.A. Kamyabi, A. Khalafi-Nezhad, M.N. Soltani Rad, Speciation of iron(II), iron(III) and full-range pH monitoring using paptode: A simple colorimetric method as an appropriate alternative for optodes, Sens.Actuators B 113 (2006) 857.

29. A. Edelmann, B. Lendl, Toward the Optical Tongue: Flow-Through Sensing of Tannin-Protein Interactions Based on FTIR Spectroscopy, J.Am.Chem.Soc. 124 (2002) 14741.

30. K. Cantrell, M.M. Erenas, I. Orbe-Paya, L.F. Capitan-Vallvey, Use of the Hue Parameter of the Hue, Saturation, Value Color Space As a Quantitative Analytical Parameter for Bitonal Optical Sensors, Anal.Chem. 82 (2010) 531.

31. L.F. Capitan-Vallvey, M.D. Fernandez-Ramos, P. Alvarez de Cienfuegos, F. Santoyo-Gonzalez, Characterization of a transparent optical test strip for quantification of water hardness, Anal.Chim.Acta 481 (2003) 139.

32. E. Bakker, P. Bühlmann, E. Pretsch, Carrier-Based Ion-Selective Electrodes and Bulk Optodes. 1. General Characteristics, Chem Rev. 97 (1997) 3083.

33. U. E. Spichiger-Keller. Chemical Sensors and Biosensors for Medical and Biological Applications, 1 ed., Wiley-VCH, Weinheim, 1998 p. 1.

34. E. Bakker, W. Simon, Selectivity of Ion-Sensitive Bulk Optodes, Anal.Chem. 64 (1992) 1805.

35. U.E. Spichiger-Keller, Ionophores, ligands and reactands, Anal.Chim.Acta 400 (1999) 65.

36. E. Alpaydim. Introduction to Machine Learning, The MIT Press, Cambridge, MA, USA, 2004.

37. D. Michie, D. J. Spiegelhalter, C. C. Taylor. Machine Learning, Neural and Statistical Classification, *Ed. Ellis Horwood*, Chichester, UK, 1994.

38. J. Gallardo, S. Alegret, R. Munoz, M. De Roman, L. Leija, P.R. Hernandez, M. Del Valle, An electronic tongue using potentiometric all-solid-state PVC-membrane sensors for the simultaneous quantification of ammonium and potassium ions in water, Anal.Bioanal.Chem. 377 (2003) 248.

39. S. Haykin. Neural Networks: A comprehensive foundation, Prentice Hall, Upper Saddle River, NJ, USA, 1999.

40. R. Linggard, D. J. Myers, C. Nightingale. Neural Networks for Vision, Speech and Natural Language, Ed. Chapman & Hall, London, UK, 1992.

41. W. Thomas-Miller, R. S. Sutton, R. J. Werbos. Neural Networks for control, 2nd ed., The MIT Press, Cambridge, MA, USA, 1991.

42. D. Mandic, J. Chambers. Recurrent Neural Networks for Prediction, John Wiley and Sons, Hoboken, NJ, USA, 2001.

43. J. Dayhoff. Neural Network architectures: An introduction, Van Nostrand Reinhold, New York, USA, 1990.

44. R. Prudencio, T. Ludemir, Neural network hybrid learning: Genetic algorithms and Levenberg-Marquardt, Proc.26th Annu.Conf.Gesellschaft for Classifikation (2003) 617.

45. M.P. Cuellar, M. Delgado, M.C. Pegalajar, Memetic Evolutionary Training for Recurrent Neural Networks: An application to time-series prediction, Expert Systems 23 (2006) 99.

46. M. P. Cuellar, M. Delgado, M. C. Pegalajar. Proc.International Conference on Enterprise and Information Systems, Miami, FL, USA, 35-42, 24-5-2005, 2005.

47. E. Antico, M. Lerchi, B. Rusterholz, N. Achermann, M. Badertscher, M. Valiente, E. Pretsch, Monitoring Pb2+ with optical sensing films, Anal.Chim.Acta 388 (1999) 327.

48. R.H. Ng, K.M. Sparks, B.E. Statland, Colorimetric determination of potassium in plasma and serum by reflectance photometry with a dry-chemistry reagent, Clin.Chem. 38 (1992) 1371.

49. A. Lapresta-Fernandez, R. Huertas, M. Melgosa, L.F. Capitan-Vallvey, Colourimetric characterisation of disposable optical sensors from spectroradiometric measurements, Anal.Bioanal.Chem. 393 (2009) 1361.

50. I.d. Orbe-Paya, M. Erenas, L.F. Capitan-Vallvey, Potassium disposable optical sensor based on transflectance measurements, Sens.Actuators B 127 (2007) 586.

51. S.L.R. Barker, B. Thorsrud, R. Kopelman, Nitrite- and Chloride-Selective Fluorescent Nano-Optodes and in In-Vitro Application to Rat Conceptuses, Anal.Chem. 70 (1998) 100.

52. D. Freiner, R.E. Kunz, D. Citterio, U.E. Spichiger, M.T. Gale, Integrated optical sensors based on refractometry of ion-selective membranes, Sens.Actuators B 29 (1995) 277.

53. A. Lapresta-Fernandez, L.F. Capitan-Vallvey, Scanometric potassium determination with ionophore-based disposable sensors, Sens.Actuators B 134 (2008) 694.

54. M. M. Erenas, K. Cantrell, M. C. Pegalajar, I. Orbe-Paya, M. P. Cuellar, L. F. Capitan-Vallvey. September 28-29, 2009 Valencia (Spain), 2009.

Capítulo 5

Uso de dispositivos digitales de imagen basados en reflexión para sensores ópticos

1. Planteamiento

La coordenada H ha demostrado ser un parámetro analítico muy robusto y estable en el caso de trabajar con imágenes tomadas con dispositivos que trabajan en modo transmisión, es decir, aquellos que iluminan por un lado la membrana, recogiendo la radiación no absorbida por el sensor por el lado contrario que es donde se encuentra el detector.

La desventaja de este tipo de dispositivos es que hace necesario el uso de una fuente de radiación para poder digitalizar la membrana, además de que la mayoría de los dispositivos de imagen portátiles comerciales trabajan en modo reflexión. Por ello, nuestro objetivo en este capítulo es demostrar la posibilidad de uso de dicho parámetro H cuando se trabaja con imágenes adquiridas de este modo, así como establecer teóricamente la relación entre la coordenada cromática H y la concentración del analito.

Se van a considerar dos modelos distintos; en el primero de ellos la radiación que llega a la membrana pasa a través de ella, produciéndose un efecto de absorción de radiación, hasta incidir sobre un soporte reflectante, que devuelve la radiación de nuevo a través de la membrana produciéndose un doble proceso de absorción de radiación antes de alcanzar el detector. En este caso se va a aplicar un modelo de transmisión basado en la ley de Lambert-Beer para establecer la radiación que llega al detector. En el segundo modelo partiremos del supuesto de que la radiación será reflejada por la membrana antes de llegar al

detector. En este caso, la radiación reflejada se calculará a partir de la expresión de Kubelka-Munk, suponiendo por tanto un modelo de reflexión.

Una vez modelado el comportamiento de la membrana con dicho parámetro, se va a estudiar la robustez del mismo. Para ello se va a establecer la influencia del valor de la coordenada tonal H cuando: a) se varía de dispositivo usado para digitalizar la membrana, para lo que se emplearán dos cámaras digitales diferentes: un escáner y la cámara de un teléfono móvil; b) se modifican las condiciones de iluminación, a través del cambio de las condiciones de balance de blancos usado, simulando de esta manera diferentes iluminaciones y c) se varían las características de las membranas usadas preparando membranas con diferentes grosores y con cantidades diferentes de cromoionóforo. Para realizar este estudio se va a utilizar de nuevo el sensor óptico desechable diseñado para la determinación de potasio que se empleó en el anterior capítulo sobre el parámetro H (Capítulo 3).

Use of digital reflection devices for measurement using hue-based optical sensors

M.M. Erenas[1], K. Cantrell[2], I. de Orbe-Payá[1], L.F. Capitán-Vallvey[1*]

[1] ECSens, Solid Phase Spectrometry Research Group, Department of Analytical Chemistry, Campus Fuentenueva, University of Granada, E-18071 Granada, Spain
[2]Department of Chemistry, The University of Portland, Portland, OR 97203, USA

Abstract

In this paper is the hue or H component of the HSV (Hue, Saturation, Value) color space is used as analytical parameter for bitonal optical sensors, from images obtained in reflection mode as an alternative to devices that acquire images in transmission mode.

This parameter is characterized by its robustness to variations in device used to obtain images, illuminant used, sensor-to-sensor variation, namely variation in sensors thickness and amount of chromoionophore. Additionally, it has a higher precision compared with traditional optical parameters, such as absorbance or transflectance, or color parameters such as R, G or B coordinates. Because of the robustness of the H parameter, it is possible to simplify the procedure used for

the optical sensors as well as the use of ubiquitous devices as digital cameras to acquire the image of the sensor.

Keywords: H coordinate; HSV color space; bitonal optical sensors; potassium sensor; imaging

2. Introduction

In a previous paper we have discussed the use of a qualitative variable to determine the amounts of analytes present by means of sensors characterized by a change in properties by reaction or interaction with the analyte if that qualitative variable can be represented by a continuous function [1]. We are concerned with the use of color - qualities that are present or represented in visual experiences coming from the human perception of electromagnetic spectrum [2] – as analytical parameter, typically used in qualitative analysis resulting from separation or identification reactions. The specification of a color by a color space, a mathematical model representing color as tuples of color components, permit their use for quantitative purposes using signals coming from different imaging devices including hand-held [3] and desktop scanners [4,5], CCD arrays [6], video cameras [7], digital photographic cameras [8] and digital color analyzers [9-11], producing very diverse color-based methods.

Among the color spaces that use the classifying descriptors hue, saturation and brightness [12] is the HSV color space. The main feature of which is the representation of the cognitive color information in a single parameter, the hue component H [13] which is independent of variations in color intensity coming from concentration and optical path. The use of this qualitative signal as a quantitative analytical signal is possible if a chemical equilibrium involving a sensor is displaced by an analyte with at least two distinct colors. The hue provides an improvement in precision, between 4 and 10 times superior CV, as compared to other optical signals such as absorbance.

Different optical techniques have been used in quantitative single-use sensors, however the most widely utilized is reflectance spectrometry. Given the structure of different types of optical single-use sensors [14], they are usually opaque, which is why the typical measurement method is by diffuse reflectance spectroscopy, with measurements at one or two wavelengths [15]. This technique involves measuring the intensity that can result from the interaction of

radiation with the reaction volume of the carrier when irradiation with electromagnetic radiation due to absorption, transmission and scattering by materials occurs. Generally, diffuse reflection coefficients of the measuring area of a disposable sensor and reference are measured, and from these measurements, the Kubelka-Munk function or its variations are calculated.

Measurement can be performed in two ways [16]. After reaction on the surface of the analytical element, the reflectance of the generated absorbing species in the sampling surface is determined. This approach has been the one adopted so far for monolayer fiber-impregnated single use sensors and the simple diffuse reflectance described by the phenomenological theory of Kubelka Munk is used for quantitative analysis. With the second approach, the sample is applied to the top surface and the color is measured by monitoring reflectance in the reverse surface of the element. This approach is common with multilayer single use sensors and makes use of a combination of both diffuse and specular reflection in the different layers, reagent layer and spreading layer mainly, that compose the analytical element [17]. In this last case the mathematical treatment is more complicated involving diffuse reflectance, ordinary transmittance, and specular reflectance of hemispherically distributed incident radiation, being typically described by the Williams-Clapper transformation [18,19].

Among the monolayer single-use sensors that use membranes made up of a single layer those with a homogenous layer are the simplest. These materials achieve a homogenous distribution of components through impregnation of an adsorbent (fiber-impregnated systems), deposition on a non-absorbent support, fabrication of a film using a film-forming material, or chemical immobilization on a support or adsorption on a membrane.

Examples of reflectance-based sensors include a calcium sensor fabricated by electrostatic immobilization of calcichrome at an anionic polymer membrane [20], a mercury sensor that uses the intensely colored reaction product with tyro-

dine adsorbed on polycaproamide membrane [21], and a test paper for the determination of aluminum based on a cellulose paper impregnated with chromeazurol S [22]. In addition to different multilayer sensors mainly used for the clinical laboratory [19,23], many lateral-flow sensors, typically based on immunoassay, have been proposed mainly for drugs and pesticides [24-26].

We are interested in quantitative disposable sensors that use the chromaticity characteristics as analytical parameters other than the typically used RGB channel intensity or a combination of such parameters [27]. Our focus is on the hue, H value, obtained from images of the sensors acquired by different imaging devices such as scanners, photographic cameras, and mobile phone cameras working in reflection mode. This approach is of particular interest for membrane optical sensors, especially those in the disposable format in order to improve their precision. Here the properties of the H coordinate are studied as an analytical parameter using a disposable K(I) sensor developed previously [28]. Two approaches, one based on reflection and another based on transflexion, are used to theoretically demonstrated that the H value can be used as a parameter to follow the behavior of the sensors and compare results with other possible analytical parameters derived from images of these sensor membranes.

3. Experimental

3.1. Reagents and membrane preparation

The potassium standard solutions were prepared weighing of analytical reagent grade dry KCl and dissolving it in water by exact weighing. All the standard solutions and samples were buffered using pH 9.0 Tris (hydroxymethyl)aminomethane 1 M buffer.

The chemicals used to prepare the potassium sensitive membranes were high molecular weight polyvinyl chloride (PVC), o-nitro-phenyloctylether

(NPOE) as plasticizer, tetrahydrofuran (THF) and the ionophore dibenzo18-crown-6-ether (DB18C6) from Sigma, the lipophilic anionic salt potassium tetrakis (4-chlorophenyl)borate (TCPB), and the chromoionophore (1,2-benzo-7-(diethylamino)-3-(octadecanoylimino) phenoxazine (liphophilized Nile Blue). All the reagents were purchased from Sigma-Aldrich (Química S.A., Madrid, Spain). To prepare potassium sensitive membranes sheets of Mylar-type polyester (Goodfellow, Cambridge, U.K.) were used. All chemicals used were of analytical- reagent grade. Reverse-osmosis quality water type III (Milli-RO 12 plus Milli-Q station from Millipore) was used throughout.

The membranes were prepared from cocktails composed by 26.0 mg of PVC, 63.0 mg of NPOE, 0.8 mg of DB18C6, 1.3 mg of liphophilized Nile Blue and 1.1 mg of TCPB, all in 1.0 mL of freshly distilled THF. Sensing membranes were prepared over 14×40×0.5 mm sheets of polyester with a spin coating technique (WS-400Ez-6NPP-Lite Single Spin Processor, Laurell Tech., USA) using two different volumes of cocktail (15 μL and 20 μL) to prepare membranes with different thickness. The red violet round-shape membrane has a diameter of 12 mm.

3.2. Measurement procedure

In all cases the membranes were activated by introduction into 10^{-2} M HCl solution for 3 minutes. Once activated, the membrane was introduced and equilibrated without shaking in the standard or sample solution for 3 minutes. Next, the sensing membrane was removed from the solution, and the image was obtained as indicated in the next section. Additionally some membranes were treated and measured after each equilibration with 10^{-2} M HCl, potassium standards and 10^{-2} M NaOH in order to calculate the robustness coefficient Rg.

The concentration of potassium tested for different purposes ranged between 10^{-7} and 0.1 M in all cases, buffered with pH 9 Tris at a final buffer concentration of 0.02 M. In the case of the real water samples, they were prepared taking 49 mL of water sample and 1 mL of pH 9 Tris 1M buffer solution.

3.3. Imaging devices, instruments and Software

Different devices were used to image the potassium membranes, namely a scanner, a reflex photographic camera, a compact camera and a mobile phone camera. The scanner was a CanoScan 8800f flatbed scanner (Canon USA, Inc., Lake Success, NY, USA) with a white LED light source and 48-bit color detection, working in reflection mode and saving the images in TIFF (Tagged Image File Format) format. The reflex camera used was a Canon EOS 500D (Digital Rebel T1i) digital SLR camera with an EF-S 60 mm f/2.8 macro lens. The detector is a 15.50-megapixel single-plate CMOS sensor with RGB primary color filters. Images were taken in JPG format. The compact camera was a Sony DSC T90 (Sony Corporation, Minato, Tokio, Japan) with 10.5 megapixel resolution and equipped with Carl Zeiss and Vario-Tessar 3.5-4.6/6.18-24.7 optic and 4x optical zoom and set at maximum resolution. The images obtained with the compact camera were in JPG format and 10.2-megapixel resolution. The integrated camera of a HTC Diamond (High Tech Computer Corporation, Taoyuan, Taiwan) mobile phone was also used to acquire images from the sensors. This camera was equipped with a 3.2 megapixel CMOS sensor, F2.8 lens, and an autofocus function. Images from the phone camera were stored in JPG format. An Ocean Optics USB2000 UV-Vis spectrophotometer (Ocean Optics, Dunedin, FL.) was use to obtain the spectrum of a light tent used for all digital camera images.

All the images acquired with cameras were obtained inside of an optical tent, PBL photo studio light tent 30", placed in a sun-lighted room, illuminated

with 3 daylight 600 W lamps (Steve Kaeser Photographic Lighting and Accessories, Ventura, CA, USA). To assure that the conditions when the images are taken are always the same, the sensing membranes, after equilibration with standards or samples, were introduced in a homemade support made of white reflective material where sensors were placed in a fixed vertical position inside the tent while the camera was in a tripod to maintain a constant distance between the camera and sensors.

The images were processed with a set of scripts and functions developed in Matlab r2007b (MathWorks, Natick, Massachusetts, USA). Statistical calculations were performed with Statgraphics software package (Manugistics Inc. and Statistical Graphics Corporation, USA, 1992), and Microsoft Excel (Microsoft Corp., Redmond, WA, USA) was used for general calculations.

3.4. Matlab Processing

All digital images were processed using the MATLAB programming environment. The basic steps image processing include: 1) Balancing: color balance and normalize the red, green, and blue channels; 2) Masking: determine which pixels in the image are colored; 3) Slicing: separate regions in the image that contain colored pixels and 4) Analyzing: calculate the most frequently occurring value of the hue in each colored region of the image

Balancing. In the balancing step the red, green, and blue channels are treated independently. First, the most frequently occurring value (mode) in the entire image is determined separately for each color channel. Because most of the pixels in the image are from the background, this value represents the "white" value for R, G, or B respectively. The RGB value of each pixel is then divided by the mode form the appropriate color channel. The result of this step is

a color-balanced image in which the RGB values range from 0 to 1 and white pixels have a value of 1 in each color channel.

Masking. In the masking step the maximum and minimum value is determined for each pixel in the image by comparing the R, G, and B values of the pixel. The difference between the maximum and minimum value is used to determine how "colored" a pixel within the image is. If the difference in the color channels is greater than a threshold value, the pixel is classified as colored. If the difference is smaller than the threshold the pixel is classified as grey (including black and white pixels as well). The threshold used for all images in this study was 30% of the maximum difference in the entire image (the most "colored" pixel). The result of this step is a logical mask with the same dimensions as the original image in which each pixel has a value of 1 if it is colored and 0 if it is grey.

Slicing. In the slicing step the logical mask produced in the previous step is searched for both rows and columns where there is a transition between lines (either horizontal rows or vertical columns) containing no colored pixels and lines containing at least one colored pixel. These transitional rows and columns then define a colored block. Blocks that do not meet a minimum size requirement (20000 pixels in most images used in this study) are discarded. Each colored block is then extracted as an individual picture. The result of this step is a set of cropped rectangular sub-images each containing the data for an individual membrane.

Analyzing. In the analyzing step the sub-images produced in the previous step are first rebalanced. This process is identical to the color balance and normalization done in the beginning of the image processing except that only the white pixels in the sub-image are used to calculate the value for each color channel's mode. The original values of R, G, and B are then re-normalized using these new values. (Note: Although the normalized values calculated in the be-

ginning of the image processing are replaced during this step, balancing is performed the first time in order for the masking step to correctly identify colored pixels. In images with poor white balance, these pixels can be misclassified as colored if the balancing is not done before masking.). The result of this step is the most frequently occurring value for RGB and Hue for each sub-image containing a membrane.

4. Rationale

The main objective of this paper is to demonstrate the use of hue, H from the HSV color space, calculated from images acquired with digital reflection devices as an analytical parameter.

Previous work demonstrated that the H parameter is suitable for monitoring the behavior of a bitonal optical sensor used for potassium determination. This sensor was based on a ionophore-chromoionophore mechanism, were a ion-exchange is performed inside the membrane, analyte ions entering in the sensor membrane result in protons leaving the membrane and causing a color change. (eq. 1 barred species means membrane phase):

$$\overline{L} + \overline{HC^+} + \overline{R^-} + K^+ \xleftrightarrow{K_{exch}} \overline{IL^+} + \overline{C} + \overline{R^-} + H^+ \quad (1)$$

The membrane is composed by an ionophore, L, which forms a complex with the analyte and retains it in the sensor; a chromoionophore, C, which is an indicator that changes its color by deprotonation; and a highly lipophilic anion, R^-, for ion-exchange purposes. All materials are contained in a plasticized PVC matrix. Based on this complexation reaction as more of the analyte goes into the bulk membrane, the chromoionophore is deprotonated and the hue of membrane changes from the acidic form, HC^+, to the basic form, C.

The ion activities ratio a_{H^+}/a_{K^+} in the aqueous phase is related to the equilibrium constant K_{exch} and the experimental parameter α through the sigmoidal-shape response function:

$$a_{K^+} = \frac{1}{K_{exch}}\left(\frac{a_{H^+}\alpha}{1-\alpha}\right)\frac{C_R-(1-\alpha)C_C}{\left(C_L-\left(C_R-(1-\alpha)C_C\right)\right)} \quad (2)$$

where C_L, C_C and C_R are the analytical concentrations of ionophore (DB18C6), chromoionophore (liphophilized Nile Blue) and lipophilic anion (TCPB), respectively and considering that the stoichiometric factor p for the complex analyte:ionophore and the charge ν of the analyte are both 1. The extent of the ion-exchange process, i.e., the recognition process, is typically followed by the normalized parameter 1-α (eq. 3) obtained from absorbance, fluorescence or other optical parameters according to eq. 3, where X is the value for a given measurement, and X_{HC^+} and X_C are the values coming from fully protonated and deprotonated chromoionophore species.

$$1-\alpha = \frac{[HC^+]}{[C]_o} = \frac{X-X_C}{X_{HC^+}-X_C} \quad (3)$$

The 1-α value can be calculated from experimental H coordinate using the three (H, H_{HC^+} and H_C) values. The shape of the sigmoid indicated by eq. 3 is the same using H (which varies between H_{HC^+} and H_C of 0.56 and 0.82 respectively) instead 1-α (which varies between 0 and 1), in a similar way as observed in a previous work [1]. Here we replace 1-α by H in the rest of the study because as a means of simplification in the calculation, necessitating only one measurement per sensor instead three, in addition to the enhanced robustness associated with the use of the qualitative hue parameter instead of an intensity based parameter.

The H parameter is calculated from images acquired with digital reflection devices, in which the sensing membrane located in a holder made with a perfect reflective material is crossed through by radiation and back being collected by the light detector.

The colorimetric behavior of the sensor membrane measured as before was predicted using the absorptivity spectra of the acid and base forms of the chromoionophore ($\varepsilon_a(\lambda)$ and $\varepsilon_b(\lambda)$ respectively), the CIE standard D65 illuminant ($P_0(\lambda)$), and the color matching functions for the CIE XYZ color space ($S_x(\lambda)$, $S_Y(\lambda)$, and $S_Z(\lambda)$). The absorbance of the membrane $A_{membrane}$ that contains a fraction of the total concentration (C_C) in the deprotonated form (α in eq. 2) can be calculated from eq. 4, where b is the thickness of the membrane.

$$A_{membrane} = \varepsilon_a bc_c(1-\alpha) + \varepsilon_b bc_c \alpha \tag{4}$$

In this study two well established models for the fraction of light reflected back to the imaging device were considered. In the first model the background is assumed to be a perfect reflector in which the incident photons must travel through the membrane, strike the background, and then travel back to the imaging device. In this transmission model the fraction of light returning is the same as the transmittance where the average pathlength (b in eq. 4) is somewhere between the film thicknesses and twice the film thickness, and the fraction of light returning to the imaging device (R) is given by eq. 5.

$$R = 10^{-A_{membrane}} \tag{5}$$

Alternatively, the fraction of reflected light (R) can be calculated according to Kubelka Munk relationship given in eq. 6 where k is the absorption coefficient and s is the scattering coefficient.

$$R = 1 + \frac{k}{s} - \sqrt{\frac{k}{s}\left(2 + \frac{k}{s}\right)} \tag{6}$$

Because k/s is directly proportional to absorbance, and the scattering coefficient is considered to be independent of wavelength, the reflectance of the semi-transparent membrane can be estimated from $A_{membrane}$ through the introduction of the adjustable parameter ω, which is proportional to the ratio of the thickness of the membrane (b) and the effective scattering coefficient of the background (s). This relationship is given in eq. 7.

$$R = 1 + A_{membrane} \cdot \omega - \sqrt{A_{membrane} \cdot \omega \cdot (2 + A_{membrane} \cdot \omega)} \quad where\ \omega \approx \frac{b}{s} \qquad (7)$$

Thus the fraction of reflected light can be calculated using either eq. 5 (transmission) or eq. 7 (reflectance). Using both of the models to calculate R, the XYZ tristimulus values were then calculated by numerically integrating (from 360 nm to 830 nm in 5 nm increments via the trapezoid rule) the intensity of each color channel according to eq. 8-10.

$$X = \int_{\lambda} P_0(\lambda\lambda) R_X(\lambda\lambda) d \qquad (8)$$

$$Y = \int_{\lambda} P_0(\lambda\lambda) R_Y(\lambda\lambda) d \qquad (9)$$

$$Z = \int_{\lambda} P_0(\lambda\lambda) R_Z(\lambda\lambda) d \qquad (10)$$

The XYZ values were then normalized by dividing each by the white point value, which was calculated by assuming that the light is not attenuated by the chromoionophore (XYZ is 0.9505, 1, 1.0890 for D65). The sRGB tristimulus values were then calculated from XYZ by linear matrix multiplication followed by gamma correction. The hue was calculated from the RGB values via eq. 11 where R, G, and B are the RGB tristimulus values.

$$H = \begin{cases} \left(\dfrac{G-B}{\max_{channel}-\min_{channel}}+0\right)\Big/6 ; \text{if } \max = R^{*} \\ \left(\dfrac{B-R}{\max_{channel}-\min_{channel}}+2\right)\Big/6 ; \text{if } \max = G \\ \left(\dfrac{R-G}{\max_{channel}-\min_{channel}}+4\right)\Big/6 ; \text{if } \max = B \end{cases} \quad (11)$$

* if H is less than 0 then add 1 to H

Using this procedure was possible theoretically calculating the values of H using α values between 0 and 1 in increments of 0.01. Similarly, the associated potassium activity to α values was calculated via eq. 2 considering that experimental value of K_{exch} is 3.85 x 10^{-8}, $C_L = C_C = C_R$ is 0.0236 m, the stoichiometric factor p for the analyte to ionophore complex is 1, and the charge of analyte ν is 1. Figure 1 show the values for the H calculated in this manner plotted as a function of the logarithm of potassium activity. Also displayed in Figure 1 are the experimentally determined values for the H of the sensing membrane as determined by flatbed scanner (+ symbols) and reflex camera (o symbols). A few things are evident in this figure. The calculated values for H are close to the observed values despite several adjustable parameters which all affect the predicted response. The transmission model, which standard error of the fit is 0.0186, (R calculated via eq. 5) gives a better fit to the experimental data than reflection model, which standard error 0.0295, but the differences are minor and may be attributed to these adjustable parameters such as the scattering coefficient or K_{exch}. In addition the experimental values for the scanner and reflex camera are very similar. The differences in the experimental measurements from these devices are primarily attributed to differences in lighting, which can be demonstrated with further modeling.

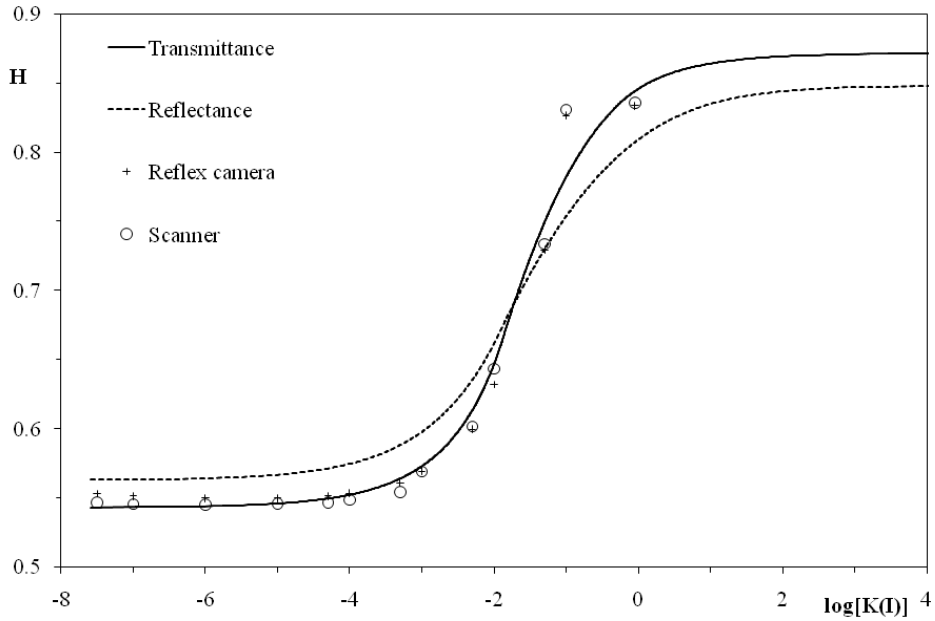

Figure 1. Adjust of experimental data to theoretical models

The effect of lighting conditions can be investigated by changing the illuminant, represented as $P_0(\lambda\lambda)$ in eq. 8-10. The D65 illuminant is representative of daylight illumination at noon, E is an equal energy illuminant in which the spectral power is the same at all wavelengths, and A is the CIE standard illuminant for incandescent/tungsten light. In this study the spectrum of the light tent used for all cameras images was measured with a spectrophotometer. The light intensities were then converted to 5 nm equally spaced values between 360 and 830 nm. Figure 2 shows the predicted values for the H using these four light sources (D65, E, A and light tent spectrum) as a function of α; additionally, the white points of each illuminant are given in Table 1. The interpretation of these results fits with intuition; the color of the sensor membranes is not exactly the same when they viewed under different types of illumination. The difference between an "ideal" source and daylight (the solid and dotted lines in Figure 2) is

negligible. But when viewed under the illumination of the light tent, the H of the indicator membrane at a half deprotonation is different; it should appear more "blue" and less "magenta". Thus modeling predicts that, at intermediate values of alpha, there will be a greater variability in the measured H of the sensor membrane as the lighting conditions (or white balance of the image) change.

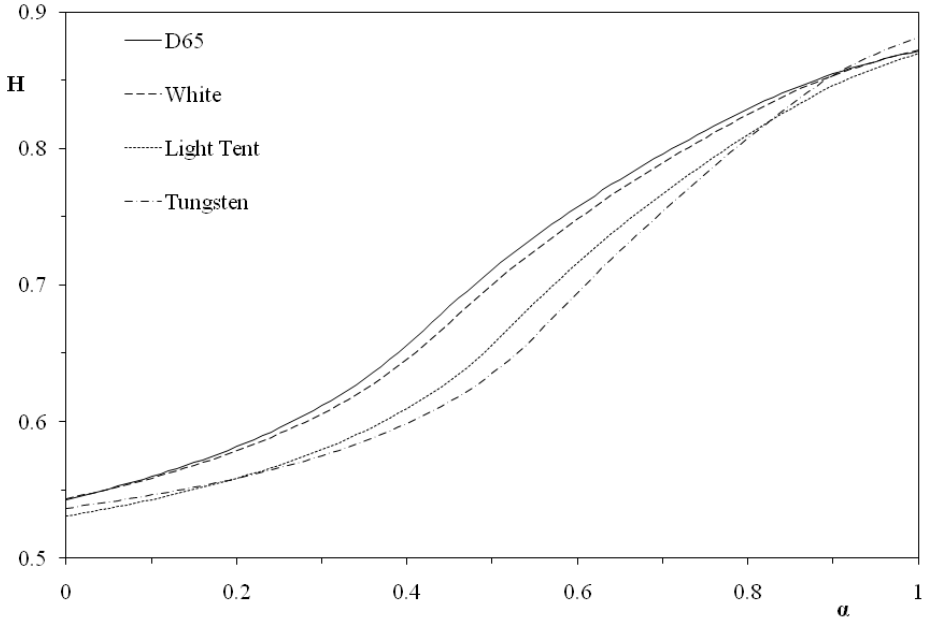

Figure 2. Variation of H value vs α depending of illuminant considered

Table 1. White points of various illuminants

Illuminant	X	Y	Z
D65	0.9505	1	1.0890
E	1.0001	1	1.0003
Light Tent	0.9177	1	0.7869
A	1.0985	1	0.3558

5. Results and discussion

Once the relationship between H and potassium concentration has been theoretically demonstrated using a transmission model that fits with the experimental data, we studied the influence of different factors on the performance of the analytical parameter H. These studies can be divided in three different groups: a) Dependence of H with the type of devices used in the imaging of the membrane, b) Membrane factors such as thickness of the sensor and chromoionophore amount, and c) Dependence of the illuminant used.

Additionally, it was necessary to define a coefficient to measure the robustness of the H parameter as these conditions were varied. For this purpose the robustness coefficient, Rb, was defined as:

$$Rb = \frac{Max_{avg} - Min_{avg}}{s_{pooled}} \tag{12}$$

where Max_{avg} is the average H value for all membranes that were equilibrated to the solution that gave the largest H value (NaOH solution, chromoionophore fully deprotonated), and Min_{avg} is the average H value for all membranes in the solution that gave the smallest value (HCl solution, chromoionophore fully protonated). S_{pooled} is the pooled standard deviation of all the membranes studied in each case. A greater the Rb coefficient indicates a more robust parameter because it implies lower S_{pooled} and/or higher range of variation of the signal; thus larger values indicate a parameter that is better suited for quantification.

5.1. Device dependence

The devices used were a scanner, a reflex digital photographic camera, a compact digital camera, and a mobile phone. With these devices the sensor was tested using 11 different potassium solutions ranged from 10^{-7} M to 10^{-1} M. Fig-

ure 3 shows the results obtained from different devices plotting the average of three replicates per device and solution. The H values obtained for each solution are comparable, showing that results do not depend on the device used to digitize the membrane. Also, the responses obtained from each device are very similar and define the same sigmoid curve.

Table 2. H values for different devices.

log[K(I)]	H value			CV
	Compact camera*	Reflex camera*	Scanner*	
-7.0	0.554	0.551	0.545	0.82%
-6.0	0.549	0.550	0.545	0.46%
-5.0	0.551	0.550	0.546	0.50%
-4.3	0.549	0.551	0.547	0.42%
-4.0	0.550	0.553	0.548	0.46%
-3.3	0.568	0.561	0.554	1.24%
-3.0	0.566	0.569	0.569	0.35%
-2.3	0.595	0.600	0.602	0.55%
-2.0	0.623	0.632	0.643	1.60%
-1.3	0.718	0.729	0.734	1.14%
-1.0	0.840	0.826	0.831	0.86%
***3 replicates per solution**			**Average CV**	0.76%

If we consider the precision obtained for each potassium concentration tested independently of the device used (Table 2), an average coefficient of variation CV of 0.76% was obtained considering images coming from the scanner and the two cameras and an average CV of 2.0% if all devices are considered.

Furthermore, the robustness coefficient Rg was calculated for the values of H parameter and other potential parameters such as R, G and B channels as shown in Table 3. This coefficient was estimated using all of the data from the scanner and the two cameras together as a single set because all points were similar and there was a large number of replicates (99). The value using the H parameter was 102 which is much greater than that obtained with the G channel,

24, which confirms that H is a parameter more suitable and robust than the others. In the case of mobile phone camera (Table 4) the Rg coefficient is higher for H, 32, with the exception of R channel, 38.

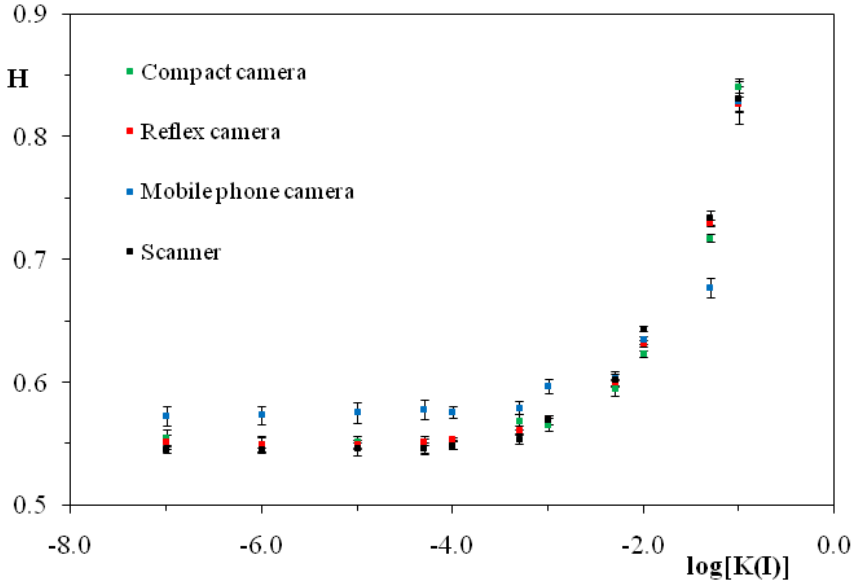

Figure 3. H dependence with potassium concentration for different devices.

Table 3. Influence of different factor on Rg coefficient.

Parameter	Rg coefficient				
	K(I) test*	Thickness*	Concentration*	Concentration and thickness*	White Balance**
R	17	8	5	5	16
G	24	7	6	5	12
B	20	7	6	5	12
H	102	55	25	27	57

*Calculated from reflex camera, compact camera and scanner data as a whole; **Calculated from compact camera

5.2. Membrane factors

The manufacture of the membranes introduces lot-to-lot variation, and hence increases the uncertainty in the measurements. The two main differences between individual membranes are the thickness and the amount of chromoionophore in the membrane. To study this variability, a set of sensors with different thicknesses was prepared with 15 μL (2.0 μm thickness) and 20 μL (2.7 μm) of cocktail, and another set was prepared with a reagent cocktail diluted by a factor of 2 with THF.

Table 4. Influence of different factor on Rg coefficient using a mobile phone camera.

	Rg coefficient			
	K(I) test	**Thickness**	**Concentration**	**Concentration and thickness**
R	38	7	10	6
G	8	3	4	3
B	6	2	2	2
H	32	23	37	22

Working with the same set of potassium solutions above described, the results obtained using sensors with the two different thickness studied (198 sensors) in terms of average CV was 0.74%. Considering the Rg coefficient, the H parameter presents the largest value (55) compared to the next closest value for the R channel (8) as shown in Table 3. In the case of mobile phone camera, the Rg coefficient calculated for H is 23 compared to the value for R channel (7) as shown in Table 4. Therefore, the differences observed using sensors with different thickness are negligible.

The precision of the measurements in terms of CV using sensors with the two different amount of chromoionophore tested (198 membranes) was

1.4%. Considering the Rg, again the value from H (25) is higher than the obtained for B channel (6) (Table 3). The value of Rg with the mobile phone was 37 for H (Table 4), better than the one for R channel (10). In conclusion, the tonal parameter H is robust to variations of chromoionophore amount.

Finally, the Rg coefficient was calculated considering all data from this study (normal cocktail/20 μL, normal cocktail/15 μL and diluted cocktail/20 μL with a total of 297 membranes). The H parameter maintains its robustness in terms of Rg, 27 for cameras and scanner (Table 3), and 37 for mobile phone, (Table 4) in opposition to the RGB channels which were 5, 5, 5 for scanner and cameras (Table 3) and 10, 4, 2 for mobile phone camera respectively (Table 4).

5.3. Illuminant dependence

The illumination is a factor that affects the H parameter as shown in the rationale section. In order to calculate the extent of this influence, images were taken with the compact camera in which the white balance setting was changed while maintaining constant illumination, resulting in images appearing as though lighted with different illuminants.

The white balances selected were sun light (5300K), cloudy (6000K), lamp (3000K), and fluorescent (4000K) and all these sets were tested over the eleven standard potassium solutions. Figure 4 shows the image of the same sensor obtained using different white balances.

Results obtained from this study, using 132 membranes, displays that a changing of the white balance has a small influence on the H value, as it is demonstrated in terms CV, the mean of which, considering all the white balances and the potassium concentrations studied, is 1.7%. Also the Rg coefficient demonstrates again that H is a robust and reliable parameter. The Rg value with the hue is 57 greater than any RGB channel, which gave values of 16, 12, and 12, re-

spectively (Table 3). This results show that illumination for sensing membrane imaging is not a very critical factor for H parameter acquisition.

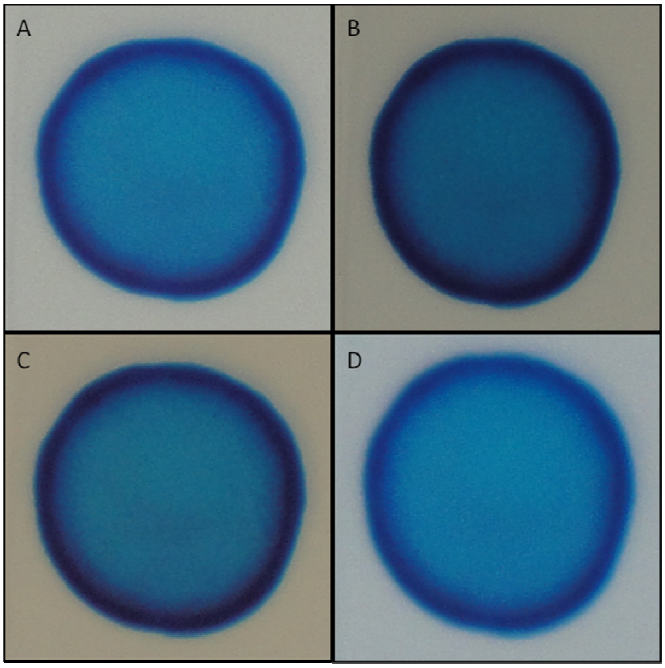

Figure 4. Membrane images acquired using different with balances. A) sun light (5300K), b) cloudy (6000K), c) lamp (3000K), d) fluorescent (4000K).

5.4. Calibration

Once the robustness of H parameter was demonstrated in reflection mode, we studied the calibration function for potassium. 11 potassium standard solutions ranging from 10^{-7} M to 10^{-1} M with three replicates each were used and the sensor membrane was imaged with the scanner and the two digital cameras.

The shape of the dependence as shown in Figure 5 is sigmoidal, as theory predicts. As usual in this type of sensors the central zone of the sigmoid can be linearized for calibration purposes and the equation $H=1.1(\pm0.1) + 0.16$

(±0.03) [K(I)]; R^2=0.998 was obtained. The limit of detection calculated as usual [29] from this regression was $3.5x10^{-4}$ M, result that is worse than the obtained working from images acquired in transmission mode ($3.6x10^{-5}$ M) [1].

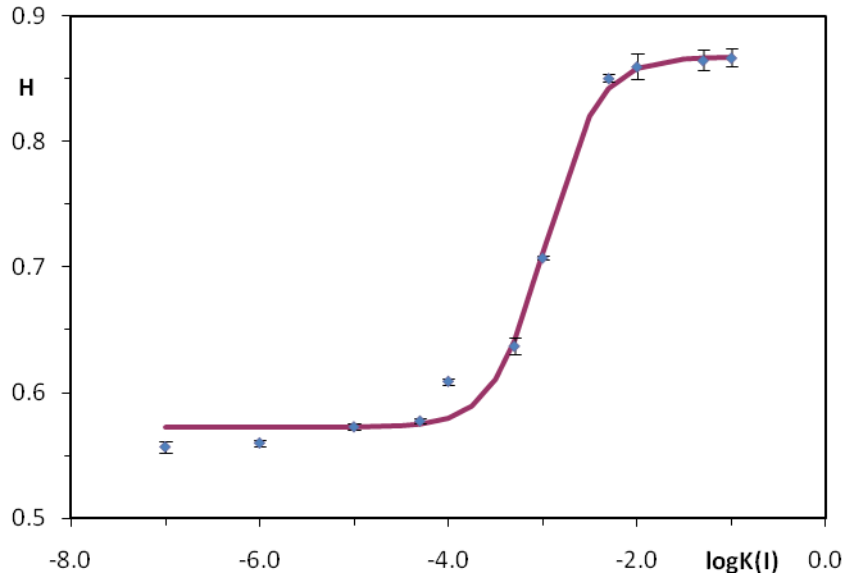

Figure 5. Calibration using an average of scanner, reflex camera and compact camera data.

However, considering the high precision of the measurements due to the high robustness of the parameter we use a Boltzmann type equation (eq. 13) to enlarge the dynamic range using the whole calibration set.

$$H = a_2 + \frac{a_2 - a_1}{1 + \exp\left(\frac{([K(I)] - a_o)}{a_3}\right)} \tag{13}$$

The constants of the Boltzmann type equation were a0 = -2.965; a1 = 0.572; a2 = 0.867; a3 = 0.280. The R^2 of the fit was 0.993 and using the IUPAC criteria to calculate the detection limit (3s), a dynamic range of $5.5x10^{-6}$ M to $1.0x10^{-1}$ M

was found. The limit of detection found is similar to that obtained working with transmission images using the same Boltzmann type equation ($4.5x10^{-6}$ M) [1].

The CV of 3 different potassium concentrations ($5.0x10^{-5}$, $5x10^{-4}$ and $5x10^{-3}$ M, 9 replicates each) were 0.42, 1.20 and 0.55%, respectively; similar values to those calculated using a scanner in transmission mode (from 0.14 to 0.75%) [1] and much better than using transflectance as analytical parameter (from 2.4 to 7.9%) [30].

To check the quality of the information obtained from the images acquired in reflection mode, different mineral water of diverse provenance (Spain) were analyzed for potassium concentration using atomic absorption spectroscopy as a reference method. The results obtained are given in Table 5 and are comparables using the p-value test.

Table 5. Determination of potassium in different types of matrices using AAS as a reference method

Samples	Phone	AAS	p-value
Mineral water 1	$4.5x10^{-5}$ M ± $0.3x10^{-5}$	$6.80x10^{-5}$ M ± $0.03x10^{-5}$	0.153
Mineral Water 2	$5.2x10^{-5}$ M ± $0.2x10^{-5}$	$6.02x10^{-5}$ M ± $0.03x10^{-5}$	0.051
Mineral Water 3	$5.8x10^{-5}$ M ± $0.4x10^{-5}$	$1.51x10^{-5}$ M ± $0.02x10^{-5}$	0.770
Mineral Water 4	$5x10^{-5}$ M ± $1.0x10^{-5}$	$4.97x10^{-5}$ M ± $0.04x10^{-5}$	0.431

6. Conclusions

The use of the H parameter from imaging devices working in reflection mode has been demonstrated to model and calibrate a potassium optical sensor.

To model the sensor behavior, two different modeling approximations were considered, one based on a transmission model and another based on a reflection model. Although both gave reasonable predictions the transmission based model gave better agreement with the experimental data.

The use of H color coordinate, as opposed to other optical parameters, as absorbance, reflectance or transflectance, permits a considerable simplification of the procedure for using the sensing membranes, requiring only one measurement in the calibration standards or samples. The use of this qualitative parameter gives good results for the quantitative determination of analytes by means bitonal optical sensors. Additionally, this parameter gives a high robustness and independence from variables such as the type of imaging device, illuminant, membrane thickness, and amount of chromoionophore in the sensing membrane.

Comparing results obtained using H in reflection mode with those obtained working in transmission mode, a very similar limit of detection was found using the whole concentration range studied modeled with a Boltzmann-type function ($5.5x10^{-6}$ M for reflection mode and $4.5x10^{-6}$ M for transmission mode), although it worsens if only the central section of the sigmoid is considered for calibration purposes ($3.5x10^{-4}$ M for reflection mode and $3.6x10^{-5}$ M for transmission mode). Considering the precision, it is better to use transmission mode (0.14 to 0.75% in transmission mode and 0.42 to 1.2% in reflection mode), although the value obtained from reflection is still good for a single use sensor.

The H parameter obtained from reflection images presents a major advantage, the possibility of use digital cameras or mobile phone cameras working in reflection mode, paving the way to in-situ analysis of real samples by non-trained personnel using these ubiquitous devices.

Acknowledgements

We acknowledge financial support from the Ministerio de Ciencia e Innovación, Dirección General de Investigación y Gestión del Plan Nacional de

I+D+i (Spain) (Projects CTQ2009-14428-C02-01 and CTQ2009-14428-C02-02); and the Junta de Andalucía (Proyecto de Excelencia P08-FQM-3535). These projects were partially supported by European Regional Development Funds (ERDF).

7. Conclusión

En este capítulo se demuestra la posibilidad de uso del parámetro H calculado a partir de imágenes adquiridas en modo reflexión. Para ello, en primer lugar se ha llevado a cabo un estudio del modelo al que se ajusta el parámetro H al variar la concentración de potasio usando un sensor óptico de un solo uso. De los dos planteados se ha visto que el que mejor se ajusta a los datos experimentales es el basado en transmisión, obteniéndose un ajuste cuya desviación estándar es de 0.0186, mientras que para el de reflexión es de 0.0295.

Tras el estudio del modelo, se estableció la influencia de diferentes factores sobre los valores de H obtenidos. El primero ellos fue la influencia del dispositivo de medida utilizado, para lo que se emplearon un escáner, una cámara fotográfica réflex, una cámara compacta y un teléfono móvil provisto de cámara. Observamos que, excepto en el caso del teléfono móvil, debido a la características de la cámara integrada, los resultados de los otros tres dispositivos son muy similares; tanto es así que el coeficiente de variación de todos los datos obtenidos es del 0.7%, por lo que decidimos en adelante utilizar todos datos procedentes de esos dispositivos como un solo grupo para así tener más réplicas y dar mayor consistencia a los resultados. No obstante, en el caso de incluir todos los resultados obtenidos incluido el teléfono móvil, la precisión empeora hasta un 2.0% solamente.

Posteriormente se estudió la influencia de factores químicos relacionados con la variabilidad de la membrana sensora, como son el grosor de la misma y la cantidad de indicador presente. Para ello se usaron todos los datos obtenidos con las dos cámaras y el escáner, obteniendo un coeficiente de variación del 0.7 y 1.4%, respectivamente.

Finalmente, se estudió la influencia de la iluminación utilizada a la hora obtener la imagen digital de la membrana. Para ello se utilizó sólo la cámara compacta modificando el ajuste seleccionado para balance de blancos a la hora

de digitalizar, y obteniendo un coeficiente de variación en las medidas del 1.7%. En todos los casos la robustez del parámetro H fue comparada con el de las coordenadas RGB, usando el coeficiente de robustez Rg, obteniendo siempre mayores valores de Rg para el parámetro H.

Una vez demostrada la estabilidad y robustez de la señal, se procedió a la calibración del sensor con las dos cámaras y el escáner. La función de calibrado se ajustó a una ecuación tipo Boltzmann, cuyo límite de detección, $5.5x10^{-6}$, es similar al obtenido usando el parámetro H calculado a partir de imágenes tomadas en modo transmisión. Además, se estudió la precisión de las medidas, que oscila entre 0.4 y 1.2%, y que son del orden de los valores obtenidos para el parámetro H en modo transmisión, 0.1 - 0.7%, y bastante mejores que para medidas de transflectancia, 2.4 - 7.9%.

Por tanto, queda demostrado que el parámetro H obtenido a partir de imágenes adquiridas en modo reflexión, origina unos resultados similares a los obtenidos a partir de dispositivos que trabajan en modo transmisión y con la gran ventaja del posible uso de gran cantidad de dispositivos de captura digital comerciales que adquieren las imágenes en modo reflexión.

8. Bibliografía

1. K. Cantrell, M.M. Erenas, I. Orbe-Paya, L.F. Capitan-Vallvey, Use of the Hue Parameter of the Hue, Saturation, Value Color Space As a Quantitative Analytical Parameter for Bitonal Optical Sensors, Anal.Chem. 82 (2010) 531.

2. Maund, Barry. Color. 2006. Metaphysics Research Lab, CSLI, Stanford University . Stanford Encyclopedie of Philosophy.

3. M. Kompany-Zareh, M. Mansourian, F. Ravaee, Simple method for colorimetric spot-test quantitative analysis of Fe(III) using a computer controlled hand-scanner, Anal.Chim.Acta 471 (2002) 97.

4. J. Gabrielson, M. Hart, A. Jarelov, I. Kuhn, D. McKenzie, R. Mollby, Evaluation of redox indicators and the use of digital scanners and spectrophotometer for quantification of microbial growth in microplates, J.Microbiol.Methods 50 (2002) 63.

5. A. Lapresta-Fernandez, L.F. Capitan-Vallvey, Scanometric potassium determination with ionophore-based disposable sensors, Sens.Actuators B 134 (2008) 694.

6. J.J. Lavigne, S. Savoy, M.B. Clevenger, J.E. Ritchie, B. McDoniel, S.J. Yoo, E.V. Anslyn, J.T. McDevitt, J.B. Shear, D. Neikirk, Solution-Based Analysis of Multiple Analytes by a Sensor Array: Toward the Development of an "Electronic Tongue", J.Am.Chem.Soc. 120 (1998) 6429.

7. K. Tohda, M. Gratzl, Micro-miniature autonomous optical sensor array for monitoring ions and metabolites 1: design, fabrication, and data analysis, Anal.Sci. 22 (2006) 383.

8. V.V. Apyari, S.G. Dmitrienko, Using a digital camera and computer data processing for the determination of organic substances with diazotized polyurethane foams, J.Anal.Chem. 63 (2008) 530.

9. E. Hirayama, T. Sugiyama, H. Hisamoto, K. Suzuki, Visual and Colorimetric Lithium Ion Sensing Based on Digital Color Analysis, Anal.Chem. 72 (2000) 465.

10. K. Suzuki, E. Hirayama, T. Sugiyama, K. Yasuda, H. Okabe, D. Citterio, Ionophore-Based Lithium Ion Film Optode Realizing Multiple Color Variations Utilizing Digital Color Analysis, Anal.Chem. 74 (2002) 5766.

11. Y. Suzuki, K. Suzuki, Optical sensors for ions and protein based on digital color analysis, Springer Series on Chemical Sensors and Biosensors 3 (2005) 343.

12. Cotton, Symon D'o,. Colour, colour spaces and the human visual system, School of Computer Science<[16] City>, 1996.

13. G. Wyszecki, W. S. Stiles. Color Science: Concepts and Methods, Quantitative Data and Formulae , Wiley Classics Library, Denver USA, 2000

14. Yu. Zolotov, V.M. Ivanov, V.G. Amelin, Test methods for extra-laboratory analysis, TrAC 21 (2002) 302.

15. Phillips, R., McGarraugh, G., Jurik, F. A., Underwood, R. D., Whole blood glucose test strip, US 5,563,042, 1996.

16. L. F. Capitan-Vallvey , in: Grimes, C. A.; Dickey, E. C.Pishko, M. V., Eds. (Ed.), Encyclopedia of Sensors, The Pennsylvania State University, Pennsylvania, USA, 2005, pp. 55-93 .

17. J. Greyson, Problems and possibilities of chemistry on dry reagent carriers, J.Autom.Chem. 3 (1981) 66.

18. F.C. Williams, F.R. Clapper, J.Opt.Soc.Am. 43 (1953) 595.

19. A. Zipp, W.E. Hornby, Solid-phase chemistry: its principles and applications in clinical analysis, Talanta 31 (1984) 863.

20. L.K. Chau, M.D. Porter, Optical Sensor for Calcium: Performance, Structure and Reactivity of Calciochrome Immobilized at an Anionic Polymer, Anal.Chem. 62 (1990) 1964.

21. R.F. Gur'eva, S.B. Savvin, A test method for the determination of mercury (I,II) on a polymer surface, J.Anal.Chem. 58 (2003) 990.

22. O.Yu. Nadzhafova, S.V. Lagodzinskaya, V. Sukhan, Test paper for the determination of aluminium in solution, J.Anal.Chem. 56 (2001) 178.

23. O. Sonntag. Dry Chemistry. Analysis with Carrier-bound Reagents, Elsevier Science Ltd, 1993.

24. W.J. Gui, S.T. Wang, Y.R. Guo, G.N. Zhu, Development of a one-step strip for the detection of triazophos residues in environmental samples, Anal.Biochem. 377 (2008) 202.

25. M. Mathai, K.J. Siebert, S.T.A. Siebert, R.A. Durst, S.G. Reeves, Development of a signal measurement technique for application in multi-analyte liposome immunomigration assays, Food Agric.Immunol. 10 (1998) 195.

26. G.P. Zhang, X.N. Wang, J.F. Yang, Y.Y. Yang, G.X. Xing, Q.M. Li, D. Zhao, S.J. Chai, J.Q. Guo, Development of an immunochromatographic lateral flow test strip for detection of beta -adrenergic agonist clenbuterol residues, J.Immunol.Methods 312 (2006) 27.

27. N.I. Ershova, V.M. Ivanov, Application of chromaticity characteristics for direct determination of trace aluminum with Eriochrome cyanine R by diffuse reflection spectroscopy, Anal.Chim.Acta 408 (2000) 141.

28. L.F. Capitan-Vallvey, M.D. Fernandez Ramos, M. Al Natsheh, A disposable single-use optical sensor for potassium determination based on neutral ionophore, Sens.Actuators B 88 (2003) 217.

29. L.F. Capitan-Vallvey, M.D. Fernandez-Ramos, P. Alvarez de Cienfuegos, Optical test strip for calcium determination based on neutral ionophore, Anal.Chim.Acta 451 (2002) 231.

30. I.d. Orbe-Paya, M. Erenas, L.F. Capitan-Vallvey, Potassium disposable optical sensor based on transflectance measurements, Sens.Actuators B 127 (2007) 586.

Capítulo 6

Uso de un teléfono móvil como analizador químico portátil

1. Planteamiento

En el capítulo anterior se ha demostrado la posibilidad de usar el parámetro H procedente de imágenes tomadas en modo reflexión como propiedad analítica para la calibración de sensores ópticos de un solo uso, para así poder cuantificar analitos utilizando estos sensores. La principal ventaja de tomar la imagen en modo reflexión es la posibilidad de utilizar dispositivos de imagen muy comunes actualmente como pueden ser cámaras fotográficas ya sean réflex, compactas o las integradas en un teléfono móvil. Todas ellas trabajan en este modo ya que capturan la imagen a partir de la luz reflejada por el objeto que vamos a fotografiar.

La principal ventaja del empleo de un teléfono móvil, entre otros dispositivos de electrónica de consumo, es su popularidad, ubicuidad, proximidad y creciente capacidad de procesamiento, lo que hace que sus aplicaciones de todo tipo se estén extendiendo incesantemente. La posibilidad de que cualquier persona sin conocimientos previos pueda llevar a cabo la determinación del analito o analitos deseados, utilizando un sensor ópticamente legible con una plataforma descentralizada, como es un teléfono móvil, va en la dirección del cambio de paradigma en ciencias analíticas, que lleva desde el laboratorio al análisis *in situ*.

Nuestro objetivo en este trabajo es trasladar y extender todo el procedimiento analítico descrito en el capítulo anterior a un teléfono móvil como plataforma completa de medida, de manera que no sólo se adquiera la imagen mediante el teléfono, sino que también se lleve a cabo el procesado de la misma así como la intrapolación del valor obtenido en la función de calibrado del sensor, pudiéndose así determinar la concentración de analito presente.

Para poder llevar a cabo todo este proceso ha sido necesario desarrollar una aplicación para teléfono móvil capaz de ejecutar el procesado de forma automática, esto es, sin intervención alguna del operador. Dicha aplicación funciona en dos pasos. El primero de ellos es el cálculo del parámetro H a partir de la imagen de la membrana sensora tomada con el teléfono móvil. Para discernir en la imagen la zona sensora del fondo y eliminar bordes, se utiliza la máscara direccional denominada operador SOBEL, aunque en una adaptación monodimensional. Ésta ha permitido la identificación de la membrana y el cálculo de un valor de H representativo, para lo que se ha utilizado la moda del conjunto, de forma compatible con su implementación en el procesador del móvil. Posteriormente dicho valor de H se introduce en la función de calibrado del sensor, realizada previamente con el propio teléfono móvil, y se obtiene el valor de concentración de analito. Para todo este estudio de prueba de concepto se ha utilizado un sensor de un solo uso para la determinación de potasio que ha sido previamente desarrollado en el grupo de investigación.

Mobile phone platform as portable chemical analyzer

A. García[a], M. M. Erenas[b], E. D. Marinetto[a], C. A. Abad[a], I. de Orbe-Payá[b], A. J. Palma[a] and L. F. Capitán-Vallvey[b]

ECsens. [a]Department of Electronics and Computer Technology, [b]Department of Analytical Chemistry, Faculty of Science. University of Granada, E-18071 Granada, Spain.

Abstract

In this work, a mobile phone platform for portable chemical analysis is presented. This platform is based on the use of the built-in camera for capturing the image of a single-use colorimetric chemical sensor, while a custom-developed software application processes this image for obtaining its characteristic H (hue) value, which is related to analyte concentration. This software application is optimized for mobile phone usage, thus preserving battery life and targeting reduced computation time through a customized image processing scheme including a modified monodimensional edge detection algorithm. Meanwhile, the influence of physical and chemical factors has been characterized, with results showing that the presented platform provides accurate results even when variations on distance from phone to sensor, image focusing, or image centering are induced. In the same way, factors such as indicator concentration and membrane thickness have been shown

to have negligible effects on the obtained H values. The calibration and testing procedures have shown that the presented platform is able to provide a detection limit of 3.1×10^{-5} M in a range of 3.1×10^{-5}- 0.1 M with a relative standard deviation for inter-membrane reproducibility lower than 1.6% for potassium concentration determination in solution.

Keywords. Mobile phone; Portable instrumentation; Imaging; Disposable optical sensor; Potassium determination

* Corresponding author; e-mail: *lcapitan@ugr.es*

2. Introduction

As mobile phone capabilities and processing power are increased, the number of applications and the size of the associated market have steadily grown. The current typical mobile phone includes high-resolution digital camera, usually above 3 Mpixels with autofocus and digital zoom, dedicated low-power high-performance processor [1], with running frequencies up to 1 GHz, and sophisticated operating systems [2,3], which usually offer multitasking, Java support, options for installing and running externally developed applications, etc. Thus, consumers have now in their hands a tool as powerful as some low-cost personal computers or netbooks, but for the inherent limitations of a hand-held device, basically screen and keyboard size and capabilities.

In this context, mobile phones have been used as supporting hardware in different applications in chemical analysis, but their capabilities may be exploited further by taking full advantage of both the hardware and software associated to mobile phones, so it is possible to transform them into valuable instruments. Most of the analytical uses rely on the concept of electronic and mobile health (e-health or m-health) or simply telemedicine, referred to the use of technology and mobile devices to improve the availability and quality of health care. Usually, an analytical module is connected to a phone that collects the health information data and communicates it to a health network platform [4-8]. Their most common use is simply as a device for imaging and transmission of pictures to a central server, which translates latent information into chemical data.

Therefore, mobile phones have been used to provide a way to easily collect, transmit, and organize data along with different analytical procedures, as it is the case in lateral flow immunoassays. In that assays, an immunochromatographic step is applied through immobilizing the antibodies and/or oligonucleotides at predetermined locations on the membrane (capture zones) that permit to read visually or by imaging devices, that is, by means of one or more optically readable lines on

a test strip. Cocaine and its major metabolite, benzoylecgonine, can be determined by imaging on a phone camera the lateral flow immunoassays that transmit the image to a central computer server, where a quantitative ratiometric pixel density analysis (QRPDA) is performed [9]. Other similar procedures have been patented based in the same concept, with the phone acting as a capturing device that does not compute the result but just send data to a server [10,11]. Another portable and quantitative assays are based on microfluidic devices, as the paper-based device proposed for the simultaneous analysis of glucose and protein in urine, along with a cellular phone that acquires images and transmits digital information to an off-site laboratory, where the data are analyzed and the results of the analysis are returned [12]. A further advance is the 3D microfluidic paper analytical devices (μPADs) fabricated by layering paper patterned into hydrophilic channels and hydrophobic walls and tape patterned with holes that connect channels in different layers of paper, with applications in telemedicine through the help of a phone camera as in the prior case [13]. A low-cost system for sensing bad-smell, oriented to the monitoring of living environments, was described based on the well known gas detector tubes in which the reading at a certain time of the length of the discoloration layer permits the estimation of gas concentration. The combination of up to six gas detector tubes with a mobile phone to acquire and transmit images and an external computer allows to calculate the discoloration speed through brightness changes and, thus, the measurement of the gas distribution [14,15]. A last example of the use of mobile phones for imaging and transmitting is a visible sensor array system proposed for simultaneous multiple SNP (Single nucleotide polymorphisms) genotyping based on alkaline phosphatase-mediated precipitation of coloured chemical substrates. The recording of the image by a mobile phone equipped with a digital camera permits the quantification in a desktop computer [16].

A different approach is presented by Filippini *et al* [17], who make use of spectral fingerprinting (computer screen photoassisted technique CSPT) for chemical sensing applications based on a standard mobile phone, where the screen is

programmed as a light source in combination with the phone's camera, also transmitting to a remote site for data evaluation. The use of a mobile phone for signal processing is proposed in some cases but not connected to image data. As an example, the inclusion of a fuel cell sensor for breath ethanol in a mobile phone permits to measure the blood ethanol content [18].

In this paper, a more complete use of a mobile phone as an analytical tool is presented. Concretely, for this proof of concept study we use a potassium sensor previously studied by us [19,20]. This optical sensing membrane for potassium is based on ion-exchange equilibrium between an aqueous solution containing the analyte and a plasticized PVC sensing membrane containing ionophore that drives the reaction and the H^+-selective chromoionophore. The more analyte enters into the bulk membrane, the more chromoionophore is deprotonated and then greater is the hue change of the membrane from the acidic form, blue for the lipophilic Nile Blue chromoionophore used in this membrane, to the magenta color of the basic form of the chromoionophore. The ion activities ratio a_{H^+}/a_{K^+} in aqueous phase is related through an equilibrium constant with the experimental parameter, a relative optical signal, which can be built from absorbance [21], fluorescence [22], reflectance [23], transflectance [24], refractive index [25], or color coordinate as could be one RGB channel [26], giving rise to a sigmoid-shape response function. Previously, we have demonstrated that the use of color, namely through hue-oriented colour space, as is the HSV, offer several advantages as analytical parameter, because it represents the colour information in one single parameter, the coordinate H (hue). In case of bitonal optical sensors that produce a colour change and hence a H change by reaction, the use of this coordinate yields a substantial improvement in precision and is better suited for quantification [20].

In this framework of image analysis as analytical tool, this paper examines the possibilities and limitations of a mobile phone as a complete analytical instrument, along with single-use optical sensors, for imaging, extracting the analytical

parameter and calculating the analyte concentration. As it will be described in the following, a custom image processing application has been developed for mobile phone usage. This paper is organized as follows: in Experimental Section the membrane preparation and the software platform development are described, indicating the measurement procedure and the algorithms for image processing and coordinate H calculation. After that, in the Results and Discussion Section, the software application is first tested with low resolution images preloaded in the mobile phone. After that, the whole measurement procedure is implemented in the mobile phone, using the built-in camera for image acquisition and then processing these images for computing the H values and thus analyte concentration. This allows characterizing the presented platform attending to both physical and chemical factors. Later, the calibration and validation procedures are described and, finally the main conclusions are summarized.

3. Experimental

3.1. Instrument and software

While there are other options for developing software applications for mobile phones, such as platform-specific Phyton or C++ [27] implementations, JavaME has been selected for a number of reasons: it is an open source language, with a variety of free development environments [28], simulators and other tools being available; development of Java-based applications is platform independent, providing that an adequate Java Virtual Machine is available for the targeted device, which is the case for most computer operating systems, mobile phones and PDAs, and a growing number of devices such as household appliances, automotive devices, etc. Thus, Java-based applications can be used on almost any platform, or even can be easily migrated if any specific or device-dependent API (Application Programming Interface) has to be used. On the other hand, while the market shares of iPhone devices and Android-based platforms are steadily growing, Nokia pro-

vides a variety of devices in the sector and is still the mobile phone market leader. Moreover, Nokia provides a handful of development resources for its Symbian-based devices, thus allowing the easy generation of applications for this type of devices.

Figure 1. Mobile phones used. a)Nokia E65; b)Nokia 6110; c)Nokia N73

In this way, the devices used as analytical instruments were the mobile phones Nokia E65, Nokia 6110 and Nokia N73 (Espoo, Finland), which run Symbian S60 operating system (Figure 1). The two first were only used for the processing of preloaded images for application debugging and testing, while the N73 was the main test platform for the complete measurement process, image capturing and subsequent concentration determination. The integrated cameras of the phones were used to acquire images from the sensing membranes, consisting on CMOS sensors ranging from 2.0 to 3.2 megapixels with autofocus function in the case of the N73 model. JavaME was selected for the development of the portable analysis platform, with Netbeans along Nokia's S60 Platform SDK for Java as development

platform. Apart from the mentioned mobile phones, the phone emulator in the SDK was also used for software debugging and testing, while Matlab software was used for the development and tuning of the image processing techniques described below. In case of images not captured by the phone camera, a commercial ScanMaker i900 scanner (Microtek, Taiwan) was used for acquisition and digitalization, with a 300 dpi resolution and 24-to-48 bits of colour.

3.2. Reagents and membrane preparation

The potassium standard solutions were prepared by exact weighing of analytical reagent grade dry KCl and dissolution in water. All the standard solutions and samples were buffered using pH 9.0 Tris(hydroxymethyl)aminomethane 1 M buffer.

The chemicals used to prepare the potassium sensitive membranes were dibenzo18-crown-6-ether (DB18C6) as ionophore, potassium tetrakis (4-chlorophenyl)borate (TCPB) as lipophilic anionic salt, (1,2-benzo-7-(diethylamino)-3-(octadecanoylimino) phenoxazine (liphophilized Nile Blue) as chromoionophore, high molecular weight polyvinyl chloride (PVC) as membrane polymer, *o*-nitro-phenyloctylether (NPOE) as plasticizer and tetrahydrofuran (THF) as solvent. All the reagents were obtained from Sigma-Aldrich (Madrid, Spain). Sheets of Mylar-type polyester (Goodfellow, Cambridge, UK) were used as plastic support for preparing the membranes. Reverse-osmosis quality water type III (Milli-RO 12 plus Milli-Q station from Millipore) was used throughout.

The membranes were prepared from cocktails composed by 26.0 mg of PVC, 63.0 mg of NPOE, 0.8 mg of DB18C6, 1.3 mg of liphophilized Nile Blue and 1.1 mg of TCPB, all in 1.0 mL of freshly distilled THF. Sensing membranes were prepared over 14×40×0.5 mm sheets of polyester with a spin coating technique (WS-400Ez-6NPP-Lite Single Spin Processor, Laurell Tech., USA) using

20µL of the cocktail. The red violet round-shape membrane has a diameter of 12 mm.

3.3. Measurement procedure

The procedure of use of the membranes was the same in all the cases. First of all, the membranes were activated by introduction in 0.01M HCl solution for 3 minutes. Once activated, the membrane was introduced and equilibrated without shaking in the standard or sample solution for other 3 minutes. Next, the sensing membrane was removed from the solution and placed in the holder, obtaining the image with the mobile phone as indicated in the next section.

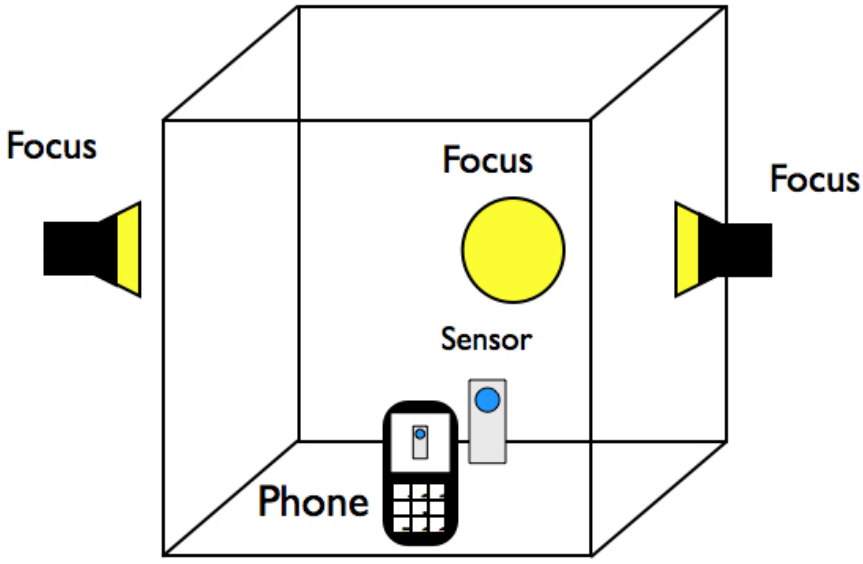

Figure 2. Schematic view of the experimental setup for the membrane image acquisition with mobile phone cameras. Illumination lamps, membrane and phone positioning are shown.

The concentration of potassium tested for different purposes ranged between 10^{-7} and 0.1 M in all cases, buffered with pH 9 Tris at a final buffer concentration of 0.02 M. In the case of the real water samples, they were prepared taking 49 mL of water sample and 1 mL of pH 9 Tris 1M buffer solution.

The membrane images were obtained using both the commercial scanner mentioned above, and the built-in camera of the mobile phone at the highest possible resolution, setting automatic white balance and automatic configurations for any other camera parameters. All the images were saved in JPEG (Joint Photographic Experts Group) format, as it is the default format in the tested Nokia mobile phones. The images acquired with the phone cameras were obtained inside of an optical PBL Photo studio light tent 30", illuminated with three daylight (D65) 600 W lamps that were distributed around the tent as shown in Figure 2. This assures a homogeneous illumination inside the tent. The sensing membranes were introduced after equilibration with standards or samples in a homemade support made of white reflective material. Thus, the membranes were placed in a fixed vertical position inside the tent in order to maintain a constant distance between the camera and the sensing membranes. The camera was fixed in the desired place inside the tent using tweezers and the distance from the sensor to the front of the phone was measured using a calibrated ruler. In this way, it is assured that the conditions for imaging are always the same.

3.4. Mobile phone software development

In the following, the image processing developed for phone application is described, as well as the implementation details, while further sections will discuss the obtained results.

3.4.1. Image processing

As it has been mentioned in the Introduction, tone (H coordinate in the HSV colour space) is the image characteristic that will be related to the analyte concentration. While the RGB colour space is the most widely utilized in chemical analysis [29-33], for the purpose of concentration determination the HSV space, obtained from a transformation of the RGB coordinates, is better suited [20] and thus will be used, specifically the H (hue) component.

The general scheme of the implemented processing requires to first transform the sensor image, usually represented in the RGB space, to HSV coordinates; after that, an image histogram is obtained, which will determine the membrane characteristic H as the maximum of this histogram, which corresponds to the mode of the H distribution. This H value will then be related to concentration, as described below. Although this processing is quite simple in its fundamentals, its computational complexity may be not as simple, even more as complex or large images have to be considered. While this is not a problem for off-line processing on an external computer, the limitations of a portable, hand-held, battery-operated mobile phone have to been taken into account. In this way, reducing the computational cost of image processing is crucial, not only in terms of computation time but also in order to preserve energy consumption and thus battery life. This is made possible by the application of border or edge detection techniques, whose aim is to differentiate the image areas containing useful information from those that do not contribute to establishing a proper value for the H coordinate. In this way, the portion of the image to be analyzed as described above is reduced, thus limiting the image processing to be carried out. While a wide range of edge detection techniques is available [34], the selected technique has to be light enough in order to not suppose a larger computational cost than this saved by its application.

Edge detection techniques are usually based on the use of masks, which allow searching for sudden changes of a certain image parameter, *i.e.*, a border or

edge, through the definition of gradients over this parameter. Thus, different masks, combined with the mathematical operations associated to the mask application, define different type of edges to be found. However, the mere application of the mask does not suffice and usually further processing is required, with the application of directional masks for improving the results, which is referred as thresholding. For the development of this work, three border detection methods have been considered: differential detection [34], Prewitt operator [35], and Sobel operator [36]. The first method relies on the application of four 3×3 masks for obtaining image derivatives at each pixel on the vertical and horizontal directions, as well as on both diagonals, with a further lineal combination of these derivative images. Thus, the computational costs associated to this method make it not adequate for its use in a mobile phone. On the other hand, the application of the Prewitt operator requires only the use of two of the previous masks, vertical and horizontal, later averaging the resulting images and performing a histogram extension for improving contrast. Although this method implies a reduction in computational costs when compared to the differential detection, both of them separate the membrane from the background but do not isolate the membrane border from the membrane body itself. On the other hand, the Sobel operator [36] comprises two masks, for vertical and horizontal edge detection, respectively, which do compute the first-order derivative combined with a Gaussian smoothing filter. This filter allows reducing noise effects during edge detection. While the computational complexity of this method is comparable to that of the Prewitt operator, the obtained results are more adequate for the proposed mobile phone chemical analysis application. However, a complete bidimensional processing is still computationally too intense, so an *ad hoc* monodimensional adaptation of the Sobel edge detection has been developed for mobile phone implementation.

For the adaptation of the Sobel edge detection, the first issue to solve is the selection of the adequate space for image processing. While edge detection is usually carried out over a grey-scale image, the transformation from RGB to grey-

scale would require extra computation. Thus, in this application, the V (value) coordinate, which corresponds to image brightness and is equivalent to a grey-scale representation, has been selected for edge detection. In this way, V values are available once the image has been transformed from RGB to HSV, so no extra computation is required. Meanwhile, the edge detection will be started looking for the central vectors of the membrane image in both directions, since they provide the areas with most significative information within, as illustrated in Figure 3. As it can be seen, apart from limiting the process to computations over vectors (pixel columns or rows in the image), the central membrane section is clearly delimited by two valleys associated to the membrane border in the V coordinate representation.

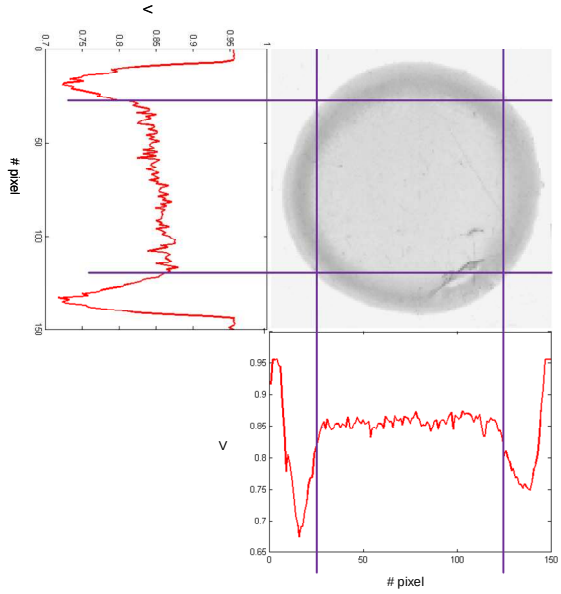

Figure 3. Use of V coordinates for delimiting membrane borders. Membrane image in V coordinates (center) and V values *vs* pixel position for two perpendicular lines passing through the image center (bottom and left) showing inner edges determination with red lines.

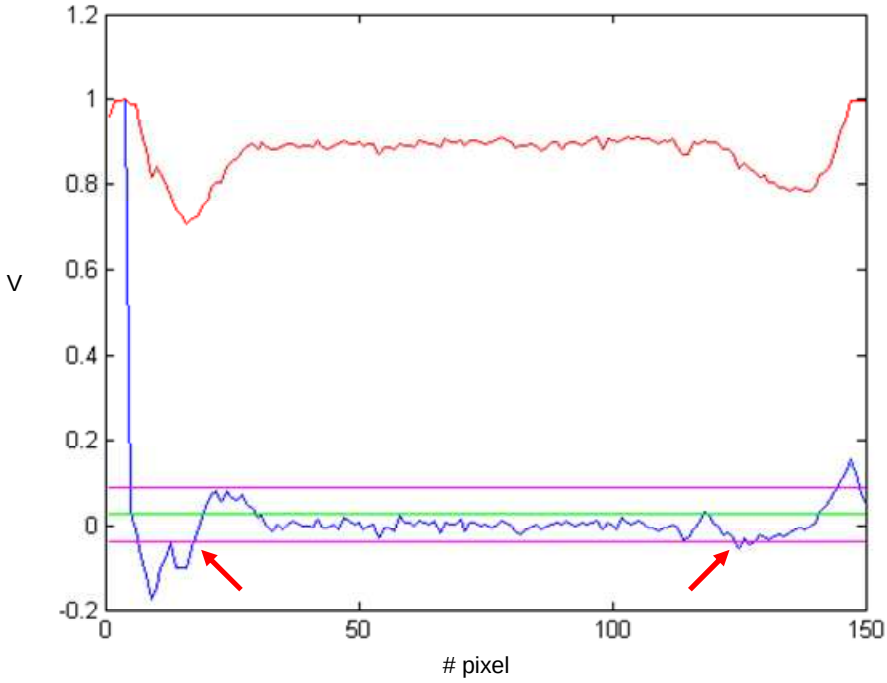

Figure 4. Original V central vertical vector (in red), processed vector with the modified Sobel operator (in blue), average processed V value (green) and variance limits (magenta). Arrows indicate edge limits.

However, given the characteristics of the membrane images and the variable width of the border, it is necessary to refine the edge detection, since the shape of the valleys in Figure 3 do not allow for an immediate decision on edge positioning. Concretely, it would be possible to use a monodimensional 3-element Sobel operator, [2 0 −2], but this may not properly process the central vectors if the membrane border is too thick, with a correspondingly wide valley in Figure 3. Thus, a modified monodimensional Sobel operator is proposed:

$$Modified\ \ Sobel\ operator = \begin{bmatrix} 2 & 0 & 0 & 0 & -2 \end{bmatrix} \quad (1)$$

that compromises 5 elements and allows the identification of thicker or out of focus edges.

Both central vectors are processed applying this modified Sobel operator, and the average and variance values are computed for the resulting vectors. In this way, the edges of the area where the H coordinate will be determined are defined as the pixels with V coordinate values not separated from the average V value more than the variance. This is illustrated in Figure 4, where an example of original vertical central vector (in red) and the processed vector (in blue) are shown, also displaying the average V value and the variance limits.

Once the edge of the useful membrane area have been defined for both vertical and horizontal directions using the modified monodimensional Sobel edge detection, the histogram of the H coordinate is performed. The membrane H-value is then computed as the mode of this histogram.

3.4.2. Platform implementation

Having in mind both software and hardware considerations, Java 2 Micro Edition (J2ME) [37] was selected for the development of the portable analysis platform, while Nokia S60 Symbian-based devices were targeted. Thus, Netbeans [38] along with Nokias's S60 Platform SDK for Java [28] was chosen as development platform. In this way, the developed applications have been tested on the device emulator included in the SDK as well as on a variety of Nokia mobile phones available in the laboratory, including several models of the E and N series, mentioned above, and some older models. While these older models do not include the same versions of the operating system and the same processors than their E- and N-series counterparts, they were used as a benchmark for the portability of the developed applications, since they were able to run every application tested providing identical results to those provided by the emulators and the E- and N-series devices.

Figure 5 shows typical several screen captures of the developed software application for two sensors equilibrated with solutions with different potassium concentration, illustrating its main features. The sensor image captures are displayed in the central pictures and, in the left, the result screens are showed, comprising the cut out images with the proposed modified Sobel algorithm and the calculated H coordinates. Comparing both sensor images (before and after edge detection), it can be observed that the edge detection procedure is a proper working tool for this task.

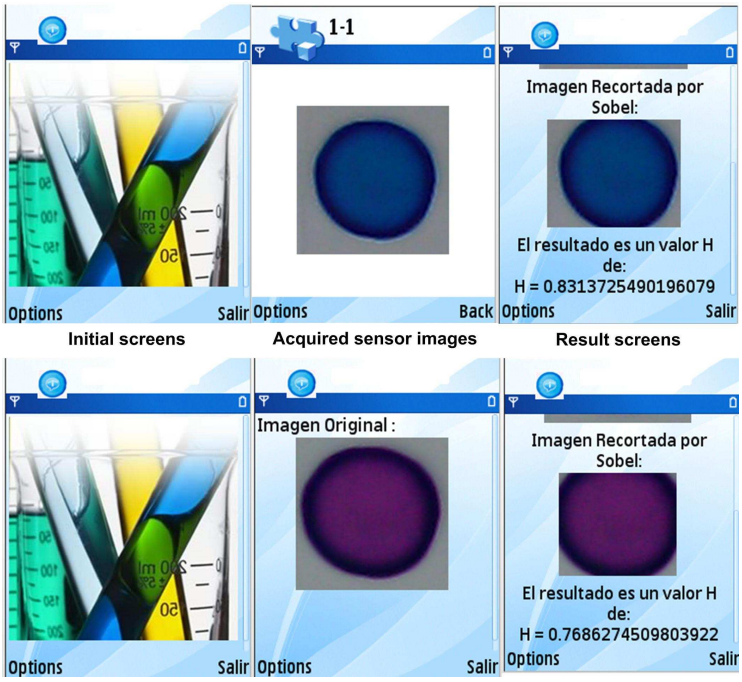

Figure 5. Screen captures of the developed software application showing: (left) the presentation screens, (center) the screens with an acquired sensor images and, (right) final screens with processed images and H coordinate results, for two different potassium concentrations.

4. Results and discussions

4.1. Preliminary results

The first step for testing the signal processing implementation in the mobile phone was to use images of the same single-use potassium sensor acquired with an external scanner, thus loading them into the phone memory for processing by the software application. Therefore, at this point, the camera of the phone was not used to acquire these images in order to separate the influence of the camera in the final analysis. Moreover, in this first version of the software, the image size was limited to 150×150 pixels.

In this way, a set of five different membranes was prepared, equilibrated with solutions of known potassium concentration in the range from 10^{-7} M to 10^{-1} M. These membranes were scanned and processed to obtain low resolution images. The resulting images were processed on a Nokia E65 in order to obtain the corresponding normalized H values. These results are depicted in Figure 6, where symbols show averaged values for the five replicas and error bars are two times the standard deviations. Figure 6 shows the typical sigmoid-trend response of this kind of ionophore-chromoionophore sensors, as mentioned above. In fact, a sigmoid function has been proposed to model these averaged data for calibration purposes:

$$H(x) = a_2 + \frac{a_1 - a_2}{1 + e^{\frac{x - a_0}{A_3}}} \tag{2}$$

where a_0 to a_3 are fitting parameters and x represents the decimal logarithm of the analyte concentration in molar units. In Figure 6, a fit between experimental H values and this model is represented by a solid line

Therefore, the calibration function is given by,

$$\log[K(I)] = a_0 + a_3 \cdot \log\left(\frac{a_1 - a_2}{H - a_2}\right) \tag{3}$$

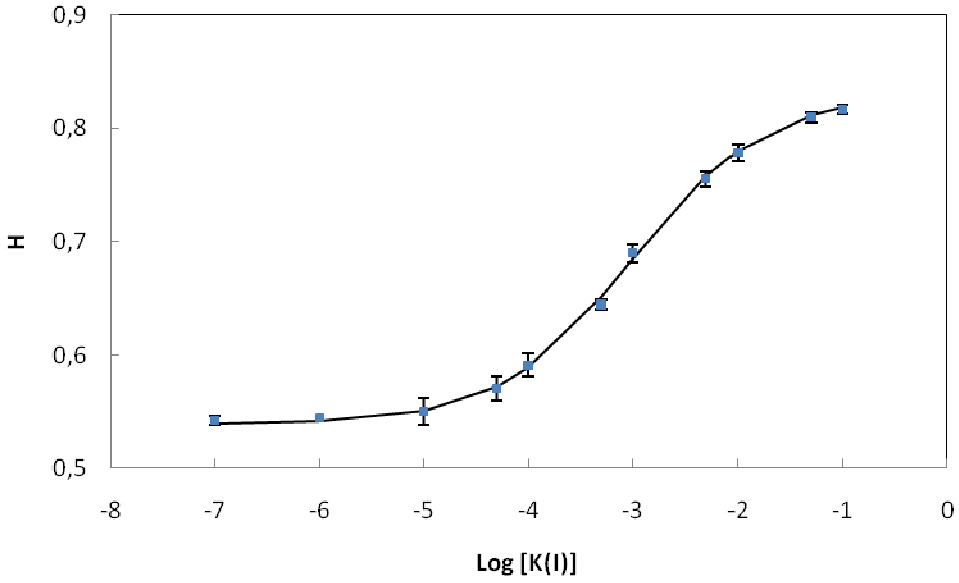

Figure 6. H coordinates *vs* potassium concentration. Symbols with error bars show H values obtained from the mobile phone with preloaded images, and solid line corresponds to a sigmoid modelization.

Equation 3 has been used to recover the concentration values, which have been compared to the theoretical data in the range from 10^{-5} to 10^{-1} M, where there was more H value variation. In this range, the maximum deviation between theoretical and experimental data is 4 % of the logarithm of the potassium concentration, which is a very acceptable agreement for this first software version with low resolution images.

4.2. Image acquisition by the phone camera

Once the software application has been shown to produce reliable results, the complete mobile phone platform is tested. As a mobile phone is not initially intended as an analytical tool, it is necessary to demonstrate its suitability for ob-

taining valid analytical information from an image of the sensor acquired directly with the phone camera. Thus, the most relevant issues that influence the physical measuring conditions, such as sensor to phone distance, focusing, centering of the sensor in the image, and hand-held operation of the phone, are addressed. Additionally, chemical factors such as membrane thickness and composition are also taken into account.

4.2.1. Influence of physical factors

As described in Section 2.3, the phone and the membrane were placed in an optical tent in order to maintain the illumination conditions as closer to daylight, controlled and homogeneous as possible, since daylight should be the typical illumination for in-situ measurement conditions. This experimental setup allowed holding the phone and the membrane at controlled distances. Thus, 11 different positions were tested, from 5 cm to 55 cm, in 5 cm intervals, and for each distance 3 images were captured for 3 different membranes equilibrated with 5×10^{-5}, 5×10^{-4} and 5×10^{-3} M potassium, respectively. These images were processed with the software application on the same phone used for image acquisition, and the corresponding H values were obtained, which are displayed in Figure 7 as a function of the distance from the phone to the membrane and for the set of images obtained with the N73 phone. It can be observed that this distance does not affect the obtained H value in the studied range. The values of relative standard deviation (RSD), calculated for each membrane using all the distance data, were 0.75%, 0.68% and 0.76%, respectively. This result was expected because the H value obtained for the membranes' images is independent of the area of the image containing membrane information, which depends on the distance from the camera to the sensor. When this distance is increased, the size of the membrane image within the total image area decreases, so there are less pixels containing useful information. However, this reduction in the number of significative pixels available to the soft-

ware application has not lead to changes of the H value. Numerically, there is a reduction in the number of useful pixels of a factor of 100 when moving the phone away from the membrane, from 5 cm to 50 cm distances. This shows that the software is robust enough to overcome this effect and that any induced variation is negligible.

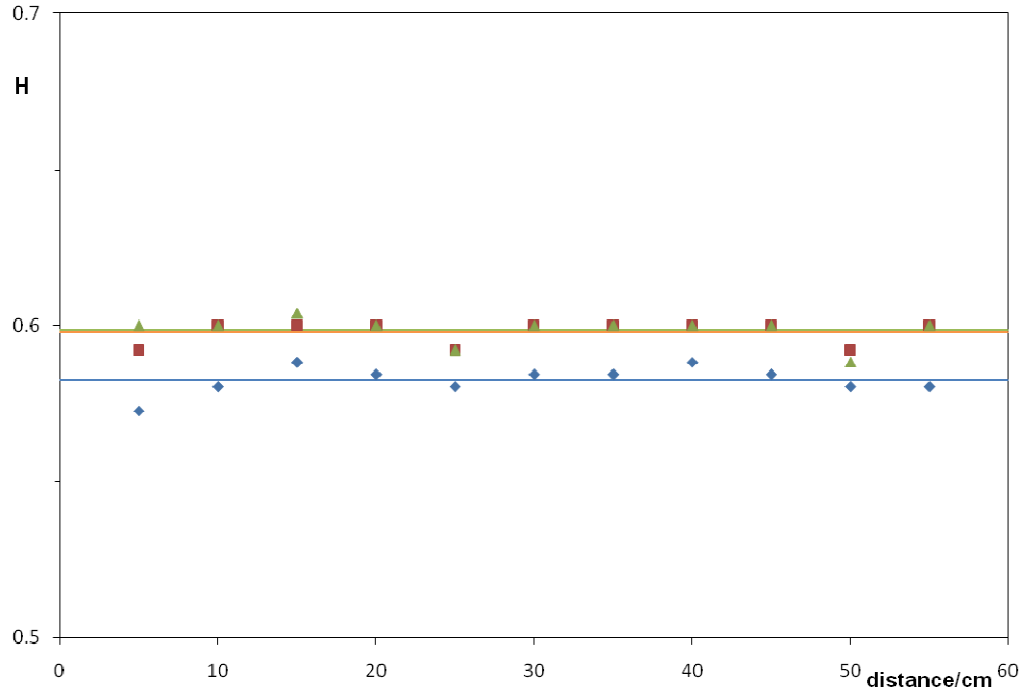

Figure 7. H coordinates as a function of the membrane-phone distance for three different sensors. Symbols show experimental H values obtained from the mobile phone and solid lines correspond to the averaged H value for each membrane. The RSD for the results

Other factor that is related to the distance from the camera to the membrane is the focusing of the image. It must be noted that usual phones include not so sophisticated optics, some of them even with fixed focus, so proper focusing is not possible for distances shorter than a predefined length. Even for phones with

cameras featuring autofocus, as it is the case for the N73 device, focus range starts at 10 cm, while the other phones available for this study with fixed focus cameras feature typical minimum focus distances up to 20 cm. Thus, data in Figure 7 for distances below 10 cm correspond to unfocused images, so it must be noted that the software application is extracting correct H values (0.588 for 5 cm and 0.593 for 10 cm) even in these conditions. It is worth noting that this is an important contribution of the proposed software application, since distances around 10 cm are a natural election for hand-held operation of the phone, while they also maximize the size of the membrane within the captured image, *i.e.*, the number of pixels containing membrane information. In this way, even if the image may not be properly focused at this distance, depending on the camera characteristics, the obtained H value will be still valid.

In order to test how hand-held operation may affect the performance of the analytical platform, other factor, in addition to distance, that should be studied when the image is acquired is centering of the sensor image within the whole picture. In this context, displaying the whole circular sensor image in the picture should be the ideal option, but hand-held operation of the mobile phone may result in pictures containing only portions of the membrane image. For this purpose, four membranes were captured in different positions within the picture, starting by placing the sensor image on the picture center and then gradually displacing the membrane image so this occupies less area of the total image, as illustrated in Figure 8. The results show that the H values obtained when the membrane is not centered are the same as when it is centered. Concretely, the relative standard deviation of the results obtained when the membrane image is displaced from the center down to occupying only 40% of the picture is 0.95%. The reason for this behaviour is that the H value was computed through its mode, so even when most of the pixels are almost white, corresponding to the image background, they do not affect the obtained result.

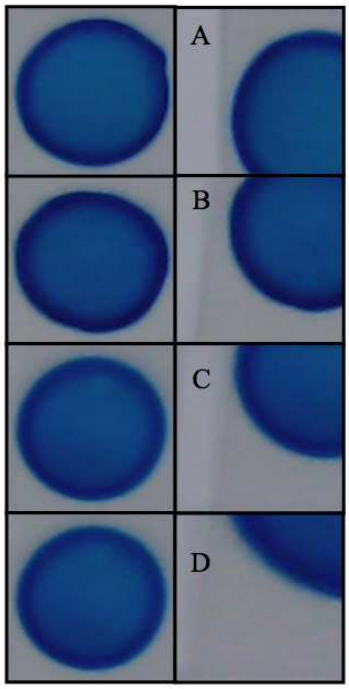

Figure 8. Centered (left) and decentered (right) membrane images showing H values and percentage of useful pixels for four different sensors. A: H_C=0.58; H_D=0.58; 59%; B: H_C=0.57; H_D=0.57; 51%; C: H_C=0.58; H_D=0.57; 43%; D: H_C=0.58; H_D=0.68; 26%

Finally, some images were captured by hand-holding the phone, thus completing the study on the influence of physical factors on the measurement process. Concretely, three membranes in three different solutions were processed in this way, and the results in terms of RSD are 0.78%, 0.77% and 0.92% for the same considered concentrations.

4.2.2. Influence of chemical factors

Regarding the chemical factors, the influence of variation in sensor composition, that could be a simile of lot-to-lot variation, was also considered through the influence of membrane thickness and indicator concentration. These deliberate changes were performed during the preparation of the membrane in order to evaluate how robust the analytical parameter H computed by the mobile phone is, by measuring its insensitivity to alterations in the operating conditions

The influence of thickness was studied by preparing a set of sensing membranes using different volumes of the same cocktail, from 10 to 25 μL, but maintaining a constant spot diameter of 12 mm. Thus, the calculated thickness varies between 1.4 and 3.5 μm. The results from three different membranes of each thickness, equilibrated with three different K(I) concentrations each, show that the H value for each K(I) concentration is almost independent of the membrane thickness, and the results do not show bias when the membrane thickness increases. Considering the precision in H using all the membranes of different thickness for the three K(I) solutions, the RSD values are 2.68, 1.34, and 1.33%.

Regarding the amount of indicator in the membrane, the chromoionophore in this case, several membranes were prepared with two different cocktails, one with the composition indicated in Section 2.2, and another with half of the concentration in all constituents previously used. Similarly to previous results, there is no bias with the increase in indicator concentration, since the hue value is maintained. The RSDs calculated from all the membranes equilibrated in the same potassium solution before testing were 2.45, 1.60, and 1.69% for each K(I) solution. Consequently, the small variations in membrane thickness and indicator concentration can be minimized by the use of the H parameter acquired with the mobile phone platform.

The independence of the results with respect to both physical and chemical factors reinforce the fact that it is possible to use a mobile phone as a platform for

obtaining analytical information, even when obviously this type of device is not designed for this purpose. This is possible because of the proposed custom software application, which is able to cope with all the factors studied, while it features a computationally-reduced image processing that allows preserving battery life and reduced processing times, still providing reliable analytical information.

4.3. Calibration with the mobile phone

As we have prior demonstrated [20], the direct use of H parameter for calibration enables simplifying the experimental procedure, avoiding the use of calibrants for the protonated and deprotonated forms of the chromoionophore, needed for the calculation of the degree of deprotonation, 1 - α, the usual analytical parameter for this type of sensors [21]. Thus, the use of H directly simplifies the procedure, only requiring one measurement, and avoids the measurement before and after equilibration with calibrants.

For calibration purposes, 12 potassium standard solutions buffered at pH 9.0 with Tris 0.02 M buffer solution and concentrations ranging from 10^{-7} to 0.1 M were prepared and used for reacting with three different potassium sensing membranes. After that, three pictures of each membrane were obtained with the mobile phone placed in the optical tent at a distance of 10 cm, according to the procedure described above. The resulting H values computed by the phone and plotted against logarithm of potassium concentration are shown in Figure 9 as a sigmoid curve, as it is usual for this class of sensing membranes.

The analytical range can be estimated by fitting a straight line to the region of maximum slope of the sigmoid for obtaining a linear function, $H = 1.17(\pm0.04) + 0.16(\pm0.01)[K(I)]$. This relationship has $R^2 = 0.9763$ and a limit of detection of 3.16×10^{-4} M, obtained from the intersection of the linear calibration function and

the linearized background at low concentration. This detection limit is higher than the calculated from absorbance measurements (1.25×10^{-5} M) [20].

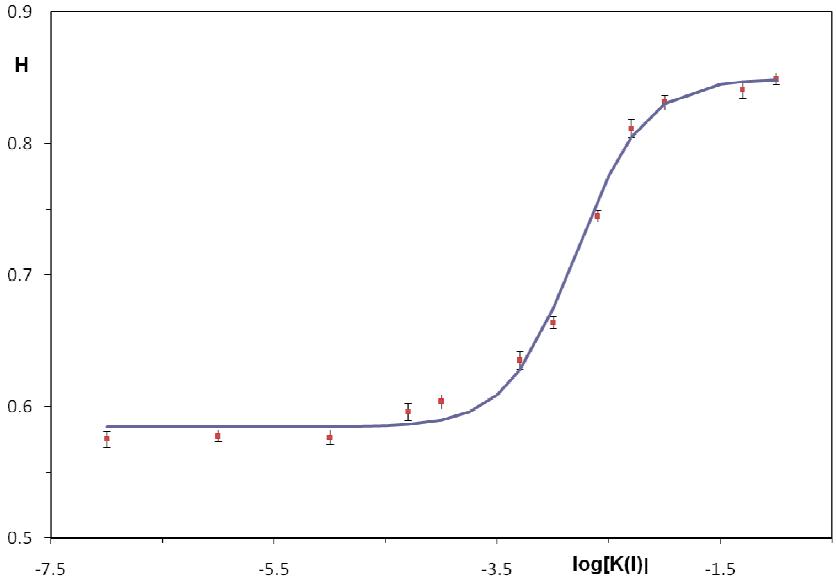

Figure 9. Calibration of the potassium concentration with experimental (symbols) H values obtained with the proposed mobile phone platform. Solid line shows sigmoid-function model.

However, the dynamic range of the procedure can be increased by fitting results to the sigmoid relationship given in Eq. 3, where the adjusting coefficients fit well (a_0 = -2.798; a_1 = 0.584; a_2 =0.849; a_3 = 0.309), also showing a good correlation (R^2 = 0.9947). The use of this function for the H parameter improves the analytical range and the detection limit of the procedure. With the use of the IUPAC criteria (3s) for the lower and upper limits, a wider measurement range (3.1×10^{-5} M to 1.0×10^{-1} M) is achieved, thus obtaining a detection limit, 3.10×10^{-5} M, similar to the calculated from absorbance measurements, 1.25×10^{-5} M, and lower than the obtained using the linear regression.

Table 1. Analytical specifications of the mobile phone platform for potassium determination

Fitting parer of the Sigmoid-function modelling	**Values**
a_0	-2.79893
a_1	0.58442
a_2	0.84908
a_3	0.30909
R^2	0.9947
Analytical parameters	**Values**
Detection limit	$3.1 \cdot 10^{-5}$ M
Range	3.1×10^{-5}-0.1 M
Inter-membrane precision	**RSD**
5×10^{-5} M	1.13%
5×10^{-4} M	1.51%
5×10^{-3} M	1.53%

The precision of the procedure using different single-use sensor was studied at three potassium concentrations, namely 5×10^{-5}, 5×10^{-4} and 5×10^{-3} M, using 10 replicas. The obtained results, also in terms of RSD, were 1.13%, 1.51% and 1.53% for the solutions mentioned above, respectively. The results of inter-membrane precision are acceptable if two facts are considered: first, the RSD values are much lower than in the case of use of analytical parameters based on intensity measurement (absorbance, reflectance, transflectance, fluorescence, RGB coordinate) and, second, the device used as analytical instrument is a very simple camera integrated in a mobile phone that digitalizes the membrane images. Moreover, the membrane precision with the developed procedure is comparable to those from other methods, such as the use of a scanner and a computer for processing the images, yielding from 0.14 to 0.75%, or the use of a scanner and custom-developed

software, providing from 0.33 to 0.92%. Thus, the results provided by the proposed mobile phone platform are slightly worse than previously mentioned data, but clearly better than other usual methods, such as diode array spectrophotometers, which provides RSD from 3.3 to 7.7%, transflectance measurements, from 2.4 to 7.9%, or a scanner using RGB colour space, 2.8 and 3.5%. As a summary, in Table 1 the analytical parameters for the mobile phone-based procedure are shown

Table 2. Validation test results. Phone *vs* atomic absorption spectroscopy potassium concentration values.

Sample	Phone	AAS	p-value
Mineral water	4.5×10^{-5} M ± 0.4×10^{-5}	3.83×10^{-5} M ± 0.01×10^{-5}	0.096
Tap Water	5×10^{-5} M ± 1.0×10^{-5}	6.22×10^{-5} M ± 0.01×10^{-5}	0.479
Spring Water	6.3×10^{-5} M ± 0.8×10^{-5}	5.29×10^{-5} M ± 0.05×10^{-5}	0.096

4.4. Validation of the mobile phone-based procedure

To test the usefulness and validate the procedure, it was applied to waters of diverse provenance (spring, mineral, tap) from Andalusia, Spain, for measuring potassium content. H values for the sensors were determined, and the concentration of potassium was calculated directly using H as the analytical parameter. The method was validated by comparison with results from atomic absorption spectroscopy. The results obtained using the described procedure were comparable to the established techniques, as shown in Table 2, which includes the p-value in order to accept the null hypothesis that confirms that there are not significant differences between results. This confirms the capability of the mobile phone-based procedure to analyze potassium using a single-use sensor, and the possibility of using optical sensors for relating hue changes to the analyte concentration.

5. Conclusions

This paper has demonstrated the capability of a mobile phone for processing and obtaining analytical information, also presenting it to the user. It has been made possible through the development of a custom software application, which includes reduced and adapted image processing in order to save computation time and preserve battery life while still providing accurate analytical measurements. Such a platform, as it has been shown, allows a non-experienced user to carry out the analysis of potassium in water, without the requirement of any chemical knowledge or laboratory equipment. Moreover, the inherent portability and battery-based operation make possible *in situ* analysis with a portable instrument, providing analytical information and analyte concentration.

The presented analytical platform has been characterized regarding both physical and chemical factors. Thus, it has been proved that physical factors such as a distance to the sensor, image centering, or even focusing, do not affect the computed H values and analyte concentrations. This has been made possible due to the custom-developed image processing, which features a monodimensional edge detection procedure, and the use of the hue component for obtaining the analyte concentration. In this way, the presented platform is well-suited for hand-held operation, enabling in-situ chemical analysis with a tool as simple as a mobile phone. Meanwhile, the study of chemical factors has confirmed that membrane thickness and indicator concentration have no significant influence on the potassium concentration determination. Thus, the performance of the presented platform is comparable to most usual procedures based on image processing on off-line computers.

Acknowledgement

We acknowledge financial support from the *Ministerio de Ciencia e Innovación, Dirección General de Investigación y Gestión del Plan Nacional de*

I+D+i (Spain) (Projects CTQ2009-14428-C02-01 and CTQ2009-14428-C02-02); and the *Junta de Andalucía* (*Proyecto de Excelencia* P08-FQM-3535). These projects were partially supported by European Regional Development Funds (ERDF).

6. Conclusión

Se ha demostrado la posibilidad de usar un teléfono móvil como plataforma analítica completa para la determinación de potasio usando un sensor óptico de un solo uso. Para ello se ha desarrollado un software adaptado a las características del teléfono que permite, a partir de una imagen de una membrana sensora, obtener la concentración del analito en cuestión, en este caso, potasio. La principal ventaja de este dispositivo es su facilidad de uso ya que sólo es necesario por parte del operador hacer la fotografía, pues el resto del proceso se realiza de manera automática por el software, dando como salida el valor de la concentración de analito.

También se ha demostrado la robustez de este método frente a diferentes factores que pueden afectar al valor de H obtenido a la hora de digitalizar la membrana. Dichos factores son tanto físicos, -distancia de adquisición de la imagen, enfoque, descentrado de la membrana en la imagen y ubicación del teléfono en un soporte para tomar la fotografía o bien hacerlo a pulso- como químicos, relativos al espesor de las membranas o la concentración de indicador presente en las mismas. Como consecuencia del estudio de estos factores, se ha calculado la precisión, expresada como desviación estándar relativa, de los resultados obtenidos frente a estas variaciones, arrojando unos valores que oscilan entre el 0.7 y el 2.2%, dependiendo del caso.

Como consecuencia de la robustez de los resultados obtenidos a partir de las imágenes adquiridas con el teléfono móvil, se ha llevado a cabo el calibrado del sistema para así poder determinar la concentración de potasio presente en muestras reales. El límite de detección calculado para dicho calibrado (3.10×10^{-5} M) es comparable al obtenido usando como instrumentación un espectrofotómetro convencional de sobremesa (1.25×10^{-5} M). De la misma manera, hablando en términos de precisión, los resultados son mejores que los conseguidos usando instrumentación específicamente diseñada para análisis químico, obteniendo una desviación estándar relativa para el caso del teléfono móvil comprendida entre 1.13-1.53%

frente a la obtenida a partir de medidas de absorción con el espectrofotómetro de diodos, 3.3-7.7%, medidas de transflectancia utilizando el refractómetro modular, 2.4-7.9% o el escáner utilizando otro espacio de color como es el RGB, 2.8-3.5%.

Por tanto, debido a la estabilidad de la señal obtenida de las imágenes frente a diferentes factores que influyen en la digitalización del sensor, como la facilidad de uso del dispositivo, concluimos que es posible el uso de un teléfono móvil como plataforma analítica por parte de usuarios sin especial formación en el campo del análisis químico, con una aceptable calidad de resultados para este tipo de análisis descentralizados.

7. Bibliografía

1. ARM,. Cortex-A8 Technical Reference Manual, http://infocenter.arm.com/help/topic/com.arm.doc.ddi0344k/index.html, 2010.

2. Android. Developers' Guide, http://developer.android.com/guide/index.html. 2010.

3. Apple iOS Developer Center. Technical Documentation, http://developer.apple.com/devcenter/ios/index.action. 2010

4. Y.T. Cheung, Test paper-type healthcare mobile phone, Patent 201388225, China, 2010.

5. Z. Dong, D. Pang, J. Li, Sports pose/blood sugar-monitoring mobile phone and on-line expert diagnosis system, Patent 201467228, China, 2010.

6. Y. Meng, M. Liu, C. Ma, G. Qu, L. Du, Real-time blood sugar monitoring system and method, blood sugar detection apparatus, and mobile phone terminal, Patent 101647703, China, 2010.

7. Y. Zhao, Method for determining blood glucose content with mobile phone, Patent 101637389, China, 2010.

8. E.H. Lee, M.K. Kim, C.H. Kim, Clinical chemistry measuring system capable of being applied to portable analysis system by using mobile phone, and method therefor, Patent 2007006304, Korea, 2007.

9. B.A. Cadle, K.C. Rasmus, L.S. Leverich, C.E. O'Neill, R.K. Bachtell, D.C. Cooper, Cellular phone-based image acquisition and quantitative ratiometric method for detecting cocaine and benzoylecgonine for biological and forensic applications, Subst.Abuse: Res.Treat. 4 (2010) 21.

10. F. Levin, Optical analytical system and methods for the determination of substances in liquids using photographic images, Patent 102008026803, Germany, 2009.

11. D. Bremnes, Method for semi-quantitative or quantitative analy. of assays including immunoassays in which method comprises assigning a barcode coded text segment on a test strip, Patent PCT 2009054729, 2009.

12. A.W. Martinez, S.T. Phillips, E. Carrilho, S.W. Thomas, H. Sindi, G.M. Whitesides, Simple Telemedicine for Developing Regions: Camera Phones

and Paper-Based Microfluidic Devices for Real-Time, Off-Site Diagnosis, Anal.Chem. 80 (2008) 3699.

13. A.W. Martinez, S.T. Phillips, G.M. Whitesides, Three-dimensional microfluidic devices fabricated in layered paper and tape, Proc.Natl.Acad.Sci.U.S.A. 105 (2008) 19606.

14. H.P. Ninh, Y. Tanaka, T. Nakamoto, K. Hamada, A bad-smell sensing network using gas detector tubes and mobile phone cameras, Sens.Actuators B 125 (2007) 138.

15. T. Nakamoto, T. Ikeda, H. Hirano, Arimoto, Humidity Compensation by Neural Network for Bad-Smell Sensing System Using Gas Detector Tube and Built-in Camera, IEEE Sensors (2009) 281.

16. Y. Michikawa, T. Suga, Y. Ohtsuka, I. Matsumoto, A. Ishikawa, K. Ishikawa, M. Iwakawa, T. Imai, Visible Genotype Sensor Array, Sensors 8 (2008) 2722.

17. Z. Iqbal, D. Filippini, Spectral Fingerprinting on a Standard Mobile Phone, J. Sensors (2010) .

18. W. Koehn, Cell phone with breath alcohol analyzer, Patent USA 2009325639, 2009.

19. L.F. Capitan-Vallvey, M.D. Fernandez Ramos, M. Al Natsheh, A disposable single-use optical sensor for potassium determination based on neutral ionophore, Sens.Actuators B 88 (2003) 217.

20. K. Cantrell, M.M. Erenas, I. Orbe-Paya, L.F. Capitan-Vallvey, Use of the Hue Parameter of the Hue, Saturation, Value Color Space As a Quantitative Analytical Parameter for Bitonal Optical Sensors, Anal.Chem. 82 (2010) 531.

21. E. Bakker, P. Bühlmann, E. Pretsch, Carrier-Based Ion-Selective Electrodes and Bulk Optodes. 1. General Characteristics, Chem Rev. 97 (1997) 3083.

22. A. Ceresa, Y. Quin, S. Peper, E. Bakker, Mechanistic insights into the development of optical chloride sensor based on the mercuracarborand-3 ionophore, Anal.Chem. 75 (2003) 133.

23. R.H. Ng, K.M. Sparks, B.E. Statland, Colorimetric determination of potassium in plasma and serum by reflectance photometry with a dry-chemistry reagent, Clin.Chem. 38 (1992) 1371.

24. I.d. Orbe-Paya, M. Erenas, L.F. Capitan-Vallvey, Potassium disposable optical sensor based on transflectance measurements, Sens.Actuators B 127 (2007) 586.

25. D. Freiner, R.E. Kunz, D. Citterio, U.E. Spichiger, M.T. Gale, Integrated optical sensors based on refractometry of ion-selective membranes, Sens.Actuators B 29 (1995) 277.

26. A. Lapresta-Fernandez, L.F. Capitan-Vallvey, Scanometric potassium determination with ionophore-based disposable sensors, Sens.Actuators B 134 (2008) 694.

27. E. Spence, Rapid Mobile Enterprise Development for Symbian OS: An introduction to OPL Application Design and Programming, 2005.

28. Nokia. S60 Platform: Introductory Guide. http://sw.nokia.com/id/fc17242f-9bb2-4509-b12c-1e6b8206085b/S60_Platform_Introductory_Guide_v1_6_en.pdf.

29. Y. Shishkin, S.G. Dmitrienko, O.M. Medvedeva, S.A. Badakova, L.N. Pyatkova, Use of a scanner and digital image-processing software for the quantification of adsorbed substances, J.Anal.Chem. 59 (2004) 102.

30. N.C. Birch, D.F. Stickle, Example of use of a desktop scanner for data acquisition in a colorimetric assay, Clin.Chim.Acta 333 (2003) 95.

31. A. Abbaspour, A. Khajehzadeh, A. Ghaffarinejad, A simple and cost-effective method, as an appropriate alternative for visible spectrophotometry: development of a dopamine biosensor, Analyst 134 (2009) 1692.

32. M. Kompany-Zareh, M. Mansourian, F. Ravaee, Simple method for colorimetric spot-test quantitative analysis of Fe(III) using a computer controlled hand-scanner, Anal.Chim.Acta 471 (2002) 97.

33. N. Maleki, A. Safavi, F. Sedaghatpour, Single-step calibration, prediction and real samples data acquisition for artificial neural network using a CCD camera, Talanta 64 (2004) 830.

34. S. E. Umbaugh. Computer Imaging: Digital Image Analysis and Processing, CRC Press, 2005

35. W. Dong, Z. Shisheng, Color Image Recognition Method Based on the Prewitt Operator, Proc.2008 IEEE International Conference on Computer Science and Software Engineering (2010) 170.

36. N. Kazakova, M. Margala, N.G. Durdle, Sobel edge detection processor for a real-time volume rendering system, Proc.2004 IEEE International Symposium on Circuits and Systems (ISCAS '04) 2 (2004) 913.

37. Sun Microsystems. Java platform. http://java.sun.com .

38. Sun Microsystems. NetBeans IDE 6.9.1. http://www.netbeans.org.

Conclusiones

Como resultado del trabajo realizado en esta Tesis Doctoral, se deducen las siguientes conclusiones:

1. Se ha propuesto el uso de medidas de transflectancia de un sensor óptico desechable diseñado para determinar la concentración de potasio presente en diferentes muestras. Para ello se utilizó una instrumentación modular portable, obteniendo resultados similares a los logrados a partir de medidas de absorción con un espectrofotómetro de sobremesa.

2. Se ha desarrollado una carta de color para la determinación semicuantitativa de potasio. Para su uso tan solo es necesario que el analista compare el color que adquiere la membrana sensora, al introducirla en una disolución que contiene el analito a determinar, con la carta de color desarrollada y así conocer el rango de concentraciones en el que se encuentra.

3. Se ha propuesto el uso de un nuevo parámetro analítico basado en el espacio de color HSV, en concreto su coordenada tonal H. Dicho parámetro destaca por su robustez frente a diferentes variables como son el grosor de la membrana, cantidad de indicador presente en la misma, iluminante y dispositivo utilizado para la digitalización de la membrana. Para el cálculo de la coordenada tonal, se ha desarrollado un software basado en Matlab que permite, a partir de una imagen digital de una membrana sensora, calcular dicha coordenada.

4. El uso del parámetro H, obtenido a partir de imágenes del sensor adquiridas en modo transmisión o reflexión, conlleva un aumento con-

siderable en la precisión de las medidas en comparación con los resultados obtenidos usando como parámetro medidas de absorción o transflexión. Dicho aumento en precisión, junto con una mayor estabilidad de la señal, va a permitir simplificar el procedimiento operatorio a la hora de emplear este tipo de sensores ya que hace posible usar el valor de H de manera directa, sin necesidad de normalizar la señal. Además, esa alta precisión permite ajustar el comportamiento de la membrana a una ecuación tipo Boltzman, consiguiendo de esta manera obtener límites de detección más bajos y por tanto mayores rangos dinámicos.

5. Se ha desarrollado una lengua electrónica para la determinación simultánea de sodio y potasio. Dicha lengua está compuesta por dos membranas sensoras no selectivas, cuya composición es similar, diferenciándose sólo en el ionóforo utilizado, que reaccionan en presencia de ambos analitos. Para la determinación de la concentración de dichos analitos a partir de valores de H procedentes de imágenes de la lengua digitalizada en modo transmisión, se han utilizado dos aproximaciones diferentes. En la primera el algoritmo k-NN y los valores de H y en la segunda una red neuronal tipo perceptrón. De esta manera se ha mostrado la versatilidad del parámetro H, usándolo en un sistema más complejo como es una lengua electrónica, manteniendo la precisión en las medidas obtenidas y la simplificación del procedimiento operatorio para usar la lengua.

6. Se ha conseguido que un teléfono móvil funcione como un sistema analítico completo capaz de digitalizar un sensor de un solo uso para la determinación de potasio y así obtener la concentración de analito presente. Para ello se portado la aplicación desarrollada en MATLAB a la plataforma Symbian. Esta aplicación calcula el valor de la coordenada tonal H de la membrana sensora digitalizada e intra-

pola su valor en una función de calibrado. El uso de un teléfono móvil permite llevar a cabo el análisis por personal no cualificado, obteniendo resultados similares a los conseguidos por personal con la formación apropiada.

7. Todos los procedimientos de medida desarrollados en la presente Memoria han sido aplicados a la determinación de los analitos objeto de estudio en muestras reales de diferente procedencia como son agua de grifo, pozo y mineral.

8. En todos los casos, el coste de los sensores de un solo uso desarrollados no sobrepasa los 10 céntimos de euro y su tiempo de vida se encuentra en torno a un mes y medio, aproximadamente.

9. En conclusión, se ha demostrado la potencialidad de las medidas colorimétricas tanto para el desarrollo de una carta de color, como para el cálculo del parámetro analítico H, obtenido de imágenes de sensores digitalizados en diferentes modos, transmisión o reflexión. El uso de este parámetro permite la simplificación del procedimiento operatorio, el aumento de la precisión de las medidas y el uso de diferentes dispositivos de captura de imagen digital, además de obtener mejores resultados que con parámetros analíticos tradicionales como la absorbancia o transflectancia. Además, el uso de estos dispositivos permite el análisis *in-situ* de las muestras a analizar por personal cualificado o no, de forma rápida, simple y a bajo costo.

Publicaciones

Artículos

Artículos publicados

1. Potassium disposable optical sensor based on transflectance and cromaticity measurements. Sensors and Actuators, B: Chemical (2007), B127(2), 586-592

2. The use of the Hue parameter of the HSV color space as a quantitative analytical parameter for bitonal optical sensor. Analytical Chemistry (2010), 82(2), 531-542

Artículos enviados

1. A surface fit approach with a disposable optical tongue for alkaline ion analysis. Talanta.

2. Disposable Optical Tongue for Alkaline Ion Analysis. Sensors and Actuators, B: Chemical.

3. Mobile phone platform as portable chemical analyzer. Sensors and Actuators, B: Chemical.

4. Use of digital reflection devices for measurement using hue-based optical sensors. Talanta.

Aportaciones a actas de congresos

Posters

1. Participación en las 11 Jornada de Análisis Instrumental con el trabajo titulado "Disposable optical sensor for potassium determination base on diffuse reflectance measurements" en Barcelona, 15 y 17 de Noviembre de 2005.

2. Participación en la X Reunión del Grupo Regional de la Sociedad Española de Química Analítica (Graseqa 2006) con el trabajo titulado "Disposable optical sensor for potassium determination base on diffuse reflectance measurements" en Cádiz, 8 y 9 de Junio de 2006.

3. Participación en EUROPTRODE IX Dublin 30 Marzo – 2 Abril 2008 con los trabajos: "Use of the H value of the HSV colour space to improve the analytical performance of optical one-shot sensors" y "Simultaneous determination of potassium and sodium by one-shot optical sensors and multivariate calibration"

4. Participación en GRASEQA 2008 XI Reunión del Grupo Regional Andaluz de la Sociedad Española de Química Analítica en Huelva 12-13 Junio con el trabajo: "Hacia un alengua óptica para la determinación de sodio y potasio con sensores ópticos de un solo uso"

5. Participación en 12as Jornadas de Análisis Instrumental (JAI) en Barcelona del 21 al 23 de Octubre de 2008 con el trabajo: "Disposable optical tongue for the simultaneous determination of alkaline ions in water"

6. Participación en XV reunión de la sociedad española de química analítica en San Sebastián del 19 al 20 de Julio de 2009 con el trabajo: "Use of HSV color space as a quantitative parameter for bitonal optical sensors"

7. Participación en EUROANALYSIS 2009 en Innsbruck (Austria) del 6 al 10 de Septiembre de 2009 con el trabajo: "Use of hue coordinate of the HSV color space as a quantitative parameter for bitonal optical sensors"

8. Participación en International workshop on multivariate image analysis en Valencia del 28 al 29 de Octubre de 2008 con el trabajo: "Automatic color feature extraction from disposable optical sensors"

9. Participación en International workshop on multivariate image analysis en Valencia del 28 al 29 de Octubre de 2008 con el trabajo: "Disposable optical tongue for simultaneous alkalyne ions determination based on color measurements"

10. Participación en EUROPT(R)ODE X european conference on optical chemical sensors and biosensors en Praga del 28 al 1 de Marzo de 2010 con el trabajo: "Disposable optical tongue for the simultaneous determination of alkaline ions in water using neuronal networks"

11. Participación en VII Colloquium Chemiometricum Mediterraneum en Granada del 21 al 24 de Junio de 2010 con el trabajo: "Use of neuronal networks for the determination of sodium and potassium using an optical tongue"

Comunicaciones orales

1. Participación en VII Colloquium Chemiometricum Mediterraneum en Granada del 21 al 24 de Junio de 2010 con el trabajo: “H value as analytical paramenter in image analysis”

2. Participación en GRASEQA 2010 XII Reunión del Grupo Regional Andaluz de la Sociedad Española de Química Analítica en Córdoba del 10 al 11 de Junio de 2010 con el trabajo: “Uso de una lengua óptica para la determinación de Na(I) y K(I) usando el tono como parámetro analítico”